Functional supramolecular additives

Functional Supramolecular Additives

PROEFSCHRIFT

ter verkrijging van de graad van doctor aan de Technische Universiteit Eindhoven, op gezag van de rector magnificus prof.dr.ir. F.P.T. Baaijens,
voor een commissie aangewezen door het College voor Promoties, in het openbaar te verdedigen op dinsdag 24 september 2019 om 16:00 uur

door

Bastiaan Dirk Ippel

geboren te Utrecht

Dit proefschrift is goedgekeurd door de promotoren en de samenstelling van de promotiecommissie is als volgt:

voorzitter:	prof.dr. J. de Boer
1e promotor:	prof.dr.dr. P.Y.W. Dankers
2e promotor:	prof.dr. C.V.C. Bouten
leden:	prof.dr. R.P. Sijbesma
	prof.dr. E.W. Meijer
	prof.dr. C. Werner (TU Dresden)
adviseur(s):	dr.ir. M.M.J. Smulders (WUR)
	dr.ir. A.I.P.M. Smits

Het onderzoek of ontwerp dat in dit proefschrift wordt beschreven is uitgevoerd in overeenstemming met de TU/e Gedragscode Wetenschapsbeoefening.

Cover design: Bastiaan Ippel

Printed by: Gildeprint, Enschede

A catalogue record is available from the Eindhoven University of Technology Library

ISBN: 978-90-386-4842-2

The research described in this thesis was funded by ZonMW as part of the LSH 2 Treat program (Project no. 436001003).

Financial support by the Dutch Society for Biomaterials and Tissue Engineering, Dutch Kidney Foundation, and Dutch Heart Foundation for publication of this thesis is gratefully acknowledged.

Content

Summary

The future of vascular access will revolve around the development of living vascular substitutes that are designed specifically for dialysis purposes and are able to grow, adapt and repair in the dynamic environment in the patient. Amongst different approaches, in situ tissue engineering features the implantation of a cell-free, but functional synthetic graft, that is remodelled by the patients own cells into living vascular tissue. To gain more insight into which cells play the most pivotal roles during the remodelling phase, and furthermore to assist in attracting and stimulating these cells, more control over the interactions between the synthetic graft material and the patients tissue is required. These improvements may be especially relevant in diseased conditions. In a multifaceted design, the functionalization of the synthetic biomaterials used for the graft with both antifouling and bio-active peptides is hypothesized to allow for the much-needed control.

Several methods for functionalizing elastomeric materials with both antifouling moieties and bioactives such as peptides exist, most of which are based on covalent chemistry. In this thesis, the polymeric base materials, which provide the mechanical properties to be suitable for application as vascular grafts, contain a supramolecular motif. These motifs, – either a ureidopyriminidinone (UPy) or a bisurea unit -, allow additives to be incorporated in a non-covalent and modular fashion. These additives were specifically engineered to add functionalities to the biomaterials for increased performance of the vascular graft directly after implantation and in the transition towards a living tissue. One key aspect in controlling cell-material interactions, is decreasing the unwanted aspecific adsorption of protein and adhesion of cells. Chapters 3 and 5 describe studies where this is achieved through incorporation of poly(ethylene glycol) containing additives in bisurea and UPy based material systems, respectively.

Specifically, different molecular designs were investigated to optimize efficacy of the modularly incorporated additives. In the bisurea system, the antifouling properties of a bifunctional additive (an oligo(ethylene glycol) (OEG) chain end-functionalized with two bisurea moieties) had superior antifouling properties compared to additives with one bisurea moiety (with an OEG chain on either or only one side) (chapter 3). Interestingly, the difference in additive design was expressed most clearly in 3D electrospun scaffolds, where the amount of OEG seemed to be the determining factor in 2D solution-cast films. In the UPy system, the non-cell adhesive properties of poly(caprolactone)diUPy (PCLdiUPy) based thin films was modified through incorporation of two bifunctional PEGdiUPy, i.e., a PEG_{2k}diUPy and a PEG_{10k}diUPy, additives and a monofunctional PEG_{5k}UPy (chapter 5). Additional hydrophobic spacers in the PEG_{5k}UPy and PEG_{10k}diUPy, flanking the UPy-moiety provided increased anchoring in the base material and superior non-cell adhesive properties. Furthermore, the mechanically more favourable chain-extended UPy-based material functionalized with the PEG_{2k}diUPy additive showed less promising results compared to PCLdiUPy. Separately, the possibilities for post-modification, that is after solution-casting or electrospinning, of a supramolecular material with antifouling polymers was investigated in chapter 6. A UPy-additive with a reactive end-group suitable for surface initiated atom transfer radical polymerization (SI-ATRP) was embedded in the hard-phase of PCLdiUPy, to which subsequently zwitterionic sulfobetaine-methacrylate (SBMA) was polymerized. The amount of SBMA and thereby the non-cell adhesive properties, was

regulated by both additive concentration and polymerization time. Moreover, translation of the post-modification approach to electrospun scaffolds was successful. Additionally, decreasing fouling of biomaterials is an often-used approach for the development of biomaterials with improved blood-compatibility, which are described in the review presented in chapter 2 of this thesis.

The next step towards increased control over cell-material interactions was pursued in chapter 4, through the combinatorial incorporation of specific cell-attracting peptide-additives and the antifouling bifunctional bisurea additive. All material mixtures with the integrin-binding RGD-peptide additive gave excellent cell-adhesive properties, illustrating the robustness of this peptide-sequence. An SDF-1α additive was also capable of refunctionalization of otherwise non-cell adhesive material mixtures, whereas the supposedly endothelial-cell specific REDV sequence showed limited activity for both endothelial and smooth muscle cells in this system. The explorative first steps towards spatial control over post-functionalization of supramolecular materials with bioactive peptides are described in chapter 8. Moreover, on the basis of preliminary results with several new additives, the design of the bisurea additives is discussed in chapter 8.

For the application as a - fully synthetic - vascular access graft, mechanical properties are particularly relevant. The impact of supramolecular additives on functional mechanical properties of electrospun scaffolds was analysed. Incorporation of a model bisurea compound, and the antifouling additives from chapter 3, resulted in minor differences in the initial modulus of the electrospun scaffolds.

The results presented in this thesis have given new insights in the efficacy of bioactivation via supramolecular functionalization strategies. Through careful engineering of additives, the next generation of vascular grafts will possess improved control over cell-material interactions, which will aid in improving the in situ regeneration of vascular scaffolds.

Samenvatting

De toekomst van alternatieve mogelijkheden voor het aanleggen van vaattoegang bij dialyse-patiënten, waarvoor geen fistula kan worden geconstrueerd, zal zich richten op het ontwikkelen van specifiek voor dit doel ontworpen levende substituten. Een van de methodes om dit te bewerkstelligen draait om de implantatie van een cel-vrij en functioneel synthetisch bloedvat, gemaakt van biologisch afbreekbare biomaterialen, die door de cellen van de patiënt zelf langzaam omgevormd zal worden tot een levend bloedvat.

Om meer inzicht te kunnen krijgen in welke cellen een cruciale rol spelen tijdens dit omvormingsproces, en om deze cellen gericht te kunnen sturen en aantrekken, is er meer controle nodig over de specifieke interacties tussen de cellen en het biomateriaal. Bovendien zouden de cellen in de patiënt een extra steuntje in de rug kunnen gebruiken om in de zieke omgeving net zo goed te kunnen functioneren en een gezond bloedvat kunnen vormen. In deze thesis wordt een ontwerp beschreven, waarin synthetische biomaterialen gefunctionalizeerd zijn met additieven die aan de ene kant ongewenste adsorptie tegengaan (zogeheten antifouling additieven), en aan de andere kant specifieke bioactiviteit toevoegen (bioactieve additieven), met het oog op de genoemde controle.

Er bestaan meerdere benaderingen voor het functionalizeren van biomaterialen met antifouling of bioactieve groepen, zoals bijvoorbeeld peptides, waarbij de meeste gebaseerd zijn op covalente chemie (door het aanleggen van chemische verbindingen). In ons onderzoek worden bijzondere polymere basis materialen gebruikt, die enerzijds de mechanische eigenschappen verschaffen om geschikt te zijn voor toepassing als artificieel bloedvat, en anderzijds een zogeheten supramoleculair motief bevatten. Deze motieven, een ureidopyrimidinone (UPy) of bisurea groep, geven de mogelijkheid om functionele additieven met eenzelfde motief op niet covalente, maar toch robuuste wijze in te mengen met het basis materiaal.

Het tegengaan van ongewenste adsorptie van cellen en eiwitten kan worden bereikt door middel van functionalizatie met hydrofiele moleculen zoals bijvoorbeeld poly(ethyleen glycol) (PEG). Hierbij zijn verschillende ontwerpen voor deze additieven onderzocht die zowel een supramoleculair motif (UPy of bisurea), als een hydrofiele PEG groep bevatten. Hierbij kwam naar voren dat in het systeem met het bisurea motief de antifouling eigenschappen het best werkten door een additief waarbij de PEG groep geflankeerd werd door twee bisurea groepen in te mengen, ten opzichte van additieven waarbij een bisurea geflankeerd werd door twee PEG groepen, of slechts aan één zijde een PEG groep had. Een interessante conclusie was hier dat dit verschil zich duidelijker manifesteerde in de materialen die verwerkt waren tot een poreuze scaffold doormiddel van electrospinnen. Dit is dezelfde methode als gebruikt kan worden voor het fabriceren van het artificiele bloedvat.In studies met materialen waarbij het UPy motief gebruikt werd, werd helder dat een extra, hydrofoob verbindings-stuk tussen de PEG en de UPy een verbeterde verankering in het basismateriaal tot gevolg had, met daarbij ook betere antifouling eigenschappen. Hiernaast is in het UPy-systeem onderzocht of het oppervlak van de synthetische biomaterialen ná fabricatie met electrospinnen gemodificeerd kon worden met antifouling groepen. Daarvoor werd een additief met een UPy groep en een reactieve groep ingemengd met het basismateriaal en verwerkt tot dunne laag of poreuze scaffold.

Daarop werd vervolgens een zwitterionisch molecuul – sulfobetaine-methacrylaat (SBMA), ook antifouling – gepolymerizeerd. In deze studie werd de hoeveelheid SBMA, en daarmee de antifouling eigenschappen, gereguleerd aan de hand van de concentratie van het additief met de reactieve groep en de reactietijd. Bovendien bleek deze methode toepasbaar op de scaffolds.

In de volgende stap naar controle over de interacties tussen de cellen en het biomateriaal spelen bioactieve additieven een centrale rol. Peptides werden gecombineerd met het bisurea-motief, met als doel specifieke cellen te laten hechten. In een materiaal gecombineerd met de bisurea-bevattende antifouling additieven werd duidelijk dat een additief gebaseerd op het generieke cel-bindende peptide RGD in alle geteste omstandigheden in staat was cellen te laten hechten op de biomaterialen. Een additief met SDF-1α (met een verhoogde specifiteit voor monocyten) was ook in staat om deze cellen te laten hechten op anderszins antifouling materialen, daar waar een vermeend endotheelcel-specifiek peptide REDV, beperkte functionaliteit presenteerde in dit systeem voor zowel endotheel als gladde spiercellen. Verder zijn de eerste stappen gezet om onze biomaterialen te kunnen functionalizeren met peptides in gedefinieerde patronen met behulp van licht-gevoelige chemie.

De mechanische eigenschappen van het verwerkte biomateriaal - inclusief eventuele additieven - zijn uitermate van belang voor de toepassing als synthetisch bloevat, wat later omgezet wordt in een levend substituut. Om het effect van de additieven op de mechanische eigenschappen te testen zijn materialen met de bisurea-bevattende antifouling additieven verwerkt met electrospinnen en onderworpen aan mechanische testen. Hieruit werd duidelijk dat het inmengen van de additieven een gering effect had op de stijfheid van deze materialen.

Concluderend hebben de resultaten in deze thesis nieuwe inzichten verschaft met betrekking tot het functionalizeren van biomaterialen via het inmengen van supramoleculaire additieven. Als deze additieven zorgvuldig ontworpen worden, kan door middel van meer gecontroleerde interacties tussen cel en biomateriaal, aan de volgende generatie synthetische bloedvaten meer sturing worden gegeven aan het omvormingsproces tot levend bloedvat..

1

Introduction to this thesis

Vascular access

Hemodialysis functions as the primary lifeline for patients with end stage renal disease. Access to the vascular system is a requirement for this procedure, where waste products are filtered from the patients' blood, outside their body. Long term access is obtained through an arteriovenous fistula, where an artery and a vein are surgically connected, or a synthetic arteriovenous graft (AVG). Surgical construction of arteriovenous fistulas is preferred over the implantation of AVGs, however in patients where no suitable homologous vasculature is available, AVGs remain the only option for permanent vascular access. Synthetic, non-degradable AVGs are most commonly fabricated from polytetrafluoroethylene (PTFE), polyethylene terephthalate (PET, or Dacron).[1] Synthetic grafts face a reduced patency compared to autologous AVFs, and complications related to vascular access grafts lead to increased and advanced interventions, with underlying causes including infection, thrombosis, stenosis, and aneurysm formation.[2,3] Moreover, due to the repeated puncturing, or cannulation, which is part of the hemodialysis procedure, the structural integrity of these synthetic grafts deteriorates rapidly. Aspects of non-degradable synthetic grafts that have been the topic of research include early cannulation possibilities, increased durability, and coating with anti-thrombotic molecules such as heparin.[1,4,5]

Tissue engineered vascular grafts

One other main limitation of traditional synthetic grafts, is the lack of incorporation in the host-tissue, and the lack of regenerative and remodeling capability due to the non-living nature of the vascular substitute.[6] This limitation especially holds true for pediatric patients that need vascular grafts. The field of vascular tissue engineering aims to (re)create living blood-vessel substitutes *in vitro* or *in vivo*, where a biomaterial substrate is often used as a template to guide tissue formation.[7] Different approaches to vascular tissue engineering can be identified, which all revolve around the appropriate combination of a biomaterial, cells and biochemical and mechanical cues for neo tissue formation (**Figure 1.1**).[6,8]

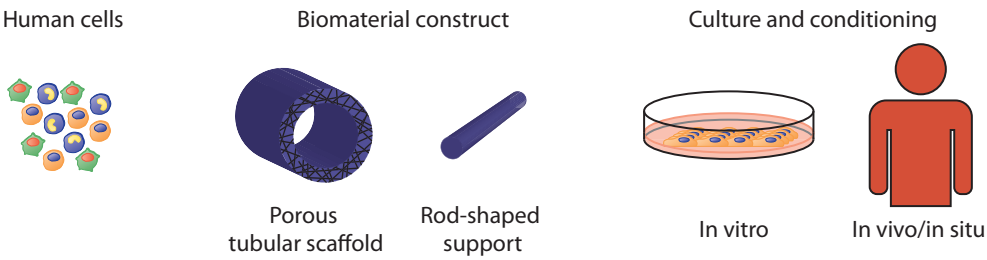

Figure 1.1. Important components of different approaches for vascular tissue engineering.

In the research by Niklason et al., tubular scaffolds, fabricated from bioresorbable polyglycolic acid are seeded with matrix producing cells and subsequently cultured *in vitro* in bioreactors that provide a pulsatile flow of medium.[9,10] The cells degrade the synthetic material and replace it with their own extracellular matrix. After decellularization, which prevents any hostile immunogenic response to the cells that created the blood-vessel, these constructs can be readily implanted for large diameter vascular applications (diameter

> 6mm).[9] Over time, cells from patients are able to repopulate this blood-vessel and transform the tissue into a native-like multi-layered structure.[11] L'Heureux et al. developed a method based on fibroblast sheets grown *in vitro*.[12,13] These fibroblast sheets were wrapped around a cylindrical support and fused through prolonged culture, after which they were decellularized. On the luminal side of this conduit endothelial cells were cultured, and around the basal side living cell-sheets were wrapped for reinforcement. Testing has progressed to human trials for such sheet-based constructs.[14,15] In an approach developed in the group of Rotmans, polymeric rods are implanted subcutaneously. The tissue capsules that form around the rod are then explanted, and used as vascular conduits.[16–18] The surface properties of the polymeric rods allow for some degree of control over the composition and structure of the formed tissue capsules.[18,19] Interestingly, after implantation the tissue capsule showed signs of remodelling towards vascular tissue.[17] In the approach by Breuer and coworkers stem cells that are harvested from the patients are used to seed porous and biodegradable scaffolds prior to implantation.[20,21] Increased patency was observed for increased cell-seeding.[22] In our group, electrospun scaffolds fabricated from biodegradable

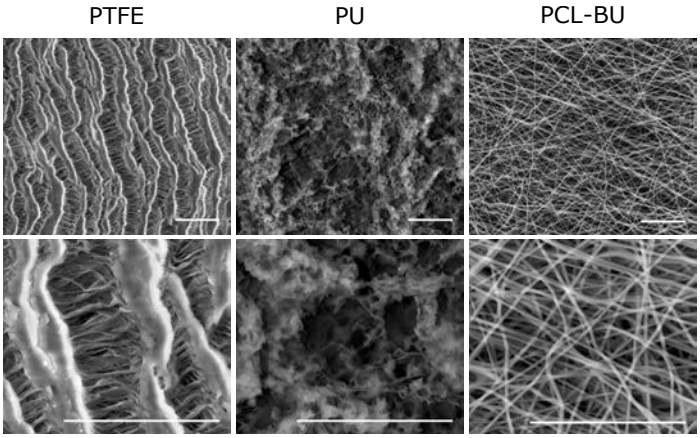

Figure 1.2. Scanning electron micrographs of vascular graft materials. Commercially available synthetic grafts made of PTFE and PU, and an example of a supramolecular electrospun scaffold, showing the clear differences in microstructure between the different approaches. Scale bars indicate 50 μm.

polymers, are used to produce acellular blood-vessel substitutes. Circulating host-cells infiltrate the scaffold, after which tissue producing cells are attracted, the polymeric material is slowly degraded and autologous vascular tissue is simultaneously deposited.[23,24] The porous and fibrous constructs used in this approach have a distinctly different microstructure (**Figure 1.2**), which has already been applied in non-degradable vascular grafts that are hypothesized to better withstand repeated cannulation. Patency rates were reported after one year that were comparable to other synthetic AVGs.[25,26] The promise of the tissue engineering approaches is highlighted by the high degree of valorisation, resulting in (spin-off) companies such as Xeltis, Aditlys, Vacis, and HumaCyte that all strive to commercialize tissue engineered vascular constructs.

However, the formation of, or remodeling towards, vascular-like tissue using these constructs is still little understood. Therefore, current and future research strives towards

enhanced understanding of - and control over - the involved processes. Several factors are known to be essential for the formation of functional tissue: Exposure to hemodynamic conditions is of great influence for the properties the tissue will develop over time, which emphasizes the importance of either in vitro hemodynamic conditioning as in the approach by Niklason et al., or directly implanting in situ, as in the approach in our group. Illustratively, both the shear stress induced by fluid flow and the cyclic stretch following from pulsatile pressure differences affect tissue formation in vascular grafts.[27] Since resorption of the biomaterial or remodeling of existing matrix proteins, and deposition of de novo extracellular matrix all occur simultaneously, the balance between the mechanical properties and degradability should be delicately managed to ensure lasting functionality after implantation.[28] The thrombogenic properties of the vascular graft, which are dictated by the biomaterial until an endothelial layer is formed, are also subject to a lot of research and biomaterial modification strategies. These principles, which range from antifouling functionalization and incorporation of anti-thrombogenic properties to methods to promote endothelialization, are discussed more elaborately in **Chapter 2**.

Many of the processes that relate to degradation of the biomaterial, and tissue formation and remodelling are cell-mediated, where immune cells are found to play a special role.[29] In biomaterial development for the next generation of vascular access grafts, a lot of effort has been placed into adapting these materials to control recruitment of cells, including immune cells, and in controlling how cells respond to the graft. The morphology, mechanical properties, susceptibility to degradation, and bioactivity are all tuneable features that can be used to tune this response. Apart from the overall morphology, which arises mostly from different variables during processing, these factors can be tuned on a molecular level: the mechanical properties change with different molecular weights of the polymer, susceptibility to degradation follows from the presence and availability of for instance groups that are easily hydrolysable, and bioactivity can be introduced through functionalization of the biomaterial with bioactive molecules such as peptides. In contrast to covalent surface functionalization or simple physisorption, in this thesis supramolecular chemistry is applied to functionalize elastomeric biomaterials with the purpose of controlling cellular behavior for vascular graft development.

Supramolecular chemistry

Supramolecular chemistry has been identified as a promising approach to synthetically mimic the complexity of the extracellular matrix.[30] Synthetically prepared supramolecular structures range in shape and complexity from random coils and nanofibers to nanoribbons and nanotubes.[31] The driving forces behind the formation of these structures are non-covalent interactions, including hydrogen bonding, electrostatic interactions, Van der Waals forces and pi-pi interactions.[32] Various molecular designs have been used to develop supramolecular materials, which rely on non-covalent interactions in different degrees. Examples that have been employed for the development of supramolecular materials include peptide amphiphiles[33], benzene-1-3-5-tricarboxamides (BTA)[34], host-guest systems based on e.g. cucurbit-urils[35] and cyclodextrins[36], and the bisurea and ureido-pyrimidinone moieties used in this thesis. Design of supramolecular polymers based on these reversible interactions can result in materials with properties such as self-healing[37,38] and stimuli-responsiveness.[39]

Bisurea supramolecular chemistry

Small molecules with closely paired urea moieties were first investigated for their ability to form organogels at low concentrations in the 1990s.[40–42] In these studies, bisurea compounds with both alkyl and aromatic spacers in between the urea groups and sidechains (**Figure 1.3**), were investigated for their gelation properties in many organic solvents and on solid substrates. These simply structured molecules could form stable and thermoreversible gels at low concentrations.[41] The proposed assembly mechanisms relies on hydrogen bonding between laterally aligned urea moieties, which can lead to the formation of filaments, tubes, sheets and multilayered nanoribbons.[41,43] The length and structure of the spacer determine the cis- or trans conformation of the assembled bisureas, as can be observed in physisorbed monolayers.[44,45] The assembly of bisurea molecules into supramolecular polymers is cooperatively driven by synergistic association of two urea moieties and the thermodynamic preference to form oligomers over dimers.[46] Considering that the association between the urea groups depends on the molecular design, the assembly can be tuned by altering the structure of the bisurea monomers. Subtle changes of molecular structure and their influence on assembly has been studied in great detail.[47] When at least one of the aliphatic side chains is substituted for a hydrophilic polymer, such as poly(ethylene glycol) (PEG), amphiphilic bisurea molecules are formed. Such molecules can possess hydrogelating properties.[48,49] Clever design of bisurea molecules that assemble in either organic or aqueous conditions, has led to materials with interesting properties. Bisurea organogelators have been used as surface modification to induce hydrophobic properties aiming at repelling surfaces,[50,51] to grow crystals of organic semiconductors[52] and prepare stimuli-responsive organogels.[53]. Bisurea based hydrogels were designed with natural protein mimicking strain-stiffening properties[54], with control over spatial organization[55], and as a polymorphic drug mimic.[56] Moreover, the specific interactions between matching bisurea moieties allows for the modular functionalization of such supramolecular assemblies.[49,57]

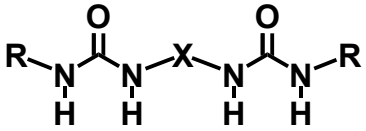

Figure 1.3. Schematic representation of small molecule bisurea structure, with X the linker between the urea groups and R the side groups.

However, for applications that require more strength, elastomeric solid materials are a more suitable candidate. Specifically, thermoplastic elastomers, which are copolymeric materials constituted of a crystalline hard-phase and a rubbery soft-phase, provide an interesting platform. If the crystalline domains classically found in thermoplastic elastomers are substituted for supramolecular building blocks such as the bisurea motif, the interactions in the hard-phase of these materials becomes highly directional and organized.

Because of these self-associating properties, development of bisurea based non chain-extended supramolecular thermoplastic elastomers was possible, [58,59] besides more traditional chain-extended supramolecular thermoplastic elastomers.[60,61] The organized nature of the hard-phase in these materials is especially evident when analyzed with atomic

force microscopy, where fibrous structures attributed to the assembled bisureas are clearly visible (**Figure 1.4**)[58,60,61] The uniformity of fiber dimensions in these AFM studies suggested a cylindrical hard segment morphology, which in turn indicates that multiple bisurea stacks co-assemble to form fibers based on dipole-dipole interactions (**Figure 1.4**).[62,63] Interestingly, it has been shown that small molecule additives with different aliphatic spacers between the urea groups self-sorted with matching bisureas in the TPE base material,[60,62,64] where the additives are randomly dispersed throughout the hard-block with matching bisurea motifs.[65] The nano-scale surface morphology of the materials and the degree of segregation depends on the design of the bisurea containing motif, the length and the properties of the polymeric soft-blocks,[66,67] and processing.[68] The mechanical properties of thermoplastic elastomers are enhanced with well-defined bisurea hard-blocks, evident by an increased tensile strength.[61] Additional urethane groups flanking the bisurea moiety change the hard-block morphology and properties, attributed to increased interaction possibilities, but do not enhance incorporation of bisurea-based additives in the elastomeric material.[62] Moreover, the specific interactions between the bisurea moieties in the hard-block can be utilized to tune the mechanical properties of the materials through incorporation of small bisurea-filler additives.[69] Also, by using a diacetylene-containing linker between the urea groups, bisurea TPEs can be crosslinked with UV after assembly.[70]

Ureidopyrimidinone supramolecular chemistry

Comparable to the bisurea, ureidopyrimidinone (UPy) moieties are capable of self-complementary assembly through fourfold hydrogen bonding.[71,72] Additional urea

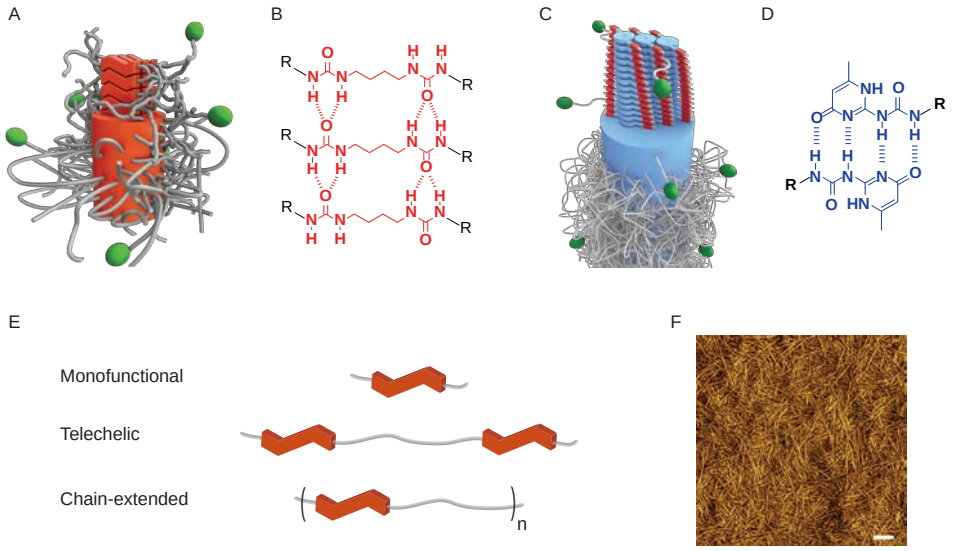

Figure 1.4. A) Schematic representation of bisurea fiber. B) Bisurea-bisurea interactions through hydrogen bonding. C) Schematic representation of UPy-fiber. D) UPy-UPy dimerization through hydrogen bonding. E) Schematic representation of possible conformations of supramolecular motifs with molecules with small, monofunctional molecules, end-functionalized polymers, or chain-extended polymer in which the supramolecular motif can function as the hard-phase. F) Atomic force microscopy phase image of a solution-cast PCLdiUPy film. Scale bar indicates 100 nm.

groups that can form hydrogen bonds stabilize lateral stacking through π-π interactions between the UPy-dimers, which bundle with 3 stacks into nano-scale fibers.[73–75] Using these interactions, telechalically functionalized supramolecular thermoplastic elastomers have been developed, as well as conventional chain-extended TPEs, with UPy-groups and additional alkyl spacers functioning as hard-segments.[76,77] Strategical grafting of UPy-groups onto a natural or synthetic polymer resulted in improved mechanical properties of hydrogels[78], and self-healing properties in an elastomeric material.[79]

Moreover, the specificity of the UPy-UPy interactions allows for modular incorporation of bioactive UPy-based additives to endow the material with properties for many applications. A mixture of UPy-RGD and UPy-PHSRN was used in an explorative study on this approach for the development of biomaterials.[80] Bioactivation of a UPy-peptide functionalized surface was probed using S-peptides in combination with an RNase assay.[81] Following these first steps, UPy-peptide conjugates have been used to create anti-microbial surfaces[82], polymeric renal basement membrane mimics[83], heparin-binding biomaterials for cytokine complexation[84], leukocyte attracting electrospun scaffolds[85], Notch-pathway activators,[86] and a bioactive cell-adhesive sides in bilayered electrospun scaffolds.[87] Using a UPy-catechol additive, cell-biomaterial interactions were improved on an inherently non-cell adhesive end-functionalized Priplast material.[88] Moreover, post-modification of supramolecular biomaterials has been the topic of recent studies, where a reactive additive was incorporated in a supramolecular TPE, to which dyes, antifouling PEG polymers, and proteins were reacted using bio-orthogonal click-chemistry.[89,90]

For applications in aqueous solutions and hydrogels, additional alkyl-spacers provide necessary hydrophobic shielding of the UPy-UPy interactions from water, in combination with hydrophilic polymers for water binding and solubility.[91] UPy-based aqueous assemblies and hydrogels have been the subject of a lot of research, focusing on dynamics[92,93] delivery of therapeutics[94–97] and clinical visualization.[98]

Aim and outline

The aim of the research described in this thesis is to exploit the versatility of the supramolecular materials platform, and introduce new functions through the incorporation of small supramolecular additives in vascular biomaterials (**Figure 1.5**). The efficacy of these newly designed additives is investigated where the relationship between material properties and functionality is of particular interest, to enhance our understanding of the impact of several additive design parameters. Antifouling additives were engineered to decrease undesired aspecific adsorption of cells and proteins. On the other hand, cell-adhesive peptide-additives were studied with the aim to increase specificity in cellularization of the biomaterials. Furthermore, additives with reactive functional groups were investigated for additional possibilities for functionalization with peptides and antifouling moieties after processing.

Through this approach, more control over the interactions cells have with the biomaterial is pursued, which can provide the tools to improve the *in situ* regeneration of the next generation of vascular access grafts.

In **Chapter 2** the strategies for the fabrication of biomaterials, *e.g.* for vascular grafts,

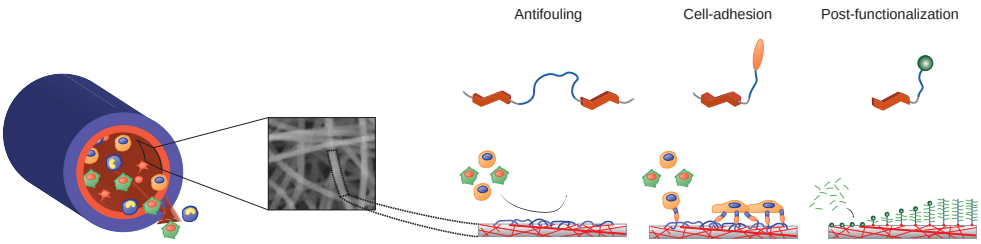

Figure 1.5. The approach featured in this thesis, where functional supramolecular additives are used to modify biomaterials used for the fabrication of vascular grafts with antifouling, cell-adhesive and post-functionalizable properties.

with improved blood-compatibility are reviewed. Antifouling, anti-thrombogenic, and endothelialization promoting functionalization approaches are discussed, and the trend towards more dynamic material systems is highlighted.

The importance of additive design in supramolecular functionalization strategies is investigated in **Chapter 3**, where three oligo(ethylene glycol) (OEG) based additives were designed and combined with a bisurea containing thermoplastic elastomer (PCL-BU). Non-cell adhesive properties were first screened on 2D thin films. Secondly, the material mixtures were processed into electrospun scaffolds, to investigate the efficacy of the functionalization in the translation from 2D to 3D structures. Furthermore, the robustness was studied by partial degradation of the electrospun scaffolds prior to cell-adhesion experiments.

Specific cellularization of our supramolecular biomaterials was studied in **Chapter 4**, through combinatorial incorporation of an antifouling additive from chapter 3 with three bisurea-peptide conjugates; a generic RGD-peptide, an endothelial cell specific REDV-peptide and a SDF-1α derived peptide. The surface properties of the functionalized materials were thoroughly characterized and related to the adhesion of vascular endothelial and smooth muscle cells.

Different UPy-based additives with hydrophilic PEG functionality were compared in **Chapter 5**. Through changes in molecular design, the effect of PEG-length and hydrophobic spacer length was investigated. Cell adhesion of various cell-types, *i.e.,* human derived kidney epithelial cells, human vascular myofibroblasts, and endothelial cells , on films fabricated with both solution-casting and spin-coating was determined.

In **Chapter 6** post-functionalization of supramolecular biomaterials via surface initiated controlled radical polymerization was studied. Zwitterionic monomers were polymerized from an initiator additive, that was embedded in the hard-phase of these materials. The efficacy of the reaction was investigated both with increasing reaction time and initiator additive concentration. Finally, this method was translated to microporous electrospun scaffolds.

For mechanically challenging applications, such as vascular grafts, mechanical properties are truly important. Therefore, the effect of additive incorporation on the mechanical behavior of electrospun scaffolds was analyzed in **Chapter 7**. The OEG-based additives described

in **Chapter 3**, and a model filler compound were mixed with the PCL-BU structural base material and processed into electrospun scaffolds followed by thermal characterization and mechanical testing.

In the final chapter, future perspectives for these material systems are described. Preliminary results for materials modified with a selection of bisurea-based additives are used to discuss the design of future supramolecular additives. Furthermore, translational aspects of this work are considered.

References

(1) Santoro, D.; Benedetto, F.; Mondello, P.; Spinelli, F.; Ricciardi, C.; Cernaro, V.; Buemi, M.; Pipito', N.; Barilla', D. Vascular Access for Hemodialysis: Current Perspectives. *Int. J. Nephrol. Renovasc. Dis.* **2014**, *7*, 281.

(2) Rotmans, J. I.; Pasterkamp, G.; Verhagen, H. J. M.; Pattynama, P. M. T.; Blankestijn, P. J.; Stroes, E. S. G. Hemodialysis Access Graft Failure: Time to Revisit an Unmet Clinical Need? *J. Nephrol.* **2005**, *18*, 9–20.

(3) Van Tricht, I.; De Wachter, D.; Tordoir, J.; Verdonck, P. Hemodynamics and Complications Encountered with Arteriovenous Fistulas and Grafts as Vascular Access for Hemodialysis: A Review. *Ann. Biomed. Eng.* **2005**, *33*, 1142–1157.

(4) Shakarchi, J. Al; Inston, N. Early Cannulation Grafts for Haemodialysis: An Updated Systematic Review. *J. Vasc. Access* **2019**, *20*, 123–127.

(5) Shemesh, D.; Goldin, I.; Hijazi, J.; Zaghal, I.; Berelowitz, D.; Verstandig, A.; Olsha, O. A Prospective Randomized Study of Heparin-Bonded Graft (Propaten) versus Standard Graft in Prosthetic Arteriovenous Access. *J. Vasc. Surg.* **2015**, *62*, 115–122.

(6) Naito, Y.; Shinoka, T.; Duncan, D.; Hibino, N.; Solomon, D.; Cleary, M.; Rathore, A.; Fein, C.; Church, S.; Breuer, C. Vascular Tissue Engineering: Towards the next Generation Vascular Grafts. *Adv. Drug Deliv. Rev.* **2011**, *63*, 312–323.

(7) Bouten, C. V. C.; Dankers, P. Y. W.; Driessen-Mol, a.; Pedron, S.; Brizard, a. M. a; Baaijens, F. P. T. Substrates for Cardiovascular Tissue Engineering. *Adv. Drug Deliv. Rev.* **2011**, *63*, 221–241.

(8) Song, H. H. G.; Rumma, R. T.; Ozaki, C. K.; Edelman, E. R.; Chen, C. S. Vascular Tissue Engineering: Progress, Challenges, and Clinical Promise. *Cell Stem Cell* **2018**, *22*, 340–354.

(9) Dahl, S. L. M.; Kypson, A. P.; Lawson, J. H.; Blum, J. L.; Strader, J. T.; Li, Y.; Manson, R. J.; Tente, W. E.; Dibernardo, L.; et al. Readily Available Tissue-Engineered Vascular Grafts. **2011**, *3*, 68ra9.

(10) Niklason, L. E.; Gao, J.; Abbott, W. M.; Hirschi, K. K.; Houser, S.; Marini, R.; Langer, R. Functional Arteries Grown in Vitro. *Science* **1999**, *284*, 489–493.

(11) Kirkton, R. D.; Santiago-Maysonet, M.; Lawson, J. H.; Tente, W. E.; Dahl, S. L. M.; Niklason, L. E.; Prichard, H. L. Bioengineered Human Acellular Vessels Recellularize and Evolve into Living Blood Vessels after Human Implantation. *Sci. Transl. Med.* **2019**, *11*, eaau6934.

(12) L'Heureux, N.; Dusserre, N.; Konig, G.; Victor, B.; Keire, P.; Wight, T. N.; Chronos, N. A F.; Kyles, A. E.; Gregory, C. R.; Hoyt, G.; et al. Human Tissue-Engineered Blood Vessels for Adult Arterial Revascularization. *Nat. Med.* **2006**, *12*, 361–365.

(13) L'Heureux, N.; McAllister, T. N.; de la Fuente, L. M. Tissue-Engineered Blood Vessel for Adult Arterial Revascularization. *N. Engl. J. Med.* **2007**, *357*, 1451–1453.

(14) McAllister, T. N.; Maruszewski, M.; Garrido, S. a.; Wystrychowski, W.; Dusserre, N.; Marini, A.; Zagalski, K.; Fiorillo, A.; Avila, H.; Manglano, X.; et al. Effectiveness of Haemodialysis Access with an Autologous Tissue-Engineered Vascular Graft: A Multicentre Cohort Study. *Lancet*

2009, *373*, 1440–1446.

(15) Wystrychowski, W.; McAllister, T. N.; Zagalski, K.; Dusserre, N.; Cierpka, L.; L'Heureux, N. First Human Use of an Allogeneic Tissue-Engineered Vascular Graft for Hemodialysis Access. *J. Vasc. Surg.* **2014**, *60*, 1353–1357.

(16) Damanik, F. F. R.; Rothuizen, T. C.; van Blitterswijk, C.; Rotmans, J. I.; Moroni, L. Towards an in Vitro Model Mimicking the Foreign Body Response: Tailoring the Surface Properties of Biomaterials to Modulate Extracellular Matrix. *Sci. Rep.* **2015**, *4*, 6325.

(17) Rothuizen, T. C.; Damanik, F. F. R.; Lavrijsen, T.; Visser, M. J. T.; Hamming, J. F.; Lalai, R. a.; Duijs, J. M. G. J.; van Zonneveld, A. J.; Hoefer, I. E.; van Blitterswijk, C. a.; et al. Development and Evaluation of in Vivo Tissue Engineered Blood Vessels in a Porcine Model. *Biomaterials* **2016**, *75*, 82–90.

(18) Rothuizen, T. C.; Damanik, F. F. R.; Anderson, J. M.; Lavrijsen, T.; Cox, M. a. J.; Rabelink, T. J.; Moroni, L.; Rotmans, J. I. Tailoring the Foreign Body Response for In Situ Vascular Tissue Engineering. *Tissue Eng. Part C Methods* **2015**, *21*, 436–446.

(19) Damanik, F. F. R.; Rothuizen, T. C.; Van Blitterswijk, C.; Rotmans, J. I.; Moroni, L. Towards an in Vitro Model Mimicking the Foreign Body Response: Tailoring the Surface Properties of Biomaterials to Modulate Extracellular Matrix. *Sci. Rep.* **2014**, *4*, 1–11.

(20) Hibino, N.; McGillicuddy, E.; Matsumura, G.; Ichihara, Y.; Naito, Y.; Breuer, C.; Shinoka, T. Late-Term Results of Tissue-Engineered Vascular Grafts in Humans. *J. Thorac. Cardiovasc. Surg.* **2010**, *139*, 431–436.e2.

(21) Shin'oka, T.; Matsumura, G.; Hibino, N.; Naito, Y.; Watanabe, M.; Konuma, T.; Sakamoto, T.; Nagatsu, M.; Kurosawa, H. Midterm Clinical Result of Tissue-Engineered Vascular Autografts Seeded with Autologous Bone Marrow Cells. *J. Thorac. Cardiovasc. Surg.* **2005**, *129*, 1330–1338.

(22) Lee, Y.; Mahler, N.; Best, C. a; Tara, S.; Sugiura, T.; Lee, A. Y.; Yi, T.; Hibino, N.; Shinoka, T.; Breuer, C. Rational Design of an Improved Tissue-Engineered Vascular Graft: Determining the Optimal Cell Dose and Incubation Time. *Regen. Med.* **2016**, *11*, 159–167.

(23) Talacua, H.; Smits, A. I. P. .; Muylaert, D. E. P.; van Rijswijk, J. W.; Vink, A.; Verhaar, M. C.; Driessen-Mol, A.; van Herwerden, L. a.; Bouten, C. V. C.; Kluin, J.; et al. In Situ Tissue Engineering of Functional Small-Diameter Blood Vessels by Host Circulating Cells Only. *Tissue Eng. Part A* **2015**, *21*, 2583–2594.

(24) Duijvelshoff, R.; van Engeland, N.; Gabriels, K.; Söntjens, S.; Smits, A.; Dankers, P.; Bouten, C. Host Response and Neo-Tissue Development during Resorption of a Fast Degrading Supramolecular Electrospun Arterial Scaffold. *Bioengineering* **2018**, *5*, 61.

(25) Wijeyaratne, S. M.; Karunanayake, L. Safety and Efficacy for Early Electrospun Polycarbonate-Urethane Vascular Graft for Rearly Hemodialysis Access: First Clinical Studies in Man. *J. Vasc. Access* **2011**, *12*, 28–35.

(26) Ferraresso, M.; Bertoli, S.; Nobili, P.; Bortolani, E. M. Early Experience with a Newly Developed Electrospun Polycarbonate-Urethane Vascular Graft for Hemodialysis Access. *J. Vasc. Access* **2013**, *14*, 252–256.

(27) van Haaften, E. E.; Wissing, T. B.; Rutten, M. C. M.; Bulsink, J. A.; Gashi, K.; van Kelle, M. A. J.; Smits, A. I. P. M.; Bouten, C. V. C.; Kurniawan, N. A. Decoupling the Effect of Shear Stress and Stretch on Tissue Growth and Remodeling in a Vascular Graft. *Tissue Eng. Part C Methods* **2018**, *24*, 418–429.

(28) Dankers, P. Y. W.; Meijer, E. W. Supramolecular Biomaterials. a Modular Approach towards Tissue Engineering. *Bull. Chem. Soc. Jpn.* **2007**, *80*, 2047–2073.

(29) Wissing, T. B.; Bonito, V.; Bouten, C. V. C.; Smits, A. I. P. M. Biomaterial-Driven in Situ Cardiovascular Tissue Engineering—a Multi-Disciplinary Perspective. *npj Regen. Med.* **2017**, *2*, 1–19.

(30) Goor, O. J. G. M.; Hendrikse, S. I. S.; Dankers, P. Y. W.; Meijer, E. W. From Supramolecular Polymers to Multi-Component Biomaterials. *Chem. Soc. Rev.* **2017**, *46*, 6621–6637.

(31) Aida, T.; Meijer, E. W.; Stupp, S. I. Functional Supramolecular Polymers. *Science* **2012**, *335*, 813–817.

(32) Fouquey, C.; Lehn, J. M.; Levelut, A. M. Molecular Recognition Directed Self-assembly of Supramolecular Liquid Crystalline Polymers from Complementary Chiral Components. *Adv. Mater.* **1990**, *2*, 254–257.

(33) Storrie, H.; Guler, M. O.; Abu-Amara, S. N.; Volberg, T.; Rao, M.; Geiger, B.; Stupp, S. I. Supramolecular Crafting of Cell Adhesion. *Biomaterials* **2007**, *28*, 4608–4618.

(34) Roosma, J.; Mes, T.; Leclère, P.; Palmans, A. R. A.; Meijer, E. W. Supramolecular Materials from Benzene-1,3,5-Tricarboxamide-Based Nanorods. *J. Am. Chem. Soc.* **2008**, *130*, 1120–1121.

(35) Appel, E. A.; Biedermann, F.; Rauwald, U.; Jones, S. T.; Zayed, J. M.; Scherman, O. A. Supramolecular Cross-Linked Networks via Host-Guest Complexation with cucurbit[8]uril. *J. Am. Chem. Soc.* **2010**, *132*, 14251–14260.

(36) Liu, S.; Chen, X.; Zhang, Q.; Wu, W.; Xin, J.; Li, J. Multifunctional Hydrogels Based on β-Cyclodextrin with Both Biomineralization and Anti-Inflammatory Properties. *Carbohydr. Polym.* **2014**, *102*, 869–876.

(37) Cordier, P.; Tournilhac, F.; Soulié-Ziakovic, C.; Leibler, L. Self-Healing and Thermoreversible Rubber from Supramolecular Assembly. *Nature* **2008**, *451*, 977–980.

(38) Diba, M.; Spaans, S.; Ning, K.; Ippel, B. D.; Yang, F.; Loomans, B.; Dankers, P. Y. W.; Leeuwenburgh, S. C. G. Self-Healing Biomaterials: From Molecular Concepts to Clinical Applications. *Adv. Mater. Interfaces* **2018**, *5*, 1800118.

(39) Yan, X.; Wang, F.; Zheng, B.; Huang, F. Stimuli-Responsive Supramolecular Polymeric Materials. *Chem. Soc. Rev.* **2012**, *41*, 6042.

(40) Hanabusa, K.; Shimura, K.; Hirose, K.; Kimura, M.; Shirai, H. Formation of Organogels by Intermolecular Hydrogen Bonding between Ureylene Segment. *Chem. Lett.* **1996**, *25*, 885–886.

(41) van Esch, J.; De Feyter, S.; Kellogg, R. M.; De Schryver, F.; Feringa, B. L. Self-Assembly of Bisurea Compounds in Organic Solvents and on Solid Substrates. *Chem. - Eur. J.* **1997**, *3*, 1238–1243.

(42) Van Esch, J.; Kellogg, R. M.; Feringa, B. L. Di-Urea Compounds as Gelators for Organic Solvents. *Tetrahedron Lett.* **1997**, *38*, 281–284.

(43) Bouteiller, L.; Colombani, O.; Lortie, F.; Terech, P. Thickness Transition of a Rigid Supramolecular Polymer. *J. Am. Chem. Soc.* **2005**, *127*, 8893–8898.

(44) De Feyter, S.; Grim, P. C. M.; van Esch, J.; Kellogg, R. M.; Feringa, B. L.; De Schryver, F. C. Nontrivial Differentiation between Two Identical Functionalities within the Same Molecule Studied by STM. *J. Phys. Chem. B* **1998**, *102*, 8981–8987.

(45) Boileau, S.; Bouteiller, L.; Lauprêtre, F.; Lortie, F. Soluble Supramolecular Polymers Based on Urea Compounds. *New J. Chem.* **2000**, *24*, 845–848.

(46) Simic, V.; Bouteiller, L.; Jalabert, M. Highly Cooperative Formation of Bis-Urea Based Supramolecular Polymers. *J. Am. Chem. Soc.* **2003**, *125*, 13148–13154.

(47) Isare, B.; Pensec, S.; Raynal, M.; Bouteiller, L. Bisurea-Based Supramolecular Polymers: From Structure to properties11Dedicated to Professor Jean-Pierre Vairon on the Occasion of His 78th Birthday. *C. R. Chim.* **2016**, *19*, 148–156.

(48) Estroff, L. A.; Hamilton, A. D. Water Gelation by Small Organic Molecules. *Chem. Rev.* **2004**, *104*, 1201–1218.

(49) Chebotareva, N.; Bomans, P. H. H.; Frederik, P. M.; Sommerdijk, N. A. J. M.; Sijbesma, R. P. Morphological Control and Molecular Recognition by Bis-Urea Hydrogen Bonding in Micelles of Amphiphilic Tri-Block Copolymers. *Chem. Commun.* **2005**, 39, 4967.

(50) Raghavanpillai, A.; Reinartz, S.; Hutchenson, K. W. Hydrophobic and Oleophobic Surface Modification Using Fluorinated Bis-Urea and Bis-Amide Gelators. *J. Fluor. Chem.* **2009**, *130*, 410–417.

(51) Cao, X.; Gao, A.; Sun, K.; Zhao, L. Formation of Hydrophobic Surface Using a Bis-Urea Derived Organogel. *Supramol. Chem.* **2014**, *27*, 484–489.

(52) Gao, S.; Wang, S.; Ma, J.; Wu, Y.; Fu, X.; Marella, R. K.; Liu, K.; Fang, Y. Salt Tunable Rheology of Thixotropic Supramolecular Organogels and Their Applications for Crystallization of Organic Semiconductors. *Langmuir* **2016**, *32*, 12805–12813.

(53) Baddi, S.; Madugula, S. S.; Sarma, D. S.; Soujanya, Y.; Palanisamy, A. Combined Experimental and Computational Study of the Gelation of Cyclohexane-Based Bis(acyl-Semicarbazides) and the Multi-Stimuli-Responsive Properties of Their Gels. *Langmuir* **2016**, *32*, 889–899.

(54) Fernandez-Castano Romera, M.; Lafleur, R. P. M.; Guibert, C.; Voets, I. K.; Storm, C.; Sijbesma, R. P. Strain Stiffening Hydrogels through Self-Assembly and Covalent Fixation of Semi-Flexible Fibers. *Angew. Chem. Int. Ed.* **2017**, *56*, 8771–8775.

(55) Van Der Asdonk, P.; Hendrikse, H. C.; Fernandez-Castano Romera, M.; Voerman, D.; Ramakers, B. E. I.; LÃ¶wik, D. W. P. M.; Sijbesma, R. P.; Kouwer, P. H. J. Patterning of Soft Matter across Multiple Length Scales. *Adv. Funct. Mater.* **2016**, *26*, 2609–2616.

(56) Foster, J. A.; Damodaran, K. K.; Maurin, A.; Day, G. M.; Thompson, H. P. G.; Cameron, G. J.; Bernal, J. C.; Steed, J. W. Pharmaceutical Polymorph Control in a Drug-Mimetic Supramolecular Gel. *Chem. Sci.* **2017**, *8*, 78–84.

(57) Vos, M. R. J.; Jardí, G. E.; Pallas, A. L.; Breurken, M.; Van Asselen, O. L. J.; Bomans, P. H. H.; Leclère, P. E. L. G.; Frederik, P. M.; Nolte, R. J. M.; Sommerdijk, N. A. J. M. The Bis-Urea Motif as a Tool to Functionalize Self-Assembled Nanoribbons. *J. Am. Chem. Soc.* **2005**, *127*, 16768–16769.

(58) Das, S.; Yilgor, I.; Yilgor, E.; Inci, B.; Tezgel, O.; Beyer, F. L.; Wilkes, G. L. Structure-Property Relationships and Melt Rheology of Segmented, Non-Chain Extended Polyureas: Effect of Soft Segment Molecular Weight. *Polymer* **2007**, *48*, 290–301.

(59) Colombani, O.; Barioz, C.; Bouteiller, L.; Chanéac, C.; Fompérie, L.; Lortie, F.; Montés, H. Attempt toward 1D Cross-Linked Thermoplastic Elastomers: Structure and Mechanical Properties of a New System. *Macromolecules* **2005**, *38*, 1752–1759.

(60) Koevoets, R. A.; Versteegen, R. M.; Kooijman, H.; Spek, A. L.; Sijbesma, R. P.; Meijer, E. W. Molecular Recognition in a Thermoplastic Elastomer. *J. Am. Chem. Soc.* **2005**, *127*, 2999–3003.

(61) Versteegen, R. M.; Kleppinger, R.; Sijbesma, R. P.; Meijer, E. W. Properties and Morphology of Segmented Copoly(ether Urea)s with Uniform Hard Segments. *Macromolecules* **2006**, *39*, 772–783.

(62) Wisse, E.; Spiering, A. J. H.; van Leeuwen, E. N. M.; Renken, R. A. E.; Dankers, P. Y. W.; Brouwer, L. A.; van Luyn, M. J. A.; Harmsen, M. C.; Sommerdijk, N. A. J. M.; Meijer, E. W. Molecular Recognition in Poly(ε-Caprolactone)-Based Thermoplastic Elastomers. *Biomacromolecules* **2006**, *7*, 3385–3395.

(63) Wisse, E.; Spiering, A. J. H.; Pfeifer, F.; Portale, G.; Siesler, H. W.; Meijer, E. W. Segmental Orientation in Well-Defined Thermoplastic Elastomers Containing Supramolecular Fillers. *Macromolecules* **2009**, *42*, 524–530.

(64) Botterhuis, N. E.; Karthikeyan, S.; Spiering, A. J. H.; Sijbesma, R. P. Self-Sorting of Guests and Hard Blocks in Bisurea-Based Thermoplastic Elastomers. *Macromolecules* **2010**, *43*, 745–751.

(65) Botterhuis, N. E.; Karthikeyan, S.; Veldman, D.; Meskers, S. C. J.; Sijbesma, R. P. Molecular Recognition in Bisurea Thermoplastic Elastomers Studied with Pyrene-Based Fluorescent Probes and Atomic Force Microscopy. *Chem. Commun.* **2008**, 33, 3915.

(66) Castagna, A. M.; Pangon, A.; Choi, T.; Dillon, G. P.; Runt, J. The Role of Soft Segment Molecular Weight on Microphase Separation and Dynamics of Bulk Polymerized Polyureas. *Macromolecules* **2012**, *45*, 8438–8444.

(67) Pangon, A.; Dillon, G. P.; Runt, J. Influence of Mixed Soft Segments on Microphase Separation of Polyurea Elastomers. *Polym. (United Kingdom)* **2014**, *55*, 1837–1844.

(68) Castagna, A. M.; Pangon, A.; Dillon, G. P.; Runt, J. Effect of Thermal History on the Microstructure of a Poly(tetramethylene Oxide)-Based Polyurea. *Macromolecules* **2013**, *46*, 6520–6527.

(69) Wisse, E.; Govaert, L. E.; Meijer, H. E. H.; Meijer, E. W. Unusual Tuning of Mechanical Properties of Thermoplastic Elastomers Using Supramolecular Fillers. *Macromolecules* **2006**, *39*, 7425–7432.

(70) Koevoets, R. a; Karthikeyan, S.; Magusin, P. C. M. M.; Meijer, E. W.; Sijbesma, R. P. Cross-Polymerization of Hard Blocks in Segmented Copoly(ether Urea)s. *Macromolecules* **2009**, *42*, 2609–2617.

(71) Sijbesma, R. P.; Beijer, F. H.; Brunsveld, L.; Folmer, B. J.; Hirschberg, J. H.; Lange, R. F.; Lowe, J. K.; Meijer, E. W. Reversible Polymers Formed from Self-Complementary Monomers Using Quadruple Hydrogen Bonding. *Science* **1997**, *278*, 1601–1604.

(72) Beijer, F. H.; Sijbesma, R. P.; Kooijman, H.; Spek, A. L.; Meijer, E. W. Strong Dimerization of Ureidopyrimidones via Quadruple Hydrogen Bonding. *J. Am. Chem. Soc.* **1998**, *120*, 6761–6769.

(73) Kautz, H.; van Beek, D. J. M.; Sijbesma, R. P.; Meijer, E. W. Cooperative End-to-End and Lateral Hydrogen-Bonding Motifs in Supramolecular Thermoplastic Elastomers. *Macromolecules* **2006**, *39*, 4265–4267.

(74) Appel, W. P. J.; Portale, G.; Wisse, E.; Dankers, P. Y. W.; Meijer, E. W. Aggregation of Ureido-Pyrimidinone Supramolecular Thermoplastic Elastomers into Nanofibers: A Kinetic Analysis. *Macromolecules* **2011**, *44*, 6776–6784.

(75) Van Beek, D. J. M.; Spiering, A. J. H.; Peters, G. W. M.; Te Nijenhuis, K.; Sijbesma, R. P. Unidirectional Dimerization and Stacking of Ureidopyrimidinone End Groups in Polycaprolactone Supramolecular Polymers. *Macromolecules* **2007**, *40*, 8464–8475.

(76) Folmer, B. J. B.; Sijbesma, R. P.; Versteegen, R. M.; Van Der Rijt, J. A. J.; Meijer, E. W. Supramolecular Polymer Materials: Chain Extension of Telechelic Polymers Using a Reactive Hydrogen-Bonding Synthon. *Adv. Mater.* **2000**, *12*, 874–878.

(77) Söntjens, S. H. M.; Renken, R. A. E.; van Gemert, G. M. L.; Engels, T. A. P.; Bosman, A. W.; Janssen, H. M.; Govaert, L. E.; Baaijens, F. P. T. Thermoplastic Elastomers Based on Strong and Well-Defined Hydrogen-Bonding Interactions. *Macromolecules* **2008**, *41*, 5703–5708.

(78) Spaans, S.; Fransen, P.-P. K. H.; Schotman, M. J. G.; van der Wulp, R.; Lafleur, R. P. M.; Kluijtmans, S. G. J. M.; Dankers, P. Y. W. Supramolecular Modification of a Sequence-Controlled Collagen-Mimicking Polymer. *Biomacromolecules* **2019**, *20*, 2360–2371.

(79) Wu, Y.; Wang, L.; Zhao, X.; Hou, S.; Guo, B.; Ma, P. X. Self-Healing Supramolecular Bioelastomers with Shape Memory Property as a Multifunctional Platform for Biomedical Applications via Modular Assembly. *Biomaterials* **2016**, *104*, 18–31.

(80) Dankers, P.Y.W.; Harmsen, M. C.; Brouwer, L.A.; van Luyn, M. J.A.; Meijer, E.W.A Modular and Supramolecular Approach to Bioactive Scaffolds for Tissue Engineering. *Nat. Mater.* **2005**, *4*, 568–574.

(81) Appel, W. P. J.; Meijer, E.W.; Dankers, P.Y.W. Enzymatic Activity at the Surface of Biomaterials via Supramolecular Anchoring of Peptides: The Effect of Material Processing. *Macromol. Biosci.* **2011**, *11*, 1706–1712.

(82) Zaccaria, S.; van Gaal, R. C.; Riool, M.; Zaat, S. A. J.; Dankers, P. Y. W. Antimicrobial Peptide Modification of Biomaterials Using Supramolecular Additives. *J. Polym. Sci. Part A: Polym. Chem.* **2018**, *56*, 1926–1934.

(83) Mollet, B. B.; Bogaerts, I. L. J.; van Almen, G. C.; Dankers, P.Y.W.A Bioartificial Environment for Kidney Epithelial Cells Based on a Supramolecular Polymer Basement Membrane Mimic and an Organotypical Culture System. *J.Tissue Eng. Regen. Med.* **2017**, *11*, 1820–1834.

(84) Bonito, V.; Smits, A. I. P. M.; Goor, O. J. G. M.; Ippel, B. D.; Driessen-Mol, A.; Münker, T. J. A. G.; Bosman, A.W.; Mes, T.; Dankers, P.Y.W.; Bouten, C.V. C. Modulation of Macrophage Phenotype and Protein Secretion via Heparin-IL-4 Functionalized Supramolecular Elastomers. *Acta Biomater.* **2018**, *71*, 1–23.

(85) Muylaert, D. E. P.; van Almen, G. C.; Talacua, H.; Fledderus, J. O.; Kluin, J.; Hendrikse, S. I. S.; van Dongen, J. L. J.; Sijbesma, E.; Bosman, A. W.; Mes, T.; et al. Early in-Situ Cellularization of a Supramolecular Vascular Graft Is Modified by Synthetic Stromal Cell-Derived Factor-1α Derived Peptides. *Biomaterials* **2016**, *76*, 187–195.

(86) Putti, M.; Stassen, O. M. J. A.; Schotman, M. J. G.; Sahlgren, C. M.; Dankers, P. Y. W. Influence of the Assembly State on the Functionality of a Supramolecular Jagged1-Mimicking Peptide Additive. *ACS Omega* **2019**, *4*, 8178–8187.

(87) Mollet, B. B.; Comellas-Aragonès, M.; Spiering, A. J. H.; Söntjens, S. H. M.; Meijer, E.W.; Dankers, P. Y. W. A Modular Approach to Easily Processable Supramolecular Bilayered Scaffolds with Tailorable Properties. *J. Mater. Chem. B* **2014**, *2*, 2483–2493.

(88) Spaans, S.; Fransen, P. P. K. H. P. K. H.; Ippel, B. D. D.; de Bont, D. F. A.; Keizer, H. M. M.; Bax, N. A. M. A. M.; Bouten, C. V. C. V. C.; Dankers, P.Y.W.Y.W. Supramolecular Surface Functionalization via Catechols for the Improvement of Cell–material Interactions. *Biomater. Sci.* **2017**, *5*, 1541–1548.

(89) Goor, O. J. G. M.; Keizer, H. M.; Bruinen, A. L.; Schmitz, M. G. J.; Versteegen, R. M.; Janssen, H. M.; Heeren, R. M. A.; Dankers, P. Y. W. Efficient Functionalization of Additives at Supramolecular Material Surfaces. *Adv. Mater.* **2017**, *29*, 1604652.

(90) Goor, O. J. G. M.; Brouns, J. E. P.; Dankers, P. Y. W. Introduction of Anti-Fouling Coatings at the Surface of Supramolecular Elastomeric Materials via Post-Modification of Reactive Supramolecular Additives. *Polym. Chem.* **2017**, *8*, 5228–5238.

(91) Dankers, P. Y. W.; Hermans, T. M.; Baughman, T. W.; Kamikawa, Y.; Kieltyka, R. E.; Bastings, M. M. C.; Janssen, H. M.; Sommerdijk, N. a J. M.; Larsen, A.; Van Luyn, M. J. a; et al. Hierarchical Formation of Supramolecular Transient Networks in Water: A Modular Injectable Delivery System. *Adv. Mater.* **2012**, *24*, 2703–2709.

(92) Hendrikse, S. I. S.; Wijnands, S. P.W.; Lafleur, R. P. M.; Pouderoijen, M. J.; Janssen, H. M.; Dankers, P.Y.W.; Meijer, E.W. Controlling and Tuning the Dynamic Nature of Supramolecular Polymers in Aqueous Solutions. *Chem. Commun.* **2017**, *53*, 2279–2282.

(93) Bastings, M. M. C.; Hermans, T. M.; Spiering, A. J. H.; Kemps, E. W. L.; Albertazzi, L.; Kurisinkal, E. E.; Dankers, P. Y. W. Quantifying Guest-Host Dynamics in Supramolecular Assemblies to Analyze Their Robustness. *Macromol. Biosci.* **2018**, *1800296*, 1800296.

(94) Bakker, M. H.; Kieltyka, R. E.; Albertazzi, L.; Dankers, P. Y. W. Modular Supramolecular Ureidopyrimidinone Polymer Carriers for Intracellular Delivery. *RSC Adv.* **2016**, *6*, 110600–110603.

(95) Bastings, M. M. C.; Koudstaal, S.; Kieltyka, R. E.; Nakano, Y.; Pape, A. C. H.; Feyen, D. A. M.; van Slochteren, F. J.; Doevendans, P. A.; Sluijter, J. P. G.; Meijer, E. W.; et al. A Fast pH-Switchable and Self-Healing Supramolecular Hydrogel Carrier for Guided, Local Catheter Injection in the Infarcted Myocardium. *Adv. Healthc. Mater.* **2014**, *3*, 70–78.

(96) Bakker, M. H.; van Rooij, E.; Dankers, P. Y. W. Controlled Release of RNAi Molecules by Tunable Supramolecular Hydrogel Carriers. *Chem. - Asian J.* **2018**, *13*, 3501–3508.

(97) Bakker, M. H.; Grillaud, M.; Wu, D. J.; Fransen, P. P. K. H.; de Hingh, I. H.; Dankers, P. Y. W. Cholesterol Modification of an Anticancer Drug for Efficient Incorporation into a Supramolecular Hydrogel System. *Macromol. Rapid Commun.* **2018**, *39*, 1–6.

(98) Bakker, M. H.; Tseng, C. C. S.; Keizer, H. M.; Seevinck, P. R.; Janssen, H. M.; Van Slochteren, F. J.; Chamuleau, S. A. J.; Dankers, P. Y. W. MRI Visualization of Injectable Ureidopyrimidinone Hydrogelators by Supramolecular Contrast Agent Labeling. *Adv. Healthc. Mater.* **2018**, *7*, 1–8.

2

Introduction of nature's complexity in engineered blood-compatible biomaterials

Abstract

Biomaterials with excellent blood-compatibility are needed for applications in vascular replacement therapies, such as vascular grafts, heart valves and stents, and in extracorporeal devices such as hemodialysis machines and blood-storage bags. The modification of materials that are being used for blood-contacting devices has advanced from passive surface modifications to the design of more complex, smart biomaterials that respond to relevant stimuli from blood to counteract coagulation. Logically, the main source of inspiration for the design of new biomaterials has been the endogenous endothelium. Endothelial regulation of hemostasis is complex and involves a delicate interplay of structural components and feedback mechanisms. Thus, challenges to develop new strategies for blood-compatible biomaterials now lie in incorporating true feedback controlled mechanisms that can regulate blood compatibility in a dynamic way. Here, supramolecular material systems are highlighted as they provide a promising platform to introduce dynamic reciprocity, due to their inherent dynamic nature.

The content of this chapter is based on:

Bastiaan D. Ippel and Patricia Y.W. Dankers, *Introduction of nature's complexity in engineered blood-compatible biomaterials,* Advanced Healthcare Materials 2018, 201700505

Introduction: blood-compatible biomaterials

Ever since medical interventions require long-term exposure of medical devices to blood, materials that are blood-compatible have been in development. Nowadays, blood-compatible materials are needed in for example vascular grafts, heart valves, stents, and catheters, and in extracorporeal devices such as hemodialysis machines and blood-storage bags. In vascular replacement therapy, applied in the construction of coronary bypasses, or arteriovenous fistulas, blood-compatible materials are of interest for both non-degradable vascular grafts and biodegradable vascular grafts that are replaced by regenerated vascular tissue. In this chapter an overview is provided of the advances in development of blood-compatible biomaterials, ranging from simple material functionalization to more complex materials and finally towards systems with life-like properties that are proposed to be controlled via feed-back controlled mechanisms in the future.

Endogenous blood-compatibility: endothelium

Blood is normally confined within the human vascular circulation. A confluent endothelial monolayer lines all blood vessels that are part of the vasculature. Cells from healthy endothelium serve an important purpose in maintaining hemostasis by regulation of coagulation, through expression of various structural and secreted components. The structure, composition and activity of healthy endothelium are important sources of inspiration for creating (synthetic) blood-compatible biomaterials, and therefore a short overview of important endothelial regulators of coagulation is given here (**Figure 2.1**).

The basement membrane to which endothelial cells adhere through cell surface receptors, is a thin and specialized layer of extracellular matrix, typically found basolateral to cellular monolayers in vivo.[1] The four major constituents of the basement membrane are collagen type IV, laminin, nidogen, and perlecan, where the self-assembled structures of collagen type IV and laminin are interconnected through nidogen and perlecan glycoproteins.[1] The integrity of the endothelial monolayer is also maintained by junctions between adjoining endothelial cells through tight and adherens junction-like molecules, that also serve as a route for communication between neighboring endothelial cells.[2,3]

Anti-coagulant functions of endothelial cells can be divided into two basic categories: those that elicit a response after secretion, comparable to paracrine signaling, and those that function through membrane-bound proteins. Secreted factors that serve as platelet inhibitors (counteracting platelet activation and aggregation) are prostacyclin (PGI_2) and nitric oxide (NO). Secreted Tissue Factor Pathway Inhibitor (TFPI) inhibits activation of factor VII and factor X, which are part of the thrombin generation cascade.[4] Besides factors inhibiting platelets and counteracting thrombin formation, tissue plasminogen activator (t-PA) is secreted by endothelial cells. The assembly of t-PA with plasminogen on fibrin activates the fibrinolytic activity necessary to break down blood-clots.[4] Binding of thrombin to protease activated receptors on the endothelial cell membrane is one of the major activators of these anti-thrombogenic functions in the endothelium.[4,5]

Membrane bound anti-thrombogenic factors include ecto-adenosine diphosphatase (ecto-ADPase), which inactivates ADP and thereby inhibits platelet aggregation. Thrombomodulin is a membrane bound protein that enhances the affinity of thrombin for protein C, which in

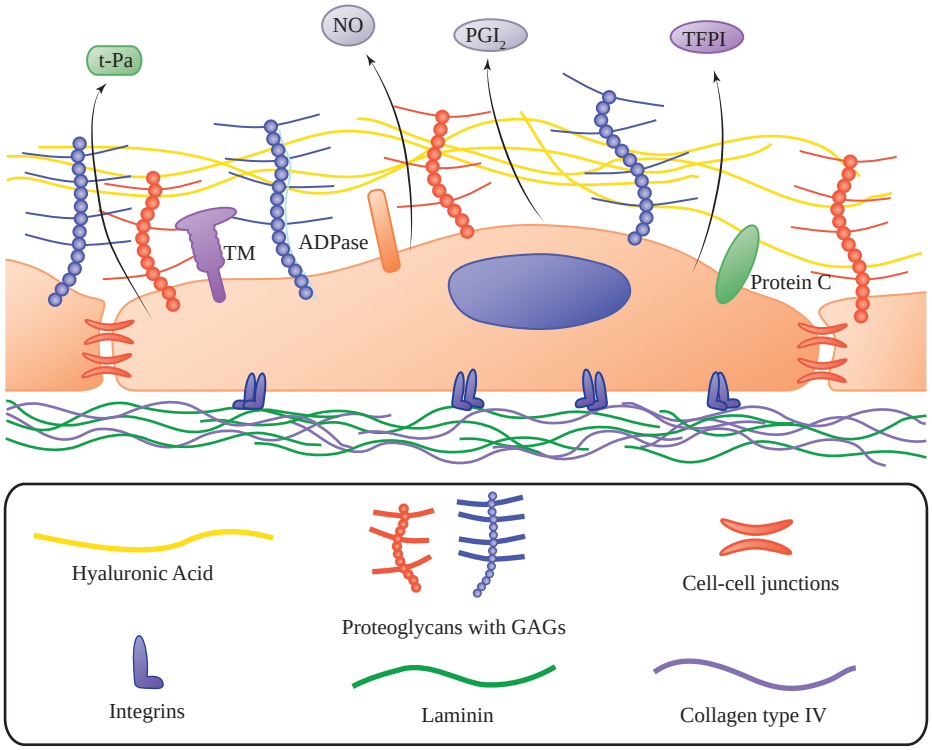

Figure 2.1. A schematic representation of the structural components and excreted factors related to endothelial anti-coagulant functions in regulating hemostasis, which are an important source of inspiration for the development of new blood-compatible biomaterials. The endothelial cells reside on a basement membrane, with laminin and collagen type IV as its major constituents. Cells adhere to the basement membrane through cell surface receptors, such as integrins, and to adjacent endothelial cells through specific cell-cell junctions. The endothelial surface is lined with a layer rich in proteoglycans and glycosaminoglycans rich layers, serving as a physical barrier between blood components and the endothelium. Several anti-coagulant factors are expressed on the endothelial membrane (for instance thrombomodulin (TM), ADPase, Protein C)) or secreted (tissue plasminogen activator (t-PA), nitric oxide (NO), prostacyclin (PGI2), tissue factor pathway inhibitor (TFPI)).

turn is responsible for cleaving and inactivating factors Va and VIIIa. Since thrombomodulin competes for binding with thrombin, it also inhibits the procoagulant functions of thrombin. Protein S, also associated with the endothelial cell membrane, promotes inactivation of factors Va and VIIIa by protein C. Endothelial heparan sulfate, a proteoglycan that is part of the endothelial glycocalyx, serves as a cofactor for antithrombin III, a direct thrombin inhibitor.[4] The endothelial cell surface is lined with a thick cell-free layer, consisting mainly of proteoglycans and glycoproteins. The size of the endothelial glycocalyx, or endothelial surface layer[6], ranges from 0.5 μm in the capillaries to over 4 μm in larger arteries.[7] Five types of glycosaminoglycans (GAG), linear poly(disaccharides), are present in the endothelial glycocalyx: heparan sulfate, chondroitin sulfate, dermatan sulfate, keratin sulfate, and hyaluronic acid. The last is not bound to one of the core proteoglycan molecules (e.g. syndecan, glypican, perlecan, versican, decorin, biglycan, and mimecan). The highly sulfonated GAGs in the glycocalyx regulate interactions with the endothelium through a vast array of binding domains for growth factors and other plasma proteins.[7–9] This glycocalyx, which

is a viscoelastic layer, also serves as a physical hydrated barrier between endothelial cells and platelets, red blood cells, and regulates interactions with leukocytes. Furthermore, mechanotransduction of shear stresses due to blood flow is also translated to endothelial cells through membrane bound constituents of the glycocalyx.[7,8] Anticoagulant factors such as antithrombin, heparin cofactor, thrombomodulin, and TFPI can bind to specific domains in the glycocalyx. Anticoagulant activity of for example antithrombin is even enhanced when bound to the glycocalyx.[7,8] The interplay between the structure and composition of the endothelial surface layer and responsiveness of an intact endothelial layer is crucial for maintenance of hemostasis.

Biomaterials based blood-compatibility

Blood-compatible biomaterials show no adverse effects such as thrombus formation after exposure to blood. Thrombus formation is largely associated with undesired protein adsorption and subsequent thrombocyte and/or cell adhesion on the biomaterial-blood interface and by intrinsic activation of blood coagulation.[10] Blood-compatibility could therefore be improved by prevention of aspecific adsorption of proteins, i.e. making blood-contacting surfaces anti-fouling (**Figure 2.2a**). Thrombus formation is also impeded by factors, normally associated with healthy endothelium, such as prostacyclin, heparan sulfate and nitric oxides.[4] Incorporation of these factors into, or their release from biomaterials might provide better blood-compatibility (**Figure 2.2b**).[10] Lastly, it is proposed that a surface that captures and can sustain nature's best blood-compatible and anti-thrombotic function is the endogenous endothelium. Endothelialization is known to greatly improve blood-contacting properties (**Figure 2.2c**).

Besides chemical and biological functionalization strategies that provide biomaterials with anti-fouling or anti-thrombogenic properties, or that promote endothelialization, the structural properties of surfaces are important in regulating the physiological response as well. Although not reviewed here, controlling surface structure can influence fouling behavior[11], cell response[12] and can even be used to tune the adhesion of endothelial cells and smooth muscle cells[13,14] and improve endothelialization *in vivo*.[15]

Anti-fouling surfaces

Anti-fouling surfaces aim at impeding protein-material interactions. Classically, self-

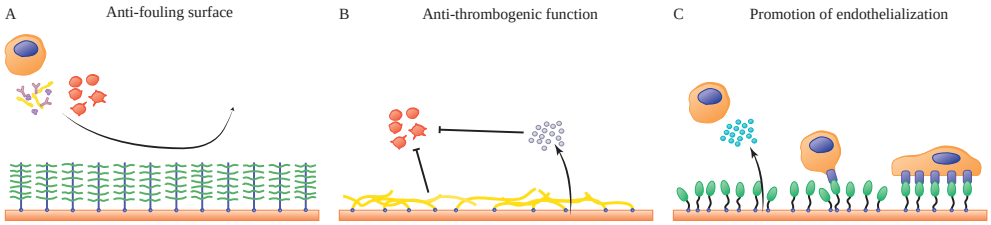

Figure 2.2. Schematic representation of the three predominant approaches for surface functionalization of biomaterials towards more blood-compatible material interfaces: A) Anti-fouling surface functionalization aimed at minimizing all surface interactions, thereby preventing thrombosis. B) Anti-thrombogenic surfaces, where coatings are composed of molecules commonly associated with anti-thrombogenic properties, or anti-coagulant factors are released. C) Surface functionalization directed to capture endothelial cells specifically and to provide an optimal base for rapid endothelialization.

assembled monolayers (SAM) that resist the adsorption of proteins meet a set of rules, deemed the Whitesides rules.[16,17] These surfaces are hydrophilic, include hydrogen-bond acceptors, but do not include hydrogen-bond donors and have an overall neutral charge. Even though exceptions have been developed[18], the majority of surfaces functionalized for anti-fouling properties still comply to these rules, and can be roughly divided into hydrophilic polymers such as poly(ethylene glycol) (PEG), zwitterionic materials and polysaccharides.[19] The driving force of the anti-fouling properties of these materials is the inclusion of a hydrated layer at the surface, serving as a physical barrier contributing to resistance to protein-fouling.[19] Surface functionalization with brushes that consist of these types of compounds, for instance polymerized onto initiator groups on the surface, yields dense coatings. This provides a versatile platform for the development of anti-fouling coatings, where the chemical composition of the grafted polymer dictates the surface properties. [20–23] Recent efforts to create anti-fouling materials have focused on surface functionalization of various materials used for blood-contacting devices. (**Figure 2.2a**)

Synthetic coatings and surface modifications

Hydrophilic polymers

Surface functionalization with hydrophilic polymers such as PEG has been applied in varying shapes and forms to produce surfaces that can resist aspecific adsorption of proteins. [11,21,24] For instance, poly(ε-caprolactone) (PCL) was end-functionalized with initiator groups before electrospinning into fibrous meshes.[25] Through controlled radical polymerization, the fiber surface could be functionalized with anti-fouling poly(oligo ethylene glycol methyl ether methacrylate) (pOEGMA) brushes, which rendered these fibrous meshes non-cell adhesive and protein resistant.[25](**Figure 2.3**)

In a similar approach, PCL fibers were functionalized with initiators for surface induced atom transfer radical polymerization (SI-ATRP) covalently attached through a polydopamine coating.[26] Anti-fouling brush coatings, which showed to resist adhesion of both proteins and other blood components from whole blood[27], were then polymerized on these initiators to create functional electrospun meshes with anti-fouling properties.[26] Also using SI-ATRP, but by functionalization with another hydrophilic polymer poly(*N*-vinylpyrrolidone), Yuan and coworkers decreased bovine serum albumin (BSA) and fibrinogen adsorption on polyurethane (PU) membranes by more than 85%.[28] Another interesting technique based on light-mediated radical polymerization, was used to gain spatial control over polymerization.[29] In this way, the chemical composition of the surface could be tuned with exposed poly(trifluoroethyl methacrylate) or anti-fouling pOEGMA.[29]

Zwitterionic molecules

Reduction of fouling is often achieved through surface functionalization with zwitterionic molecules.[11,20,21,30,31] Various zwitterionic compounds, such as sulfobetaine, phosporylcholine, or carboxybetaine, and various coating compositions can be applied for the effective introduction of anti-fouling properties.[30,31] Moreover, the molecular weight of zwitterionic brushes can have an effect on the degree of fouling on the functionalized substrates[32], which indicates that several design parameters are key in fabrication of functional zwitterionic coatings and modifications. An illustration of recent efforts in zwitterionic surface

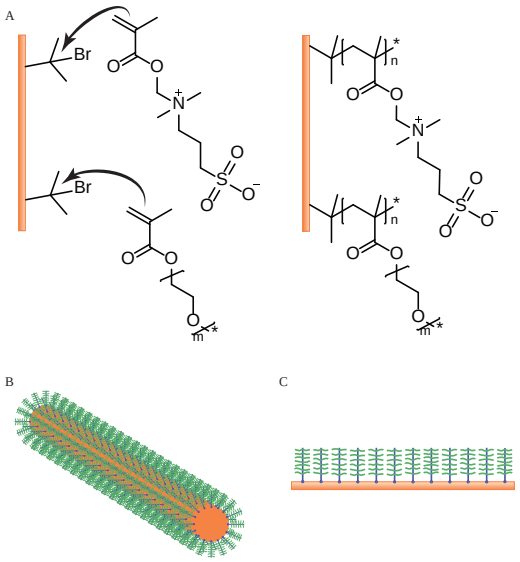

Figure 2.3. A) Schematic representation of surface functionalization using SI-ATRP with zwitterionic sulfobetaine methacrylate and oligo(ethylene glycol) methyl methacrylate, which results in anti-fouling bottle-brush like coatings. These coatings can be applied on the exposed initiator groups on B) electrospun fibers, such as in [25] C) or on other substrates as in.[35]

functionalization is given below.

Poly(lactic acid) (PLA) membranes were functionalized with bromoalkyl initiator groups, anchored on a polydopamine coating, onto which poly(sulfobetaine methacrylate) (pSBMA) brushes were formed with SI-ATRP. It was shown that this coating decreased protein adsorption and platelet adhesion, indicative of improved hemocompatibility.[33] Ultrathin zwitterionic anti-fouling coatings, applicable to various substrates with different chemical compositions and surface roughness, were fabricated by initiated chemical vapor deposition (iCVD).[34] These versatile ultrathin coatings showed a significant reduction of BSA adsorption as measured with a quartz crystal microbalance with dissipation monitoring (QCM-D).[34] Silicon surfaces were grafted with pSBMA using ATRP. These brushes have been demonstrated to be stable without signs of hydrolysis or a diminished protein repellency after one week in PBS, thereby maintaining over 99% reduction in fibrinogen adsorption.[35] (**Figure 2.3**)

Retention of anti-fouling properties with these types of coatings in a dynamic environment remains a challenge, due to the hydrophilic nature of the coatings. Via crosslinking of poly(carboxybetaine methacrylate) (pCBMA) brushes using a covalently incorporated macro-crosslinker on a polyurethane surface, zwitterionic coatings remained stable and as anti-fouling as freshly prepared coatings after a week in a hydrodynamic environment.[36] Another method to improve stability in anti-fouling zwitterionic coatings combined layer-by-layer fabrication of pSBMA and tannic acid, which resulted in stable multilayer films. These films decreased the adsorption of BSA (to below 1 ng cm^{-2}), lysozyme and hemoglobin significantly.[37]

Versatility of the techniques used to covalently tether hydrophilic or zwitterionic coatings

to surfaces is demonstrated by a few research groups that report on both hydrophilic and zwitterionic functionalization on the same substrates.

Silanized polycarbonate substrates were functionalized with anti-fouling brushes from e.g. pOEGMA and poly(carboxy betaine acryl amide) (pCBAA), that decreased the platelet adhesion on these coatings.[38] When these coatings were prepared on silica and studied with highly sensitive electromagnetic piezoelectric acoustic sensors (EMPAS), the protein adsorption from whole blood correlated strongly to the results with platelet adhesion.[38] PU membranes were activated using air-plasma, to get hydroxyl groups exposed at the surface in order to immobilize the bromium initiator groups, that provide the possibility for polymerization of anti-fouling sulfobetaine- and phosphobetaine-based and PEG-based brushes.[39] These brushes significantly reduced protein adsorption, cell and platelet adhesion, without changing the mechanical properties of the PU membranes.[39]

Coatings consisting of biological molecules

An approach that most closely resembles the composition of the endothelial glycocalyx, is the use of sugar-based molecules, such as glycoproteins and polysaccharides.[7,8] In these examples, multilayers were fabricated with inclusion of glycoproteins or polysaccharides. Lubricin glycoprotein was adsorbed as a coating onto a variety of substrates. Even after prolonged storage, these coatings were more anti-adhesive for blood-plasma proteins than PEG-based SAMs.[40] Layer-by-layer fabrication was also utilized to form polysaccharide-based multilayers on a cellulose acetate membrane. These membranes inhibited bacterial growth and platelet adhesion, however, protein adsorption was not notably decreased.[41] Chitosan/alginate multilayered films were deposited onto poly(ethylene imine) (PEI) coated polystyrene (PS) surfaces, using the electrostatic interactions between the chitosan and alginate.[42] In an effort to further improve layer stability, the films were crosslinked with genipin, which forms covalent crosslinks between the alginate and chitosan strands. The degree of crosslinking however negatively influenced the anti-fouling properties of these surfaces.[42] Deposition of a new bilayer of chitosan/alginate on top of the crosslinked multilayer was able to decrease cell adhesion again.[42]

Surfaces with extreme wetting and fluid repelling properties

Another method to introduce anti-fouling properties on materials is the use of surfaces with extreme wetting and repulsion of aqueous and organic fluids.[43] Surfaces with extremely low surface tensions that repel both aqueous and organic fluids (omniphobic) could provide excellent anti-fouling properties.[43] For vascular replacement therapies, application of this principle remains a challenge however, since the function of these materials relies heavily on a combination of surface morphology, roughness and wettability.[44,45] This principle was applied to electrospun meshes by incorporation of ZnO nanoparticles in poly(vinylidene fluoride) (PVF) electrospun membranes, which resulted in superhydrophobic electrospun membranes.[46] Also, electrospun cellulose acetate membranes with a coating of self-assembling chitin nanocrystals, showed superhydrophilic properties, for which it was shown that bacterial adhesion was decreased on these surfaces.[47] However, the structural investigation of surfaces with different surface morphologies (untextured, or decorated with nanoscale flower-like structures or nanotubes) and surface chemistries (unmodified, PEGylated, or fluorinated) revealed that not all combinations lead to superhemophobic

surfaces that can induce decreased thrombocyte adhesion and activation, when compared to hemophilic and hemophobic sufaces.[48]

Self-healing anti-fouling materials

One of the challenges in the fabrication of anti-fouling coatings for biomaterials is the control of the time the material remains functional. If anti-fouling properties are lost over time, the chance of thrombosis in blood-contacting devices with these coatings will increase. Several recent studies have therefore focused on retaining or restoring anti-fouling properties after physical damage by the development of self-healing coatings or materials.

Based on anti-fouling properties related to omniphobic surfaces, slippery liquid-infused porous surfaces (SLIPS) were developed.[49] In this method, a porous surface is infused with a lubricant that serves as a biofouling repellent, which results in a self-healing surface that resists for instance blood-staining and bacterial adhesion.[49,50] Applied with clinically used perfluorocarbon liquids a commonly used vascular graft material, i.e. expanded polytetrafluoroethylene (ePTFE) can be modified according to this method in order to reduce bacterial adhesion *in vivo*.[51] PEI-PEG co-polymers and hyaluronic acid were combined to develop self-assembled polyelectrolyte. Protein fouling and cell adhesion were significantly decreased on these multilayers. Moreover, the multilayers showed spontaneous healing of imposed physical defects, thereby restoring the anti-fouling function.[52] Superhydrophobic coatings were prepared by grafting of fluoropolymer brushes onto nanostructured silicon surfaces with SI-ATRP. These brushes were capable of restoring anti-fouling properties through heating for 30 minutes after damage induced by air-plasma.[53] A significant decrease in protein adsorption was measured on spin-coated layers containing self-assembling microspheres in a matrix with hydrophilic poly(hydroxyl ethyl methacrylate) (pHEMA) and zwitterionic phosphorylcholine polymers. These films were shown to be capable of self-healing, in aqueous conditions after physical damage, thereby reducing protein adsorption even after physical damage to the coating.[54] Kuroki et al. grafted poly(2-vinylpyridine) P2VP films with PEG. In their study, a comparison was made between regular surface grafting of PEG on the P2VP structure, and PEGylation of the bulk of the P2VP material. When the PEG was grafted to the P2VP throughout the material, self-healing behavior was observed, attributed to rearrangement of the PEG chains to and at the surface of the substrate.[55] Due to this replenishment from the bulk, the anti-fouling properties of the functionalized substrates were maintained for significantly longer time then the surface grafted materials.[55]

Despite the effort to create stable coatings with complete surface coverage, it remains a challenge to prevent protein adsorption below a critical level, even in controlled laboratory settings. It was shown that only 5 ng cm^{-2} fibrinogen adsorption can result in thrombocyte adhesion and subsequent activation, which leads to thrombus formation.[56–59]

Anti-thrombogenic surfaces

The next approach that aims at improved blood-compatibility, which is highlighted here, focusses on the use of anti-thrombogenic moieties, which can be used to functionalize biomaterials in the form of a coating, or mediate the release of such factors.

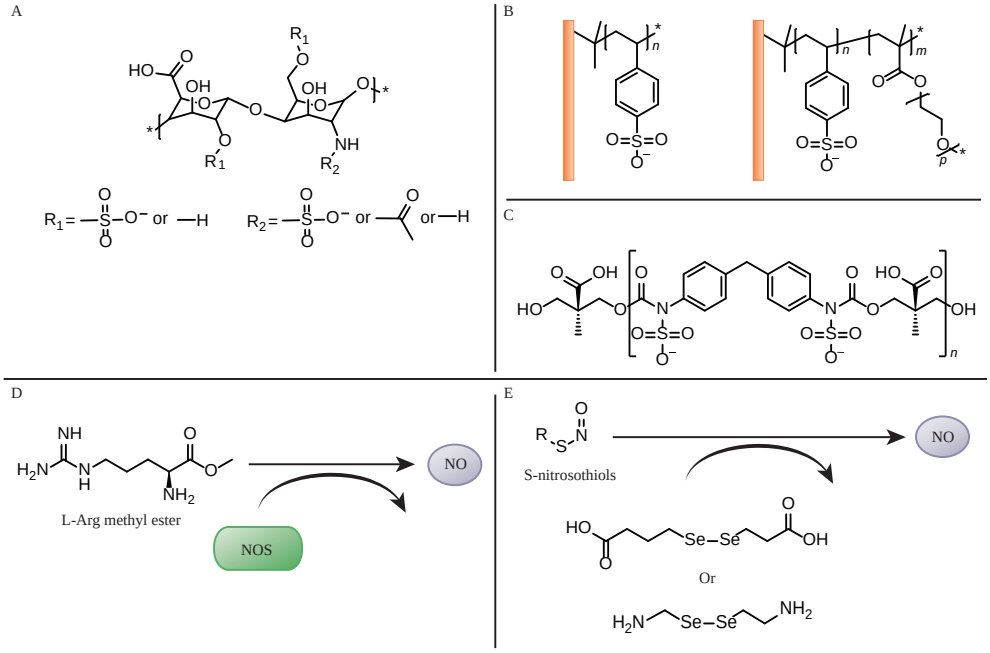

Figure 2.4. A) Schematic representation of the disaccharide of heparan sulfate and heparin. The sites of variable sulfonation are indicated.[9,65] B) Example of a sulfonated heparan/heparin mimicking polymer, grafted onto a surface using ATRP, possibly in combination with anti-fouling pOEGMA.[66] C) Example of a sulfonated PU polymer, with heparin/heparan mimicking properties.[70] D) Function of L-AME incorporation in biomaterials, which results in increased NOS mediated NO formation.[85] E) Schematic representation of the conversion from endogenous S-nitrosothiols into NO, mediated by diselenide containing materials that have glutathione peroxidase-like activity.[81]

Coating of anti-thrombogenic molecules

Heparin functionalization of vascular grafts and stents has already been used in clinical practice for a few decades.[60,61] Recently, heparin was coupled to ePTFE vascular graft material. These heparin functionalized vascular grafts were shown to decrease clot formation and platelet adhesion in whole-blood, while the material maintained the ability to sustain functional – determined through NO production - endothelial and blood outgrowth endothelial cell (BOEC) culture.[62] Multilayers of poly-l-lysine and heparin, present as the outer layer, were shown to prevent adsorption of blood proteins.[63] Furthermore, the adsorption of proteins was increasingly reduced with an increasing number of layers in the multilayer.[63] The electrostatic interactions between heparin and poly-l-lysine were used to create hybrid nanoparticles, which were immobilized on dopamine coated substrates.[64] These heparin-nanoparticle functionalized surfaces decreased adhesion and activation of platelets and had a positive effect by increasing blood-clotting times.[64]

Heparin and its less sulfonated biological counterpart heparan sulfate, have a variety of functions, including binding important factors regulating coagulation.[9,65] Polymeric mimics of these sulfonated polysaccharides allow for control over for instance the degree of sulfonation, influencing binding affinity to factors associated with anti-coagulative activity.[65] Application of such sulfonated molecules or polymers in biomaterials, can also improve

blood-compatibility properties.(**Figure 2.4**) Sulfonated heparin mimicking polymers, based on the combination of sodium styrene sulfonate and pOEGMA,[66] were conjugated to carbon nanotubes with SI-ATRP. These modifications decreased protein adsorption and thrombocyte adhesion, and positively increased clotting time as well.[67] Similar heparin mimics were used to prepare multilayers through a layer-by-layer assembly process.[68] Such coatings could be suitable for various materials to improve blood-compatibility.[68] A surface induced free radical polymerization technique in aqueous environment was employed to functionalize poly(ether sulfone) (PES) membranes with varying ratios of poly(sodium p-styrene sulfonate –co- sulfobetaine methacrylate) brushes. Brushes with high sulfobetaine content resisted adsorption of platelets and proteins in a closely related fashion. The p-styrene sulfonate incorporation prolonged and thereby improved blood coagulation times on the membranes, but this effect was lost with only a small amount of sulfobetaine.[69] A blend of sulfonated PU and PES was used to fabricate membranes with improved blood-compatibility, as was evident from an *in vitro* decrease in protein adsorption and platelet adhesion, increased blood coagulation times, and a lower thrombin generation activation.[70] As an alternative to heparin, direct thrombin inhibitors such as hirudin have been of interest for non-thrombogenic functionalization of biomaterials. [71,72] A coating with bivalirudin, a hirudin derived peptide, increased whole blood clotting time, decreased platelet adhesion and fibrinogen adsorption and also showed clear thrombin inactivation.[73] Polyurethane was functionalized with another direct, small molecule, thrombin inhibitor argatroban for increased blood compatibility.[74,75] Coupling of argatroban to free amines on the PU with a hexamethylene di-isocyanate linker resulted in promising decreases in thrombus formation in a extracorporeal circulation experiment.[75] Argatroban functionalization of a NO releasing polymer blend showed promising results with regards to maintaining platelet quiescence and decrease in thrombus formation.[74] Interestingly, fibrinogen, a fast adsorbing blood protein that is seen as a mediator for undesirable thrombocyte adhesion, has also been used as a coating with positive results related to vascular graft patency[76] and decreased cell and platelet adhesion on coated PTFE and polyethylene terephthalate (PET) substrates.[77]

Release of anti-thrombogenic agents

Heparin was not only used as coating but also as compound to be released from a depot. Yao et al. incorporated heparin in a multilayered electrospun PCL/chitosan scaffold based on ionic interactions between heparin and chitosan.[78] The vascular graft showed sustained release of heparin for more than 1 month *in vitro,* and improved patency *in vivo* in a rat abdominal aorta interposition model after 1 month.[78] A biodegradable poly(urethane urea) was co-electrospun with dipyridamole, an anti-coagulatory drug. This method ensued continuous release of dipyridamole *in vitro* for 90 days, and reduced thrombogenicity as measured by thrombin anti-thrombin complex formation, hemolysis and platelet formation *in vitro*.[79] Where NO is produced by endothelial cells with nitric oxide synthase (NOS), it can also be generated from endogenous NO donors, such as S-nitrosothiols, by selenium-containing molecules with glutathione peroxidase like activity.[80] (**Figure 2.4**) Functionalized biomaterial mediated NO production might prove beneficial towards improved blood-compatibility. A bioactive coating was prepared by coupling of 3,3-diselenodipropionic acid to an amine rich substrate. This 3,3-diselenodipropionic acid has peroxidase-like activity and can generate NO from S-nitrosothiols via a specific catalytic reaction.[81] This bioactive coating showed long-term and continuous production of NO and also inhibited platelet

activation.[81]

The combination of anti-fouling coatings, such as zwitterionic polycarboxybetaine and hydrophilic poly-2-methoxyethyl acrylate, with physiological NO release reduces platelet adsorption on membranes more than the two methods separate, even with evidence for a synergistic effect.[82,83] SLIPS can be used too for a sustained release method. A PEI and PVDMA multilayer was combined with an anti-bacterial triclosan-infused hydrophobic oil.[84] These infused SLIPS decreased bacterial viability and suppressed the adhesion of a range of bacterial and mammalian cells.[84] L-arginine methyl ester (L-AME) was incorporated in a poly(carbonate urethane)urea (PCU) base material.[85] Upon blood-contact, L-AME releases from the PCU, acting both as a porogen, and a substrate to NOS, to catalyze NO production,[85] a potent anti-thrombogenic agent normally secreted by endothelial cells (**Figure 2.4d**).[4] Thromboelastography data showed improved clotting times with increasing L-AME concentrations.[85] Moreover, endothelial progenitor cell (EPC) viability improved with L-AME incorporation when evaluated *in vitro*[85] and *in vivo*.[86] A surface that combines fibrinolytic functionality with Lysine incorporation[87], and inhibition of platelet activation and aggregation with surface mediated NO production, was prepared on a pOEGMA brush base material. 6-amino-2-(2-methacylamido)-hexanoic acid)(LysMA) was copolymerized with pOEGMA and grafted to a PU surface. This resulted in a surface with anti-fouling properties due to the pOEGMA and clot lysing properties attributed to the poly(LysMA). The poly(LysMA) functionalization ensued increased plasminogen mediated clot-lysis. Furthermore, selenocystamine, which catalyzes NO generation from S-nitrosothiols, was covalently coupled onto the surface complementing the system with NO generating properties. The NO production contributed to reduced platelet adhesion and smooth muscle cell adhesion and proliferation on the surfaces.[88]

Specific bioactivation

In contrast to previously discussed approaches for improvement of blood-compatibility in biomaterials, which focused on making the surface as inert as possible, or grafting with anti-thrombogenic molecules, functionalization of biomaterials that promote endothelialization is another promising approach.

One of the methods through which biomaterial surfaces can specifically be bioactivated, is via the combination of such bioactivation strategies with anti-fouling or anti-thrombogenic functionalization. Recently, several methods have been developed to further functionalize such coatings for incorporation of more biofunctionalities.[89] pSBMA brushes that were shown to have excellent anti-fouling properties[35] were further functionalized with an initiator group for ATRP, to which bacterium specific antibodies were coupled.[90] This resulted in coatings with highly specific detection of these bacteria from complex media, while still maintaining a high reduction in aspecific adsorption of proteins from these mixtures.[90] Sulfobetaine containing zwitterionic brush-coatings were adapted for specific functionalization using azide-based click-chemistry in which a bicyclononyne (BCN)-functionalized biotin conjugate was covalently coupled in order to specifically recognize avidins from solution.[91] Anti-fouling properties were maintained without reducing specificity of the avidin-biotin recognition.[91] Click-chemistry was also employed in a design where they covalently coated electrospun polystyrene based materials with PEG-brushes through

SI-ATRP.[92] A portion of these PEG-chains had trimethylsilyl groups used for coupling with azide-RGD moieties.[92] Non-specific adsorption of BSA was significantly decreased on the PEGylated scaffolds, but cells were able to adhere on the RGD-functionalized scaffolds.[92]

RGD functionalization of block copolymer brushes consisting poly(acrylamide), pOEGMA, and poly(acrylic acid) showed stable cell adhesion, while the non-functionalized coatings were resistant to cell adhesion for up to 1 month in culture medium.[93] One-step processing with electrospinning of PEG-block-poly(D,L-lactide) (PEG-*b*-PDLLA) block-copolymers resulted in meshes that were resistant to BSA adsorption.[94] Incorporation of RGD-functionalized block-copolymers before processing makes these scaffolds adhesive for cells.[94] In a similar approach, poly(D,L-lactide-co-glycolide) PLGA) scaffolds were functionalized with PEG containing star-shaped molecules resulting in protein-repellent fibers.[95] This material mixture was bioactivated with RGD-peptides that reacted to exposed isocyanate groups, prior to electrospinning, which resulted in scaffolds that sustain cell-adhesion.[95]

Also anti-microbial bioactivity can be applied in combination with PEG-brushes.[96] Polydimethylsulfoxide (PDMS)-PEG brushes were end-functionalized with antimicrobial peptides (AMP), which resulted in functionalized surfaces that showed decreased plasma protein adsorption, regardless of the PEG-block length and presence of the AMPs.[96] Interestingly, the bioactive films showed L929 cell compatibility, but significant anti-microbial activity, killing 99% of three bacterial species.[96]

Endothelial cell-specific bioactivation

Bioactivation strategies, such as described here, can also be beneficial for the formation and stimulation of endothelial layers on biomaterial surfaces. Bioactive functionalization, for instance based on methods that incorporate the general cell-binding peptide RGD as described in the examples above, can already benefit endothelialization. Chen et al. combined zwitterionic phosphobetaine for anti-fouling properties, a peptide with high affinity to EPCs, and DOPA groups for adhesion to the material substrate on a single polymer backbone.[97] This combinatorial approach slightly increased EPC adhesion.[97] A polydopamine coating was employed to functionalize a material surface with DNA nanoparticles, with plasmid DNA encoding for the hepatocyte growth factor (HGF) gene.[98] These immobilized nanoparticles increased expression of HGF in both endothelial and smooth muscle cells, and due to the nature of HGF, increased endothelial cell proliferation, and thereby their competitiveness over smooth muscle cells.[98] Multilayered electrospun PU vascular grafts were functionalized with heparin and the cell adhesion peptides, RGD and YIGSR, all coupled by a 1 kDa PEG-linker.[99] *In vitro* studies showed an increase in human umbilical cord endothelial cell (HUVEC) adhesion and proliferation on surfaces with cell adhesive peptides present.[99] Patency of vascular grafts modified with the combination of heparin, RGD and YIGSR was increased from 46.2% to 71.4% after implantation in a rabbit abdominal aorta interposition model for 9 weeks.[99]

EPCs or BOECs could provide a promising source of endothelial cells that can be attracted from the circulation.[100,101] Many approaches try to capture these progenitor cells or endothelial cells themselves using cell-specific targeting molecules. For instance, Xi et al. used EPC specific DNA aptamers electrostatically attached to a dopamine poly(ethylene

–co- imine) copolymer film to increase EPC adhesion and proliferation.[102] The aptamer modified surfaces promoted EPC adhesion and proliferation over smooth muscle cells and endothelial cells to a lesser extent, proving its potential for use in specific stimulation of EPC adhesion.[102] Another approach showed that vascular endothelial growth factor (VEGF) immobilized onto substrates through a heparin/poly-l-lysine coating was able to specifically attract endothelial cells under flow *in vitro*.[103] Specificity for endothelial cells was even retained in complex cell-mixtures and endothelial cell suspensions in whole blood. Increased flow and shear stress did decrease the effectivity of cell-capture through VEGF functionalization.[103] Heparin mediated crosslinking of VEGF or anti-CD34 antibodies was utilized to functionalize poly(glycolic acid) (PGA)-based vascular grafts.[104] After 2 weeks in an *in vivo* study in a mouse inferior vena cava interposition model, the anti-CD34 functionalization showed slightly more endothelialization compared to the VEGF functionalized vascular graft, but both performed better than unmodified vascular grafts.[104]

The QK-peptide (KKLTWQELYQL[K(ac)Y[K(ac)]GI), which mimics the receptor binding region of VEGF, was covalently immobilized on elastin-like polypeptide (ELP) hydrogels.[105] Endothelial cell proliferation was significantly increased on the ELP hydrogels upon functionalization.[105] The VEGF-mimicking QK peptide was also incorporated in poly(l-lactide-co-ε-caprolactone) (PELCL) electrospun membranes, which resulted in increased proliferation of endothelial cells on the functionalized scaffolds.[106]

Several endothelial (progenitor) cell specific peptides have also been of interest for stimulating endothelialization (**Table 2.1**).[107–109] The REDV-peptide was immobilized on a heparin/chitosan multilayer on PET sheets, which showed specific endothelial cell adhesion and suppression of smooth muscle cell adhesion *in vitro*.[110] Immobilization of REDV on PEG-b-PELCL electrospun membranes through 1-ethyl-3-(3-dimethylaminopropyl) carbodiimide (EDC)/N-hydroxysuccinimide (NHS) chemistry improved endothelial cell adhesion compared to non-functionalized scaffolds, and additionally decreased BSA and fibrinogen adsorption slightly as well.[111] REDV conjugation to PTFE surfaces with a PEG linker through NHS-chemistry promoted HUVEC adhesion, decreased platelet adsorption and showed beneficial effects on antibacterial behavior, by resisting *S. aureus* adhesion.[112] In a similar fashion, PEG-based anti-fouling properties and an endothelial cell specific peptide were combined by conjugation of collagen type IV derived CAG-peptides to pOEGMA brushes on a PU-based material.[113] This resulted in a decreased platelet adhesion on all pOEGMA brush covered surfaces, and a selective surface towards endothelial cell adhesion, both in single-cell culture and in co-culture with smooth muscle cells.[113] Moreover, incorporation of a CAG-peptide promoted endothelialization in small-diameter vascular grafts. Endothelialization was improved from 77% to 98% in a carotid arterial replacement model in rats after 6 weeks. This resulted in a slightly improved overall patency. Endothelial function on CAG-functionalized vascular graft surfaces was also improved as assessed by endothelial NOS activity.[114] PCL electrospun scaffolds functionalized with pCBMA were further modified with EPC specific TPS peptides (TPSLEQRTVYAK) using azide-based click chemistry. Platelet adhesion on the scaffolds with zwitterionic functionalization was significantly decreased, where the addition of the TPS peptide resulted in increases specificity for EPC adhesion compared to mesenchymal stromal cells (MSC) and HUVECs.[115] Heparin immobilization can also be used to promote endothelialization. The density of immobilized heparin on substrates however is crucial for the effect on cells, i.e.

higher heparin densities leads to inhibition of all cell adhesion, while lower densities favor endothelial cell adhesion over smooth muscle cell adhesion.[64]

Table 2.1. Overview of peptides that have been used for the stimulation of endothelialization on the surface of biomaterials to improve blood-compatibility.

Peptide (full sequence)	Sequence derived from
REDV-peptide	*Human plasma Fibronectin*[107]
CAG-peptide	*Collagen IV, with high affinity for ECs* [109]
TPS-peptide (TPSLEQRTVYAK)	*Glycoprotein with high specificity for BOECs*[108]
QK-peptide (KKLTWQELYQL[K(ac)Y[K(ac)]GI)	*VEGF receptor binding region* [105]

Stimulation of endothelialization via release of agents

Besides covalent conjugation of endothelial attracting moieties, release of non-thrombogenic factors from biomaterials can also improve endothelialization. Dipyridamole or heparin released from small diameter vascular grafts results in a biomaterial to which endothelial cells prefer to adhere and proliferate on over smooth muscle cells.[78,79] NO production mediated by biomaterial-catalyst conjugates has similar inhibitory effects on smooth muscle cell adhesion and proliferation.[81] Dai et al. electrospun polyurethane scaffolds loaded with PEG-VEGF nanoparticles.[116] Prolonged release of these nanoparticles improved endothelial progenitor cell proliferation and differentiation and thus increased endothelialization.[116] A star-shaped copolymer of (poly(lactide-co-3(S)-methyl-morpholine-2,5-dione)$_6$, or a star-(PLMD)$_6$ was grafted with PEI, PEG and a REDV peptide. This combination formed stable micelles and was used to condense pEGFP-ZNF580 utilizing electrostatic reactions with the PEI core-shell. These complexes were used to specifically transfect endothelial cells with the ZNF580 gene, resulting in increased transfection rates and migration in endothelial cells.[117]

Responsive material systems

The next step in the development of blood-compatible synthetic biomaterials is the introduction of responsiveness, such as triggered release of anti-coagulant factors. Uncontrolled activity of anti-thrombogenic moieties could for instance even lead to unwanted bleeding. Great effort has been put into the fabrication of systems that are responsive to certain stimuli. Material systems have been developed that respond to light, change in pH, mechanical stimuli, change in temperature, and that possess redox sensitivity[118,119]. With regards to blood-compatible materials, recent studies on responsive systems are discussed here, which concern anti-fouling or anti-thrombogenic response, or responsiveness to biologically relevant cues, such as proteases and enzymes.

Responsive anti-fouling materials

An early example of a blood-compatible responsive material is a system composed of an electrosensitive polypyrrole-heparin conjugate that is able to increase heparin exposure upon stimulation, which thereby supports endothelial cell culture.[120] Spin-coated thin films were prepared by Xu et al. with different compositions of amphiphilic PEG-PS copolymer brushes. The amount of exposed PEG at the surface of these films was varied

through exposure to different solvent vapors, which allowed the authors to tune the fouling behavior of these brush coatings.[121] The anti-fouling properties of zwitterionic or mixed charged brush-coatings depend on the pH of the solution they are exposed to. For instance, zwitterionic poly(3-(1-(4-vinylbenzyl)-H-imidazol-3-ium-3-yl)propane-1-sulfonate) (polyVBIPS) brushes, grafted onto substrates with ATRP, showed reversible surface hydration effects in different solutions, rendering the surfaces either anti-fouling, or less fouling.[122] Similar results were seen for a mixed charged copolymer brush coating, consisting of positively charged [2-(Acryloyloxy)ethyl] trimethyl ammonium chloride (TMA) and negatively charged 2-carboxy ethyl acrylate (CAA), which showed anti-fouling behavior in neutral pH, but was fouling in acidic conditions.[123] Moreover, adhered bacteria could be released from the surface by changing the pH of the exposed solution.[123] A multi-layered approach was applied to build in selectivity to cells or bacteria. The multi-layered construct consisted of a short anti-fouling PEG-linker, followed by a responsive peptide linker, either susceptive to degradation by gelatinase or coagulase, both excreted by bacteria, and an adhesive RGD peptide in the top layer.[124] This surface was shown to be adhesive to cells. However when bacteria adhered that secrete either gelatinase or the coagulase, the sensitive peptide was cleaved, and the adhesive properties of the surface were lost, rendering the surface no longer adhesive to these bacteria.[124]

Biologically relevant responsive systems

Systems that display one-directional responsiveness to biological cues, similar like the ones that regulate anticoagulant functions of endothelium *in vivo*, can be used to fabricate responsive blood-compatible materials. Materials that are of interest contain peptides or other sequences that are recognized by similar biological cues as those that elicit a response in endothelium. A self-assembling peptide hydrogel was used as a base for sustained release of NO. A caged NO donor molecule was attached to the peptide hydrogelator. Upon cleavage by the enzyme ß-galactosidase, the cage was broken and NO was released from the hydrogel.[125]

Another method to release NO in a responsive system was developed by Wang et al., using a material system in which an electrospun vascular graft was covalently functionalized with biotin. The graft was further modified with an avidin-galactosidase. After administration of a glycosylated NO-prodrug, the exposed enzyme on the vascular graft surface released the NO from the prodrug locally, thereby decreasing thrombus formation and platelet adhesion on the graft surface. The enzyme in this method showed catalytic activity *in vivo* for up to 1 month.[126]

Some responsive materials systems are based on the differences between physiological conditions *in vivo* and possible conditions *ex vivo*, for instance for easy application in combination with increased retention times *in vivo.* Contreras-García et al. grafted co-polymers of N-isopropyl acrylamide (pNIPAM) and N-(3-aminopropyl) methacrylamide hydrochloride on polypropylene films. These films were loaded in swollen conditions at room temperature, whereas at physiological temperature the polymer structures were collapsed due to the thermal behavior of pNIPAM, which resulted in better retention of encapsulated drugs.[127] An example of a supramolecular materials platform where this principle was used, is described by our group.[128] A PEG-based hydrogel was end-

functionalized with ureido-pyrimidinone (UPy) moieties that form reversible crosslinks through fourfold hydrogen bonding. At high pH, the hydrogel is liquid, allowing for injection through a catheter. At physiological pH, the material was shown to gelate, and increase the localization and retention time of incorporated growth factors.[128]

Thrombin related responsive systems

The main activator of an anti-thrombogenic phenotype in endothelial cells is thrombin. Thrombin is therefore also a promising candidate to develop biomaterial systems with responsive anti-coagulative activity. In recent years, several material systems have been developed that respond to the presence of thrombin in various manners.

In a very elegant catch-and-release microfluidic system, a thrombin-specific DNA aptamer is used on top of flexible epoxy micropillars embedded in a hydrogel.[129] This microfluidic system has two laminar fluid flows on top of each other, where the tops of the pillars are in the top flow-layer, and the hydrogel that supports the pillars is in the bottom flow-layer. When a solution with thrombin is flowed through the upper channel, the DNA aptamers on top of the posts will bind to the thrombin. Both the thrombin aptamer and the hydrogel are pH sensitive: the aptamer loses its affinity for thrombin in acidic pH, and the hydrogel shrinks at lower pH.[129] Thus, when the fluid in the bottom flow-layer is changed from a neutral pH to an acidic pH, the hydrogel shrinks and the pillars collapse thereby exposing the pH-sensitive thrombin-aptamer to the same acidic pH. This results in the release of thrombin into the solution of the bottom flow-layer, which can be collected separately from the top flow-layer.[129] This system is a good demonstration of the versatility of reversible thrombin binding by specific DNA aptamers. A similar thrombin-specific pH-responsive system that has potential as a biosensor, used an increased FRET signal in more acidic conditions and thrombin release from the aptamer as a read-out.[130]

A bioresponsive hydrogel system was developed in which the specific binding of a DNA-aptamer to thrombin caused a gel-sol transition.[131] A DNA-aptamer, with a high affinity for thrombin, was part of a crosslinker in a polyacrylamide gel. In the presence of thrombin, the crosslinking function of the aptamer was lost, and the content of the hydrogel was released through the gel-sol transition.[131] A comparable gel-sol transition as a result of thrombin presence was reported by Zhang et al.[132] A double thrombin-DNA aptamer was part of a Y-shaped DNA hydrogel in which gold-nanoparticles were released from the gel in the presence of thrombin. The release of the gold-nanoparticles resulted in an increased FRET-signal in combination with positively charged quantum dots.[132] A thrombin-sensitive cage was developed for protease responsive delivery, by incorporating thrombin sensitive peptide (TSP) GGLPVR/GSGAS into a nanoscale protein cage. The TSP sequence was included in the sequence for the ferritin from hyperthermophilic archaeon *Pyrococcus furiosus*. The internal domain, conjugated to the payload, was externalized upon cleavage of the peptide by thrombin, without damaging the cage structure.[133] Another example of reactivity to protease-cleavable peptides is a PEG-based anti-fouling hydrogel coating in whichthe anti-inflammatory chemokine IL-1Ra was incorporated.[134] This method showed sustained release of the chemokine upon activation by proteases.[134] An example that employs reactivity to thrombin in order to maintain hemostasis, is presented by Du et al. A t-PA loaded polyacrylamide hydrogel was crosslinked with a TSP (Gly-dPhe-Pro-Arg-Gly-

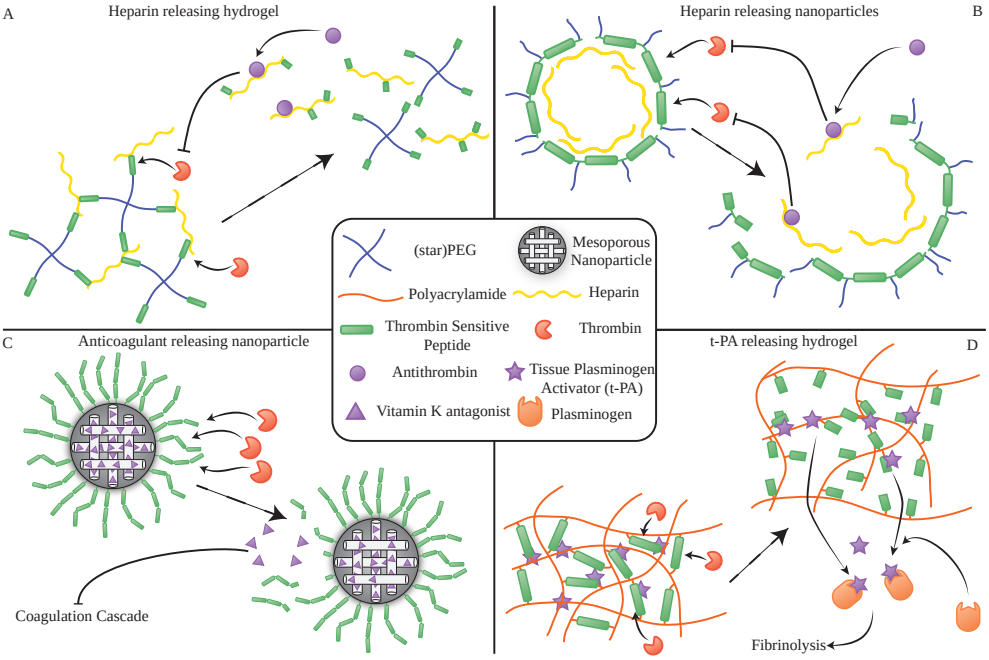

Figure 2.5. Schematic representation of thrombin sensitive systems that regulate coagulation: A) A starPEG hydrogel crosslinked through heparin and thrombin sensitive peptides (TSP). Upon degradation of these peptides by thrombin, heparin is released from the hydrogel. Subsequently, heparin-antithrombin complexes inhibit thrombin activity and further gel degradation and heparin release.[138] B) Heparin is released from heparin-TSP nanoparticles, upon cleavage of the TSP by thrombin, resulting in decreased thrombin activity and further nanoparticle degradation, also mediated by heparin-antithrombin complexes.[139] C) Mesoporous nanoparticles, loaded with a Vitamin K antagonist are covered in TSP. When the TSP is cleaved by thrombin, the content of the nanoparticle is released, inhibiting coagulation and thrombin activity.[140] D) A polyacrylamide hydrogel is crosslinked by TSPs, and loaded with tissue plasminogen activator (t-PA). Upon degradation of the gel by thrombin, t-PA is released, which subsequently induces fibrinolysis after the activation of plasminogen.[135]

Phy-Pro-Ala-Gly-Gly, that can be cleaved between the Arg and Gly by thrombin), terminated at both ends with methacrylamide.[135] In the presence of thrombin t-PA was released from the hydrogel and subsequently lysed thrombi. An increased degree of crosslinking led to a decrease in thrombin mediated degradation rates, which shows the tunability of the activity. Clotting was prevented in a whole blood incubation experiment with these responsive t-PA releasing hydrogels.[135] (**Figure 2.5**)

Introduction of feedback-controlled response mechanisms

The next step in the introduction of complexity into blood-compatible materials is the development of intrinsic (negative) feedback-controlled response mechanisms.[136] In most cases, this means that the stimuli that induce the bioactivity of such a system decrease the activity of the stimuli. For instance in the study by Purcell et al. matrix metalloproteinase (MMP) sensitive peptide crosslinkers were incorporated in a polysaccharide-based hydrogel system.[137] This hydrogel was loaded with tissue inhibitor of MMPs (TIMP) through electrostatic interactions. Upon cleavage of the MMP-sensitive peptide, the TIMP was

released, inhibiting the function of the MMPs, limiting further hydrogel digestion.[137] This method was used to attenuate adverse remodeling in the left ventricle of pig heart post-MI by decreasing the amount of matrix degradation, leading to improved cardiac output.[137]

Below the first approaches that truly implement negative feedback-controlled response mechanisms to control hemostasis are reviewed. A star-PEG hydrogel based system was end-functionalized with TSP sequences, i.e. (Gly- (D)Phe-Pip-Arg-Ser-Trp-Gly-Cys-Gly) that were crosslinked through heparin molecules.[138] In the presence of thrombin, the TSPs were cleaved, and the heparin was released from the hydrogel. The released heparin subsequently served as a substrate for antithrombin, which increases the affinity of antithrombin for thrombin, and inhibits thrombin function and further heparin release from the hydrogel.[138] Application of this hydrogel system showed remarkable reduction in blood-clot formation in contact with the responsive hydrogel, in comparison with clinically applied PTFE and heparin-coated PTFE samples.[138] (**Figure 2.5**) Nanoscale self-titrating activatable therapeutic nanoparticles, or nanoSTAT, were developed to locally prevent thrombosis.[139] The nanoSTAT is formed by self-assembly of a positively charged TSP, and negatively charged heparin. Covalent functionalization of the thrombin-sensitive peptide with PEG stabilized the particles, and nonspecific interactions were minimized. When cleaved by thrombin, the positively charged peptide casing released the heparin payload, thereby inhibiting thrombin via binding to antithrombin. This locally prevented thrombosis.[139] (**Figure 2.5**)

A technique that involves acenocoumarol loaded nanoparticles has thrombin-regulated anti-coagulating activity.[140] The drug acenocoumarol functions as an anticoagulant via Vitamin K antagonistic activity.[141] Vitamin K is involved in coagulation as a Gla-protein activator, including prothrombin, factors VII, IX, X, and protein C and S. The nanoparticles contained a thrombin-mediated hydrolysable peptide sequence with LVPRGS repeats. Upon cleavage by thrombin the drug was released from the nanoparticles, interfering in the coagulation cascade and subsequently preventing clot formation and further release from the nanoparticles.[140] (**Figure 2.5**) These examples show that feedback systems that regulate coagulation are mostly based on thrombin reactivity. A good overview of bioresponsive systems with other applications is presented in a recent review by Wagner and colleagues.[142]

Supramolecular systems for blood-compatibility

Supramolecular materials may be the ideal candidates for incorporation of autonomous feedback mechanisms owing to the inherently dynamic nature of the major interactions in these types of materials. Supramolecular materials form a class of materials that employ highly specific non-covalent interactions as the major driving force of assembly and functionalization.[143] In recent years, supramolecular material systems have been employed to develop biomaterials with anti-fouling, anti-thrombogenic and responsive properties, of which examples are highlighted below.

Anti-fouling supramolecular systems

Host-guest interactions between ß-cyclodextrin and adamantane-functionalized molecules were implemented by Cai et al. to render microporous membranes less susceptible for aspecific protein adsorption.[144] Propargyl methacrylate (PMA) was grafted on a

poly(vinylidene fluoride)(PVF) base material. The alkyne endgroups on the PMA are able to undergo a click-reaction with azide-moieties used to post-functionalize the membranes with mono(6-azideo-6-dexosy)-ß-cyclodextrin that serve as supramolecular hosts. Subsequent addition of PEG-molecules end-functionalized with adamantane guest moieties resulted in a PEG-mediated reduction in protein adsorption.[144] The versatility of cyclodextrin-adamantane host-guest chemistry was shown by Deng et al. via anchoring of cyclodextrin host molecules onto PES membranes to which subsequently adamantane modified functional polymers were grafted.[145] Upon addition of adamantane modified PEG the surfaces were more resistant to protein adsorption and platelet adhesion. Supramolecular incorporation of heparin mimicking poly(styrenesulfonate-co-sodium acrylates) conjugated to the adamantane resulted in an anti-thrombogenic surface that prolonged blood clotting times. Addition of adamantane-poly(methyl chloride-quaternized 2-(dimethylamino)ethyl methacrylate) complemented the system with antibacterial functionality.[145]

Similar host-guest chemistry was employed in the formulation of a layer-by-layer assembled multilayer coating.[146] One layer consisted of polyethylenimine-ß-cyclodextrin (PEI-ß-CD) and the other of ferrocene-modified chitosan (Fc-CHT). The host-guest interactions between the cyclodextrin and the ferrocene improved long-term stability of the multilayers that showed inhibition of bacterial adhesion and growth.[146]

In a modular approach we showed that UPy-functionalized PEG molecules were incorporated in UPy-modified PCL base materials based on the hydrogen bonding interactions between UPy molecules.[147] These mixtures were shown to decrease cell-adhesion on thin films[148–150] and electrospun scaffolds, both *in vitro*[148,149] and *in vivo*.[149] (**Figure 2.6**) The same modular approach was employed to introduce bioactivity in these materials, as shown by cell adhesion on materials produced from mixtures containing RGD peptides conjugated to UPy moieties.[148,151]

Improved anti-coagulant properties

To include anti-thrombogenic properties in supramolecular biomaterials, Zhan et al. employed a combinatorial approach. In their research, a PU substrate was modified with a poly(2-hydroxyethyl methacrylate-co-1-adamantan-1-ylmethyl methacrylate) copolymer, to which both REDV peptide and a ß-CD decorated with seven lysines were coupled, through covalent coupling and ß-CD-adamantane host-guest interactions, respectively.[152] The REDV-peptide serves as a promotor for endothelialization, while the lysine-rich molecule acts as a ligand for plasminogen and t-PA, enhancing lysis of thrombi at the biomaterial surface. The combination of these two strategies stimulated clot-lysis and endothelial cell adhesion, without impairment of function of either peptide.[152] In a comparable approach, an ARMAPE peptide with high t-PA affinity was covalently coupled instead of the REDV-peptide.[153] Aspecific protein adsorption on these surfaces was intrinsically low due to the used HEMA linkers, and did not increase significantly compared to control surfaces upon functionalization with both the peptides and the lysine decorated ß-CD.[152,153] The dual affinity for t-PA and plasminogen also resulted in improved clot lysis when the functionalized surfaces were exposed to plasma.[153]

A supramolecular system based on rotoxanes was used for material-mediated NO generation.[154] L-arginine was covalently immobilized to α-cyclodextrins (α-CD) through

a hydrolysable ester linker onto the polyrotoxane. Upon separation of the L-arginine, the mechanical properties and biocompatibility of the polyrotaxane biomaterial were retained.[154] Calixarenes, which are known for their function as host in supramolecular host-guest interactions[155], have been shown to function as a direct inhibitor of fibrin polymerization, preventing the final step in blood-clot formation.[156] Using supramolecular host-guest chemistry based on cyclodextrin-adamantane interactions, PCL surfaces were functionalized with mixtures of PEG and TPS peptide, where the adhesion of EPCs on these surfaces could be modulated.[157] These examples of material systems based on host-guest chemistry show the potential of supramolecular systems with anti-coagulant function.

Responsive supramolecular systems

In recent years, several supramolecular systems with responsivity to different cues and with different functions have been developed.[158]

A thermoresponsive supramolecular system that is either anti-fouling, or kills adhered bacteria was developed by Shi et al.: ß-CD covered surfaces were functionalized with adamantane terminated pNIPAM (Ad-pNIPAM) and poly[2(methacryloyloxy)ethyl]-trimethylammonium chloride (Ad-PMT) using host-guest interactions between the ß-CD and the adamantane.[159] At temperatures below the lower critical temperature (lower critical solution temperature, or LCST) the hydrated pNIPAM-brush provides anti-fouling properties. Above the LCST the longer pNIPAM molecules collapse which renders the surface adhesive for bacteria, and simultaneously exposes the bacteria to Ad-PMT. This effectively kills the bacteria, including those that may have attached before the temperature transition.[159]

Some supramolecular approaches have been developed for stimulative control over cell adhesion to functionalized biomaterials. An et al. functionalized RGD peptides with an N-terminal tryptophan-glycine-glycine (WGG) motif. The WGG peptide is capable to act as a guest, together with the electrosensitive viologen-moiety inside a cucurbit[8]uril (CB[8]) host molecule. In this approach, PEG-coated anti-fouling surfaces were functionalized with viologen molecules attached via an alkyl spacer through disulphide coupling.[160] In combination with the CB[8] and WGGRGD peptides, the surfaces were made bioactive and cell adhesive. Upon electrical stimulation of the substrates however, the viologen was reduced and the complex with the WGGRGD peptide dissociates, which resulted in release of the adherent cells.[160] (**Figure 2.6**)

Employing the difference in affinity of the guest molecules napthalane and adamantane to cyclodextrin, another responsive cell-adhesive system was developed.[161] Covalent modification of alginate surfaces with cyclodextrin molecules was described. Acting as guest for the cyclodextrin host, 1-adamantane-carboxylic acid was conjugated to RGDS (ada-RGDS) and RGES (ada-RGES, an RGD analog without biological activity) peptides. As a guest with a slightly lower affinity for interaction with the cyclodextrin, RGDS was coupled to 1-napthalene-amide (naphtyl-RGDS). On the bare alginate, cells kept a rounded morphology. Upon supramolecular functionalization with the RGD-guest molecules, cells were able to spread on the surfaces. When the ada-RGES was added to the substrates with napthyl-RGDS, the napthyl-RGDS guests were replaced by ada-RGES guests, by which the surfaces lost bioactivity and cell-adhesive properties.[161]

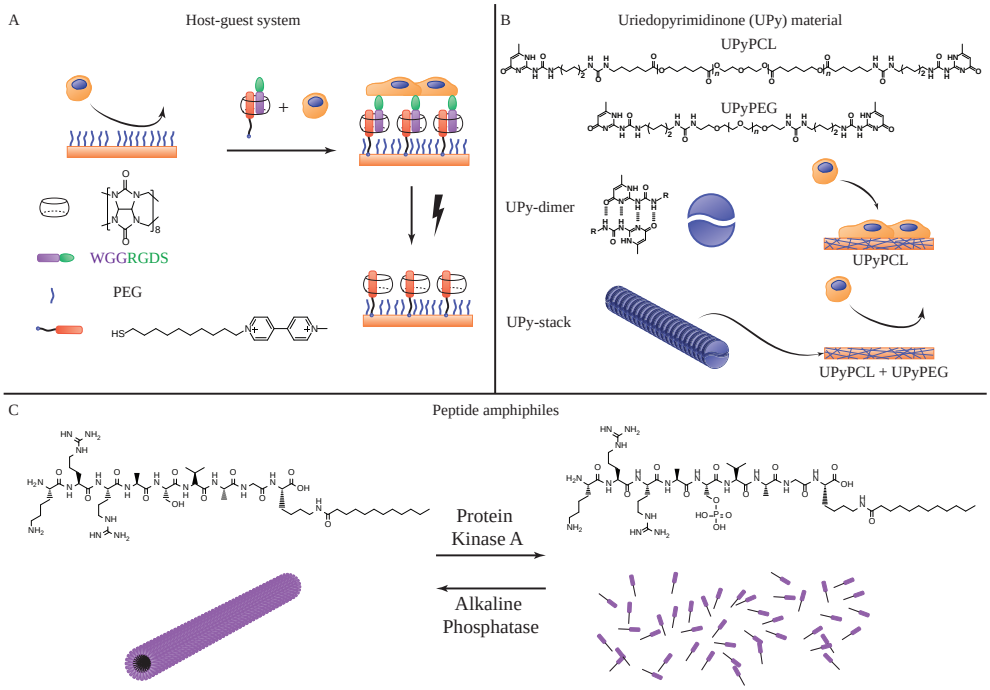

Figure 2.6. Schematic representation of supramolecular material systems. A) Stimulative control over cell-adhesion through electrosensitive viologen-WGG-peptide-cucurbit[8]uril (CB[8]) disassociation: A surface is functionalized with viologen moieties, and through complexation with a WGGRGDS peptide as hosts in the cucurbit[8]uril guest molecule, cells are able to adhere on the functionalized surface. Upon reduction of the viologen, the peptide disassociates from the CB[8] and causes cells to release from the surface.[160] B) Modular functionalization of materials based on specific interactions between ureidopyrimidinone (UPy)-conjugated molecules. These UPy moieties form dimers that can stack into fibrous structures. Simple mixtures of UPyPCL and UPyPEG result in non-cell adhesive surfaces.[148–150] C) Enzyme sensitive self-assembly of peptide amphiphiles, where specific phosphorylation by Protein Kinase A causes disassembly of supramolecular nanofibers and dephosphorylation by Alkaline Phosphatase allows again for self-assembly into nanofibers.[163]

A nice example of a supramolecular material system, with responsivity resulting in conformational changes, is with a water soluble block-copolymer, consisting of PEG and pHEMA, of which 32% of the methacrylate monomers is grafted with a biguanidine-ß-CD moiety.[162] Adenosine triphosphate (ATP) can specifically interact with this conjugate, through a combination of hydrogen-bonding between the triphosphate group and the biguanidine linker, and the host-guest interactions of the nucleotide group and the cyclodextrin. Dependent on the concentration of ATP, the polymers form different structures, ranging from spheres, to fibers and vesicles.[162]

An enzyme-responsive system based on self-assembling peptide amphiphiles (PA) was developed by Webber and coworkers.[163] The self-assembly into nanofibers is driven by collapse of the hydrophobic tail, in combination with ß-sheet formation of the peptides. The peptide sequence, that contains a serine, is specifically recognized by the enzyme Protein Kinase A, which phosphorylates this serine. The phosphate group on the serine disrupts the ß-sheet and causes disassembly of the PA nanofibers. In presence of another enzyme, alkaline phosphatase, the original PA is restored by dephosphorylation, which allows the

molecules to self-assemble into fibrous structures again. In this way, the supramolecular assembly is regulated in an enzymatic way, in close resemblance to phosphorylation cycles in nature.[163] (**Figure 2.6**)

The self-assembly into either nanosheets or nanotubes in another system with two Fmoc PAs depends on the ratio between these peptides. The balance between the two dipeptides used in this study, Fmoc-cysteic acid-phenylalananine (CAF) and Fmoc-lysine phenylananine (KF) is regulated by thermolysin mediated hydrolysis and amide formation. Interestingly, in the presence of the cationic polysaccharide chitosan, the formation of CAF is favored, which results in nanosheet formation. In the presence of the anionic polysaccharide heparin, KF is formed more, which gives rise to nanotubular structures,[164] showing biomolecule dependent self-assembly for this peptide-based system.

Outlook

The scientific development of new biomaterials with improved blood-compatibility has been shown to progress from passive functionalization strategies, towards responsivity to relevant biological cues. Insights in this field will lead to better understanding and control over blood-biomaterial interactions, even though not all complexity can eventually be translated for clinical applications.[165]

The dynamic material systems described have shown to modulate thrombus formation, either in solution or in a hydrogel state. One of the key challenges in further development of biomaterials that counteract coagulation in a dynamic fashion would be the implementation of these feedback-controlled mechanisms into biomaterials that are mechanically suitable as structural materials in applications such as vascular grafts and heart valve constructs. One could think of recent advances in combining hydrogels with elastomeric biomaterials, by covalently coating with thin hydrogel layers[166,167], or in the form of interpenetrating polymer networks.[168–170]

Supramolecular materials could provide the ideal platform for the incorporation of dynamic reciprocity, since the properties of such biomaterials are governed by non-covalent supramolecular interactions, which are intrinsically dynamic. This will lead to materials that better mimic the natural environment, e.g. the extracellular matrix, and could lead to the development of life-like materials.

In the design of blood-contacting materials based on the strong but non-covalent supramolecular interactions care should be taken to ensure prolonged stability, since these materials will be subjected to a constantly diluting environment *in vivo*. Even though dilution-based self-assembly has been described in literature[171], the self-assembly of supramolecular materials in solution can change with biologically relevant changes in e.g. pH, ionic strength or protein concentrations.[143,158] In more stable elastomeric supramolecular materials, such as described by our group,[148–150] these factors have a limited effect, but the dynamicity is lower in these materials. The challenge lies in finding the delicate balance where supramolecular materials have sufficient robustness and dynamic properties simultaneously.[172,173]

Another aspect, in which progress can be made, is the design of ligands that serve as the

reactive components in dynamic materials. In most material systems described, these reactive sites, such as thrombin-sensitive peptide sequences, are consumed over time, such that eventually dynamic functionality of the system is lost. Many processes in nature, the main source of inspiration in the development of new biomaterials, are governed through non-covalent and, importantly, reversible interactions. The same holds for the anti-coagulative functionalities of endothelium, where for instance the complexation of thrombin to thrombomodulin activates anti-coagulant properties of protein C bound to endothelial protein C receptor[174], or the conformational change that antithrombin undergoes when bound to specific pentasaccharide domains in heparan sulfate through hydrogen bonding, which results in increased affinity for thrombin.[175] Promising examples of compounds that can serve as ligands with reversible interactions in dynamic systems include DNA aptamers[102,129–131] As described, complexation with specific DNA aptamers can be fully reversible,[102,129,130] and can be used to modulate gel-sol transitions.[131] Reversible enzyme mediated responsivity, as shown for the dephosphorylation and phosphorylation in the self-assembling peptide amphiphiles system,[163] is another example of how life-like processes can be used to modulate material properties. In future research, we propose that the design of new synthetic biomaterials with a combination of feedback controlled anti-coagulant activity and smart use of reversible interactions will provide the edge for a new generation of blood-compatible biomaterials; en route to meet nature's complexity in a synthetic way.

References

(1) LeBleu, V. S.; Macdonald, B.; Kalluri, R. Structure and Function of Basement Membranes. *Exp. Biol. Med.* **2007**, *232*, 1121–1129.

(2) Dejana, E. Endothelial Cell–cell Junctions: Happy Together. *Nat. Rev. Mol. Cell Biol.* **2004**, *5*, 261–270.

(3) Bazzoni, G.; Dejana, E. Endothelial Cell-to-Cell Junctions: Molecular Organization and Role in Vascular Homeostasis. *Physiol Rev.* **2004**, *84*, 869–901.

(4) Wu, K. K.; Thiagarajan, P. Role of Endothelium in Thrombosis and Hemostasis. *Annu. Rev. Med.* **1996**, *47*, 315–331.

(5) Coughlin, S. R. Thrombin Signalling and Protease-Activated Receptors. *Nature* **2000**, *407*, 258–264.

(6) Pries, A. R.; Secomb, T. W.; Gaehtgens, P. The Endothelial Surface Layer. *Pflugers Arch.* **2000**, *440*, 653–666.

(7) Reitsma, S.; Slaaf, D. W.; Vink, H.; Van Zandvoort, M. A. M. J.; Oude Egbrink, M. G. A. The Endothelial Glycocalyx: Composition, Functions, and Visualization. *Pflugers Arch. Eur. J. Physiol.* **2007**, *454*, 345–359.

(8) Weinbaum, S.; Tarbell, J. M.; Damiano, E. R. The Structure and Function of the Endothelial Glycocalyx Layer. *Annu. Rev. Biomed. Eng.* **2007**, *9*, 121–167.

(9) Sasisekharan, R.; Venkataraman, G. Heparin and Heparan Sulfate: Biosynthesis, Structure and Function. *Current Opinion in Chemical Biology*. 2000, pp 626–631.

(10) Lavery, K. S.; Rhodes, C.; Mcgraw, A.; Eppihimer, M. J. Anti-Thrombotic Technologies for Medical Devices. *Adv. Drug Deliv. Rev.* **2017**, *112*, 2–11.

(11) Banerjee, I.; Pangule, R. C.; Kane, R. S. Antifouling Coatings: Recent Developments in the Design of Surfaces That Prevent Fouling by Proteins, Bacteria, and Marine Organisms. *Adv. Mater.* **2011**, *23*, 690–718.

(12) Unadkat, H.V; Hulsman, M.; Cornelissen, K.; Papenburg, B. J.; Turckenmüller, R. K.; Carpenter, A. E.; Wessling, M.; Post, G. F.; Uetz, M.; Reinders, M. J. T.; et al. An Algorithm-Based Topographical Biomaterials Library to Instruct Cell Fate. *Proc. Natl. Acad. Sci. U. S. A.* **2011**, *108*, 16565–16570.

(13) Gong, T.; Zhao, K.; Liu, X.; Lu, L.; Liu, D.; Zhou, S. A Dynamically Tunable, Bioinspired Micropatterned Surface Regulates Vascular Endothelial and Smooth Muscle Cells Growth at Vascularization. *Small* **2016**, *12*, 5769–5778.

(14) Stefopoulos, G.; Robotti, F.; Falk, V.; Poulikakos, D.; Ferrari, A. Endothelialization of Rationally Microtextured Surfaces with Minimal Cell Seeding Under Flow. *Small* **2016**, 4113–4126.

(15) Liang, C.; Hu, Y.; Wang, H.; Xia, D.; Li, Q.; Zhang, J.; Yang, J.; Li, B.; Li, H.; Han, D.; et al. Biomimetic Cardiovascular Stents for In??vivo Re-Endothelialization. *Biomaterials* **2016**, *103*, 170–182.

(16) Chapman, R. G.; Ostuni, E.; Takayama, S.; Holmlin, R. E.; Yan, L.; Whitesides, G. M. Surveying for Surfaces That Resist the Adsorption of Proteins [3]. *J. Am. Chem. Soc.* **2000**, *122*, 8303–8304.

(17) Ostuni, E.; Chapman, R. G.; Liang, M. N.; Meluleni, G.; Pier, G.; Ingber, D. E.; Whitesides, G. M. Self-Assembled Monolayers That Resist the Adsorption of Cells. *Langmuir* **2001**, *17*, 6336–6343.

(18) Rodriguez-Emmenegger, C.; Brynda, E.; Riedel, T.; Houska, M.; Šubr, V.; Alles, A. B.; Hasan, E.; Gautrot, J. E.; Huck, W. T. S. Polymer Brushes Showing Non-Fouling in Blood Plasma Challenge the Currently Accepted Design of Protein Resistant Surfaces. *Macromol. Rapid Commun.* **2011**, *32*, 952–957.

(19) Chen, S.; Li, L.; Zhao, C.; Zheng, J. Surface Hydration: Principles and Applications toward Low-Fouling/nonfouling Biomaterials. *Polymer* **2010**, *51*, 5283–5293.

(20) Higaki, Y.; Kobayashi, M.; Murakami, D.; Takahara, A. Anti-Fouling Behavior of Polymer Brush Immobilized Surfaces. *Polym. J.* **2016**, *48*, 325–331.

(21) Wei, Q.; Becherer, T.; Angioletti-Uberti, S.; Dzubiella, J.; Wischke, C.; Neffe, A. T.; Lendlein, A.; Ballauff, M.; Haag, R. Protein Interactions with Polymer Coatings and Biomaterials. *Angew. Chem., Int. Ed.* **2014**, *53*, 8004–8031.

(22) Hucknall, A.; Rangarajan, S.; Chilkoti, A. In Pursuit of Zero: Polymer Brushes That Resist the Adsorption of Proteins. *Adv. Mater.* **2009**, *21*, 2441–2446.

(23) Krishnamoorthy, M.; Hakobyan, S.; Ramstedt, M.; Gautrot, J. E. Surface-Initiated Polymer Brushes in the Biomedical Field: Applications in Membrane Science, Biosensing, Cell Culture, Regenerative Medicine and Antibacterial Coatings. *Chem. Rev.* **2014**, *114*, 10976–11026.

(24) Liu, M.; Leroux, J. C.; Gauthier, M. A. Conformation-Function Relationships for the Comb-Shaped Polymer pOEGMA. *Prog. Polym. Sci.* **2014**, *48*, 111–121.

(25) Harrison, R. H.; Steele, J. A. M.; Chapman, R.; Gormley, A. J.; Chow, L. W.; Mahat, M. M.; Podhorska, L.; Palgrave, R. G.; Payne, D. J.; Hettiaratchy, S. P.; et al. Modular and Versatile Spatial Functionalization of Tissue Engineering Scaffolds through Fiber-Initiated Controlled Radical Polymerization. *Adv. Funct. Mater.* **2015**, *25*, 5748–5757.

(26) Kostina, N. Y.; Pop-Georgievski, O.; Bachmann, M.; Neykova, N.; Bruns, M.; Michálek, J.; Bastmeyer, M.; Rodriguez-Emmenegger, C. Non-Fouling Biodegradable Poly(ϵ-Caprolactone) Nanofibers for Tissue Engineering. *Macromol. Biosci.* **2016**, *16*, 83–94.

(27) Surman, F.; Riedel, T.; Bruns, M.; Kostina, N. Y.; Sedláková, Z.; Rodriguez-Emmenegger, C. Polymer Brushes Interfacing Blood as a Route toward High Performance Blood Contacting Devices. *Macromol. Biosci.* **2015**, *15*, 636–646.

(28) Yuan, H.; Qian, B.; Zhang, W.; Lan, M. Protein Adsorption Resistance of PVP-Modified Polyurethane Film Prepared by Surface-Initiated Atom Transfer Radical

Polymerization. *Appl. Surf. Sci.* **2016**, *363*, 483–489.

(29) Pester, C. W.; Poelma, J. E.; Narupai, B.; Patel, S. N.; Su, G. M.; Mates, T. E.; Luo, Y.; Ober, C. K.; Hawker, C. J.; Kramer, E. J. Ambiguous Anti-Fouling Surfaces: Facile Synthesis by Light-Mediated Radical Polymerization. *J. Polym. Sci. Part A: Polym. Chem.* **2015**, 253–262.

(30) Li, Q.; Imbrogno, J.; Belfort, G.; Wang, X.-L. Making Polymeric Membranes Antifouling Via "grafting From" polymerization of Zwitterions. *J. Appl. Polym. Sci.* **2015**, *132*, 41781-.

(31) Schlenoff, J. B. Zwitteration: Coating Surfaces with Zwitterionic Functionality to Reduce Nonspecific Adsorption. *Langmuir* **2014**, *30*, 9625–9636.

(32) Shih, Y. J.; Chang, Y. Tunable Blood Compatibility of Polysulfobetaine from Controllable Molecular-Weight Dependence of Zwitterionic Nonfouling Nature in Aqueous Solution. *Langmuir* **2010**, *26*, 17286–17294.

(33) Zhu, L. J.; Liu, F.; Yu, X. M.; Gao, A. L.; Xue, L. X. Surface Zwitterionization of Hemocompatible Poly(lactic Acid) Membranes for Hemodiafiltration. *J. Memb. Sci.* **2015**, *475*, 469–479.

(34) Yang, R.; Gleason, K. K. Ultrathin Antifouling Coatings with Stable Surface Zwitterionic Functionality by Initiated Chemical Vapor Deposition (iCVD). *Langmuir* **2012**, *28*, 12266–12274.

(35) Nguyen, A. T.; Baggerman, J.; Paulusse, J. M. J.; van Rijn, C. J. M.; Zuilhof, H. Stable Protein-Repellent Zwitterionic Polymer Brushes Grafted from Silicon Nitride. *Langmuir* **2011**, *27*, 2587–2594.

(36) Wang, W.; Lu, Y.; Xie, J.; Zhu, H.; Cao, Z. A Zwitterionic Macro-Crosslinker for Durable Non-Fouling Coatings. *ChemComm* **2016**, *52*, 4671–4674.

(37) Ren, P. F.; Yang, H. C.; Liang, H. Q.; Xu, X. L.; Wan, L. S.; Xu, Z. K. Highly Stable, Protein-Resistant Surfaces via the Layer-by-Layer Assembly of Poly(sulfobetaine Methacrylate) and Tannic Acid. *Langmuir* **2015**, *31*, 5851–5858.

(38) de los Santos Pereira, A.; Sheikh, S.; Blaszykowski, C.; Pop-Georgievski, O.; Fedorov, K.; Thompson, M.; Rodriguez-Emmenegger, C. Antifouling Polymer Brushes Displaying Antithrombogenic Surface Properties. *Biomacromolecules* **2016**, acs.biomac.6b00019.

(39) Liu, P.; Huang, T.; Liu, P.; Shi, S.; Chen, Q.; Li, L.; Shen, J. Zwitterionic Modification of Polyurethane Membranes for Enhancing the Anti-Fouling Property. *J. Colloid Interface Sci.* **2016**, *480*, 91–101.

(40) Greene, G. W.; Martin, L. L.; Tabor, R. F.; Michalczyk, A.; Ackland, L. M.; Horn, R. Lubricin: A Versatile, Biological Anti-Adhesive with Properties Comparable to Polyethylene Glycol. *Biomaterials* **2015**, *53*, 127–136.

(41) Peng, L.; Li, H.; Meng, Y. Layer-by-Layer Structured Polysaccharides-Based Multilayers on Cellulose Acetate Membrane: Towards Better Hemocompatibility, Antibacterial and Antioxidant Activities. *Appl. Surf. Sci.* **2017**, *401*, 25–39.

(42) Silva, J. M.; García, J. R.; Reis, R. L.; García, A. J.; Mano, J. F. Tuning Cell Adhesive Properties via Layer-by-Layer Assembly of Chitosan and Alginate. *Acta Biomater.* **2017**, 1–15.

(43) Brown, P. S.; Bhushan, B. Bioinspired, Roughness-Induced, Water and Oil Super-Philic and Super-Phobic Coatings Prepared by Adaptable Layer-by-Layer Technique. *Sci. Rep.* **2015**, *5*, 1–16.

(44) Tuteja, A.; Choi, W.; Ma, M.; Mabry, J. M.; Mazzella, S. a; Rutledge, G. C.; McKinley, G. H.; Cohen,

R. E. Designing Superoleophobic Surfaces. *Science* **2007**, *318*, 1618–1622.

(45) Deng, X.; Mammen, L.; Butt, H. J.; Vollmer, D. Candle Soot as a Template for a Transparent Robust Superamphiphobic Coating. *Science* **2012**, *335*, 67–70.

(46) Liu, Z.; Wang, H.; Wang, E.; Zhang, X.; Yuan, R.; Zhu, Y. Superhydrophobic Poly(vinylidene Fluoride) Membranes with Controllable Structure and Tunable Wettability Prepared by One-Step Electrospinning. *Polymer* **2016**, *82*, 105–113.

(47) Goetz, L. A.; Jalvo, B.; Rosal, R.; Mathew, A. P. Superhydrophilic Anti-Fouling Electrospun Cellulose Acetate Membranes Coated with Chitin Nanocrystals for Water Filtration. *J. Memb. Sci.* **2016**, *510*, 238–248.

(48) Movafaghi, S.; Leszczak, V.; Wang, W.; Sorkin, J. a.; Dasi, L. P.; Popat, K. C.; Kota, A. K. Hemocompatibility of Superhemophobic Titania Surfaces. *Adv. Healthcare Mater.* **2017**, 1600717.

(49) Wong, T.-S.; Kang, S. H.; Tang, S. K. Y.; Smythe, E. J.; Hatton, B. D.; Grinthal, A.; Aizenberg, J. Bioinspired Self-Repairing Slippery Surfaces with Pressure-Stable Omniphobicity. *Nature* **2011**, *477*, 443–447.

(50) Epstein, A. K.; Wong, T.-S.; Belisle, R. A.; Boggs, E. M.; Aizenberg, J. Liquid-Infused Structured Surfaces with Exceptional Anti-Biofouling Performance. *Proc. Natl. Acad. Sci. U. S. A.* **2012**, *109*, 13182–13187.

(51) Chen, J.; Howell, C.; Haller, C. A.; Patel, M. S.; Ayala, P.; Moravec, K. A.; Dai, E.; Liu, L.; Sotiri, I.; Aizenberg, M.; et al. An Immobilized Liquid Interface Prevents Device Associated Bacterial Infection in Vivo. *Biomaterials* **2017**, *113*, 80–92.

(52) Chen, D.; Wu, M.; Li, B.; Ren, K.; Cheng, Z.; Ji, J.; Li, Y.; Sun, J. Layer-by-Layer-Assembled Healable Antifouling Films. *Adv. Mater.* **2015**, *27*, 5882–5888.

(53) Wang, Z.; Zuilhof, H. Self-Healing Superhydrophobic Fluoropolymer Brushes as Highly Protein-Repellent Coatings. *Langmuir* **2016**, *32*, 6310–6318.

(54) Chen, K.; Zhou, S.; Wu, L. Self-Healing Underwater Superoleophobic and Antibiofouling Coatings Based on the Assembly of Hierarchical Microgel Spheres. *ACS Nano* **2016**, *10*, 1386–1394.

(55) Kuroki, H.; Tokarev, I.; Nykypanchuk, D.; Zhulina, E.; Minko, S. Stimuli-Responsive Materials with Self-Healing Antifouling Surface via 3D Polymer Grafting. *Adv. Funct. Mater.* **2013**, *23*, 4593–4600.

(56) Zhang, M.; Horbett, T. A. Tetraglyme Coatings Reduce Fibrinogen and von Willebrand Factor Adsorption and Platelet Adhesion under Both Static and Flow Conditions. *J. Biomed. Mater. Res., Part A* **2009**, *89*, 791–803.

(57) Zhang, Z.; Zhang, M.; Chen, S.; Horbett, T. A.; Ratner, B. D.; Jiang, S. Blood Compatibility of Surfaces with Superlow Protein Adsorption. *Biomaterials* **2008**, *29*, 4285–4291.

(58) Shen, M.; Martinson, L.; Wagner, M. S.; Castner, D. G.; Ratner, B. D.; Horbett, T. A. PEO-like Plasma Polymerized Tetraglyme Surface Interactions with Leukocytes and Proteins: In Vitro and in Vivo Studies. *J. Biomater. Sci. Polym. Ed.* **2002**, *13*, 367–390.

(59) Tsai, W. B.; Grunkemeier, J. M.; Horbett, T. A. Human Plasma Fibrinogen Adsorption and Platelet Adhesion to Polystyrene. *J. Biomed. Mater. Res.* **1999**, *44*, 130–139.

(60) Serruys, P. W.; Emanuelsson, H.; van der Giessen, W.; Lunn, A. C.; Kiemeney, F.; Macaya, C.; Rutsch, W.; Heyndrickx, G.; Suryapranata, H.; Legrand, V.; et al. Heparin-Coated Palmaz-Schatz Stents in Human Coronary Arteries. *Circulation* **1996**, *93*.

(61) Tanzi, M. C. Bioactive Technologies for Hemocompatibility. *Expert Rev. Med. Devices* **2005**, *2*, 473–492.

(62) Hoshi, R. A.; Lith, R. Van; Jen, M. C.; Allen, J. B.; Lapidos, K. A.; Ameer, G. Biomaterials The Blood and Vascular Cell Compatibility of Heparin-Modi Fi Ed ePTFE Vascular Grafts. *Biomaterials* **2013**, *34*, 30–41.

(63) Barrantes, A.; Wengenroth, J.; Arnebrant, T.; Haugen, H. J. Poly-L-Lysine/heparin Multilayer Coatings Prevent Blood Protein Adsorption. *J. Colloid Interface Sci.* **2017**, *485*, 288–295.

(64) Liu, T.; Liu, Y.; Chen, Y.; Liu, S.; Maitz, M. F.; Wang, X.; Zhang, K.; Wang, J.; Wang, Y.; Chen, J.; et al. Immobilization of Heparin/poly-L-Lysine Nanoparticles on Dopamine-Coated Surface to Create a Heparin Density Gradient for Selective Direction of Platelet and Vascular Cells Behavior. *Acta Biomater.* **2014**, *10*, 1940–1954.

(65) Paluck, S. J.; Nguyen, T. H.; Maynard, H. D. Heparin-Mimicking Polymers: Synthesis and Biological Applications. *Biomacromolecules* **2016**, *17*, 3417–3440.

(66) Nguyen, T. H.; Kim, S.-H.; Decker, C. G.; Wong, D. Y.; Loo, J. a; Maynard, H. D. A Heparin-Mimicking Polymer Conjugate Stabilizes Basic Fibroblast Growth Factor. *Nat. Chem.* **2013**, *5*, 221–227.

(67) Nie, C.; Ma, L.; Xia, Y.; He, C.; Deng, J.; Wang, L.; Cheng, C.; Sun, S.; Zhao, C. Novel Heparin-Mimicking Polymer Brush Grafted Carbon nanotube/PES Composite Membranes for Safe and Efficient Blood Purification. *J. Memb. Sci.* **2015**, *475*, 455–468.

(68) Nie, C.; Ma, L.; Cheng, C.; Deng, J.; Zhao, C. Nanofibrous Heparin and Heparin-Mimicking Multilayers as Highly Effective Endothelialization and Antithrombogenic Coatings. *Biomacromolecules* **2015**, *16*, 992–1001.

(69) Xie, Y.; Wang, R.; Li, S.; Xiang, T.; Zhao, C. S. A Robust Way to Prepare Blood-Compatible and Anti-Fouling Polyethersulfone Membrane. *Colloids Surf., B* **2016**, *146*, 326–333.

(70) Ma, L.; Su, B.; Cheng, C.; Yin, Z.; Qin, H.; Zhao, J.; Sun, S.; Zhao, C. Toward Highly Blood Compatible Hemodialysis Membranes via Blending with Heparin-Mimicking Polyurethane: Study in Vitro and in Vivo. *J. Memb. Sci.* **2014**, *470*, 90–101.

(71) Freitas, S. C.; Barbosa, M. A.; Martins, M. C. L. The Effect of Immobilization of Thrombin Inhibitors onto Self-Assembled Monolayers on the Adsorption and Activity of Thrombin. *Biomaterials* **2010**, *31*, 3772–3780.

(72) Maitz, M. F.; Sperling, C.; Werner, C. Immobilization of the Irreversible Thrombin Inhibitor D-Phe-Pro-Arg- Chloromethylketone: A Concept for Hemocompatible Surfaces? *J. Biomed. Mater. Res., Part A* **2010**, *94*, 905–912.

(73) Yang, Z.; Tu, Q.; Maitz, M. F.; Zhou, S.; Wang, J.; Huang, N. Direct Thrombin Inhibitor-Bivalirudin Functionalized Plasma Polymerized Allylamine Coating for Improved Biocompatibility of Vascular Devices. *Biomaterials* **2012**, *33*, 7959–7971.

(74) Major, T. C.; Brisbois, E. J.; Jones, A. M.; Zanetti, M. E.; Annich, G. M.; Bartlett, R. H.; Handa, H. The Effect of a Polyurethane Coating Incorporating Both a Thrombin Inhibitor and Nitric Oxide on Hemocompatibility in Extracorporeal Circulation. *Biomaterials* **2014**, *35*, 7271–7285.

(75) Yu, J.; Brisbois, E.; Handa, H.; Annich, G.; Meyerhoff, M.; Bartlett, R.; Major, T. The Immobilization of a Direct Thrombin Inhibitor to a Polyurethane as a Nonthrombogenic Surface Coating for Extracorporeal Circulation. *J. Mater. Chem. B* **2016**, *4*, 2264–2272.

(76) Hasegawa, T.; Okada, K.; Takano, Y.; Hiraishi, Y.; Okita, Y. Autologous Fibrin-Coated Small-Caliber Vascular Prostheses Improve Antithrombogenicity by Reducing Immunologic Response. *J. Thorac. Cardiovasc. Surg.* **2007**, *133*, 1268–1276.e1.

(77) Safiullin, R.; Christenson, W.; Owaynat, H.; Yermolenko, I. S.; Kadirov, M. K.; Ros, R.; Ugarova, T. P. Fibrinogen Matrix Deposited on the Surface of Biomaterials Acts as a Natural Anti-

Adhesive Coating. *Biomaterials* **2015**, *67*, 151–159.

(78) Yao, Y.; Wang, J.; Cui, Y.; Xu, R.; Wang, Z.; Zhang, J.; Wang, K.; Li, Y.; Zhao, Q.; Kong, D. Effect of Sustained Heparin Release from PCL/chitosan Hybrid Small-Diameter Vascular Grafts on Anti-Thrombogenic Property and Endothelialization. *Acta Biomater.* **2014**, *10*, 2739–2749.

(79) Punnakitikashem, P.; Truong, D.; Menon, J. U.; Nguyen, K. T.; Hong, Y. Electrospun Biodegradable Elastic Polyurethane Scaffolds with Dipyridamole Release for Small Diameter Vascular Grafts. *Acta Biomater.* **2014**, *10*, 4618–4628.

(80) Cha, W.; Meyerhoff, M. E. Catalytic Generation of Nitric Oxide from S-Nitrosothiols Using Immobilized Organoselenium Species. *Biomaterials* **2007**, *28*, 19–27.

(81) Yang, Z.; Yang, Y.; Xiong, K.; Li, X.; Qi, P.; Tu, Q.; Jing, F.; Weng, Y.; Wang, J.; Huang, N. Nitric Oxide Producing Coating Mimicking Endothelium Function for Multifunctional Vascular Stents. *Biomaterials* **2015**, *63*, 80–92.

(82) Gupta, S.; Amoako, K. A.; Suhaib, A.; Cook, K. E. Multi-Modal, Surface-Focused Anticoagulation Using Poly-2-Methoxyethylacrylate Polymer Grafts and Surface Nitric Oxide Release. *Adv. Mater. Interfaces* **2014**, *1*, 1–7.

(83) Amoako, K. A.; Sundaram, H. S.; Suhaib, A.; Jiang, S.; Cook, K. E. Multimodal, Biomaterial-Focused Anticoagulation via Superlow Fouling Zwitterionic Functional Groups Coupled with Anti-Platelet Nitric Oxide Release. *Adv. Mater. Interfaces* **2016**, *3*, 1–9.

(84) Manna, U.; Raman, N.; Welsh, M. A.; Zayas-Gonzalez, Y. M.; Blackwell, H. E.; Palecek, S. P.; Lynn, D. M. Slippery Liquid-Infused Porous Surfaces That Prevent Microbial Surface Fouling and Kill Non-Adherent Pathogens in Surrounding Media: A Controlled Release Approach. *Adv. Funct. Mater.* **2016**, *26*, 3599–3611.

(85) Everett, W.; Scurr, D. J.; Rammou, A.; Darbyshire, A.; Hamilton, G.; de Mel, A. A Material Conferring Hemocompatibility. *Sci. Rep.* **2016**, *6*, 26848.

(86) Chaves, C.; Gao, C.; Hunckler, J.; Elsawy, M.; Legagneux, J.; Renault, G.; Masquelet, A. C.; de Mel, A. Dual-Acting Biofunctionalised Scaffolds for Applications in Regenerative Medicine. *J. Mater. Sci. Mater. Med.* **2017**, *28*, 32.

(87) Tang, Z.; Liu, X.; Luan, Y.; Liu, W.; Wu, Z.; Li, D.; Chen, H. Regulation of Fibrinolytic Protein Adsorption on Polyurethane Surfaces by Modification with Lysine-Containing Copolymers. *Polym. Chem.* **2013**, *4*, 5597.

(88) Gu, H.; Chen, X.; Liu, X.; Zhan, W.; Lyu, Z.; Yu, Q.; Wu, Z.; Chen, H. A Hemocompatible Polyurethane Surface Having Dual Fibrinolytic and Nitric Oxide Generating Functions. *J. Mater. Chem. B* **2017**, *5*, 980–987.

(89) Jiang, H.; Xu, F.-J. Biomolecule-Functionalized Polymer Brushes. *Chem. Soc. Rev.* **2013**, *42*, 3394.

(90) Nguyen, A. T.; Baggerman, J.; Paulusse, J. M. J.; Zuilhof, H.; Van Rijn, C. J. M. Bioconjugation of Protein-Repellent Zwitterionic Polymer Brushes Grafted from Silicon Nitride. *Langmuir* **2012**, *28*, 604–610.

(91) Lange, S. C.; van Andel, E.; Smulders, M. M. J.; Zuilhof, H. Efficient and Tunable Three-Dimensional Functionalization of Fully Zwitterionic Antifouling Surface Coatings. *Langmuir* **2016**, *32*, 10199–10205.

(92) Rodda, A. E.; Ercole, F.; Glattauer, V.; Gardiner, J.; Nisbet, D. R.; Healy, K. E.; Forsythe, J. S.; Meagher, L. Low Fouling Electrospun Scaffolds with Clicked Bioactive Peptides for Specific Cell Attachment. *Biomacromolecules* **2015**, *16*, 2109–2118.

(93) Lilge, I.; Schönherr, H. Synthesis and Characterization of Well-Defined Ligand-Terminated Block Copolymer Brushes for Multifunctional Biointerfaces. *Polym. (United Kingdom)* **2016**, *98*, 409–420.

(94) Grafahrend, D.; Calvet, J. L.; Klinkhammer, K.; Salber, J.; Dalton, P. D.; Möller, M.; Klee, D. Control of Protein Adsorption on Functionalized Electrospun Fibers. *Biotechnol. Bioeng.* **2008**, *101*, 609–621.

(95) Grafahrend, D.; Heffels, K.-H.; Beer, M.V; Gasteier, P.; Möller, M.; Boehm, G.; Dalton, P. D.; Groll, J. Degradable Polyester Scaffolds with Controlled Surface Chemistry Combining Minimal Protein Adsorption with Specific Bioactivation. *Nat. Mater.* **2011**, *10*, 67–73.

(96) Gao, Q.; Yu, M.; Su, Y.; Xie, M.; Zhao, X.; Li, P.; Ma, P. X. Rationally Designed Dual Functional Block Copolymers for Bottlebrush-like Coatings: In Vitro and In Vivo Antimicrobial, Antibiofilm, and Antifouling Properties. *Acta Biomater.* **2017**.

(97) Chen, H.; Li, X.; Zhao, Y.; Li, J.; Chen, J.; Yang, P.; Maitz, M. F.; Huang, N. Construction of a Multifunctional Coating Consisting of Phospholipids and Endothelial Progenitor Cell-Specific Peptides on Titanium Substrates. *Appl. Surf. Sci.* **2015**, *347*, 169–177.

(98) Li, B. C.; Chang, H.; Ren, K. F.; Ji, J. Substrate-Mediated Delivery of Gene Complex Nanoparticles via Polydopamine Coating for Enhancing Competitiveness of Endothelial Cells. *Colloids Surf., B* **2016**, *147*, 172–179.

(99) Choi, W. S.; Joung, Y. K.; Lee, Y.; Bae, J. W.; Park, H. K.; Park, Y. H.; Park, J. C.; Park, K. D. Enhanced Patency and Endothelialization of Small-Caliber Vascular Grafts Fabricated by Coimmobilization of Heparin and Cell-Adhesive Peptides. *ACS Appl. Mater. Interfaces* **2016**, *8*, 4336–4346.

(100) Hill, J. M.; Zalos, G.; Halcox, J. P. J.; Schenke, W. H.; Waclawiw, M. A.; Quyyumi, A. A.; Finkel, T. Circulating Endothelial Progenitor Cells, Vascular Function, and Cardiovascular Risk. *N. Engl. J. Med.* **2003**, *348*, 593–600.

(101) Peters, E. B.; Christoforou, N.; Leong, K. W.; Truskey, G. A.; West, J. L. Poly(Ethylene Glycol) Hydrogel Scaffolds Containing Cell-Adhesive and Protease-Sensitive Peptides Support Microvessel Formation by Endothelial Progenitor Cells. *Cell. Mol. Bioeng.* **2015**, *9*, 38–54.

(102) Li, X.; Deng, J.; Yuan, S.; Wang, J.; Luo, R.; Chen, S.; Wang, J.; Huang, N. Fabrication of Endothelial Progenitor Cell Capture Surface via DNA Aptamer Modifying Dopamine/polyethyleneimine Copolymer Film. *Appl. Surf. Sci.* **2016**, *386*, 138–150.

(103) Smith, R. J.; Koobatian, M. T.; Shahini, A.; Swartz, D. D.; Andreadis, S. T. Capture of Endothelial Cells under Flow Using Immobilized Vascular Endothelial Growth Factor. *Biomaterials* **2015**, *51*, 303–312.

(104) Melchiorri, A. J.; Hibino, N.; Yi, T.; Lee, Y. U.; Sugiura, T.; Tara, S.; Shinoka, T.; Breuer, C.; Fisher, J. P. Contrasting Biofunctionalization Strategies for the Enhanced Endothelialization of Biodegradable Vascular Grafts. *Biomacromolecules* **2015**, *16*, 437–446.

(105) Cai, L.; Dinh, C. B.; Heilshorn, S. C. One-Pot Synthesis of Elastin-like Polypeptide Hydrogels with Grafted VEGF-Mimetic Peptides. *Biomater. Sci.* **2014**, *2*, 757.

(106) Yang, Y.; Yang, Q.; Zhou, F.; Zhao, Y.; Jia, X.; Yuan, X.; Fan, Y. Electrospun PELCL Membranes Loaded with QK Peptide for Enhancement of Vascular Endothelial Cell Growth. *J. Mater. Sci. Mater. Med.* **2016**, *27*, 1–10.

(107) Hubbell, J.A.; Massia, S. P.; Desai, N. P.; Drumheller, P. D. Endothelial Cell-Selective Materials for Tissue Engineering in the Vacular Graft via a New Receptor. *Nat. Biotechnol.* **1991**, *9*, 568–572.

(108) Veleva, A. N.; Cooper, S. L.; Patterson, C. Nanoparticles and Microparticles for Drug and Vaccine Delivery. *Biotechnol. Bioeng.* **2007**, *98*, 312.

(109) Kanie, K.; Narita, Y.; Zhao, Y.; Kuwabara, F.; Satake, M.; Honda, S.; Kaneko, H.; Yoshioka, T.; Okochi, M.; Honda, H.; et al. Collagen Type IV-Specific Tripeptides for Selective Adhesion of Endothelial and Smooth Muscle Cells. *Biotechnol. Bioeng.* **2012**, *109*, 1808–1816.

(110) Lin, Q. K.; Hou, Y.; Ren, K. F.; Ji, J. Selective Endothelial Cells Adhesion to Arg-Glu-Asp-Val Peptide Functionalized Polysaccharide Multilayer. *Thin Solid Films* **2012**, *520*, 4971–4978.

(111) Zhou, F.; Jia, X.; Yang, Y.; Yang, Q.; Gao, C.; Zhao, Y.; Fan, Y.; Yuan, X. Peptide-Modified PELCL Electrospun Membranes for Regulation of Vascular Endothelial Cells. *Mater. Sci. Eng. C* **2016**, *68*, 623–631.

(112) Gabriel, M.; Niederer, K.; Becker, M.; Raynaud, C. M.; Vahl, C. F.; Frey, H. Tailoring Novel PTFE Surface Properties: Promoting Cell Adhesion and Antifouling Properties via a Wet Chemical Approach. *Bioconjugate Chem.* **2016**, *27*, 1216–1221.

(113) Khan, M.; Yang, J.; Shi, C.; Lv, J.; Feng, Y.; Zhang, W. Surface Tailoring for Selective Endothelialization and Platelet Inhibition via a Combination of SI-ATRP and Click Chemistry Using Cys-Ala-Gly-Peptide. *Acta Biomater.* **2015**, *20*, 69–81.

(114) Kuwabara, F.; Narita, Y.; Yamawaki-Ogata, A.; Kanie, K.; Kato, R.; Satake, M.; Kaneko, H.; Oshima, H.; Usui, A.; Ueda, Y. Novel Small-Caliber Vascular Grafts with Trimeric Peptide for Acceleration of Endothelialization. *Ann. Thorac. Surg.* **2012**, *93*, 156–163.

(115) Li, Q.; Wang, Z.; Zhang, S.; Zheng, W.; Zhao, Q.; Zhang, J.; Wang, L.; Wang, S.; Kong, D. Functionalization of the Surface of Electrospun Poly(epsilon-Caprolactone) Mats Using Zwitterionic Poly(carboxybetaine Methacrylate) and Cell-Specific Peptide for Endothelial Progenitor Cells Capture. *Mater. Sci. Eng. C* **2013**, *33*, 1646–1653.

(116) Dai, W.; Guo, H.; Qian, D.; Qin, Z.; Lei, Y.; Hou, X.; Wen, C. Improving Endothelialization by the Combined Application of Polyethylene Glycol Coated Cerium Oxide Nanoparticles and VEGF in Electrospun Polyurethane Scaffolds. *J. Mater. Chem. B* **2017**, *5*, 1053–1061.

(117) Lv, J.; Hao, X.; Li, Q.; Akpanyung, M.; Nejjari, A.; Neve, A. L.; Ren, X.; Feng, Y.; Shi, C.; Zhang, W. Star-Shaped Copolymer Grafted PEI and REDV as a Gene Carrier to Improve Migration of Endothelial Cells. *Biomater. Sci.* **2017**, *5*, 511–522.

(118) Yan, X.; Wang, F.; Zheng, B.; Huang, F. Stimuli-Responsive Supramolecular Polymeric Materials. *Chem. Soc. Rev.* **2012**, *41*, 6042.

(119) Cole, M. A.; Voelcker, N. H.; Thissen, H.; Griesser, H. J. Stimuli-Responsive Interfaces and Systems for the Control of Protein-Surface and Cell-Surface Interactions. *Biomaterials* **2009**, *30*, 1827–1850.

(120) Garner, B.; Georgevich, A.; Hodgson, A.; Liu, L.; Wallace, G. G. Polypyrrole-Heparin Composites as Stimulus-Responsive Substrate for Endothelial Cell Growth. *J. Biomed. Mater. Res.* **1999**, *44*, 121–129.

(121) Xu, B.; Feng, C.; Hu, J.; Shi, P.; Gu, G.; Wang, L.; Huang, X. Spin-Casting Polymer Brush Films for Stimuli-Responsive and Anti-Fouling Surfaces. *ACS Appl. Mater. Interfaces* **2016**, *8*, 6685–6692.

(122) Yang, J.; Chen, H.; Xiao, S.; Shen, M.; Chen, F.; Fan, P.; Zhong, M.; Zheng, J. Salt-Responsive Zwitterionic Polymer Brushes with Tunable Friction and Antifouling Properties. *Langmuir* **2015**, *31*, 9125–9133.

(123) Mi, L.; Bernards, M. T.; Cheng, G.; Yu, Q.; Jiang, S. pH Responsive Properties of Non-Fouling Mixed-Charge Polymer Brushes Based on Quaternary Amine and Carboxylic Acid Monomers. *Biomaterials* **2010**, *31*, 2919–2925.

(124) Li, L. L.; Qi, G. Bin; Yu, F.; Liu, S. J.; Wang, H. An Adaptive Biointerface from Self-Assembled Functional Peptides for Tissue Engineering. *Adv. Mater.* **2015**, *27*, 3181–3188.

(125) Gao, J.; Zheng, W.; Zhang, J.; Guan, D.; Yang, Z.; Kong, D.; Zhao, Q. Enzyme-Controllable Delivery of Nitric Oxide from a Molecular Hydrogel. *Chem. Commun.* **2013**, *49*, 9173–9175.

(126) Wang, Z.; Lu, Y.; Qin, K.; Wu, Y.; Tian, Y.; Wang, J.; Zhang, J.; Hou, J.; Cui, Y.; Wang, K.; et al. Enzyme-Functionalized Vascular Grafts Catalyze in-Situ Release of Nitric Oxide from Exogenous NO

Prodrug. *J. Control. Release* **2015**, *210*, 179–188.

(127) Contreras-García, A.; Alvarez-Lorenzo, C.; Taboada, C.; Concheiro, A.; Bucio, E. Stimuli-Responsive Networks Grafted onto Polypropylene for the Sustained Delivery of NSAIDs. *Acta Biomater.* **2011**, *7*, 996–1008.

(128) Bastings, M. M. C.; Koudstaal, S.; Kieltyka, R. E.; Nakano, Y.; Pape, A. C. H.; Feyen, D. A. M.; van Slochteren, F. J.; Doevendans, P. A.; Sluijter, J. P. G.; Meijer, E. W.; et al. A Fast pH-Switchable and Self-Healing Supramolecular Hydrogel Carrier for Guided, Local Catheter Injection in the Infarcted Myocardium. *Adv. Healthcare Mater.* **2014**, *3*, 70–78.

(129) Shastri, A.; McGregor, L. M.; Liu, Y.; Harris, V.; Nan, H.; Mujica, M.; Vasquez, Y.; Bhattacharya, A.; Ma, Y.; Aizenberg, M.; et al. An Aptamer-Functionalized Chemomechanically Modulated Biomolecule Catch-and-Release System. *Nat. Chem.* **2015**, *7*, 447–454.

(130) McConnell, E. M.; Bolzon, R.; Mezin, P.; Frahm, G.; Johnston, M.; DeRosa, M. C. PHAST (pH-Driven Aptamer Switch for Thrombin) Catch-and-Release of Target Protein. *Bioconjugate Chem.* **2016**, *27*, 1493–1499.

(131) Yang, H.; Liu, H.; Kang, H.; Tan, W. Engineering Target-Responsive Hydrogels Based on Aptamer-Target Interactions. *J. Am. Chem. Soc.* **2008**, *130*, 6320–6321.

(132) Zhang, L.; Lei, J.; Liu, L.; Li, C.; Ju, H. Self-Assembled DNA Hydrogel as Switchable Material for Aptamer-Based Fluorescent Detection of Protein. *Anal. Chem.* **2013**, *85*, 11077–11082.

(133) Kang, Y. J.; Park, D. C.; Shin, H. H.; Park, J.; Kang, S. Incorporation of Thrombin Cleavage Peptide into a Protein Cage for Constructing a Protease-Responsive Multifunctional Delivery Nanoplatform. *Biomacromolecules* **2012**, *13*, 4057–4064.

(134) Gutowski, S. M.; Shoemaker, J. T.; Templeman, K. L.; Wei, Y.; Latour, R. A.; Bellamkonda, R. V.; LaPlaca, M. C.; García, A. J. Protease-Degradable PEG-Maleimide Coating with on-Demand Release of IL-1Ra to Improve Tissue Response to Neural Electrodes. *Biomaterials* **2015**, *44*, 55–70.

(135) Du, H.; Li, C.; Luan, Y.; Liu, Q.; Yang, W.; Yu, Q.; Li, D.; Brash, J. L.; Chen, H. An Antithrombotic Hydrogel with Thrombin-Responsive Fibrinolytic Activity: Breaking down the Clot as It Forms. *Mater. Horiz.* **2016**, *3*, 556–562.

(136) Morris, E.; Chavez, M.; Tan, C. Dynamic Biomaterials: Toward Engineering Autonomous Feedback. *Curr. Opin. Biotechnol.* **2016**, *39*, 97–104.

(137) Purcell, B. P.; Lobb, D.; Charati, M. B.; Dorsey, S. M.; Wade, R. J.; Zellars, K. N.; Doviak, H.; Pettaway, S.; Logdon, C. B.; Shuman, J. A.; et al. Injectable and Bioresponsive Hydrogels for on-Demand Matrix Metalloproteinase Inhibition. *Nat. Mater.* **2014**, *13*, 653–661.

(138) Maitz, M. F.; Freudenberg, U.; Tsurkan, M. V; Fischer, M.; Beyrich, T.; Werner, C. Bio-Responsive Polymer Hydrogels Homeostatically Regulate Blood Coagulation. *Nat. Commun* **2013**, *4*, 2168.

(139) Lin, K. Y.; Lo, J. H.; Consul, N.; Kwong, G. a.; Bhatia, S. N. Self-Titrating Anticoagulant Nanocomplexes That Restore Homeostatic Regulation of the Coagulation Cascade. *ACS Nano* **2014**, *8*, 8776–8785.

(140) Bhat, R.; Ribes, À.; Mas, N.; Aznar, E.; Sancenón, F.; Marcos, M. D.; Murguía, J. R.; Venkataraman, A.; Martínez-Máñez, R. Thrombin-Responsive Gated Silica Mesoporous Nanoparticles As Coagulation Regulators. *Langmuir* **2016**, *32*, 1195–1200.

(141) Ufer, M. Comparative Pharmacokinetics of Vitamin K Antagonists. *Clin. Pharmacokinet.* **2005**, *44*, 1227–1246.

(142) Wagner, H. J.; Sprenger, A.; Rebmann, B.; Weber, W. Upgrading Biomaterials with Synthetic Biological Modules for Advanced Medical Applications. *Adv. Drug Deliv. Rev.* **2016**, *105*, 77–95.

(143) Webber, M. J.; Appel, E. a.; Meijer, E. W.; Langer, R. Supramolecular Biomaterials. *Nat. Mater.* **2015**, *15*, 13–26.

(144) Cai, T.; Neoh, K. G.; Kang, E. T. Poly(vinylidene Fluoride) Graft Copolymer Membranes With "clickable" surfaces and Their Functionalization. *Macromolecules* **2011**, *44*, 4258–4268.

(145) Deng, J.; Liu, X.; Zhang, S.; Cheng, C.; Nie, C.; Zhao, C. Versatile and Rapid Postfunctionalization from Cyclodextrin Modified Host Polymeric Membrane Substrate. *Langmuir* **2015**, *31*, 9665–9674.

(146) Xu, G.; Pranantyo, D.; Xu, L.; Neoh, K. G.; Kang, E. T.; Teo, S. L. M. Antifouling, Antimicrobial, and Antibiocorrosion Multilayer Coatings Assembled by Layer-by-Layer Deposition Involving Host-Guest Interaction. *Ind. Eng. Chem. Res.* **2016**, *55*, 10906–10915.

(147) Sijbesma, R. P.; Beijer, F. H.; Brunsveld, L.; Folmer, B. J.; Hirschberg, J. H.; Lange, R. F.; Lowe, J. K.; Meijer, E. W. Reversible Polymers Formed from Self-Complementary Monomers Using Quadruple Hydrogen Bonding. *Science* **1997**, *278*, 1601–1604.

(148) Mollet, B. B.; Comellas-Aragonès, M.; Spiering, A. J. H.; Söntjens, S. H. M.; Meijer, E. W.; Dankers, P. Y. W. A Modular Approach to Easily Processable Supramolecular Bilayered Scaffolds with Tailorable Properties. *J. Mater. Chem. B* **2014**, *2*, 2483–2493.

(149) Van Almen, G. C.; Talacua, H.; Ippel, B. D.; Mollet, B. B. B.; Ramaekers, M.; Simonet, M.; Smits, A. I. P. M.; Bouten, C. V. C.; Kluin, J.; Dankers, P. Y. W. Development of Non-Cell Adhesive Vascular Grafts Using Supramolecular Building Blocks. *Macromol. Biosci.* **2016**, *16*, 350–362.

(150) Pape, A. C. H.; Ippel, B. D.; Dankers, P. Y. W. Cell and Protein Fouling Properties of Polymeric Mixtures Containing Supramolecular Poly(ethylene Glycol) Additives. *Langmuir* **2017**, *33*, 4076–4082.

(151) Dankers, P. Y. W.; Harmsen, M. C.; Brouwer, L. A.; van Luyn, M. J. A.; Meijer, E. W. A Modular and Supramolecular Approach to Bioactive Scaffolds for Tissue Engineering. *Nat. Mater.* **2005**, *4*, 568–574.

(152) Zhan, W.; Shi, X.; Yu, Q.; Lyu, Z.; Cao, L.; Du, H.; Liu, Q.; Wang, X.; Chen, G.; Li, D.; et al. Bioinspired Blood Compatible Surface Having Combined Fibrinolytic and Vascular Endothelium-Like Properties via a Sequential Coimmobilization Strategy. *Adv. Funct. Mater.* **2015**, *25*, 5206–5213.

(153) Liu, Q.; Li, D.; Zhan, W.; Luan, Y.; Du, H.; Liu, X.; Brash, J. L.; Chen, H. Surfaces Having Dual Affinity for Plasminogen and Tissue Plasminogen Activator: In Situ Plasmin Generation and Clot Lysis. *J. Mater. Chem. B* **2015**, *3*, 6939–6944.

(154) Lee, W. K.; Kobayashi, J.; Ooya, T.; Park, K. I. D.; Yui, N. Synthesis and Characterization of Nitric Oxide Generative Polyrotaxane. *Polymer* **2002**, *13*, 1153–1161.

(155) Rebek Jr., J. Host–guest Chemistry of Calixarene Capsules. *Chem. Commun.* **2000**, No. 8, 637–643.

(156) Lugovskoy, E. V.; Gritsenko, P. G.; Koshel, T. A.; Koliesnik, I. O.; Cherenok, S. O.; Kalchenko, O. I.; Kalchenko, V. I.; Komisarenko, S. V. Calix[4]arene Methylenebisphosphonic Acids as Inhibitors of Fibrin Polymerization. *FEBS J.* **2011**, *278*, 1244–1251.

(157) Ji, Q.; Zhang, S.; Zhang, J.; Wang, Z.; Wang, J.; Cui, Y.; Pang, L.; Wang, S.; Kong, D.; Zhao, Q. Dual Functionalization of Poly(??-Caprolactone) Film Surface through Supramolecular Assembly with the Aim of Promoting in Situ Endothelial Progenitor Cell Attachment on Vascular Grafts. *Biomacromolecules* **2013**, *14*, 4099–4107.

(158) Webber, M. J. Engineering Responsive Supramolecular Biomaterials: Toward Smart Therapeutics. *Bioeng. Transl. Med.* **2016**, No. August, 1–15.

(159) Shi, Z.-Q.; Cai, Y.-T.; Deng, J.; Zhao, W.-F.; Zhao, C.-S. Host–Guest Self-Assembly Toward

Reversible Thermoresponsive Switching for Bacteria Killing and Detachment. *ACS Appl. Mater. Interfaces* **2016**, *8*, 23523–23532.

(160) An, Q.; Brinkmann, J.; Huskens, J.; Krabbenborg, S.; De Boer, J.; Jonkheijm, P. A Supramolecular System for the Electrochemically Controlled Release of Cells. *Angew. Chem., Int. Ed.* **2012**, *51*, 12233–12237.

(161) Boekhoven, J.; Rubertpérez, C. M.; Sur, S.; Worthy, A.; Stupp, S. I. Dynamic Display of Bioactivity through Host-Guest Chemistry. *Angew. Chem., Int. Ed.* **2013**, *52*, 12077–12080.

(162) Yan, Q.; Zhao, Y. ATP-Triggered Biomimetic Deformations of Bioinspired Receptor-Containing Polymer Assemblies. *Chem. Sci.* **2015**, *6*, 4343–4349.

(163) Webber, M. J.; Newcomb, C. J.; Bitton, R.; Stupp, S. I. Switching of Self-Assembly in a Peptide Nanostructure with a Specific Enzyme. *Soft Matter* **2011**, *7*, 9665–9672.

(164) Abul-Haija, Y. M.; Ulijn, R. V. Sequence Adaptive Peptide-Polysaccharide Nanostructures by Biocatalytic Self-Assembly. *Biomacromolecules* **2015**, *16*, 3473–3479.

(165) Holzapfel, B. M.; Reichert, J. C.; Schantz, J. T.; Gbureck, U.; Rackwitz, L.; Nöth, U.; Jakob, F.; Rudert, M.; Groll, J.; Hutmacher, D. W. How Smart Do Biomaterials Need to Be? A Translational Science and Clinical Point of View. *Adv. Drug Deliv. Rev.* **2013**, *65*, 581–603.

(166) He, M.; Jiang, H.; Wang, R.; Xie, Y.; Zhao, W.; Zhao, C. A Versatile Approach towards Multi-Functional Surfaces via Covalently Attaching Hydrogel Thin Layers. *J. Colloid Interface Sci.* **2016**, *484*, 60–69.

(167) Quilitzsch, M.; Osmond, R.; Krug, M.; Heijnen, M.; Ulbricht, M. Macro-Initiator Mediated Surface Selective Functionalization of Ultrafiltration Membranes with Anti-Fouling Hydrogel Layers Applicable to Ready-to-Use Capillary Membrane Modules. *J. Memb. Sci.* **2016**, *518*, 328–337.

(168) Stenger, M.; Klein, K.; Grønnemose, R. B.; Klitgaard, J. K.; Kolmos, H. J.; Lindholt, J. S.; Alm, M.; Thomsen, P.; Andersen, T. E. Co-Release of Dicloxacillin and Thioridazine from Catheter Material Containing an Interpenetrating Polymer Network for Inhibiting Device-Associated Staphylococcus Aureus Infection. *J. Control. Release* **2016**, *241*, 125–134.

(169) Peng, H. T.; Martineau, L.; Shek, P. N. Hydrogel-Elastomer Composite Biomaterials: I. Preparation of Interpenetrating Polymer Networks and in Vitro Characterization of Swelling Stability and Mechanical Properties. *J. Mater. Sci. Mater. Med.* **2007**, *18*, 975–986.

(170) Li, L.; Zhao, N.; Liu, S. Versatile Surface Biofunctionalization of Poly(ethylene Terephthalate) by Interpenetrating Polymerization of a Butynyl Monomer Followed By "click Chemistry." *Polymer* **2012**, *53*, 67–78.

(171) Hermans, T. M.; Broeren, M. A. C.; Gomopoulos, N.; van der Schoot, P.; van Genderen, M. H. P.; Sommerdijk, N. A. J. M.; Fytas, G.; Meijer, E. W. Self-Assembly of Soft Nanoparticles with Tunable Patchiness. *Nat. Nanotechnol.* **2009**, *4*, 721–726.

(172) Rybtchinski, B. Adaptive Supramolecular Nanomaterials Based on Strong Noncovalent Interactions. *ACS Nano* **2011**, *5*, 6791–6818.

(173) Mattia, E.; Otto, S. Supramolecular Systems Chemistry. *Nat. Nanotechnol.* **2015**, *10*, 111–119.

(174) Mosnier, L. O.; Zlokovic, B. V.; Griffin, J. H. The Cytoprotective Protein C Pathway. *Blood* **2007**, *109*, 3161–3172.

(175) Jin, L.; Abrahams, J. P.; Skinner, R.; Petitou, M.; Pike, R. N.; Carrell, R. W. The Anticoagulant Activation of Antithrombin by Heparin. *Med. Sci.* **1997**, *94*, 14683–14688.

3

Supramolecular antifouling additives for robust and efficient functionalization of elastomeric materials: molecular design matters

Abstract

The ultimate functionality of elastomeric materials can be largely influenced by the molecular design of antifouling additives that interact through directed hydrogen bonding bisurea motifs. Herein, three additives, composed of matching bisurea groups and antifouling oligo(ethylene glycol) (OEG) functionalities, are judiciously designed. The first additive is composed of one bisurea and one OEG, the second additive of one bisurea and two OEGs, and the third additive of two bisurea and one OEG. On solution-cast films, non-cell adhesive properties are dependent on the amount of incorporated OEG irrespective of the bisurea design; however, on 3D electrospun scaffolds only the additive that consists of two bisurea moieties connected via an OEG functionality ensures proper non-cell adhesive properties. Interestingly, robust non-cell adhesive properties are maintained, both with repeated cell seeding and after partial enzymatic degradation of the scaffold. These results highlight the importance of additive design in supramolecular functionalization and show that translation from simple 2D solution-cast films to 3D electrospun scaffolds is not trivial with respect to additive presentation and functionality.

The content of this chapter is based on:

Bastiaan D. Ippel, Henk M. Keizer, Patricia Y.W. Dankers, *Supramolecular antifouling additives for robust and efficient functionalization of elastomeric materials: molecular design matters,* Advanced Functional Materials 2019, 1805375

Introduction

In the fabrication of everyday polymeric materials, additives are commonly mixed with polymers to provide the materials with desired and improved properties. Well-known examples include plasticizers, stabilizers, UV-absorbers, pigments and lubricants.[1] For biomedical applications, control over the adhesion of cells and adsorption of proteins at the biomaterial surface is important to tune the response to tissue the biomaterial is exposed to.[2,3] Antifouling functionalization is often used to improve biomaterial performance to resist fouling, or to aid in specific bioactivation.[4–6] Besides covalent strategies[7–9] functional antifouling additives can be simply mixed with base polymers to create biomaterials with antifouling properties. The antifouling function is introduced either via hydrophilic compounds, such as poly and oligo(ethylene glycols),[10–15] or via hydrophobic fluorinated groups[16,17]. Interactions of such additives with the base material are important to ensure both robust incorporation and functionality through sufficient surface exposure of the functional groups. Macromolecular additives, such as amphiphilic block copolymers, in which the hydrophobic block contributes to incorporation in the base material, and hydrophilic block provides the antifouling properties, have been reported. In studies by Park et al.[12], Freij-Larsson et al.[10], and Lee et al.[11] polyurethane (PU) materials were functionalized with macromolecular additives composed of hydrophobic poly(tetrahydrofuran) PTHF or poly(propylene glycol) (PPG) blocks providing easy incorporation, and PEG functionalities for antifouling properties. The additives in the research by Tan et al.[13], Xu et al.[15], and Zhang et al.[14] had macromolecular hydrophobic blocks that matched the base materials. We propose that for biomaterials development the interaction of the additive with the base polymer should be delicately managed. When this interaction is constituted by hydrogen bonding, directionality and specificity can be introduced. A well-known class of hydrogen bonded polymers is formed by segmented PUs and poly(urethane urea)s (PUU) consisting of macromolecular soft blocks, and hard blocks that are formed by urethane and/or urea functionalities. Such materials have been used in numerous biomedical applications ranging from cardiac patches[18], heart valves[19] to vascular grafts.[20,21]

In supramolecular thermoplastic elastomers the hard-blocks, that assemble through directed hydrogen-bonding, can be specifically functionalized with supramolecular additives that have matching hard-blocks.[22] This principle has been extensively studied by our group with the fourfold hydrogen bonding ureido-pyrimidinone (UPy) moiety as a supramolecular motif.[23] UPy-based materials were modified with UPy-additives to incorporate both antifouling[24–26] and bioactive[24,27–29] functionalities. However, this approach has been left relatively unexplored in more traditional hydrogen bonded elastomeric materials. Thermoplastic elastomers with highly defined bisurea hard-blocks follow the same principle, *i.e.,* specific, robust modification via matching small-molecule bisurea additives (**Figure 3.1**).[30] Importantly, it was previously shown that additives and thermoplastic elastomers with bisurea motifs that have a different spacer length between the urea groups are able to self-sort with matching motifs.[31,32]

Here, OEG-based bisurea containing additives were judiciously designed to be incorporated in bisurea-based elastomers in order to arrive at robust antifouling materials. Comparison of three different OEG-based bisurea containing additives allows us to investigate the importance of molecular design of additives with highly specific interactions with the base

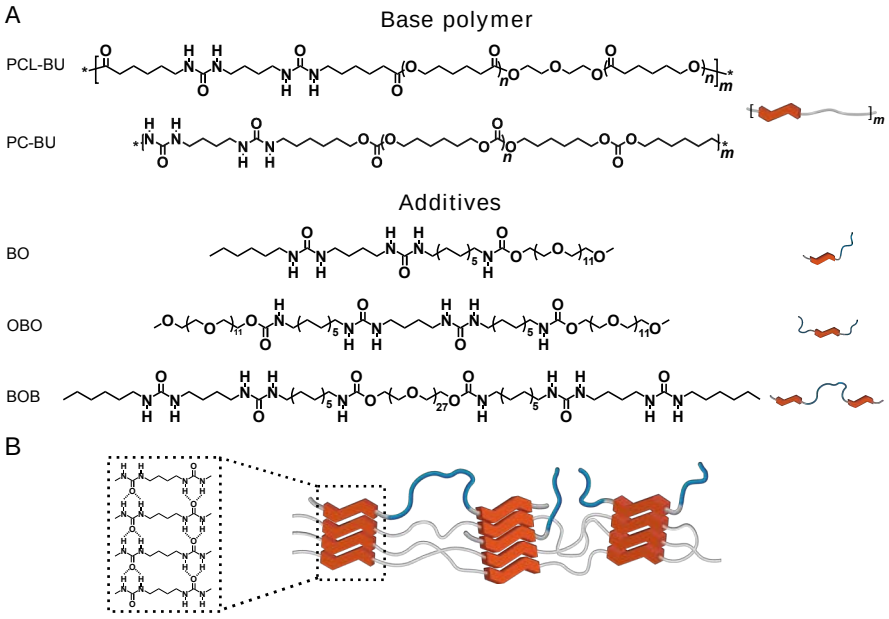

Figure 3.1. A) Structural representation of the base polymers polycaprolactone-bisurea (PCL-BU) and polycarbonate-bisurea (PC-BU), and the three additives, BU-OEG (BO), OEG-BU-OEG (OBO) and BU-OEG-BU (BOB). B) Schematic representation of self-assembly of bisurea moieties (in red) into a fibrous hard-block.

material for functional antifouling properties. First, surface properties and functionality of solution-cast thin films were assessed, followed by the characterization of functional electrospun scaffolds.

Materials design

The two urea groups in the bisurea moieties of the additives are spaced with a C_4, to match the bisurea in the base polymer (**Figure 3.1**). To further facilitate supramolecular anchoring in the base material, small hydrophobic alkyl spacers flank the bisurea motifs in the additives.

The first additive, BU-OEG (BO) is a monovalent (*i.e.*, with one bisurea moiety) additive, which comprises of one OEG chain (OEG_{12}) and one bisurea moiety. The second additive, OEG-BU-OEG (OBO), is a monovalent additive, in which the bisurea moiety is flanked by two OEG chains, equal in length to the OEG chain in BO (OEG_{12}). The third additive, BU-OEG-BU (BOB) is a bivalent additive, with an OEG chain that is approximately two times the size of the OEGs in OBO and BO (OEG_{27}), end-functionalized with two bisurea moieties.

These additive designs allow to study the effect of additive design independent from OEG concentration. The choice of soft-block of the elastomeric base polymer vastly influences the degradability of the biomaterial.[19,33] Here we have chosen to investigate the influence of both a polyester, *i.e.*, polycaprolactone (PCL), and a polycarbonate, *i.e.*, poly(hexamethylene carbonate) (PC), backbone.

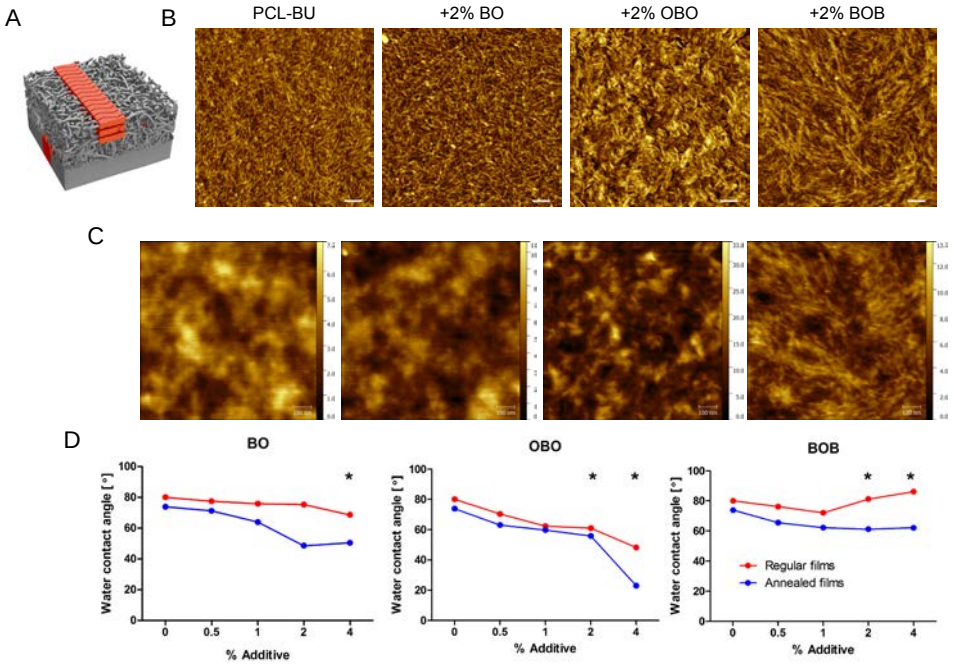

Figure 3.2. A) Schematic representation of a self-assembled nanofiber at the surface of a film. B) AFM phase micrographs of solution-cast films of PCL-BU with 2 mol% of the three additives. Scale bars represent 100 nm. C) AFM height images of PCL-BU with 2 mol% additive. The false color ruler shows height in nm. Scale bars represent 100 nm. D) Water contact angles measured on solution-cast films of PCL-BU with 0, 0.5, 1, 2, and 4 mol% of the additives. Regular films are indicated by the blue data points, water annealed films by the red data points. Non-cell adhesive solution-cast films are indicated with asterisks. Data is represented as mean ± SEM.

Solution-cast surface characterization and functionality

The effect on surface morphology of addition of the three OEG-based additives to the PCL-BU base polymer was probed using tapping mode atomic force microscopy, in which the self-assembled fibrous structure of thin films with bisurea hard blocks are visualized as brighter domains.[30,31,34,35] The pristine PCL-BU material showed characteristic fibers that are formed by organized self-assembly of the bisurea hard-blocks. (Figure 3.2). A fibrous morphology was also observed for the solution-cast films with 2 mol% of each of the additives, which suggests proper supramolecular incorporation of the additives, even though the exact morphology was different for each additive. An increase in lighter domains on the surface of the solution-cast films with BOB and especially the OBO additive indicates the presence of crystalline OEG domains. Moreover, no obvious changes were observed in the presence of OEG domains at the surface of the films with additive after annealing in aqueous environment for 24 hours (data not shown). Thus, these additives were properly incorporated in the PCL-BU base polymer and OEG presence at the surface remained stable in aqueous environment. The hydrophilicity of the solution-cast films was assessed with static water contact angle measurements, where a decreased contact angle (*i.e.,* increased hydrophilicity) can be attributed to an increase of hydrophilic OEG at the surface of the films. Increased hydrophilicity in turn is an indication of the non-cell adhesive

properties of the films.[36] The pristine material shows a contact angle of 80 ± 1°, which decreased to 48 ± 5° with 4 mol% OBO, and to 69 ± 2° with 4 mol% BO, but slightly increased to 86 ± 2° with 4 mol% BOB (Figure 3.2). Incubating the solution-cast samples in aqueous environment for 24 hours resulted in decreased contact angles for all additive concentrations, which indicates an increase in OEG at the surface of the films, as opposed to what was observed in the AFM on water annealed samples with 2 mol% additive.

Table 3.1. Atomic surface composition of solution-cast films derived from narrow scan XPS spectra.

Surface	Surface Composition [At %]		
	C	**O**	**N**
Pristine PCL-BU	76.4	22.2	1.5
+ 1% OBO	74.4	22.8	2.8
+ 2% OBO	74.1	22.4	3.5
+ 4% OBO	73.4	23.3	3.3
Pure OBO	72.2	23.6	4.3
+ 1% BOB	74.9	21.9	3.2
+ 2% BOB	73.7	20.3	6.0
+ 4% BOB	74.3	20.4	5.3
Pure BOB	69.8	24.0	6.2

Table 3.2. Quantification of components in XPS C1s narrow scan of solution-cast films of PCL-BU with the OBO and BOB additive

Scaffold	Atomic Composition [At %]				
	C-C	**C-N**	**C-O**	**O=C-O**	**O=C-N**
Pristine PCL-BU	63.9	6.6	14.4	14.1	1.0
+ 1% OBO	49.0	9.9	29.9	8.8	2.5
+ 2% OBO	40.3	12.8	36.6	7.0	3.3
+ 4% OBO	38.8	11.2	40.9	5.8	3.3
Pure OBO	31.7	14.8	45.1	4.0	4.4
+ 1% BOB	55.5	10.2	21.3	10.8	2.2
+ 2% BOB	44.8	12.4	32.4	7.3	3.0
+ 4% BOB	47.5	10.6	32.1	6.5	3.4
Pure BOB	40.2	17.9	34.4	3.3	4.3

Contractile and adhesive primary vascular derived myofibroblast-like cells, *i.e.,* human vena saphena cells, were cultured on thin films of material mixtures with 0.5, 1, 2 and 4 mol% of the additives to investigate the non-cell adhesive properties. On the pristine PCL-BU surface, and the mixtures with 0.5 or 1 mol% additive, cells adhered and displayed a clear spread morphology with a well-defined actin cytoskeleton (Figure 3.4). For the OBO and BOB, incorporation of only 2 mol% was required for significant non-cell adhesive properties, whereas the BO additive is virtually non-cell adhesive at 4 mol%. Strikingly, the hydrophilicity of those surfaces that resist cell adhesion did not differ from the surfaces

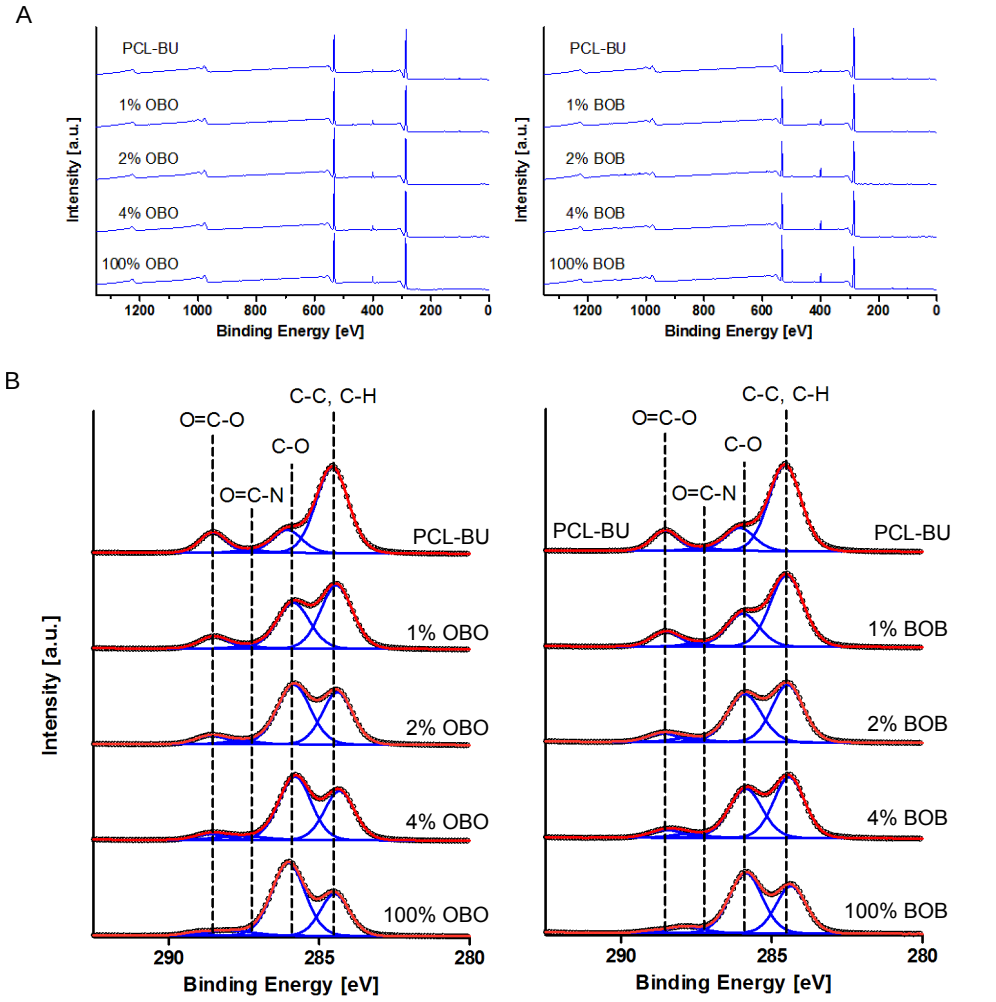

Figure 3.3. A) XPS survey spectra for solution-cast films of PCL-BU with the OBO and BOB additive. B) XPS carbon narrow scans of solution-cast films of PCL-BU with the OBO and BOB additive, and pure OBO and BOB additive, with the measured data represented by the black circles, the modelled atomic components by the blue curves, and the sum of these components by the red curve.

that do. Only upon incorporation of higher concentrations of OEG-additive, the water contact angle decreased. With X-ray photoelectron spectroscopy (XPS) an increase in nitrogen content and characteristic C-O species was observed with increasing additive concentration (**Figure 3.3**, **Table 3.1**, **Table 3.2**), which indicates increased OEG content at the surface.

Moreover, these concentrations are relatively low, in comparison to previous studies where PEG-based UPy-additives were non-covalently incorporated in UPy-functionalized materials.[24–26] In the studies by Van Almen et al. and Mollet et al., respectively, ratios of base material to additive of 90:10 and 70:30 were used for non-cell adhesive properties.[24,25] In the study by Pape et al. a ratio of 95:5 was used, but non-cell adhesive properties were

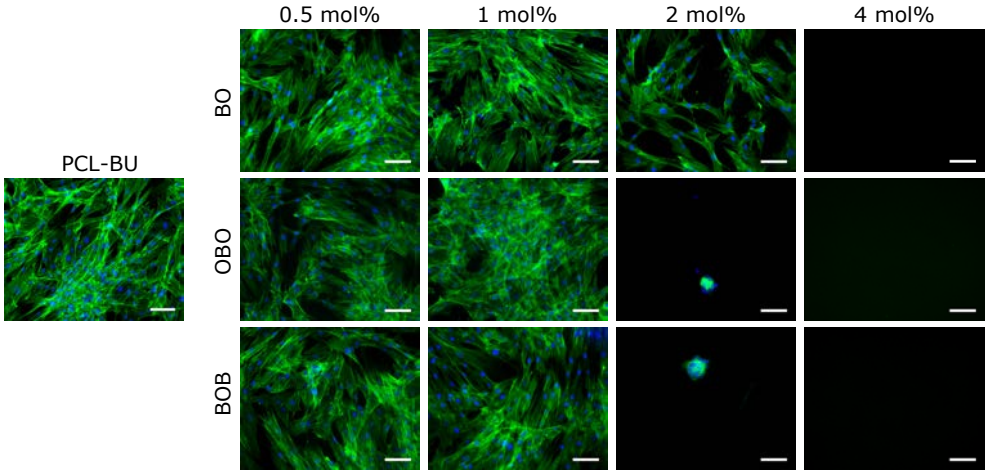

Figure 3.4. Fluorescence micrographs of HVSCs cultured on PCL-BU based solution-cast films for 24 hours. The actin cytoskeleton is presented in green, and nuclei in blue. Scale bars represent 100 µm.

less significant.[26] Incubation with culture medium for 24 hours, which would allow for adsorption of serum proteins prior to cell seeding, yielded similar results (Figure 3.5). When polycarbonate is used as the soft-block in the base material (Figure 3.1), mixtures with the three additives show similar non-cell adhesive properties (Figure 3.6). These results highlight the modularity of the material system and show efficient non-cell adhesive properties at low additive concentrations.

In conclusion, the primary screening of the OEG-based additives showed that the BOB and OBO require the lowest degree of incorporation –2 mol%– for non-cell adhesive properties, and would therefore be the candidates that are used for further processing into electrospun scaffolds. The amount of OEG seems to be the dictating factor for non-cell adhesive properties in the functionality of a single additive.

Electrospun scaffold characterization

Electrospinning of these bisurea elastomeric materials yields fibrous and porous constructs, and when deposited on a rotating mandrel can be readily fabricated into tubular vascular grafts and heart valves.[19,37,38] Since the functionalization strategy relies on non-covalent interactions, varying processing conditions can however affect the self-assembly of the polymeric materials and therefore also the incorporation of the additive and the resulting representation of the OEG-additives at the surface of the processed material. The two OEG-additives that required lower concentrations for non-cell adhesive properties were further processed into electrospun scaffolds at increased additive concentrations of 4, 10 and 20 mol%. To ensure that the changes in cell-adhesive properties can be attributed to the difference in chemical make-up of the material, the morphologies of the scaffolds should be roughly the same, since it is known that electrospun scaffold properties such as fiber diameter and porosity can have a significant effect on for instance cell spreading and proliferation, and platelet adhesion[39]. The desired fiber diameter for these scaffolds was ≤ 1 µm, to prevent cellular infiltration in the *in vitro* cell adhesion experiments. The average fiber diameter of the scaffolds ranged from 0.6 ± 0.1 µm to 0.9 ± 0.1 µm, which is relatively

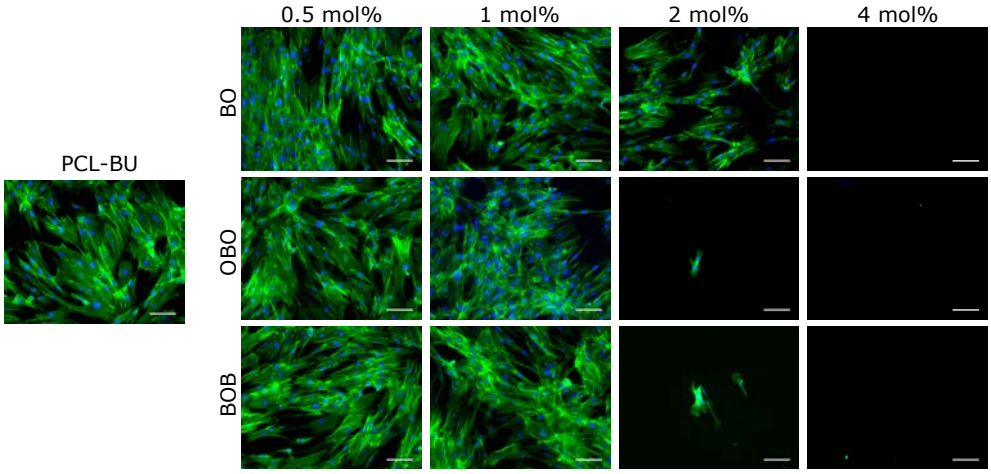

Figure 3.5. Fluorescence micrographs of HVSCs cultured on PCL-BU based solution-cast films for 24 hours, prior to which these films were incubated in growth medium for 24 hours at 37°C. The actin cytoskeleton is presented in green, and nuclei in blue. Scale bars represent 100 µm.

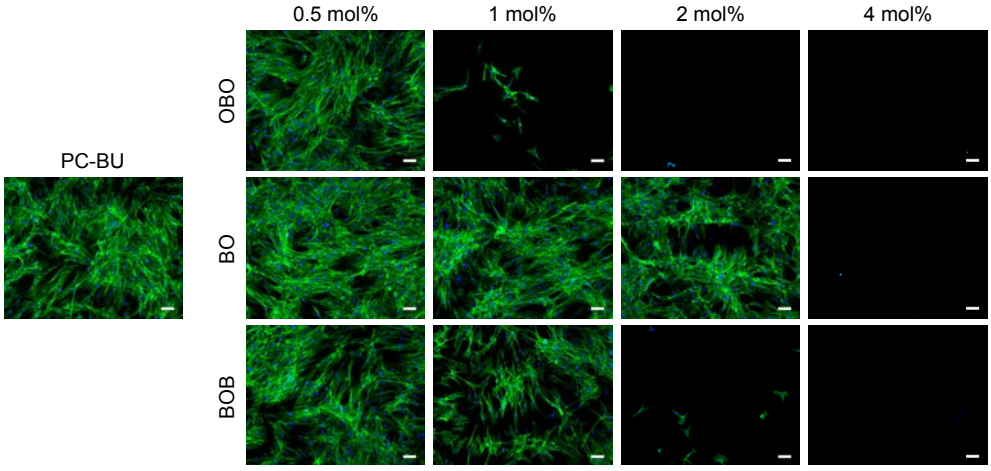

Figure 3.6. Fluorescence micrographs of HVSCs cultured on PC-BU based solution-cast films for 24 hours. The actin cytoskeleton is presented in green, and nuclei in blue. Scale bars represent 100 µm.

close to the desired 1 µm (**Table 3.3**) Moreover, the overall morphology of the fibers was smooth, no obvious surface roughness was detected with SEM (**Figure 3.7**).

Water contact angle measurements on the electrospun scaffolds showed an increased contact angle for the pristine PCL-BU mesh (128 ± 2 °), attributed to the roughness of the electrospun scaffold surface, compared to the smooth solution-cast films. All scaffolds with an additive showed very fast absorption (< 5 seconds), which made the determination of contact angles for these scaffolds impossible, but did indicate that incorporation of all concentrations of additive resulted in more hydrophilic constructs.

Similar to the solution-cast films, the surface chemistry of the electrospun scaffolds can

be assessed by means of XPS. For both the OBO and the BOB additive, an increase in the characteristic C-O component of the high-resolution carbon scan was observed, which indicates an increased OEG coverage at the surface of the fibers (Figure 3.7, Table 3.4).

Interestingly, the carbon spectrum of the 20 mol% OBO additive closely resembled the spectrum of the solution-cast film from the pure additive (**Figure 3.3**, **Figure 3.7**). For BOB however, this did not hold. This suggests that the incorporation of the two additives in the electrospun fiber is different; on the surface of the fiber more OBO than BOB additive is presented. Since the interactions that enable incorporation of the additives are non-covalent, it is detrimental that no additive leaks from the scaffold and functionality is maintained. Leakage of the additives was assessed using liquid chromatography-mass spectrometry (LC-MS). Seven days incubation of the scaffolds with 10 mol% of OBO in Milli-Q or PBS resulted in the release of 5 ± 2% or 26 ± 3% OBO, respectively. It is proposed that the presence of salts influences the leakage of the OBO additive. In contrast,

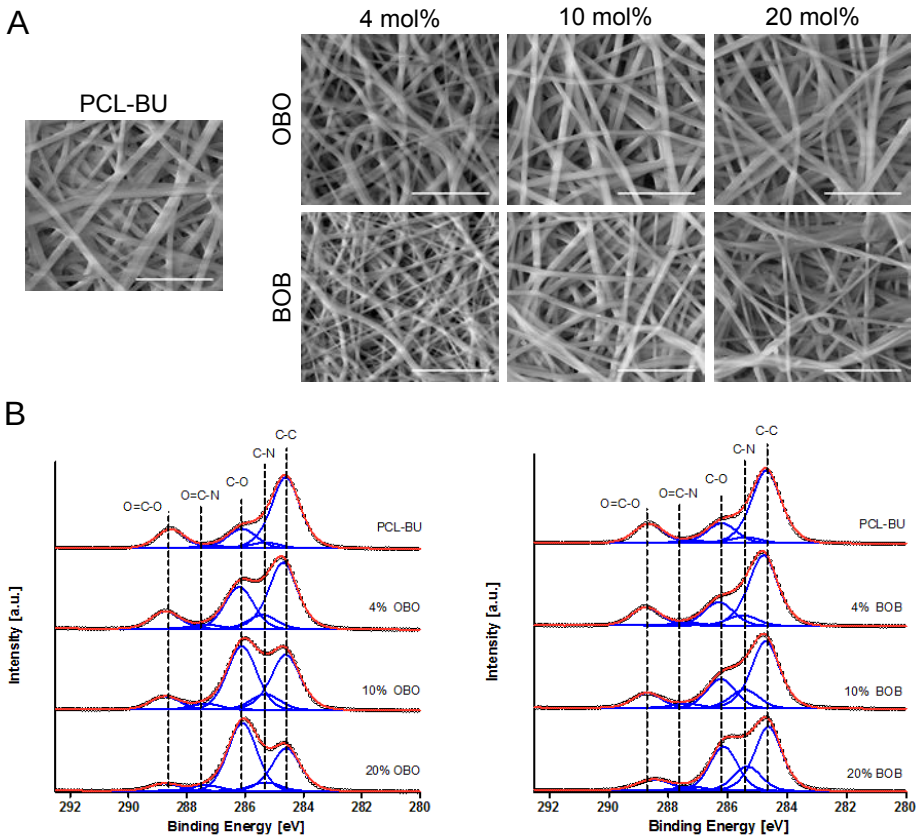

Figure 3.7. A) Scanning electron micrographs of electrospun scaffolds with 4, 10 and 20 mol% OBO and BOB additive (composite image of secondary and backscattered electrons). Scale bars represent 10 µm. B) XPS carbon spectra of electrospun scaffolds with 4, 10 and 20 mol% OBO and BOB additive. The data is presented by the black circles, the individual modelled components by blue curves (left to right, O=C-O, O=C-N, C-O, C-N, C-C) and the sum of the components, or the total fit by the red curves.

Table 3.3. Average fiber diameter of electrospun scaffolds with 4, 10, and 20 mol% BOB and OBO in PCL-BU

Material	Fiber diameter [mean ± SD]
PCL-BU	0.8 ± 0.1 µm
+ 4% OBO	0.7 ± 0.1 µm
+ 10% OBO	0.9 ± 0.1 µm
+ 20% OBO	0.8 ± 0.1 µm
+ 4% BOB	0.6 ± 0.2 µm
+ 10% BOB	0.7 ± 0.1 µm
+ 20% BOB	0.6 ± 0.1 µm

Table 3.4. Quantification of components in XPS C1s narrow scan of electrospun scaffolds of PCL-BU with the OBO and BOB additive

Scaffold	Atomic Composition [At %]				
	C-C	**C-N**	**C-O**	**O=C-O**	**O=C-N**
Pristine PCL-BU	61.7	4.7	16.0	15.6	1.9
+ 4% OBO	47.4	9.4	28.5	2.8	11.9
+ 10% OBO	37.0	10.0	40.7	3.7	8.5
+ 20% OBO	33.4	6.5	50.5	4.1	5.6
+ 4% BOB	57.3	8.1	18.2	2.2	14.2
+ 10% BOB	51.3	13.5	21.2	3.0	11.0
+ 20% BOB	44.0	15.9	28.8	2.5	8.9

the BOB additive was not detected with LC-MS after 7 days in Milli-Q and PBS, which indicates that this additive is retained in the scaffold. The cytotoxicity of the additives from the scaffold was investigated by means of a resazurin assay. This revealed that the additives had no cytotoxic effect in both direct and indirect cytoxicity assays (**Figure 3.8**).

Antifouling properties of electrospun scaffolds

Human Vena Saphena Cells show a clear spread morphology on the pristine PCL-BU scaffold (**Figure 3.9**). Upon incorporation of either 4 mol% OBO or 4 mol% BOB, the adhesion was decreased, even though patches of cells were still able to adhere, in contrast to the solution-cast films with 4 mol% additive. A striking difference between the two additives was observed in the cell adhesion on scaffolds with 10 and 20 mol% additive. Cell adhesion was reduced to a minimum on electrospun meshes with 10 and 20 mol% BOB, where non-spreading cell(-cluster)s were still present on the surfaces with 10 and 20 mol% OBO. For scaffolds with 4, 10 and 20 mol% BO, large patches of adhered cells were observed (**Figure 3.9**). Similar to the solution-cast films, the electrospun scaffolds can be fabricated with polycarbonate as the soft-block in the base polymer. The cell adhesion on

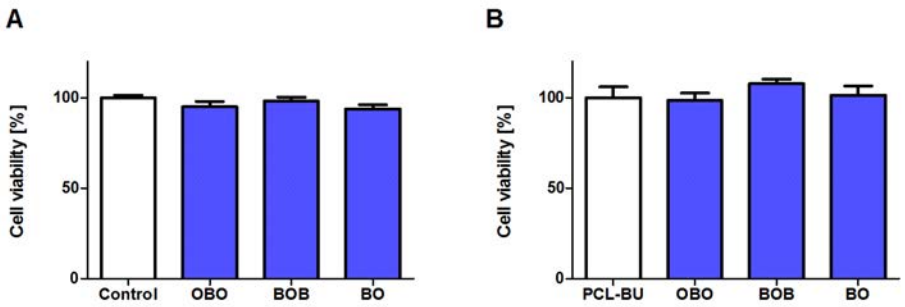

Figure 3.8. Cell viability as measured with the resazurin assay for direct cytotoxicity (A) and indirect cytotoxicity (B). Data is represented as mean ± SEM.

an electrospun scaffold of PC-BU with 10 mol% BOB was significantly decreased (**Figure 3.9**), which confirms once again the modularity of this system and the ability to tune other relevant material properties towards different applications. Interestingly, when the cells seeded on the scaffolds with 10 mol% OBO were cultured for 7 days, these were able to spread resulting in patches with spread cells on the scaffold (**Figure 3.11**), which may be attributed to the possible leakage of the OBO additive from the scaffold in a period of 7 days. The scaffold with 10 mol% BOB showed no spreading cells and retained the non-cell adhesive properties. Even when the scaffold was repeatedly seeded, up to 3 times, no spreading cell patches were observed, though the amount of rounded cell clusters slightly increased.

The material system used here has applications in vascular regeneration therapy. In this case, the material would slowly degrade *in vivo*. Since the modular approach relies on functionalization prior to processing, the bulk of the material is functionalized, apart from possible segregation during the electrospinning process. To investigate whether the non-cell adhesive functionality is retained upon degradation, cell adhesion was studied on scaffolds that were partially degraded *in vitro* with a lipase enzyme (**Figure 3.11**). The SEM images showed a different morphology in the degraded scaffolds, where the fibers on the surface in the PCL-BU scaffold were thinner and perforated, and the scaffold with additive showed more segmented fiber fragments on the surface of the scaffold. The change in surface morphology on the PCL-BU scaffold even seemed to increase the cell-adhesive properties of the material. Strikingly though, the non-cell adhesive properties of the scaffold with 10 mol% BOB was largely maintained after partial degradation of the scaffold material.

The protein fouling properties of the functionalized scaffolds was assessed on the basis of adsorption of the first three proteins from the Vroman series[40], *i.e.*, albumin, γ-globulin, and fibrinogen, that would normally be the first to adsorb from blood. Interestingly, a similar amount of protein adsorbed from a 1 mg protein mL^{-1} solution on the pristine scaffolds samples for all of the tested proteins. Albumin adsorption was significantly reduced on all scaffolds with additive, and was even reduced to below the detection limit for 10 and 20 mol% BOB incorporation (**Figure 3.9**), which nicely corresponds to the trend seen in cell adhesion on these scaffolds. However, even though the adsorption of γ-globulin and fibrinogen was drastically decreased on scaffolds upon incorporation of the additives, no clear difference in adsorption of these proteins was observed with different concentrations

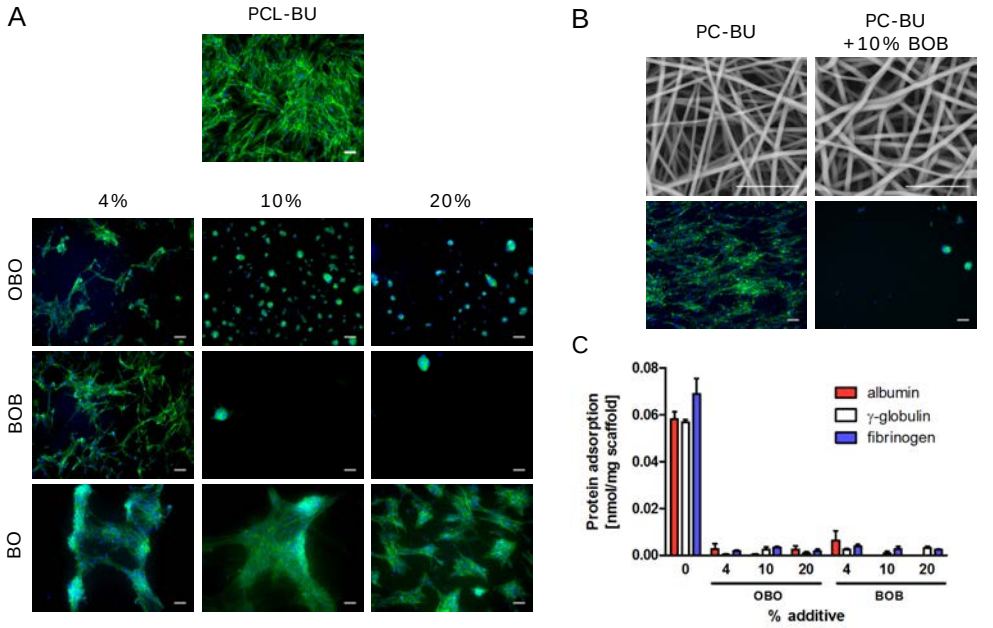

Figure 3.9. Fluorescence micrographs of HVSCs cultured for 24 hours on A) electrospun PCL-BU scaffolds with 0, 4, 10 and 20 mol% of the OBO, BOB and BO additive and B) electrospun PC-BU scaffolds with 0 and 10 mol% of the BOB additive. Actin cytoskeleton is presented in green, and nuclei in blue. Scale bars represent 100 µm. Scanning electron micrographs are included for the PC-BU based scaffolds. Scale bars in the SEM images represent 10 µm. C) Adsorption of albumin, γ-globulin and fibrinogen on electrospun scaffolds of PCL-BU with 0, 4, 10, and 20 mol% OBO and BOB additive. Data is represented as mean ± SEM.

of the two additives. Adsorption from a 10% FBS solution, which corresponds to roughly 3 mg mL^{-1} total protein (measured with Bradford Assay, data not shown), might provide results that can be better correlated to the cell adhesion studies. A decreased protein adsorption of protein was still observed for the scaffolds with additive compared to pristine PCL-BU (**Figure 3.10**). A distinct decrease in adsorption was observed when the BOB concentration was increased from 4 to 10 and 20 mol%, similar to the albumin adsorption. However, the decreased adsorption with 10 and 20 mol% did not clearly differ from the scaffolds with the OBO additive, whereas the cell adhesion did show significant differences for these two additives. Similar differences between a reduction in protein adsorption and cell adhesion was observed previously on UPy-based functionalized supramolecular surfaces, which confirms no direct correlation may be possible between quantification of protein adsorption and cell adhesion.[26]

The first obvious difference between functionalization of simple solution-cast films and electrospun scaffolds is the increased additive concentration that is required for non-cell adhesive properties. Firstly, this could be attributed to an increase in surface area to bulk volume ratio, which increases roughly 30 times. This would of course hold true for any material system that is developed on simple 2D substrates and later further processed into more complex 3D structures. However, since the increase in required additive is only 5 times, it could be hypothesized that a certain gradient of additive concentration is present from the bulk to the surface of the material, as was seen before in another supramolecular

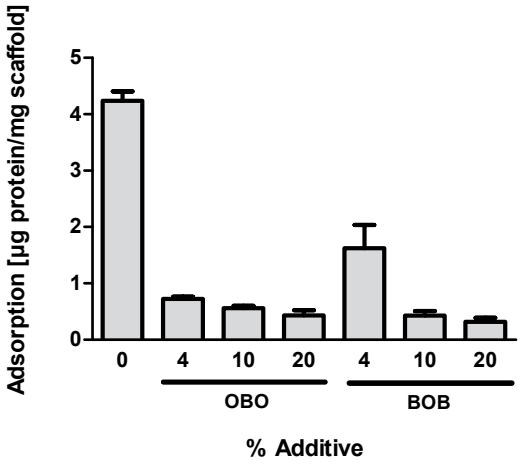

Figure 3.10. Protein adsorption from 10% fetal bovine serum in PBS, compared to an albumin standard, on electrospun scaffolds of PCL-BU with 0, 4, 10, and 20 mol% OBO and BOB additive. Data is represented as mean ± SEM

functionalization study.[41] If this gradient is present, the cross-sectional shape and surface area would influence this gradient, which is different for one solid layer and a thin electrospun fiber. For instance, the distance over which this gradient can be present is in the order of micrometers for the thin film, where this is a few hundred nanometers for the electrospun fibers.

Also the processing involved influences this distribution, which is governed by self-assembly during solvent evaporation, where for the solution-cast films the solvent is evaporated to the air, and in electrospinning, an electric field is applied while the solvent evaporates fairly fast. For the functionalized electrospun scaffolds, a clear distinction can be made between the efficacy of OBO and BOB. Even though the data from the XPS measurements points towards an increased OEG content at the surface of the electrospun fibers for both additive designs, the scaffolds with OBO are not able to prevent cell adhesion completely, whereas the BOB is able to do this. The improved non-cell adhesive properties of the BOB could be attributed to molecular design: in a study on polyethyloxazoline brushes, that were grafted to a surface in either a loop or as linear grafts, it was shown that a loop can indeed be more efficient in resisting biofouling than linear chains.[42] This finding can be attributed to the ability of hydrophilic loops to form significantly more hydrated brushes.[43] The importance of hydration has previously also been shown for OEG-based self-assembled monolayers, where the protein repelling properties depend on the conformation of the OEG chains and the resulting hydration of the monolayer. [44–46]

Interestingly, in our results the difference between additive designs was only observed in the electrospun scaffolds, where the small increments in additive concentrations in solution-cast films did not result in clear differences. In previous studies with UPy-based materials, the comparison was also made between a looped and linear configuration, or rather a monovalent and bivalent additive in terms of supramolecular motifs. In Pape et al.[26] no obvious difference was found between a bivalent PEG_{10k}diUPy and a monovalent

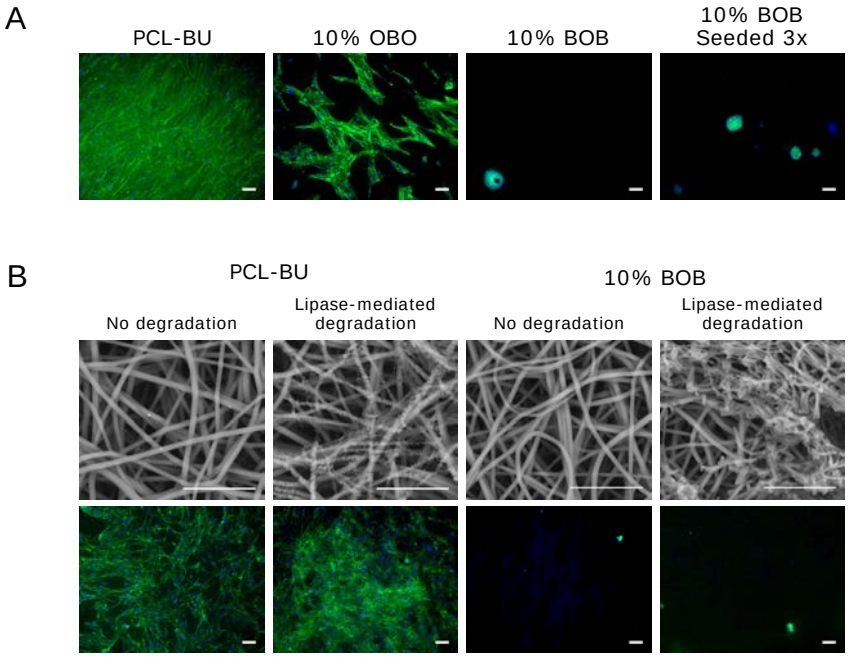

Figure 3.11. A) Fluorescence micrographs of HVSCs cultured up to 7 days on electrospun scaffolds of PCL-BU with 10 mol% OBO and BOB additive. Cells were seeded on day 0, and for the graph on the far right also on day 2 and 4. Actin cytoskeleton is presented in green, and nuclei in blue. Scale bars represent 100 µm. B) Top row: scanning electron micrographs of PCL-BU scaffolds with 0 and 10 mol% BOB, both before and after lipase-mediated degradation (only backscattered electrons). Scale bars represent 10 µm. Bottom row: Fluorescence micrographs of HVSCs cultured for 24 hours on scaffolds that have undergone lipase-mediated degradation. Scale bars represent 100 µm.

PEG_{5k}diUPy in spin-coated 2D films. In a post-modification approach however, in which molecular design has been shown to be important for functionalization efficiency[47], we have reported that bivalent PEG-additives outperformed monovalent PEG in terms of antifouling properties when the additives were reacted to the surface using a click-reaction.[48]

Besides the efficacy of antifouling functionalization, retention of the additives is paramount for proper functionality. In previously reported studies, where antifouling amphiphilic additives were incorporated, macromolecular hydrophobic blocks were used to facilitate incorporation of the additives. Either leaching of the additives was not quantified[10,13], or significant leaching of the additives was reported[11,12]. Similar to these amphiphilic *tri*-block copolymers the OBO additive reported here leaches from the base material. However, the design of the BOB additive provides proper anchoring in the base polymer through the two bisurea moieties.

Conclusions

Here we have demonstrated the feasibility of incorporation of antifouling properties in supramolecular elastomers. The robustness and functionality of the OEG-based additives is dependent on the molecular design of the additive, and therefore great care should be taken in the development of new supramolecular additives for other possible functionalities.

It is also evident that the translation from simple 2D solution-cast films to 3D electrospun scaffolds is not completely trivial in terms of additive presentation and functionality. However, a slight increase in additive concentration proved sufficient to regain non-cell adhesive functionality on the electrospun scaffolds. Even though the design of these additives was optimized for incorporation in a highly defined PCL-BU polymer, it would be interesting to apply the findings presented in this work on more generic PUU biomaterials.

Experimental section

Materials
PCL-BU and PC-BU were synthesized by SyMO-CHEM B.V. as described previously.[19,32,38] The BU-OEG, BU-OEG-BU, and OEG-BU-OEG were kindly synthesized by Henk M. Keizer from SyMO-Chem B.V.. The full description of the synthesis can be found in the publication related to this chapter.[49]

Preparation of solution-cast samples
The PCL-BU and additives were dissolved in 1,1,1,3,3,3, hexofluorisopropanol (HFIP, Sigma) at a concentration of 7.4 mM – where the molar mass of a single repeating unit, as shown in figure 1, is used - , which is equal to 20 mg mL^{-1} for the base polymer. These solutions were mixed in molar ratios PCL-BU:additive of 0.5:99.5, 1:99, 2:98, and 4:96, prior to casting 50-60 µL on 13 or 14 mm glass coverslips. The polymer films were air-dried for several hours, before final drying in vacuum overnight. For cell culture experiments, the coverslips were sterilized under UV for 15 minutes. For AFM and water contact angle experiments after water annealing, solution-cast films were incubated covered with MQ for 24 hours at 37 °C and dried to air overnight prior to the measurement.

Preparation of electrospun samples
Mixtures of PCL-BU or PC-BU and additive were simultaneously dissolved at 12% w/w in HFIP by mixing with a magnetic stirrer at room temperature overnight. The viscous solution was transferred to a 3 mL syringe, which was connected to a steel needle with an inner diameter of 0.8 mm via tubing with an inner diameter of 1 mm. An electrospinning setup by IME technologies (Geldrop, Netherlands) was used, equipped with a.o. climate control, and an antistatic module. A voltage of 25 kV was applied between the needle and a mandrel, rotating at 500 rpm. Polymer solution was extruded from the needle at a flowrate of 10-20 µL min^{-1}. The electrospun scaffolds were dried in vacuo overnight after removal from the mandrel.

Atomic Force Microscopy
A Digital Instruments Multimode Nanoscope IV, operating in the tapping mode regime, was used to record phase and height images of solution-cast films at room temperature with silicon cantilever tips (PPP-NCHR, NanoSensors^{tm}, 204-497 kHz, 10-130 N m^{-1}). Images were processed using Gwyddion software (version 2.43).

Water Contact Angle measurements
Static water contact angles were determined using an OCA30 machine (DataPhysics) at room temperature. Water droplets of 5 µL were applied and the contact angle was measured at the polymer-air-water interface at 5 seconds.

X-ray Photoelectron Spectroscopy (XPS)
XPS was performed using a Thermo Scientific K-Alpha spectrometer equipped with a monochromatic, small-spot X-ray source and a 180° double focusing hemispherical analyzer with a 128-channel detector. Coverslips were secured using double sided carbon tape and spectra were obtained using an Aluminium anode (Al Kα, 1486.7 eV, 72W). Survey scans were measured at a pass energy of 200 eV and region scans at a pass energy of 50 eV. Analysis and quantification of the spectra were performed using CasaXPS software (version 2.3.17).

Cell culture
Human vena saphena cells, which are vascular derived matrix producing myofibroblasts[50] were

harvested from the human vena saphena magna according to the Dutch guidelines for secondary use of materials. HVSCs were expanded in culture medium, which consisted of Dulbecco's modified Eagle medium (DMEM, #41966 Gibco) supplemented with 10% fetal bovine serum, 1% Glutamax (Gibco) and 1% penicillin/streptomycin, and used for experiments up to passage 7.

Cell adhesion analysis
Solution-cast films on glass were secured in adapted 12 well Transwell inserts (Corning), from which the membrane was removed and custom made PEEK rings were used to mount the samples. For the electrospun scaffolds 8 mm circular shaped samples were punched from the sheet with a biopsy punch (Kai Medical) and mounted in similarly adapted 24 well Transwell inserts. Samples were sterilized under UV on both sides for 15 minutes. Cells were collected from the culture flasks using trypsin and seeded at a concentration of 25,000 cells/cm^2 on the solution-cast films and 60,000 cells cm^{-2} for the electrospun scaffolds. For the pre-incubation, 500 µL culture medium was incubated in the inserts for 24 hours and removed just prior to seeding. For the 7 day cultures, medium was refreshed 1 and 3 days after seeding. For the repeatedly seeded samples, cells were seeded in a similar fashion on day 2 and day 4 after initial seeding. Non-adherent cells were aspirated and samples were washed twice with PBS prior to fixation with 3.7% formaldehyde. The actin cytoskeleton was stained with ATTO 488 conjugated phalloidin (Invitrogen) and nuclei with DAPI, after removal of the samples from the adapted Transwell inserts. Samples were visualized with a Zeiss Axiovert 200M fluorescence microscope.

Cytotoxicity assay
For an indirect cytotoxicity assay circular samples of PCL-BU electrospun scaffolds with 0 and 10 mol% OBO, BOB and BO additive were incubated in 1 mL culture medium for 7 days at 37 °C. For a direct cytotoxicity assay 1 mL growth medium was supplemented with the amount of additive that would be present in 1 mg of electrospun scaffold, *i.e.*, 66 µg mL^{-1} for OBO, 83 µg mL^{-1} for BOB and 41 µg mL^{-1} for BO.

HVSCs were seeded at 25,000 cells cm^{-2} in 24 wells culture plates and left to adhere in between 8 hours and overnight. The medium was changed with either the conditioned medium for indirect cytotoxicity or the additive supplemented medium for direct cytotoxicity and cells were cultured for a further 24 hours. Cell viability was determined using a resazurin assay, where cells were incubated in culture medium supplemented with 44 µM resazurin for 24 hours at 37 °C. Fluorescence of the reduced form of resazurin, resorufin, (λ_{ex} = 550 , λ_{em}= 584 nm) was measured using a Synergy HT plate reader and Gen5 software.

In vitro enzymatic degradation
Electrospun scaffold samples were mounted in the adapted 24 well Transwell inserts, similar as for regular cell culture, and incubated in milli-Q water overnight. Subsequently scaffolds were incubated overnight in 20 U/mL Lipase (from Thermomyces Lanuginosus) solution, followed by washes in milli-Q and PBS.

Scanning Electron Microscopy
Scaffolds were analyzed using a FEI Quanta 600 scanning electron microscope and Xt Microscope control software. Images were recorded in low vacuum (~0.6 mbar) with water vapor, of samples fixed on metal stubs with adhesive carbon conductive tape. Secondary and backscattered electrons were detected with an accelerating voltage of 10 kV and a working distance of 10 mm. Compound images were constructed by overlaying the resulting images from both detectors.

Additive leakage
Leakage of the OEG-additives from electrospun scaffolds was measured using analytical reversed phase high pressure liquid chromatography-mass spectrometry (LC-MS) on a system consisting of the following components: Shimadzu SCL-10A VP system controller, Shimadzu LC-10AD VP liquid chromatography pumps (with an Alltima C18 3u (50 mm x 2.1 mm) reversed phase column and gradients of water-acetonitrile supplemented with 0.1% (v/v) formic acid), a Shimadzu DGU 20A3 prominence degasser, a Thermo Finnigan surveyor autosampler, a Thermo Finnigan surveyor detector

and Thermo Scientific LCQ Fleet.

For the OBO a standard curve was prepared by dissolving OBO in PBS at 100, 10, 1, and 0.1 μg mL^{-1} and in Milli-Q supplemented with 0.1 % (v/v) Formic Acid at 100, 50, 1, 0.5, 0.1 and 0.05 μg mL^{-1}. In the PBS samples the total ion count for three hydrogen adducts ($[M+H]^+$, $[M+2H]^{2+}$, $[M+3H]^{3+}$) was determined with the genesis algorithm and for the samples in Milli-Q for three sodium adducts (($[M+Na]^+$, $[M+H+Na]^{2+}$, $[M+2H+Na]^{3+}$). Electrospun scaffolds were incubated with 1 mL PBS or Milli-Q for 7 days at 37 °C. The solutions were filtered over a 0.2 μm filter prior to the measurement.

For the BOB no standard curve could be prepared due to poor solubility. Nevertheless, the electrospun scaffolds were incubated with 1 mL PBS or Milli-Q for 7 days at 37 °C. The solutions were filtered of a 0.2 μm filter prior to measurement with LC-MS.

Protein adsorption
Adsorption of bovine serum albumin (BSA), γ-globulin, fibrinogen and 10% FBS was measured with a bicinchoninic acid assay (BCA assay, QuantiPro, Sigma). Scaffold samples were individually incubated in eppendorf tubes with PBS for 24 hours, to completely wet the scaffolds. Each scaffold was incubated in 500 μL of 1 mg mL^{-1} protein solution, or 10% FBS in PBS at 37 °C for 2 hours on a shaking table. The scaffolds were then washed three times for 5 minutes, by transferring to new Eppendorf tubes with PBS. Then the adsorbed protein was washed from the scaffolds in 500 μL 1% SDS solution at 37 °C for 2 hours and measured subsequently with the BCA assay. Amount of adsorbed protein was corrected for the initial weight of the scaffold samples. The measured adsorption of albumin, γ-globulin and fibrinogen was divided by the molecular weight of the protein.

References

(1) Al-Malaika, S.; Axtell, F.; Rothon, R.; Gilbert, M. Additives for Plastics. In *Brydson's Plastics Materials*; Elsevier, 2017; pp 127–168.

(2) Tang, L.; Thevenot, P.; Hu, W. Surface Chemistry Influences Implant Biocompatibility. *Curr. Top. Med. Chem.* **2008**, *8*, 270–280.

(3) Anderson, J. M.; Rodriguez, A.; Chang, D. T. Foreign Body Reaction to Biomaterials. *Semin. Immunol.* **2008**, *20*, 86–100.

(4) Ippel, B. D.; Dankers, P. Y. W. Introduction of Nature's Complexity in Engineered Blood-Compatible Biomaterials. *Adv. Healthc. Mater.* **2018**, *7*, 1700505.

(5) Holzapfel, B. M.; Reichert, J. C.; Schantz, J. T.; Gbureck, U.; Rackwitz, L.; Nöth, U.; Jakob, F.; Rudert, M.; Groll, J.; Hutmacher, D. W. How Smart Do Biomaterials Need to Be? A Translational Science and Clinical Point of View. *Adv. Drug Deliv. Rev.* **2013**, *65*, 581–603.

(6) Yu, Q.; Zhang, Y.; Wang, H.; Brash, J.; Chen, H. Anti-Fouling Bioactive Surfaces. *Acta Biomater.* **2011**, *7*, 1550–1557.

(7) Ye, S.; Hong, Y.; Sakaguchi, H.; Shankarraman, V.; Luketich, S. K.; D'Amore, A.; Wagner, W. R. Nonthrombogenic, Biodegradable Elastomeric Polyurethanes with Variable Sulfobetaine Content. *ACS Appl. Mater. Interfaces* **2014**, *6*, 22796–22806.

(8) Banerjee, I.; Pangule, R. C.; Kane, R. S. Antifouling Coatings: Recent Developments in the Design of Surfaces That Prevent Fouling by Proteins, Bacteria, and Marine Organisms. *Adv. Mater.* **2011**, *23*, 690–718.

(9) Harrison, R. H.; Steele, J. A. M.; Chapman, R.; Gormley, A. J.; Chow, L. W.; Mahat, M. M.; Podhorska, L.; Palgrave, R. G.; Payne, D. J.; Hettiaratchy, S. P.; et al. Modular and Versatile Spatial Functionalization of Tissue Engineering Scaffolds through Fiber-Initiated Controlled Radical Polymerization. *Adv. Funct. Mater.* **2015**, *25*, 5748–5757.

(10) Freij-Larsson, C.; Jannasch, P.; Wesslén, B. Polyurethane Surfaces Modified by Amphiphilic Polymers: Effects on Protein Adsorption. *Biomaterials* **2000**, *21*, 307–315.

(11) Lee, J. H.; Ju, Y. M.; Kim, D. M. Platelet Adhesion onto Segmented Polyurethane Film Surfaces Modified by Addition and Crosslinking of PEO-Containing Block Copolymers. *Biomaterials* **2000**, *21*, 683–691.

(12) Park, J. H.; Bae, Y. H. Physicochemical Properties and in Vitro Biocompatibility of PEO/PTMO Multiblock Copolymer/segmented Polyurethane Blends. *J. Biomater. Sci. Polym. Ed.* **2002**, *13*, 527–542.

(13) Tan, J.; L. Brash, J. Nonfouling Biomaterials Based on Polyethylene Oxide-Containing Amphiphilic Triblock Copolymers as Surface Modifying Additives: Synthesis and Characterization of Copolymers and Surface Properties of Copolymer–polyurethane Blends. *J. Appl. Polym. Sci.* **2008**, *108*, 1617–1628.

(14) Zhang, Q.; Liu, Y.; Chen, K. C.; Zhang, G.; Shi, X.; Chen, H. Surface Biocompatible Modification of Polyurethane by Entrapment of a Macromolecular Modifier. *Colloids Surf., B* **2013**, *102*, 354–360.

(15) Xu, M.; Qiu, J.; Lin, Y.; Shi, X.; Chen, H.; Xiao, T. Surface Biocompatible Modification of Polypropylene by Entrapment of Polypropylene-Block-Poly(vinylpyrrolidone). *Colloids Surf., B* **2010**, *80*, 200–205.

(16) Guex, A. G.; Weidenbacher, L.; Maniura-Weber, K.; Rossi, R. M.; Fortunato, G. Hierarchical Self-Assembly of Poly(Urethane)/Poly(Vinylidene Fluoride-Co-Hexafluoropropylene) Blends into Highly Hydrophobic Electrospun Fibers with Reduced Protein Adsorption Profiles. *Macromol. Mater. Eng.* **2017**, *302*, 1–8.

(17) Jahangir, A. R.; McClung, W. G.; Cornelius, R. M.; McCloskey, C. B.; Brash, J. L.; Santerre, J. P. Fluorinated Surface-Modifying Macromolecules: Modulating Adhesive Protein and Platelet Interactions on a Polyether-Urethane. *J. Biomed. Mater. Res.* **2002**, *60*, 135–147.

(18) Gu, X.; Matsumura, Y.; Tang, Y.; Roy, S.; Hoff, R.; Wang, B.; Wagner, W. R. Sustained Viral Gene Delivery from a Micro-Fibrous, Elastomeric Cardiac Patch to the Ischemic Rat Heart. *Biomaterials* **2017**, *133*, 132–143.

(19) Kluin, J.; Talacua, H.; Smits, A. I. P. M. P. M.; Emmert, M. Y.; Brugmans, M. C. P.; Fioretta, E. S.; Dijkman, P. E.; Söntjens, S. H. M.; Duijvelshoff, R.; Dekker, S.; et al. In Situ Heart Valve Tissue Engineering Using a Bioresorbable Elastomeric Implant – From Material Design to 12 Months Follow-up in Sheep. *Biomaterials* **2017**, *125*, 101–117.

(20) Seifalian, A. M.; Salacinski, H. J.; Tiwari, A.; Edwards, A.; Bowald, S.; Hamilton, G. In Vivo Biostability of a Poly(carbonate-Urea)urethane Graft. *Biomaterials* **2003**, *24*, 2549–2557.

(21) Hong, Y.; Ye, S. H.; Nieponice, A.; Soletti, L.; Vorp, D. A.; Wagner, W. R. A Small Diameter, Fibrous Vascular Conduit Generated from a Poly(ester Urethane)urea and Phospholipid Polymer Blend. *Biomaterials* **2009**, *30*, 2457–2467.

(22) Goor, O. J. G. M.; Hendrikse, S. I. S.; Dankers, P. Y. W.; Meijer, E. W. From Supramolecular Polymers to Multi-Component Biomaterials. *Chem. Soc. Rev.* **2017**, *46*, 6621–6637.

(23) Aida, T.; Meijer, E. W.; Stupp, S. I. Functional Supramolecular Polymers. *Science* **2012**, *335*, 813–817.

(24) Mollet, B. B.; Comellas-Aragonès, M.; Spiering, A. J. H.; Söntjens, S. H. M.; Meijer, E. W.; Dankers, P. Y. W. A Modular Approach to Easily Processable Supramolecular Bilayered Scaffolds with Tailorable Properties. *J. Mater. Chem. B* **2014**, *2*, 2483–2493.

(25) Van Almen, G. C.; Talacua, H.; Ippel, B. D.; Mollet, B. B. B.; Ramaekers, M.; Simonet, M.; Smits, A. I. P. M.; Bouten, C. V. C.; Kluin, J.; Dankers, P. Y. W. Development of Non-Cell Adhesive Vascular

Grafts Using Supramolecular Building Blocks. *Macromol. Biosci.* **2016**, *16*, 350–362.

(26) Pape, A. C. H.; Ippel, B. D.; Dankers, P. Y. W. Cell and Protein Fouling Properties of Polymeric Mixtures Containing Supramolecular Poly(ethylene Glycol) Additives. *Langmuir* **2017**, *33*, 4076–4082.

(27) Dankers, P. Y. W.; Harmsen, M. C.; Brouwer, L. A.; van Luyn, M. J. A.; Meijer, E. W. A Modular and Supramolecular Approach to Bioactive Scaffolds for Tissue Engineering. *Nat. Mater.* **2005**, *4*, 568–574.

(28) Muylaert, D. E. P.; van Almen, G. C.; Talacua, H.; Fledderus, J. O.; Kluin, J.; Hendrikse, S. I. S.; van Dongen, J. L. J.; Sijbesma, E.; Bosman, A. W.; Mes, T.; et al. Early in-Situ Cellularization of a Supramolecular Vascular Graft Is Modified by Synthetic Stromal Cell-Derived Factor-1α Derived Peptides. *Biomaterials* **2016**, *76*, 187–195.

(29) Bonito, V.; Smits, A. I. P. M.; Goor, O. J. G. M.; Ippel, B. D.; Driessen-Mol, A.; Münker, T. J. A. G.; Bosman, A. W.; Mes, T.; Dankers, P. Y. W.; Bouten, C. V. C. Modulation of Macrophage Phenotype and Protein Secretion via Heparin-IL-4 Functionalized Supramolecular Elastomers. *Acta Biomater.* **2018**, *71*, 1–23.

(30) Botterhuis, N. E.; Karthikeyan, S.; Veldman, D.; Meskers, S. C. J.; Sijbesma, R. P. Molecular Recognition in Bisurea Thermoplastic Elastomers Studied with Pyrene-Based Fluorescent Probes and Atomic Force Microscopy. *Chem. Commun.* **2008**, No. 33, 3915.

(31) Botterhuis, N. E.; Karthikeyan, S.; Spiering, A. J. H.; Sijbesma, R. P. Self-Sorting of Guests and Hard Blocks in Bisurea-Based Thermoplastic Elastomers. *Macromolecules* **2010**, *43*, 745–751.

(32) Wisse, E.; Spiering, A. J. H.; van Leeuwen, E. N. M.; Renken, R. A. E.; Dankers, P. Y. W.; Brouwer, L. A.; van Luyn, M. J. A.; Harmsen, M. C.; Sommerdijk, N. A. J. M.; Meijer, E. W. Molecular Recognition in Poly(ε-Caprolactone)-Based Thermoplastic Elastomers. *Biomacromolecules* **2006**, *7*, 3385–3395.

(33) Brugmans, M. C. P.; SÖntjens, S. H. M.; Cox, M. A. . J.; Nandakumar, A.; Bosman, A. W.; Mes, T.; Janssen, H. M.; Bouten, C. V. C.; Baaijens, F. P. T.; Driessen-Mol, A. Hydrolytic and Oxidative Degradation of Electrospun Supramolecular Biomaterials: In Vitro Degradation Pathways. *Acta Biomater.* **2015**, *27*, 21–31.

(34) Castagna, A. M.; Pangon, A.; Dillon, G. P.; Runt, J. Effect of Thermal History on the Microstructure of a Poly(tetramethylene Oxide)-Based Polyurea. *Macromolecules* **2013**, *46*, 6520–6527.

(35) Koevoets, R. A.; Versteegen, R. M.; Kooijman, H.; Spek, A. L.; Sijbesma, R. P.; Meijer, E. W. Molecular Recognition in a Thermoplastic Elastomer. *J. Am. Chem. Soc.* **2005**, *127*, 2999–3003.

(36) Chen, S.; Li, L.; Zhao, C.; Zheng, J. Surface Hydration: Principles and Applications toward Low-Fouling/nonfouling Biomaterials. *Polymer* **2010**, *51*, 5283–5293.

(37) van Haaften, E. E.; Wissing, T. B.; Rutten, M. C. M.; Bulsink, J. A.; Gashi, K.; van Kelle, M. A. J.; Smits, A. I. P. M.; Bouten, C. V. C.; Kurniawan, N. A. Decoupling the Effect of Shear Stress and Stretch on Tissue Growth and Remodeling in a Vascular Graft. *Tissue Eng., Part C* **2018**, *24*, 418–429.

(38) Duijvelshoff, R.; van Engeland, N.; Gabriels, K.; Söntjens, S.; Smits, A.; Dankers, P.; Bouten, C. Host Response and Neo-Tissue Development during Resorption of a Fast Degrading Supramolecular Electrospun Arterial Scaffold. *Bioengineering* **2018**, *5*, 61.

(39) Milleret, V.; Hefti, T.; Hall, H.; Vogel, V.; Eberli, D. Influence of the Fiber Diameter and Surface Roughness of Electrospun Vascular Grafts on Blood Activation. *Acta Biomater.* **2012**, *8*, 4349–4356.

(40) Leonard, E. F.; Vroman, L. Is the Vroman Effect of Importance in the Interaction of Blood with

Artificial Materials? *J. Biomater. Sci. Polym. Ed.* **1991**, *3*, 95–107.

(41) Goor, O. J. G. M.; Keizer, H. M.; Bruinen, A. L.; Schmitz, M. G. J.; Versteegen, R. M.; Janssen, H. M.; Heeren, R. M. A.; Dankers, P. Y. W. Efficient Functionalization of Additives at Supramolecular Material Surfaces. *Adv. Mater.* **2017**, *29*, 1604652.

(42) Morgese, G.; Trachsel, L.; Romio, M.; Divandari, M.; Ramakrishna, S. N.; Benetti, E. M. Topological Polymer Chemistry Enters Surface Science: Linear versus Cyclic Polymer Brushes. *Angew. Chem., Int. Ed.* **2016**, *55*, 15583–15588.

(43) Yan, W.; Divandari, M.; Rosenboom, J. G.; Ramakrishna, S. N.; Trachsel, L.; Spencer, N. D.; Morgese, G.; Benetti, E. M. Design and Characterization of Ultrastable, Biopassive and Lubricious Cyclic poly(2-Alkyl-2-Oxazoline) Brushes. *Polym. Chem.* **2018**, *9*, 2580–2589.

(44) Pertsin, A. J.; Grunze, M. Computer Simulation of Water near the Surface of Oligo(ethylene Glycol)-Terminated Alkanethiol Self-Assembled Monolayers. *Langmuir* **2000**, *16*, 8829–8841.

(45) Harder, P.; Grunze, M.; Dahint, R.; Whitesides, G. M.; Laibinis, P. E. Molecular Conformation in Oligo(ethylene Glycol)-Terminated Self-Assembled Monolayers on Gold and Silver Surfaces Determines Their Ability To Resist Protein Adsorption. *J. Phys. Chem. B* **1998**, *102*, 426–436.

(46) Wang, R. L. C.; Kreuzer, H. J.; Grunze, M. Molecular Conformation and Solvation of Oligo(ethylene Glycol)-Terminated Self-Assembled Monolayers and Their Resistance to Protein Adsorption. *J. Phys. Chem. B* **1997**, *101*, 9767–9773.

(47) Schulz, A.; Stocco, A.; Bethry, A.; Lavigne, J. P.; Coudane, J.; Nottelet, B. Direct Photomodification of Polymer Surfaces: Unleashing the Potential of Aryl-Azide Copolymers. *Adv. Funct. Mater.* **2018**, *28*, 1–7.

(48) Goor, O. J. G. M.; Brouns, J. E. P.; Dankers, P. Y. W. Introduction of Anti-Fouling Coatings at the Surface of Supramolecular Elastomeric Materials via Post-Modification of Reactive Supramolecular Additives. *Polym. Chem.* **2017**, *8*, 5228–5238.

(49) Ippel, B. D.; Keizer, H. M.; Dankers, P. Y. W. Supramolecular Antifouling Additives for Robust and Efficient Functionalization of Elastomeric Materials: Molecular Design Matters. *Adv. Funct. Mater.* **2019**, *29*, 1805375.

(50) Mol, A.; Rutten, M. C. M.; Driessen, N. J. B.; Bouten, C. V. C.; Zünd, G.; Baaijens, F. P. T.; Hoerstrup, S. P. Autologous Human Tissue-Engineered Heart Valves: Prospects for Systemic Application. *Circulation* **2006**, *114*, 152–159.

4

Combinatorial functionalization with bisurea-peptide and antifouling bisurea additives of a supramolecular elastomeric biomaterial

Abstract

The bioactive additive toolbox to functionalize supramolecular elastomeric materials expands rapidly. Here we have set an explorative step towards screening of complex combinatorial functionalization with antifouling and three peptide-containing additives in a bisurea-based supramolecular system. Thorough investigation of surface properties of thin films with contact angle measurements, x-ray photoelectron spectroscopy and atomic force microscopy, was correlated to cell-adhesion of endothelial and smooth muscle cells to apprehend their respective predictive values for functional biomaterial development. Peptides were presented at the surface alone, and in combinatorial functionalization with the oligo(ethylene glycol) based non-cell adhesive additive. The bisurea-RGD additive was cell-adhesive in all conditions, whereas the endothelial cell-specific bisurea-REDV showed limited bioactive properties in all chemical nano-environments. Also, aspecific functionality was observed for a bisurea-SDF1α peptide. These results emphasize that special care should be taken in changing the chemical nano-environment with peptide functionalization.

The content of this chapter is based on:

Bastiaan D. Ippel, Boris Arts, Henk M. Keizer, Patricia Y.W. Dankers, *Combinatorial functionalization with bisurea-peptide and antifouling bisurea additives of a supramolecular elastomeric biomaterial,* submitted

Introduction

Biomaterial functionalization with various bioactive cues has been studied for several decades to be able to steer cellular behaviour and positively influence the response upon implantation of the biomaterial.[1] Inspiration for the design of these cues is often taken from natural extracellular matrix components.[2] In direct approaches, extracellular matrix proteins have been used to coat or covalently functionalize biomaterials for improved bioactivity.[3,4] To induce or enhance adhesion of cells to synthetic materials, functionalization with short peptide mimics of adhesion sites in extracellular matrix proteins is a popular strategy. One of the most studied examples of such a peptide is the RGD sequence[5–9], found in for instance fibronectin and vitronectin. Besides peptides such as RGD, which induce cell adhesion in general, peptide sequences have been discovered for which specific cell types have an increased affinity over other cell types, due to increased expression of the binding motif on these cells.[2] The REDV peptide, for which endothelial cell-specificity has been reported,[10,11] attributed to binding to integrin α4β1,[11,12] has been extensively applied to enhance endothelialization of biomaterials.[13–39] In another approach, a peptide derived from stromal cell derived factor-1α (SDF1α), a chemoattractant of lymphocytes, monocytes and progenitors cells, has been applied for improved *in-situ* cellularization.[40]

Several parameters in the method of covalent tethering of peptides to a biomaterial surface influence the resulting functionality of the peptide. This includes, but is not limited to, the spacing between adhesive peptides[41], the length of the linker that is used to attach the peptide,[42–47] and the amino-acids that flank the essential peptide sequence[6], which all suggest that tuning the chemical nano-environment of peptides is of great importance for functionality of the peptides. However, a popular approach features the functionalization with both bioactive peptides, and antifouling moieties, to enhance specificity of the bioactivation and reduce adhesion of undesired entities to the functionalized biomaterial[48–51], where the chemical environment of the peptides is designed to repel any aspecific interactions.

In our group we apply a functionalization strategy based on specific supramolecular interactions,[52,53] that facilitate the non-covalent incorporation of functional additives. In the past, adhesive properties of supramolecular biomaterials were improved through incorporation of additives, including additives with peptide functionality.[54–56] Here the bisurea moiety is employed as the supramolecular motif, as an integral part of a segmented block-copolymer as the hard-segment. The mechanical properties of such hydrogen bonded elastomeric materials allow for application in biomedical applications ranging from heart valves[57] and cardiac patches[58], to vascular grafts[59–61] Bisurea-based additives have been shown to self-sort with matching motifs. [62–65] Furthermore, antifouling materials were formulated with oligo(ethylene glycol) (OEG) based bisurea additives, with a strong dependence of functionality on molecular design of the additive.[66]

Here, as a first step towards screening of bioactive supramolecular additives, using a combination of extensive surface characterization and functionality assessment, we functionalized the polycaprolactone-bisurea (PCL-BU) base material in combinatorial fashion with the best performing antifouling OEG-based bisurea additive from our previous work, BU-OEG-BU (BOB),[66], and three bioactive peptide additives. To this end three

bisurea-peptide conjugates, i.e., BU-RGD, BU-REDV, and BU-SDF1α (**Figure 4.1**), were synthesized. Solution-cast thin films of PCL-BU, mixed with BOB and BU-RGD, BU-REDV, or BU-SDF1α were characterized with water contact angle measurements (WCA), atomic force microscopy (AFM) and X-ray photoelectron spectroscopy (XPS). The cell-adhesion of vascular endothelial and smooth muscle cells was studied to gain insight in the efficacy of the incorporated BU-peptide additives, in co-formulation with the antifouling BOB. Moreover, this combinatorial approach allowed us to systematically study the functionality of the mixtures with bisurea-peptides in different supramolecular nano-environments. These results can determine the predictive value of extensive surface characterization, in view of further screening of new bioactive supramolecular additives.

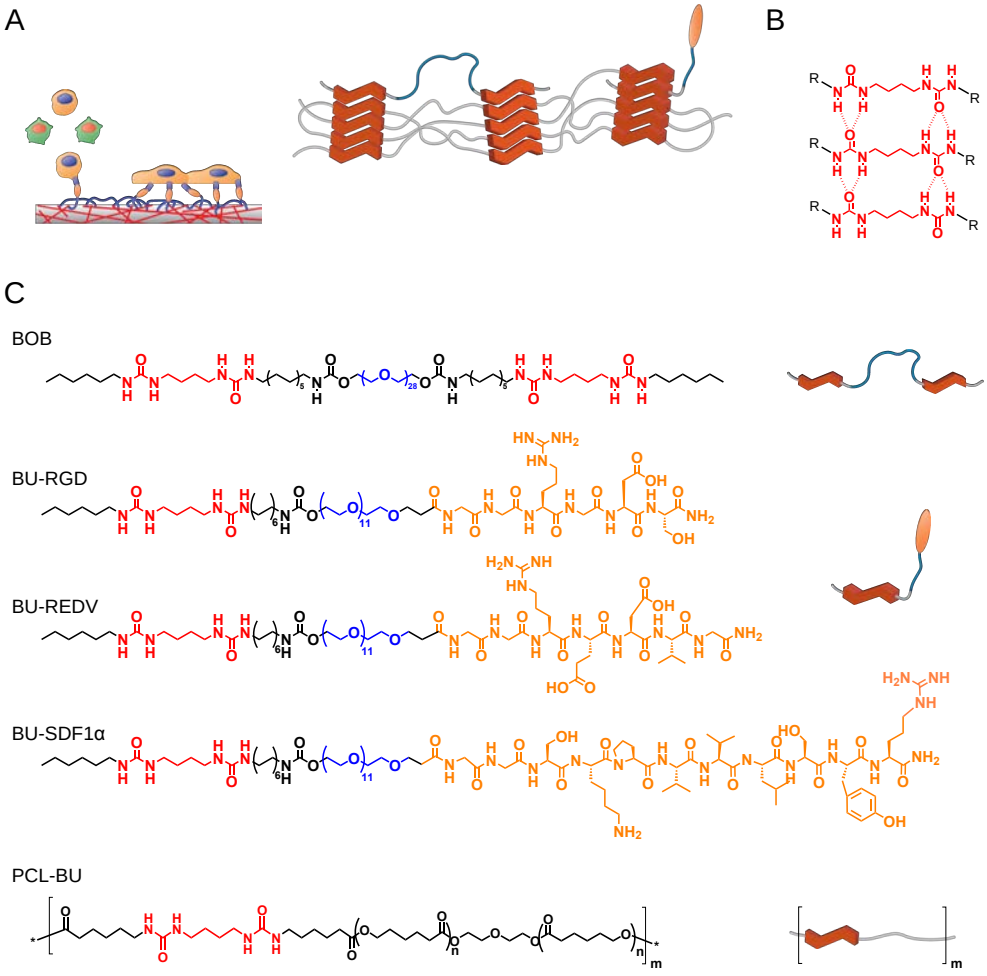

Figure 4.1. A) Schematic representation of supramolecular approach for the combinatorial functionalization of BU-peptides and BOB additives in the PCL-BU base material and the resulting cell adhesion functionality. B) Structural representation of the bifurcated hydrogen bonding pattern between bisurea moieties that facilitate the supramolecular assembly and incorporation of bisurea-containing additives. C) Structural representations of the PCL-BU base material, BU-OEG-BU (BOB) antifouling additive, and the BU-peptide conjugates (BU-RGD, BU-REDV, and BU-SDF1α).

Material toolbox

A materials toolbox was designed for the first step towards screening complex combinatorially functionalized supramolecular biomaterials, where we aimed to use structure-property relations to predict functionality for these mixtures. The bisurea-peptide conjugates were successfully synthesized with fmoc solid phase peptide synthesis and subsequent coupling of a bisurea-OEG-COOH to the N-terminus on the resin. The ethylene glycol linker should ensure proper exposure at the surface of the mixtures, and is hypothesized to facilitate better mixing in the combination with the OEG-based antifouling BOB,[67] of which the design was described previously.[66]

Surface characterization

Atomic force microscopic analysis allows for the surface morphology of the solution-cast films to be probed, which can give insight in the influence of additives on the combinatorial self-assembly with the supramolecular base material and the other additives. In phase images of the pristine PCL-BU a characteristic fibrous morphology was visible (**Figure 4.2**),[62,64,65,68] where the brighter domains were attributed to the hard-phase made up of self-assembled bisurea fibers. Upon incorporation of the non-cell adhesive BOB additive, a fibrous morphology was retained, which indicated proper incorporation of the additive in the base material. The increased presence of brighter domains such as with 2 and 4% BOB, were associated with presence of poly(ethylene glycol) at the surface, similar to previously reported results.[66] When the bisurea-peptide additives were mixed with the PCL-BU polymer, brighter domains were again observed, but here in a different capacity. For the BU-RGD and BU-SDF1α, small fibrillar structures could be resolved within the brighter domains. The BU-REDV formed larger domains, in which these fibrous structures were clearly present. In the background darker areas, the fibrous structure that resembled the pristine PCL-BU could still be detected, which was especially apparent in the surfaces with only BU-REDV. Such a fibrous morphology was not self-evident upon incorporation of a supramolecular peptide additive.[69] For all the surfaces with combinations of the BU-peptides and the BOB additive in the PCL-BU base material, the surface appeared to be saturated with additive. The fibrous morphology that was observed for the bisurea-peptides separately was retained upon combination with BOB, except for the combination of 4% BOB and 1% BU-SDF1α, where the surface was more of an amorphous nature. However, the separated domains of peptide, that were present most obvious with BU-REDV and to a lesser extent with BU-SDF1α and BU-RGD, were no longer discernible upon combination with BOB and the distribution of the additives over the surfaces was more homogeneous. In the height images the same trend was observed (**Figure 4.3**) and the nanoscale roughness of these surfaces was highest for the surfaces with only BOB, and smaller than 4 nm for all films with BU-peptide additives (**Table 4.1**). These observations indicated a retained presence of the peptides at the surface, in the case of co-formulation with the BOB additive.

WCA measurements give an indication for the macroscale hydrophilic properties of an interface. In general, functionalization with hydrophilic moieties will result in an increased hydrophilicity of the surface.[70] However, when the BOB additive was incorporated in PCL-BU previously, no increase in hydrophilicity was observed similar to what was observed

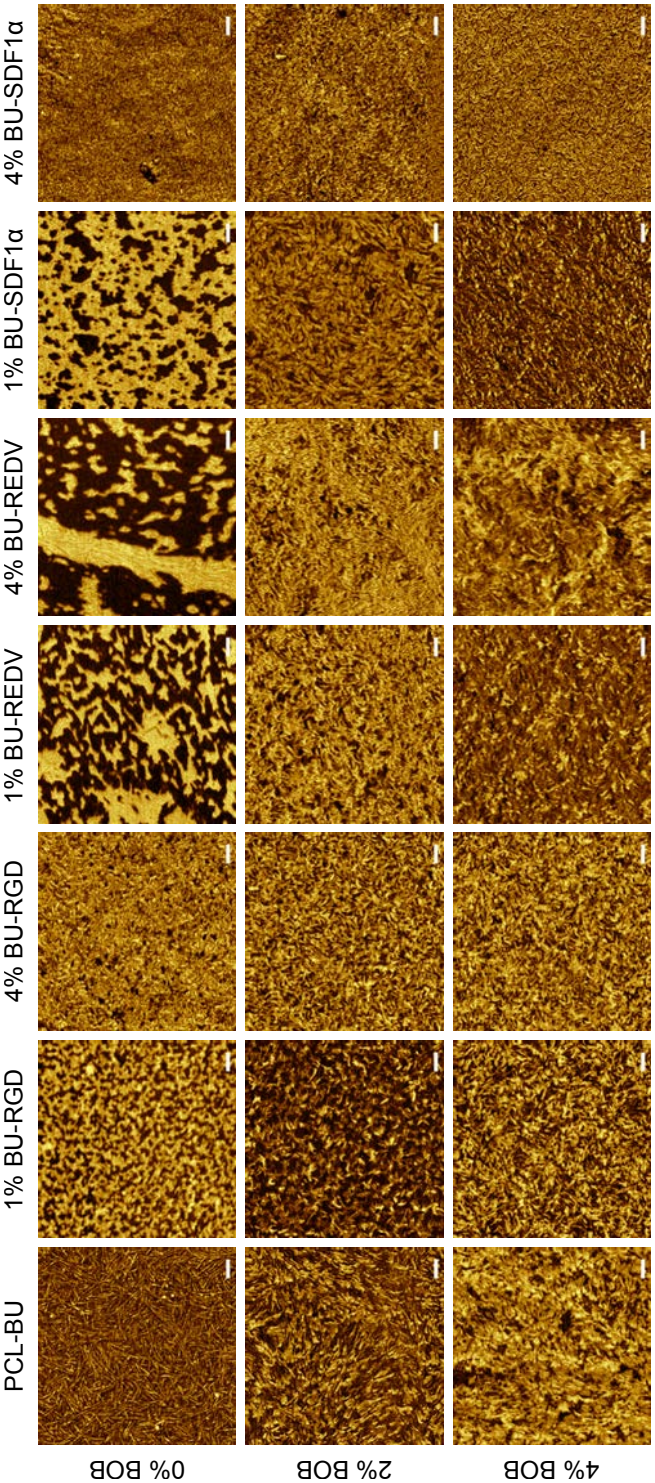

Figure 4.2. Atomic Force Microscopy phase images recorded in tapping mode in air of solution-cast films of PCL-BU with mixtures of BU-OEG-BU and the BU-peptide conjugates. Scale bars represent 100 nm.

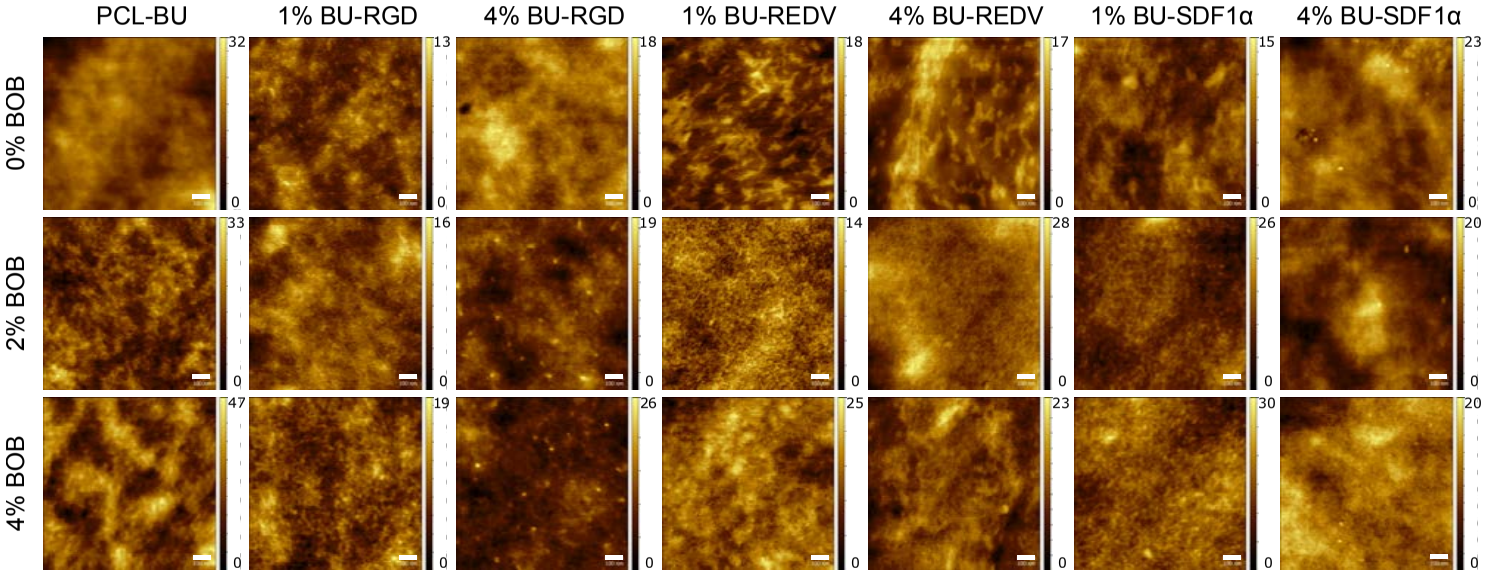

Figure 4.3. Atomic Force Microscopy height images recorded in tapping mode in air of solution-cast films of PCL-BU with mixtures of BU-OEG-BU and the BU-peptide conjugates. Scale bars represent 100 nm.

Table 4.1. RMS roughness in nm of solution-cast films of PCL-BU with mixtures of BU-OEG-BU and the BU-peptide additives

	PCL-BU	1% BU-RGD	4% BU-RGD	1% BU-REDV	4% BU-REDV	1% BU-SDF1α	4% BU-SDF1α
0% BOB	3.95	1.56	2.08	2.51	2.68	1.83	2.76
2% BOB	4.26	2.08	2.16	1.74	3.41	3.02	2.97
4% BOB	7.37	2.49	2.61	3.25	2.86	3.47	2.76

here (**Figure 4.3**).[66] The inclusion of the different BU-peptide conjugates in the PCL-BU base material led to different changes in surface hydrophilicity. Incorporation of 1 and 4% BU-RGD resulted in a stark decrease in contact angle. A similar concentration dependent decrease in contact angle resulted from the incorporation of BU-REDV, which was in line with previous efforts with REDV surface functionalization.[19,23,35,71] Interestingly, the incorporation of 1% BU-SDF1α resulted in a lower contact angle compared to 4% BU-SDF1α, which was comparable to that of pristine PCL-BU. In combination with the non-cell adhesive BOB additive, the incorporation of BU-peptide conjugates resulted in contact angles that did not deviate considerably from pristine PCL-BU, and no concentration dependence could be discerned.

Using XPS, the chemical composition of the surfaces with these self-assembled complex mixtures was investigated. In general, an increase in the contribution of nitrogen was detected upon incorporation of the additives, which could be explained by the presence of additional urea, urethane and amide bonds in both the BOB and BU-peptide additives (**Table 4.2**). More direct evidence for the presence of the peptides at the surface arose from deconvolution of the C 1s narrow scans of these surfaces, where the contribution of different carbon species was fitted (**Figure 4.4**). Evidently, the fraction of carbon species that could be attributed to O=C-N bonds, which are abundant in the backbone

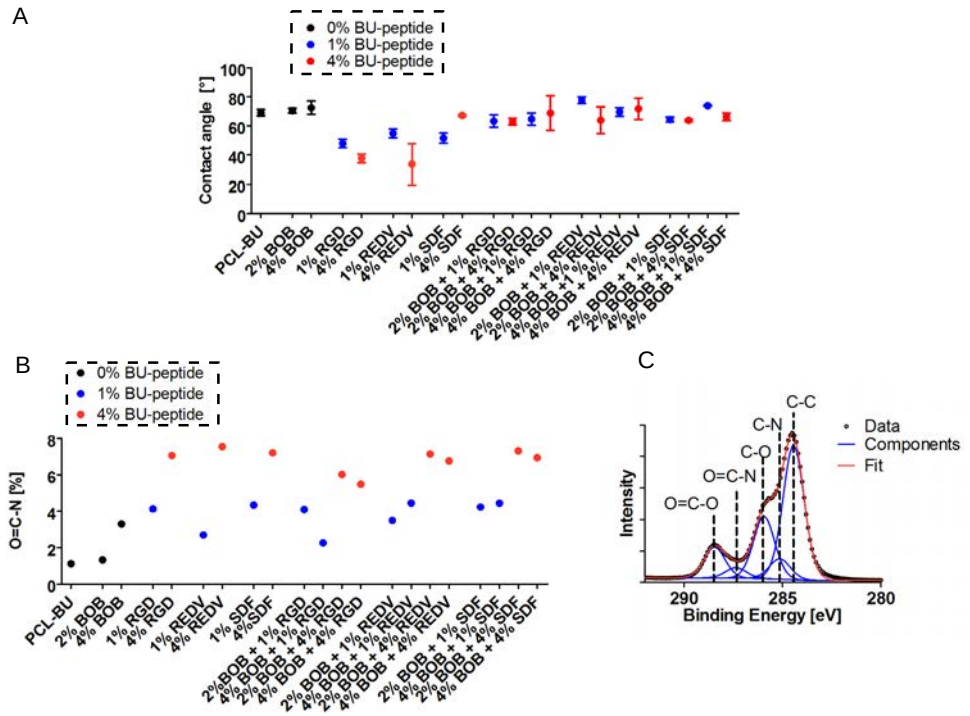

Figure 4.4. A) Water contact angles measured on solution-cast films of PCL-BU with mixtures of BU-OEG-BU and the BU-peptide conjugates. Data is represented as mean ± SD B) Quantification of fraction of O=C-N carbon species from narrow scan XPS carbon spectra. C) Example of fit in narrow scan XPS carbon spectra for PCL-BU + 1% BU-RGD. The data are represented by the black circles, the individual modelled components by blue curves and the sum of the components, or the total fit by the red curve.

Table 4.2. Elemental Composition of surface of solution-cast films of PCL-BU functionalized with mixtures of BOB and BU-peptide conjugates.

Surface	Surface Composition [at %]			Ratio
	C	**O**	**N**	**C/N**
PCL-BU	77.4	21.43	1.17	66.2
+ 2% BU-OEG-BU	75.2	22.6	2.16	34.8
+ 4% BU-OEG-BU	73.2	20.2	6.6	11.1
+ 1% BU-RGD	73.09	22.12	4.79	15.3
+ 4% BU-RGD	70.44	22.03	7.54	9.3
+ 1% BU-REDV	74.14	22.03	3.83	19.4
+ 4% BU-REDV	70.65	21.76	7.59	9.3
+ 1% BU-SDF1α	73.2	21.71	5.09	14.4
+ 4% BU-SDF1α	71.56	21.13	7.31	9.8
+ 2% BU-OEG-BU + 1% BU-RGD	72.9	21.98	5.13	14.2
+ 4% BU-OEG-BU +1% BU-RGD	75.28	21.84	2.88	26.1
+ 2% BU-OEG-BU + 4% BU-RGD	71.64	21.73	6.63	10.8
+ 4% BU-OEG-BU + 4% BU-RGD	72.58	21.66	5.76	12.6
+ 2% BU-OEG-BU + 1% BU-REDV	73.67	21.53	4.8	15.3
+ 4% BU-OEG-BU + 1% BU-REDV	72.54	21.23	6.23	11.6
+ 2% BU-OEG-BU + 4% BU-REDV	70.68	21.5	7.82	9.0
+ 4% BU-OEG-BU + 4% BU-REDV	70.71	21.33	7.96	8.9
+ 2% BU-OEG-BU + 1% BU-SDF1α	73.47	21.48	5.06	14.5
+ 4% BU-OEG-BU + 1% BU-SDF1α	72.95	20.87	6.18	11.8
+ 2% BU-OEG-BU + 4% BU-SDF1α	71.04	21.03	7.92	9.0
+ 4% BU-OEG-BU + 4% BU-SDF1α	71.24	20.74	8.02	8.9

Table 4.3. Quantification of components in XPS C1s narrow scan of solution-cast films of PCL-BU functionalized with mixtures of BOB and BU-peptide conjugates.

Surface	Carbon species				
	C-C	**C-O**	**C-N**	**O=C-N**	**O=C-O**
PCL-BU	65.17	18.05	1.05	1.12	14.61
+ 2% BU-OEG-BU	61.17	22.53	2.11	1.33	12.86
+ 4% BU-OEG-BU	45.01	36.69	7.64	3.31	7.35
+ 1% BU-RGD	51.84	24.18	7.85	4.13	12
+ 4% BU-RGD	42.5	29.04	12.11	7.07	9.27
+ 1% BU-REDV	57.14	20.62	5.78	2.7	13.75
+ 4% BU-REDV	44.32	27.49	11.29	7.56	9.34
+ 1% BU-SDF1α	54.2	22.53	7.73	4.34	11.2
+ 4% BU-SDF1α	48.29	27.22	9.33	7.22	7.95
+ 2% BU-OEG-BU + 1% BU-RGD	47.82	29.02	8.98	4.1	10.08
+ 4% BU-OEG-BU +1% BU-RGD	52.49	26.6	7.21	2.27	11.43
+ 2% BU-OEG-BU + 4% BU-RGD	42.52	31.61	11.2	6.03	8.64
+ 4% BU-OEG-BU + 4% BU-RGD	43.18	33.85	9.44	5.49	8.05
+ 2% BU-OEG-BU + 1% BU-REDV	51.12	25.96	8.35	3.5	11.06
+ 4% BU-OEG-BU + 1% BU-REDV	43.65	35.81	8.58	4.45	7.51
+ 2% BU-OEG-BU + 4% BU-REDV	43.26	30.09	11.02	7.15	8.47
+ 4% BU-OEG-BU + 4% BU-REDV	41.94	32.8	10.7	6.77	7.8
+ 2% BU-OEG-BU + 1% BU-SDF1α	51.46	25.64	8.29	4.24	10.37
+ 4% BU-OEG-BU + 1% BU-SDF1α	45.99	32.66	8.76	4.44	8.15
+ 2% BU-OEG-BU + 4% BU-SDF1α	45.93	30.47	9.37	7.32	6.91
+ 4% BU-OEG-BU + 4% BU-SDF1α	45.17	32.42	8.9	6.95	6.55

of peptides, could be correlated to the extent of the incorporation of the BU-peptide additives (**Figure 4.4, Table 4.3, Figure 4.5**), which further substantiated the determined peptide presence at the surface of these films. The C 1s component attributed to C-O that is distinctive of the ethylene glycol in both the BOB additive and the OEG linker present in the bisurea-peptide additives, increased clearly with BOB concentration, but had a poor positive correlation to amount of OEG (**Figure 4.5**) The chemical and morphological characterization of these complex material interfaces suggested a persistent exposure of the peptides at the surface, which was not negated by combinatorial self-assembly with the antifouling BOB additive. The analysis of macro-scale hydrophilic properties however could not distinguish for surfaces with or without BU-peptides.

Screening of cell-adhesive properties of complex co-formulations for endothelial and smooth muscle cells.

Human umbilical vein endothelial cells (HUVEC) and human aortic smooth muscle cells (hASMC) were cultured on the solution-cast films as a measure for the effectivity and bioactive properties of these co-assemblies of bisurea-peptide additives and antifouling BOB. On PCL-BU the HUVECs adhered and spread and showed the tendency to form small colonies (**Figure 4.6**). Upon functionalization with BOB, the adhesion and spreading of

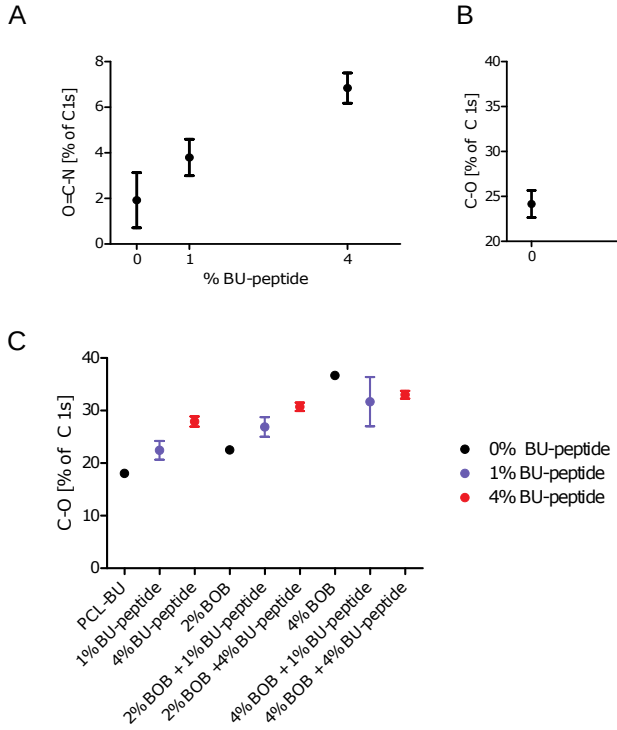

Figure 4.5. A) O=C-N component of Carbon 1s spectrum as a function of BU-peptide concentration. B) C-O component of C 1s spectrum as a function of BOB concentration, also in combination with the BU-peptide additives. C) C-O component of C 1s spectrum related to the concentration of both the antifouling and BU-peptide additives, for which the absolute amount of oligo(ethylene glycol) units increases incrementally. Data is represented as mean ± SD.

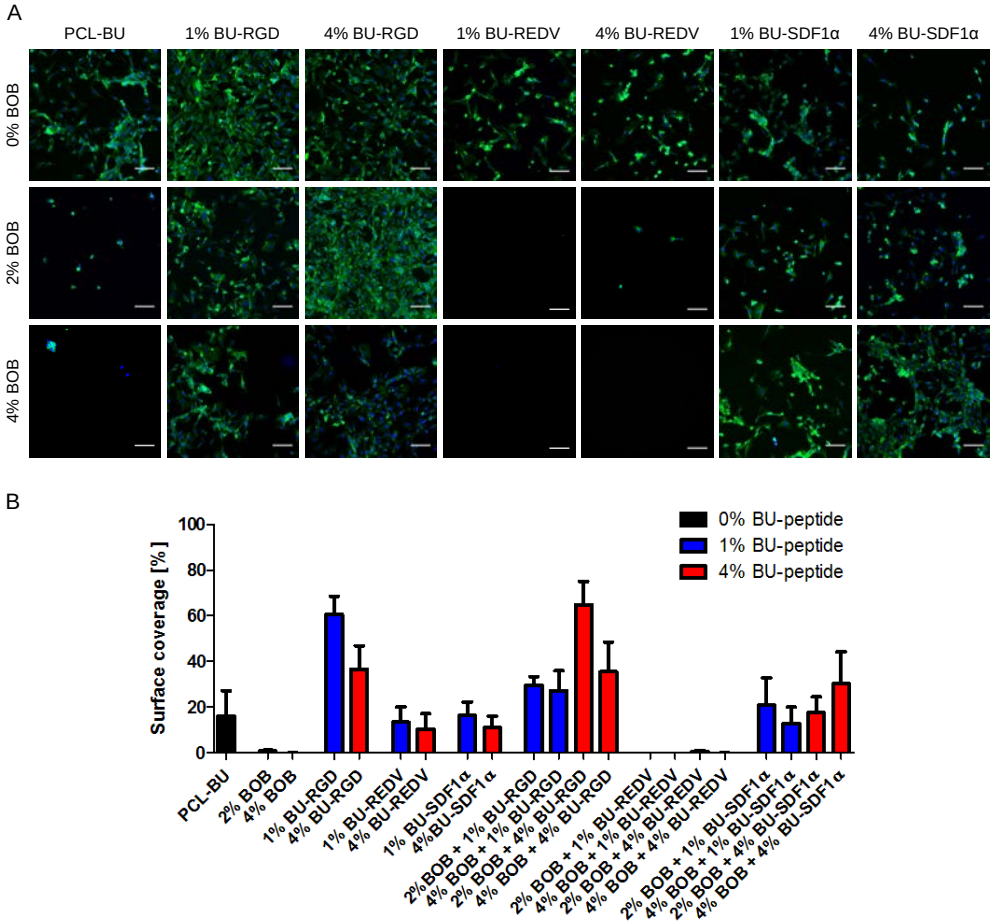

Figure 4.6. A) Fluorescence micrographs of human umbilical vein endothelial cells cultured for 24 hours on solution-cast films of PCL-BU functionalized with mixtures of anti-fouling BOB, and BU-peptide conjugates. The actin cytoskeleton is represented in green, nuclei in blue. Scale bars indicate μm. B) Surface coverage of the endothelial cells on the solution-cast films. Data is represented as mean ± SD.

HUVECs was significantly decreased, and only small clusters of rounded cells were present, similar to results on the same mixtures with a myofibroblast-like cells.[66] Incorporation of the generic cell-adhesive BU-RGD increased the adhesion and spreading of the HUVECs and more actin stress-fibers can be seen (**Figure 4.6**). Supramolecular incorporation of BU-REDV only did not improve adhesion of the HUVECs. Functionalization with 1% BU-SDF1α resulted in similar HUVEC adhesion and spreading compared to pristine PCL-BU, whereas the adhesion on surfaces with 4% BU-SDF1α may even have been slightly decreased. The adhesion of the endothelial cells to the surfaces with the mixtures of BOB and BU-SDF1α might be explained by the presence of the CXCR4 receptor on the endothelial cell membrane, even though this receptor has no obvious adhesive function for the endothelial cells.[72] Strikingly, the integrin α4β1 that has been shown to be present in endothelial cells,[11] was not able to induce cell adhesion through binding with the REDV on

the passivated BOB-functionalized surfaces. An increased concentration of 6 and 8 mol% BU-REDV, both alone and in combination with the non-cell adhesive BOB, also did not result in an increased adhesion for the endothelial cells (**Figure 4.9**)

For human Aortic Smooth Muscle cells this panel of material mixtures showed similar cell-adhesive properties, even though the adhesion on pristine PCL-BU was not particularly good. Cell spreading and adhesion was significantly decreased through incorporation of the non-cell adhesive BOB additive. The adhesive properties were efficiently restored in the combinatorial functionalization with BU-RGD, which resulted in clearly spread cells that depicted a defined actin cytoskeleton (**Figure 4.7**) Here, expectedly the functionalization with BU-REDV did not increase smooth muscle cell adhesion compared to pristine, and neither did the combination of BOB and BU-REDV result in adhesion of SMCs. However, comparable to the endothelial cells, both incorporation of BU-SDF1α alone and the composite of BU-SDF1α and BOB resulted in the adhesion of SMCs. Yet the morphology

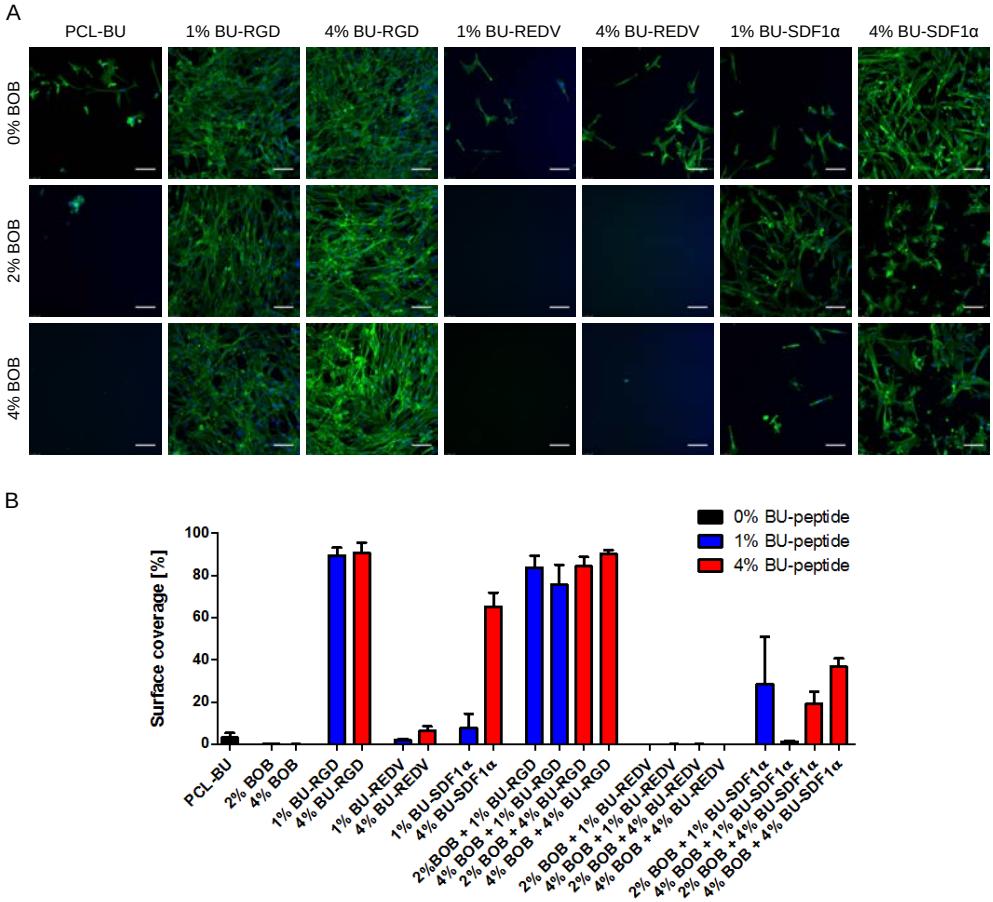

Figure 4.7. Fluorescence micrographs of human aortic smooth muscle cells cultured for 24 hours on solution-cast films of PCL-BU functionalized with mixtures of anti-fouling BU-OEG-BU and BU-peptide conjugates. The actin cytoskeleton is represented in green, nuclei in blue. Scale bars indicate 100 µm. B) Surface coverage of the smooth muscle cells on the solution-cast films. Data is represented as mean ± SD.

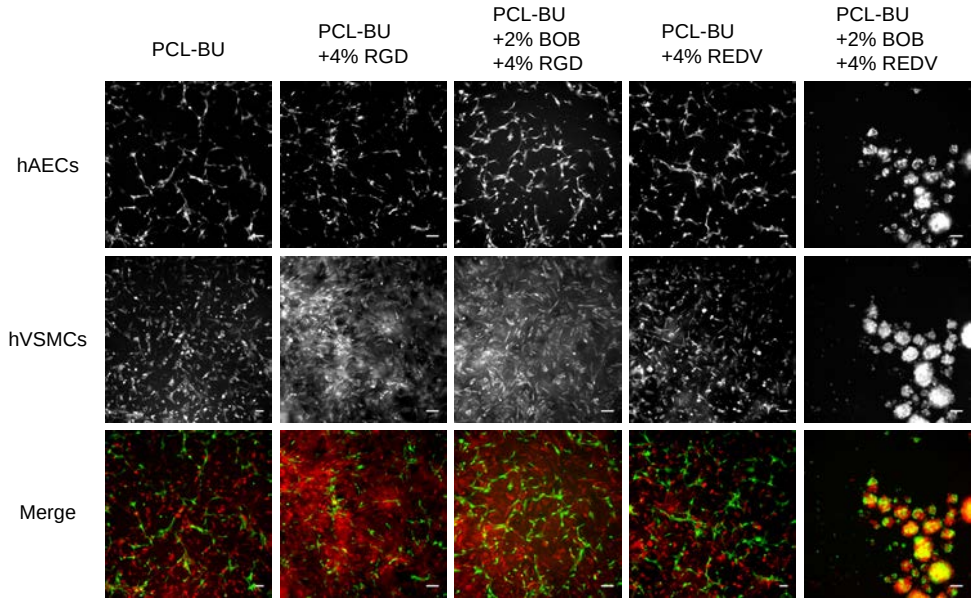

Figure 4.8. Fluorescence micrographs of endothelial cells and smooth muscle cells co-cultured on thin films op PCL-BU with Endothelial cells (top row) are stained in green and smooth muscle cells (middle row) are stained in red. Scale bars represent 100 µm.

of these cells was less spread compared to BU-RGD functionalized surfaces, and the actin cytoskeleton was less defined, which may indicate less tight attachment to the biomaterial surface. Interestingly, the amount of cells that adhered on the materials containing both BOB and BU-SDF1α showed a negative correlation to the BU-SDF1α concentration for 2% BOB, where less cells adhered on the surface with 4% BU-SDF1α compared to 1% BU-SDF1α, whereas this correlation was positive for the combination with 4% BOB, where more cells adhered with 4% BU-SDF1α compared to 1% BU-SDF1α. This observation cannot be correlated to neither the macro-scale hydrophilicity, which was comparable for all four combinations and close to that of pristine PCL-BU, nor the amount of peptide, if the O=C-N component was taken as a measure.

In the single cell-type cultures comparable adhesive behaviour was observed. Since literature states the ability of the REDV peptide to provide specificity in adhesion for endothelial cells over smooth muscle cells, a co-culture experiment was conducted. For this human Aortic Endothelial Cells were used, which showed a similar response in single culture to REDV functionalized surfaces (**Figure 4.9**), and the human aortic Smooth Muscle Cells for a more fair comparison. For pristine PCL-BU, less ECs adhere compared to the SMCs (**Figure 4.8**), which was not altered by incorporation of 4% BU-RGD, 4% BU-REDV, or the combination of 2% BOB and 4% BU-RGD. However, the adhesion of SMCs seemed to be increased for BU-RGD functionalized films. Congruent with the results for the single-cell cultures, the co-formulation of BU-REDV with BOB was not able to negate the non-cell adhesive functionality of BOB for both ECs and SMCs in co-culture.

General discussion

The modular supramolecular approach allowed for this study on the functionality and presentation of BU-peptide conjugates, both alone and in combination with the non-cell adhesive BOB additive, in varying ratios. The combination of BU-RGD and antifouling BOB in the PCL-BU base polymer resulted in surface where RGD presentation restored biofunctional properties. Cells adhered readily, despite the OEG of the BOB being present at the surface. Even though obvious differences between the co-assemblies of the BU-peptides and the BOB did not emerge from screening of their surface properties, the BU-REDV and BU-SDF1α functionalized surfaces had unequivocally different functionality in terms of cellular adhesion. Many reports in literature describe the functionalization of biomaterials with RGD peptides for increased bioactivity through improved adhesion of numerous cell types.

Numerous studies describe the functionalization of biomaterials with the RGD peptide for increased bioactivity through improved adhesion of numerous cell types,[6,9] including on materials where antifouling linkers or substrates were applied as the base.[73] Sufficient anchoring of RGD-moieties to biomaterials is a prerequisite for functionality of the peptides. Loosely bound RGD, or RGD present in solution actually inhibits adhesion.[6,11] The proper

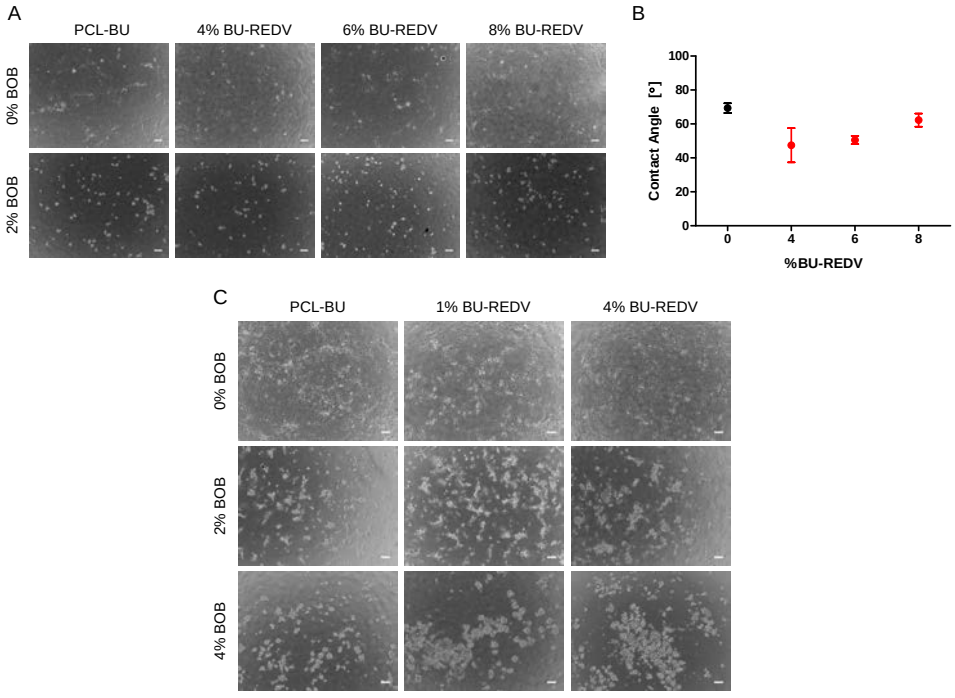

Figure 4.9. A) Phase contrast micrographs of human umbilical vein endothelial cells cultured for 24 hours on solution-cast films of PCL-BU functionalized with mixtures of 2 mol% BU-OEG-BU and increased BU-REDV concentrations. Scale bars represent 100 μm. B) Water contact angles on solution-cast films of PCL-BU with 4, 6, and 8 mol% BU-REDV. Data is represented as mean ± SD. C) Phase contrast micrographs of human Aortic Endothelial Cells cultured for 24 hours on solution-cast films of PCL-BU functionalized with mixtures of BU-OEG-BU and BU-REDV. Scale bars represent 100 μm.

attachment of both endothelial cells and smooth muscle cells in this study on the RGD functionalized material, alone and in combination with the antifouling BOB additive, shows that our supramolecular system allows for proper anchoring of peptide ligands of similar design. Surprisingly, the non-integrin binding SDF1α peptide did show refunctionalization capability. It is known that cell-binding is not necessarily integrin mediated,[74] but impaired focal adhesion formation may result in altered cellular morphology, just as was observed here for the SDF1α functionalized surfaces. Besides proper incorporation, grafting density and distribution of biomimetic adhesive ligands can influence their efficacy. For RGD grafting densities as low as 1 fmol cm^{-2} have been reported to induce cell adhesion and spreading[75] and for REDV a density of 10 pmol cm^{-2} was reported.[10] The additives and base material are self-assembled into structures described here, and therefore the peptide concentration at the surface is unknown, and would be particularly hard to quantify. However, in a system with mesoscopically similar assembly that relies on a quadruple hydrogen bonding motif, an additive with a OEG_6 spacer was shown to accumulate at the surface of the supramolecular material.[76] Theoretically, if all the incorporated peptide for 4 mol% BU-peptide is present at the surface, a density of approximately 10 nmol cm^{-2} is obtained. Note that, in the unlikely scenario where only a fraction of the incorporated additive is available at the surface, the density would still be relatively high.[21] Comparing the affinity to different peptide-functionalized surfaces is non-trivial, since the chemistry used to tether the peptide to a material, and the amino-acids that flank the principal sequence can influence this affinity. The thresh-hold for cell-spreading has been shown to be 6x higher for REDV when compared to RGD.[77] This suggested difference in ligand density required for effective functionalization with REDV, compared to RGD, may indicate a difference in affinity of integrins binding to these receptors. Moreover, half of the integrins is able to bind RGD motifs,[6] whereas REDV binding relies on the α4β1 integrin. Nonetheless, inconsistent results have been reported for the efficacy of REDV functionalization. Some studies report improved adhesion of endothelial cells, but do not compare to RGD or other peptides for functionalization,[14–20,22–24,27–30,33,34,36,39,78,79] or adhesion of other mammalian cell types.[19,20,23,26–28,32–34,36,39,71,80], or show unexpected failed refunctionalization for other cell-types with RGD[10]. Other studies also unexpectedly show reduced endothelial cell adhesion on REDV functionalized surfaces compared to RGD.[21,37,71,80–82] Yet, taking into account the concerns raised above, the comparison between different biomaterial platforms, with different functionalization chemistries, ligand densities, and experimental methods remains hampered.

Conclusion

These results serve as a reminder that in the design and fabrication of biomimetic materials we should heed to capture the complexity that is found in nature. Ligand chemical nano-environment, spacing, ordening, density and affinity all influence the cellular responses in both natural and synthetic systems. Here we have demonstrated in a combinatorial non-covalent approach that a supramolecular mixture of a polymeric base material , non-cell adhesive BOB, and the generic BU-peptide conjugate BU-RGD results in re-activated and cell adhesive surface. However, the supramolecular incorporation of BU-REDV showed little activity, whereas the BU-SDF1α exhibited aspecific functionality, both alone and in combined formulation with the BOB. These results were hard to correlate to physical and chemical properties of these surfaces, and the chemical nano-environment of the peptides,

which highlights that care should be taken with the predictive value of such read-outs for future screening purposes.

Experimental section

Materials and instrumentation
All reagents, chemicals, materials and solvents were obtained from commercial sources and were used as received. All solvents were of AR quality. In the synthetic procedures, equivalents (eq) are molar equivalents. HPLC-PDA/ESI-MS analyses were performed using a Shimadzu LC-10 AD VP series HPLC coupled to a diode array detector (Finnigan Surveyor PDA Plus detector, Thermo Electron Corporation) and an ion-trap (LCQ Fleet, Thermo Scientific), applying a 95/5 to 5/95 water/acetonitrile gradient, with this eluent always containing 0.1 v/v% formic acid.

Syntheses
PCL-BU and BU-OEG-BU were synthesized as described previously by SyMO-Chem.[60,63,66] The BU-COOH precursor and BU-SDF1α were synthesized by SyMO-Chem. GGREDVG was manually synthesized through Fmoc-based solide phase peptide synthesis. The peptide was synthesized on a Rink-amide resin (0.61 mmol g^{-1}, 50 µmol scale) in dimethylformamide (DMF) as solvent with O-(1H-6-Chlorobenzotriazole-1-yl)-1,1,3,3-tetramethyluronium hexafluorophosphate (HCTU) as activator and DIPEA as a base (4:4:16 equivalent of amino acid/HCTU/DIPEA to the resin). All amino acids were coupled in duplicate. Fmoc deprotection was achieved with 20 (v/v)% piperidine in DMF. Bisurea-carboxylic acid was coupled on the solid support to the N-terminus of the peptide with a ratio of 2:1,2:5 equivalent of BU-COOH/HATU/DIPEA to the resin. After overnight reaction bisurea-peptide was cleaved using a mixture of TFA, TIS and mQ (95/2.5/2.5 (v/v)%). The BU-peptide conjugate was obtained pure directly after synthesis indicated by HPLC-MS(ESI). TFA ions were exchanged by chloride ions *via* two cycles of dissolving the peptide in 2 mM HCl and freeze drying. Lyophilisation yielded a white powder. HPLC-MS(ESI) R_t = 5.31 min m/z calcd ($C_{78}H_{146}N_{16}O_{28}$) 1755.1 g mol^{-1}; found $[M+1H]^{1+}$ = 1756.20 g mol^{-1}, $[M+2H]^{2+}$ = 879.00 g mol^{-1}, $[M+3H]^{3+}$ = 586.42 g mol^{-1}.

Preparation of polymer films
PCL-BU and additives were dissolved in 1,1,1,3,3,3-hexafluoroisopropanol (HFIP, Fluorochem) at a concentration of 7.4 mM, where the molar mass of a single repeating unit was used for PCL-BU, which is depicted in figure 4.1. The solutions were mixed in appropriate molar ratios through the combination of volumes in the same respective ratios. This resulted in solutions of approximately 20 mg mL^{-1}, of which 25 or 50 µL was cast on 10 or 14 mm glass coverslips respectively. The films were dried to air for several hours, before final drying in vacuum overnight.

Atomic Force Microscopy
Atomic Force Microscopy was performed on a Digital Instruments Multimode Nanoscope IIIa, and a Digitial Instruments Dimension 3100 Nanoscope IIIa. Phase and height images of solution-cast films were recorded in the tapping mode regime in air at room temperature using silicon cantilever tips (PPP-NCHR). Images were processed using Gwyddion software (version 2.43), and the root mean square roughness was extracted from 1 x 1 µm height images.

X-ray Photoelectron Spectroscopy
XPS was performed using a Thermo Scientific K-Alpha spectrometer equipped with a monochromatic, small- spot X-ray source, and a 180° double focusing hemispherical analyzer with a 128-channel detector. Coverslips were secured using double sided carbon tape and spectra were obtained using an aluminum anode (Al Kα , 1486.7 eV, 72 W). Survey scans were measured at a pass energy of 200 eV and region scans at a pass energy of 50 eV. Scans were analysed using CasaXPS software (version 2.3.18). For quantification the high resolution scans of carbon, oxygen and nitrogen were used.

Water Contact Angle Measurements
An OCA30 machine (DataPhysics), operated with SCA20 software (version 4.1.13), was used to determine static water contact angles on solution-cast films at room temperature. 5 µL Milli-Q water droplets were applied to the surface through a needle and the contact angle was measured at the

polymer-air-water interface 5 seconds after deposition of the droplet.

Endothelial cell culture
Both Human Umbilical Vein Endothelial Cells (HUVEC, Lonza) and human Aortic Endothelial Cells (hAECs, Lonza) were cultured in endothelial growth medium (Lonza and PromoCell, endothelial basal medium supplemented with endothelial cell growth factors, and additional Pen/Strep for the supplemented PromoCell medium). Culture flasks were coated with 0.1% gelatin in PBS for approximately 15 minutes at 37 °C prior to seeding the cells, which were passaged before reaching 80% confluency. Cells were harvested using trypsin/EDTA and used for experiments up to passage 6.

Smooth muscle cell culture
Human aortic smooth muscle cells (hASMCs, Lonza) were cultured in smooth muscle growth medium, consisting of medium 231 supplemented with smooth muscle cell growth factors and additional Pen/Strep. Cells were harvested using trypsin/EDTA and used for experiments up to passage 5.

Cell adhesion assay
Solution-cast films on 14 mm glass coverslips were secured in an adapted Transwell as described before[66,83]and sterilized under UV for 15 minutes. Endothelial cells were seeded at a density of 40,000 cells cm^{-2} and smooth muscle cells at 25,000 cm^{-2}. 500 µL cell-suspension was used inside the inserts, and 1 mL appropriate growth medium was added outside the insert after establishing the inserts did not leak immediately. Cells were cultured for 24 hours at 37 °C and 5% CO_2, after which non-adherent cells were aspirated and the surfaces were washed with PBS with subsequent fixation in 3.7% formaldehyde. The actin-cytoskeleton was stained with ATTO488 conjugated phalloidin and nuclei were counterstained with 4′,6-diamidino-2-phenylindole (DAPI). Samples were visualized using a Leica DMi8s microscope. Furthermore, the surface covered by cells was determined by binarizing fluorescence micrographs of the phalloidin-stained samples into background and cells in ImageJ (NIH, version 1.48). The percentage of foreground pixels was used as a measure for the area occupied by cells. Three images taken with a 10x objective were measured per condition.

Endothelial Cell and Smooth Muscle Cell co-culture
HAECs and hASMCs were expanded as before. Prior to harvesting, medium was aspirated from the cells, and cells were incubated for 30 minutes with 10 µM CellTracker Green CMFDA and Orange CMTMR (Invitrogen) respectively for 30 minutes. The cells were then washed with PBS twice and harvested. Both HAECs and HASMCs were resuspended in smooth muscle cell growth medium and combined 1:1 for a total of 80,000 cells mL^{-1}. 500 µL of mixed-cell suspension was seeded on each of the coverslip, which corresponds to approximately 20,000 hAECs and 20,000 hASMCS cm^{-2}. After 24 hours of culture, the cells were visualized before and after fixation in 3.7% formaldehyde and counterstaining with DAPI using a Leica DMI8s microscope.

References

(1) Hubbell, J. A. Bioactive Biomaterials. *Curr. Opin. Biotechnol.* **1999**, *10*, 123–129.

(2) Shin, H.; Jo, S.; Mikos, A. G. Biomimetic Materials for Tissue Engineering. *Biomaterials* **2003**, *24*, 4353–4364.

(3) Wilson, C. J.; Clegg, R. E.; Ph, D.; Leavesley, D. I.; Ph, D.; Pearcy, M. J.; Ph, D. Mediation of Biomaterial – Cell Interactions by Adsorbed Proteins : A Review. **2005**, *11*.

(4) Goddard, J. M.; Hotchkiss, J. H. Ã. Polymer Surface Modification for the Attachment of Bioactive Compounds. **2007**, *32*, 698–725.

(5) Pierschbacher, M. D.; Ruoslahti, E. Cell Attachment Activity of Fibronectin Can Be Duplicated by Small Synthetic Fragments of the Molecule. *Nature* **1984**, *309*, 30–33.

(6) Hersel, U.; Dahmen, C.; Kessler, H. RGD Modified Polymers: Biomaterials for Stimulated Cell Adhesion and beyond. *Biomaterials* **2003**, *24*, 4385–4415.

(7) Perlin, L.; MacNeil, S.; Rimmer, S. Production and Performance of Biomaterials Containing RGD Peptides. *Soft Matter* **2008**, *4*, 2331–2349.

(8) Delaittre, G.; Greiner, A. M.; Pauloehrl, T.; Barner-kowollik, C.; Verne, D. P. J.; Bastmeyer, M.; Barner-kowollik, C. Chemical Approaches to Synthetic Polymer Surface Biofunctionalization for Targeted Cell Adhesion Using Small Binding Motifs. *Soft Matter* **2012**, *8*, 7323–7347.

(9) Rahmany, M. B.; Van Dyke, M. Biomimetic Approaches to Modulate Cellular Adhesion in Biomaterials: A Review. *Acta Biomater.* **2013**, *9*, 5431–5437.

(10) Hubbell, J. A.; Massia, S. P.; Desai, N. P.; Drumheller, P. D. Endothelial Cell-Selective Materials for Tissue Engineering in the Vacular Graft via a New Receptor. *Nat. Biotechnol.* **1991**, *9*, 568–572.

(11) Massia, S. P.; Hubbell, J. A. Vascular Endothelial Cell Adhesion and Spreading Promoted by the Peptide REDV of the IIICS Region of Plasma Fibronectin Is Mediated by Integrin a4b1. *J. Biol. Chem.* **1992**, *267*, 14019–14026.

(12) Mould, A. P.; Komoriya, A.; Yamada, K. M.; Humphries, M. J. The CS5 Peptide Is a Second Site in the IIICS Region of Fibronectin Recognized by the Integrin α4β1: Inhibition of α4β1function by RGD Peptide Homologues. *J. Biol. Chem.* **1991**, *266*, 3579–3585.

(13) Park, C. H.; Hong, Y. J.; Park, K.; Han, D. K. Peptide-Grafted Lactide-Based Poly(ethylene Glycol) Porous Scaffolds for Specific Cell Adhesion. *Macromol. Res.* **2010**, *18*, 526–532.

(14) Ji, Y.; Wei, Y.; Liu, X.; Wang, J.; Ren, K.; Ji, J. Zwitterionic Polycarboxybetaine Coating Functionalized with REDV Peptide to Improve Selectivity for Endothelial Cells. *J. Biomed. Mater. Res., Part A* **2012**, *100 A*, 1387–1397.

(15) Lin, Q. K.; Hou, Y.; Ren, K. F.; Ji, J. Selective Endothelial Cells Adhesion to Arg-Glu-Asp-Val Peptide Functionalized Polysaccharide Multilayer. *Thin Solid Films* **2012**, *520*, 4971–4978.

(16) Wei, Y.; Ji, Y.; Xiao, L.-L.; Lin, Q.; Xu, J.; Ren, K.; Ji, J. Surface Engineering of Cardiovascular Stent with Endothelial Cell Selectivity for in Vivo Re-Endothelialisation. *Biomaterials* **2013**, *34*, 2588–2599.

(17) Liu, Y.; Yang Tan, T. T.; Yuan, S.; Choong, C. Multifunctional P(PEGMA)-REDV Conjugated Titanium Surfaces for Improved Endothelial Cell Selectivity and Hemocompatibility. *J. Mater. Chem. B* **2013**, *1*, 157–167.

(18) Yang, J.; Khan, M.; Zhang, L.; Ren, X.; Guo, J.; Feng, Y.; Wei, S.; Zhang, W. Antimicrobial Surfaces Grafted Random Copolymers with REDV Peptide Beneficial for Endothelialization. *J. Mater. Chem. B* **2015**, *3*, 7682–7697.

(19) Yuan, S.; Xiong, G.; He, F.; Jiang, W.; Liang, B.; Choong, C. Multifunctional REDV-Conjugated Zwitterionic Polycarboxybetaine-Polycaprolactone Hybrid Surfaces for Enhanced Antibacterial Activity, Anti-Thrombogenicity and Endothelial Cell Proliferation. *J. Mater. Chem. B* **2015**, *3*, 8088–8101.

(20) Castellanos, M. I.; Zenses, A. S.; Grau, A.; Rodríguez-Cabello, J. C.; Gil, F. J.; Manero, J. M.; Pegueroles, M. Biofunctionalization of REDV Elastin-like Recombinamers Improves Endothelialization on CoCr Alloy Surfaces for Cardiovascular Applications. *Colloids Surf., B* **2015**, *127*, 22–32.

(21) Noel, S.; Hachem, A.; Merhi, Y.; De Crescenzo, G. Development of a Polyester Coating Combining Antithrombogenic and Cell Adhesive Properties: Influence of Sequence and Surface Density of Adhesion Peptides. *Biomacromolecules* **2015**, *16*, 1682–1694.

(22) Wang, Y.; Chen, S.; Pan, Y.; Gao, J.; Tang, D.; Kong, D.; Wang, S. Rapid in Situ Endothelialization of a Small Diameter Vascular Graft with Catalytic Nitric Oxide Generation and Promoted Endothelial Cell Adhesion. *J. Mater. Chem. B* **2015**, *3*, 9212–9222.

(23) Kakinoki, S.; Yamaoka, T. Single-Step Immobilization of Cell Adhesive Peptides on a Variety of Biomaterial Substrates via Tyrosine Oxidation with Copper Catalyst and Hydrogen Peroxide. *Bioconjugate Chem.* **2015**, *26*, 639–644.

(24) Zhan, W.; Shi, X.; Yu, Q.; Lyu, Z.; Cao, L.; Du, H.; Liu, Q.; Wang, X.; Chen, G.; Li, D.; et al. Bioinspired Blood Compatible Surface Having Combined Fibrinolytic and Vascular Endothelium-Like Properties via a Sequential Coimmobilization Strategy. *Adv. Funct. Mater.* **2015**, *25*, 5206–5213.

(25) Wei, Y.; Zhang, J. xun; Ji, Y.; Ji, J. REDV/Rapamycin-Loaded Polymer Combinations as a Coordinated Strategy to Enhance Endothelial Cells Selectivity for a Stent System. *Colloids Surf., B* **2015**, *136*, 1166–1173.

(26) Zhou, F.; Jia, X.; Yang, Y.; Yang, Q.; Gao, C.; Zhao, Y.; Fan, Y.; Yuan, X. Peptide-Modified PELCL Electrospun Membranes for Regulation of Vascular Endothelial Cells. *Mater. Sci. Eng. C* **2016**, *68*, 623–631.

(27) Gabriel, M.; Niederer, K.; Becker, M.; Raynaud, C. M.; Vahl, C. F.; Frey, H. Tailoring Novel PTFE Surface Properties: Promoting Cell Adhesion and Antifouling Properties via a Wet Chemical Approach. *Bioconjugate Chem.* **2016**, *27*, 1216–1221.

(28) Butruk-Raszeja, B. a.; Dresler, M. S.; Ku??mi??ska, A.; Ciach, T. Endothelialization of Polyurethanes: Surface Silanization and Immobilization of REDV Peptide. *Colloids Surf., B* **2016**, *144*, 335–343.

(29) Yu, S.; Gao, Y.; Mei, X.; Ren, T.; Liang, S.; Mao, Z.; Gao, C. Preparation of an Arg-Glu-Asp-Val Peptide Density Gradient on Hyaluronic Acid-Coated Poly(μ-Caprolactone) Film and Its Influence on the Selective Adhesion and Directional Migration of Endothelial Cells. *ACS Appl. Mater. Interfaces* **2016**, *8*, 29280–29288.

(30) Wei, Y.; Zhang, J.; Feng, X.; Liu, D. Bioactive Zwitterionic Polymer Brushes Grafted from Silicon Wafers via SI-ATRP for Enhancement of Antifouling Properties and Endothelial Cell Selectivity. *J. Biomater. Sci. Polym. Ed.* **2017**, *28*, 2101–2116.

(31) Castellanos, M. I.; Mas-Moruno, C.; Grau, A.; Serra-Picamal, X.; Trepat, X.; Albericio, F.; Joner, M.; Gil, F. J.; Ginebra, M. P.; Manero, J. M.; et al. Functionalization of CoCr Surfaces with Cell Adhesive Peptides to Promote HUVECs Adhesion and Proliferation. *Appl. Surf. Sci.* **2017**, *393*, 82–92.

(32) Kambe, Y.; Murakoshi, A.; Urakawa, H.; Kimura, Y.; Yamaoka, T. Vascular Induction and Cell Infiltration into Peptide-Modified Bioactive Silk Fibroin Hydrogels. *J. Mater. Chem. B* **2017**, *5*, 7557–7571.

(33) Li, Z.; Zhou, P.; Zhou, F.; Zhao, Y.; Ren, L.; Yuan, X. Antimicrobial Eugenol-Loaded Electrospun Membranes of Poly(ε-Caprolactone)/gelatin Incorporated with REDV for Vascular Graft Applications. *Colloids Surf., B* **2018**, *162*, 335–344.

(34) Kakinoki, S.; Takasaki, K.; Mahara, A.; Ehashi, T.; Hirano, Y.; Yamaoka, T. Direct Surface Modification of Metallic Biomaterials via Tyrosine Oxidation Aiming to Accelerate the Re-Endothelialization of Vascular Stents. *J. Biomed. Mater. Res., Part A* **2018**, *106*, 491–499.

(35) Ding, X.; Chin, W.; Lee, C. N.; Hedrick, J. L.; Yang, Y. Y. Peptide-Functionalized Polyurethane Coatings Prepared via Grafting-To Strategy to Selectively Promote Endothelialization. *Adv. Healthcare Mater.* **2018**, *7*, 1–9.

(36) Zhou, F.; Wen, M.; Zhou, P.; Zhao, Y.; Jia, X.; Fan, Y.; Yuan, X. Electrospun Membranes of PELCL/PCL-REDV Loading with miRNA-126 for Enhancement of Vascular Endothelial Cell Adhesion and Proliferation. *Mater. Sci. Eng. C* **2018**, *85*, 37–46.

(37) Colak, B.; Di Cio, S.; Gautrot, J. E.; Cio, S. Di; Gautrot, J. E. Biofunctionalized Patterned Polymer Brushes via Thiol-Ene Coupling for the Control of Cell Adhesion and the Formation of Cell Arrays. *Biomacromolecules* **2018**, *19*, 1445–1455.

(38) Flora, T.; de Torre, I. G.; Quintanilla, L.; Alonso, M.; Rodríguez-Cabello, J. C. Spatial Control and

Cell Adhesion Selectivity on Model Gold Surfaces Grafted with Elastin-like Recombinamers. *Eur. Polym. J.* **2018**, *106*, 19–29.

(39) Devalliere, J.; Chen, Y.; Dooley, K.; Yarmush, M. L.; Uygun, B. E. Improving Functional Re-Endothelialization of Acellular Liver Scaffold Using REDV Cell-Binding Domain. *Acta Biomater.* **2018**, *78*, 151–164.

(40) Muylaert, D. E. P.; van Almen, G. C.; Talacua, H.; Fledderus, J. O.; Kluin, J.; Hendrikse, S. I. S.; van Dongen, J. L. J.; Sijbesma, E.; Bosman, A. W.; Mes, T.; et al. Early in-Situ Cellularization of a Supramolecular Vascular Graft Is Modified by Synthetic Stromal Cell-Derived Factor-1α Derived Peptides. *Biomaterials* **2016**, *76*, 187–195.

(41) Massia, S. P. An RGD Spacing of 440 Nm Is Sufficient for Integrin Alpha V Beta 3- Mediated Fibroblast Spreading and 140 Nm for Focal Contact and Stress Fiber Formation. *J. Cell Biol.* **2004**, *114*, 1089–1100.

(42) Han, X.; Liu, Y.; Wu, F. G.; Jansensky, J.; Kim, T.; Wang, Z.; Brooks, C. L.; Wu, J.; Xi, C.; Mello, C. M.; et al. Different Interfacial Behaviors of Peptides Chemically Immobilized on Surfaces with Different Linker Lengths and via Different Termini. *J. Phys. Chem. B* **2014**, *118*, 2904–2912.

(43) Wilson, M. J.; Liliensiek, S. J.; Murphy, C. J.; Murphy, W. L.; Nealey, P. F. Hydrogels with Well-Defined Peptide-Hydrogel Spacing and Concentration: Impact on Epithelial Cell Behavior. *Soft Matter* **2012**, *8*, 390–398.

(44) Sur, S.; Tantakitti, F.; Matson, J. B.; Stupp, S. I. Epitope Topography Controls Bioactivity in Supramolecular Nanofibers. *Biomater. Sci.* **2015**, *3*, 520–532.

(45) Beer, J. H.; Springer, K. T.; Coller, B. S. Immobilized Arg-Gly-Asp (RGD) Peptides of Varying Lenghts as Structural Probes of the Platelet Glycoprotein IIb/IIIa Receptor. *Blood* **1992**, *79*, 117–129.

(46) Attwood, S. J.; Cortes, E.; Haining, A. W. M.; Robinson, B.; Li, D.; Gautrot, J.; del Río Hernández, A. Adhesive Ligand Tether Length Affects the Size and Length of Focal Adhesions and Influences Cell Spreading and Attachment. *Sci. Rep.* **2016**, *6*, 34334.

(47) Houseman, B. T.; Mrksich, M. The Microenvironment of Immobilized Arg-Gly-Asp Peptides Is an Important Determinant of Cell Adhesion. *Biomaterials* **2001**, *22*, 943–955.

(48) Grafahrend, D.; Heffels, K.-H.; Beer, M. V; Gasteier, P.; Möller, M.; Boehm, G.; Dalton, P. D.; Groll, J. Degradable Polyester Scaffolds with Controlled Surface Chemistry Combining Minimal Protein Adsorption with Specific Bioactivation. *Nat. Mater.* **2011**, *10*, 67–73.

(49) Rodda, A. E.; Ercole, F.; Glattauer, V.; Gardiner, J.; Nisbet, D. R.; Healy, K. E.; Forsythe, J. S.; Meagher, L. Low Fouling Electrospun Scaffolds with Clicked Bioactive Peptides for Specific Cell Attachment. *Biomacromolecules* **2015**, *16*, 2109–2118.

(50) Lange, S. C.; van Andel, E.; Smulders, M. M. J.; Zuilhof, H. Efficient and Tunable Three-Dimensional Functionalization of Fully Zwitterionic Antifouling Surface Coatings. *Langmuir* **2016**, *32*, 10199–10205.

(51) Ippel, B. D.; Dankers, P. Y. W. Introduction of Nature's Complexity in Engineered Blood-Compatible Biomaterials. *Adv. Healthcare Mater.* **2018**, *7*, 1700505.

(52) Goor, O. J. G. M.; Hendrikse, S. I. S.; Dankers, P. Y. W.; Meijer, E. W. From Supramolecular Polymers to Multi-Component Biomaterials. *Chem. Soc. Rev.* **2017**, *46*, 6621–6637.

(53) Aida, T.; Meijer, E. W.; Stupp, S. I. Functional Supramolecular Polymers. *Science* **2012**, *335*, 813–817.

(54) Spaans, S.; Fransen, P. P. K. H. P. K. H.; Ippel, B. D. D.; de Bont, D. F. A.; Keizer, H. M. M.; Bax, N. A. M. A. M.; Bouten, C. V. C. V. C.; Dankers, P. Y. W. Y. W. Supramolecular Surface Functionalization via Catechols for the Improvement of Cell–material Interactions. *Biomater. Sci.* **2017**, *5*,

1541–1548.

(55) Storrie, H.; Guler, M. O.; Abu-Amara, S. N.; Volberg, T.; Rao, M.; Geiger, B.; Stupp, S. I. Supramolecular Crafting of Cell Adhesion. *Biomaterials* **2007**, *28*, 4608–4618.

(56) Dankers, P.Y.W.; Harmsen, M. C.; Brouwer, L.A.; van Luyn, M. J.A.; Meijer, E.W.A Modular and Supramolecular Approach to Bioactive Scaffolds for Tissue Engineering. *Nat. Mater.* **2005**, *4*, 568–574.

(57) Kluin, J.; Talacua, H.; Smits, A. I. P. M. P. M.; Emmert, M. Y.; Brugmans, M. C. P.; Fioretta, E. S.; Dijkman, P. E.; Söntjens, S. H. M.; Duijvelshoff, R.; Dekker, S.; et al. In Situ Heart Valve Tissue Engineering Using a Bioresorbable Elastomeric Implant – From Material Design to 12 Months Follow-up in Sheep. *Biomaterials* **2017**, *125*, 101–117.

(58) Gu, X.; Matsumura, Y.; Tang, Y.; Roy, S.; Hoff, R.; Wang, B.; Wagner, W. R. Sustained Viral Gene Delivery from a Micro-Fibrous, Elastomeric Cardiac Patch to the Ischemic Rat Heart. *Biomaterials* **2017**, *133*, 132–143.

(59) Hong, Y.; Ye, S. H.; Nieponice, A.; Soletti, L.; Vorp, D. A.; Wagner, W. R. A Small Diameter, Fibrous Vascular Conduit Generated from a Poly(ester Urethane)urea and Phospholipid Polymer Blend. *Biomaterials* **2009**, *30*, 2457–2467.

(60) Duijvelshoff, R.; van Engeland, N.; Gabriels, K.; Söntjens, S.; Smits, A.; Dankers, P.; Bouten, C. Host Response and Neo-Tissue Development during Resorption of a Fast Degrading Supramolecular Electrospun Arterial Scaffold. *Bioengineering* **2018**, *5*, 61.

(61) Seifalian, A. M.; Salacinski, H. J.; Tiwari, A.; Edwards, A.; Bowald, S.; Hamilton, G. In Vivo Biostability of a Poly(carbonate-Urea)urethane Graft. *Biomaterials* **2003**, *24*, 2549–2557.

(62) Koevoets, R. A.; Versteegen, R. M.; Kooijman, H.; Spek, A. L.; Sijbesma, R. P.; Meijer, E. W. Molecular Recognition in a Thermoplastic Elastomer. *J. Am. Chem. Soc.* **2005**, *127*, 2999–3003.

(63) Wisse, E.; Spiering, A. J. H.; van Leeuwen, E. N. M.; Renken, R. A. E.; Dankers, P. Y. W.; Brouwer, L. A.; van Luyn, M. J. A.; Harmsen, M. C.; Sommerdijk, N. A. J. M.; Meijer, E. W. Molecular Recognition in Poly(ε-Caprolactone)-Based Thermoplastic Elastomers. *Biomacromolecules* **2006**, *7*, 3385–3395.

(64) Botterhuis, N. E.; Karthikeyan, S.; Veldman, D.; Meskers, S. C. J.; Sijbesma, R. P. Molecular Recognition in Bisurea Thermoplastic Elastomers Studied with Pyrene-Based Fluorescent Probes and Atomic Force Microscopy. *Chem. Commun.* **2008**, No. 33, 3915.

(65) Botterhuis, N. E.; Karthikeyan, S.; Spiering, A. J. H.; Sijbesma, R. P. Self-Sorting of Guests and Hard Blocks in Bisurea-Based Thermoplastic Elastomers. *Macromolecules* **2010**, *43*, 745–751.

(66) Ippel, B. D.; Keizer, H. M.; Dankers, P. Y. W. Supramolecular Antifouling Additives for Robust and Efficient Functionalization of Elastomeric Materials: Molecular Design Matters. *Adv. Funct. Mater.* **2019**, *29*, 1805375.

(67) Mollet, B. B.; Comellas-Aragonès, M.; Spiering, A. J. H.; Söntjens, S. H. M.; Meijer, E. W.; Dankers, P. Y. W. A Modular Approach to Easily Processable Supramolecular Bilayered Scaffolds with Tailorable Properties. *J. Mater. Chem. B* **2014**, *2*, 2483–2493.

(68) Castagna, A. M.; Pangon, A.; Dillon, G. P.; Runt, J. Effect of Thermal History on the Microstructure of a Poly(tetramethylene Oxide)-Based Polyurea. *Macromolecules* **2013**, *46*, 6520–6527.

(69) Bonito, V.; Smits, A. I. P. M.; Goor, O. J. G. M.; Ippel, B. D.; Driessen-Mol, A.; Münker, T. J. A. G.; Bosman, A. W.; Mes, T.; Dankers, P. Y. W.; Bouten, C. V. C. Modulation of Macrophage Phenotype and Protein Secretion via Heparin-IL-4 Functionalized Supramolecular Elastomers. *Acta Biomater.* **2018**, *71*, 1–23.

(70) Chen, S.; Li, L.; Zhao, C.; Zheng, J. Surface Hydration: Principles and Applications toward Low-

Fouling/nonfouling Biomaterials. *Polymer* **2010**, *51*, 5283–5293.

(71) Lei, Y.; Remy, M.; Labrugere, C.; Durrieu, M. C. Peptide Immobilization on Polyethylene Terephthalate Surfaces to Study Specific Endothelial Cell Adhesion, Spreading and Migration. *J. Mater. Sci. Mater. Med.* **2012**, *23*, 2761–2772.

(72) Volin, M.V.; Joseph, L.; Shockley, M. S.; Davies, P. F. Chemokine Receptor CXCR4 Expression in Endothelium. *Biochem. Biophys. Res. Commun.* **1998**, *242*, 46–53.

(73) Yu, Q.; Zhang, Y.; Wang, H.; Brash, J.; Chen, H. Anti-Fouling Bioactive Surfaces. *Acta Biomater.* **2011**, *7*, 1550–1557.

(74) Albelda, S. M.; Buck, C. A. Integrins and Other Cell Adhesion Molecules. *FASEB J.* **1990**, *4*, 2868–2880.

(75) Massia, S. P.; Hubbell, J. A. An RGD Spacing of 440 Nm Is Sufficient for Integrin A„ß 3 -Mediated Fibroblast Spreading and 140 Nm for Focal Contact and Stress Fiber Formation. **1991**, *c*.

(76) Goor, O. J. G. M.; Keizer, H. M.; Bruinen, A. L.; Schmitz, M. G. J.; Versteegen, R. M.; Janssen, H. M.; Heeren, R. M. A.; Dankers, P. Y. W. Efficient Functionalization of Additives at Supramolecular Material Surfaces. *Adv. Mater.* **2017**, *29*, 1604652.

(77) By, F.; Peptide, R. G. D.; Mould, A. P.; Komoriyae, A.; Yamadall, K. M.; Humphriess, M. J. The CS5 Peptide Is a Second Site in the IIICS Region of Fibronectin. **1991**, No. 6, 3579–3585.

(78) Wei, Y.; Zhang, J.; Li, H.; Zhang, L.; Bi, H. Multifunctional Copolymer Coating of Polyethylene Glycol, Glycidyl Methacrylate, and REDV to Enhance the Selectivity of Endothelial Cells. *J. Biomater. Sci. Polym. Ed.* **2015**, *26*, 1357–1371.

(79) Wei, Y.; Ji, Y.; Xiao, L.; Lin, Q.; Ji, J. Different Complex Surfaces of Polyethyleneglycol (PEG) and REDV Ligand to Enhance the Endothelial Cells Selectivity over Smooth Muscle Cells. *Colloids Surf., B* **2011**, *84*, 369–378.

(80) De Torre, I. G.; Wolf, F.; Santos, M.; Rongen, L.; Alonso, M.; Jockenhoevel, S.; C.Rodríguez-Cabello, J.; Mela, P. Elastin-like Recombinamer-Covered Stents: Towards a Fully Biocompatible and Non-Thrombogenic Device for Cardiovascular Diseases. *Acta Biomater.* **2015**, *12*, 146–155.

(81) Heilshorn, S. C.; DiZio, K. A.; Welsh, E. R.; Tirrell, D. A. Endothelial Cell Adhesion to the Fibronectin CS5 Domain in Artificial Extracellular Matrix Proteins. *Biomaterials* **2003**, *24*, 4245–4252.

(82) Jung, J. P.; Moyano, J. V.; Collier, J. H. Multifactorial Optimization of Endothelial Cell Growth Using Modular Synthetic Extracellular Matrices. *Integr. Biol.* **2011**, *3*, 185–196.

(83) Zaccaria, S.; van Gaal, R. C.; Riool, M.; Zaat, S. A. J.; Dankers, P. Y. W. Antimicrobial Peptide Modification of Biomaterials Using Supramolecular Additives. *J. Polym. Sci. Part A: Polym. Chem.* **2018**, *56*, 1926–1934.

5

Non-cell adhesive properties of UPy-PEG additive functionalized thin films

Abstract

Fouling properties of new biomaterials are important for the performance of a material in a biological environment. In this chapter, thin supramolecular material films were formulated using end-functionalized PCLdiUPy and chain-extended CE-UPyPCL as structural base materials, to assess the influence of base material design, and three UPy-functionalized poly(ethylene glycol) additives, where the influence of the design of these additives was investigated. The films were fabricated with both solution-casting and spin-coating. The antifouling properties were determined through cell adhesion assays with 4 different cell-types. The results described in this chapter compare the results from these studies with the cell adhesion assays described throughout this thesis.

The content of this chapter is based on:

A.C.H. Pape, Bastiaan D. Ippel, Patricia Y.W. Dankers, *Cell and protein fouling properties of polymeric mixtures containing supramolecular poly(ethylene glycol) additives*, Langmuir 2017, 201700505

Geert C. van Almen, Hanna Talacua, Bastiaan D. Ippel, Björne B. Mollet, Mellany Ramaekers, Marc Simonet, Anthal I.P.M. Smits, Carlijn V.C. Bouten, Jolanda Kluin, Patricia Y.W. Danekrs, *Development of non-cell adhesive vascular grafts using supramolecular building blocks*, Macromolecular Bioscience 2016, 16, 350-362

Introduction

Control of the fouling properties of biomaterials, *e.g.* protein adsorption and cell adhesion, is essential for ultimate functioning of these materials as implants and prostheses. Surface coating of implants using antifouling compounds is often applied. Functional antifouling properties are most frequently added through physisorption or chemical tethering of antifouling moieties. Covalently attached layers are more durable than physisorbed adlayers, but making stable coatings on more complex surfaces as efficient in reducing biofouling as self-assembling monolayers (SAM) on gold remains a challenge.[1]

Initial investigation on properties of antifouling SAMs revealed that moieties that resist the adsorption of proteins and cells typically are hydrophilic, include hydrogen-bond acceptors, lack hydrogen-bond donors, and have an overall neutral charge.[2,3] Since then, hydrophilic poly(ethylene glycol) (PEG)-based materials have been widely used to develop antifouling surfaces using varying surface preparation techniques.[4] Similar to hydrophilic polysaccharide containing materials and coatings based on zwitterionic molecules, the antifouling properties of PEG-based materials have been attributed to the presence of an hydration layer near the surface, which acts as a physical barrier.[5]

To design antifouling materials, ethylene glycol-based materials have been used in varying designs. Recently, the functionalization of substrates with polymer brushes has proven to increase surface coverage and thereby increase effectivity of the applied coating.[1,6] Brush-like coatings based on PEG, often in the form of a poly[oligo(ethylene glycol) methyl methacrylate] (pOEGMa), have for instance been successfully applied via surface-initiated atom transfer radical polymerization (SI-ATRP) on 2D substrates[7,8] and on electrospun fibers.[9,10]

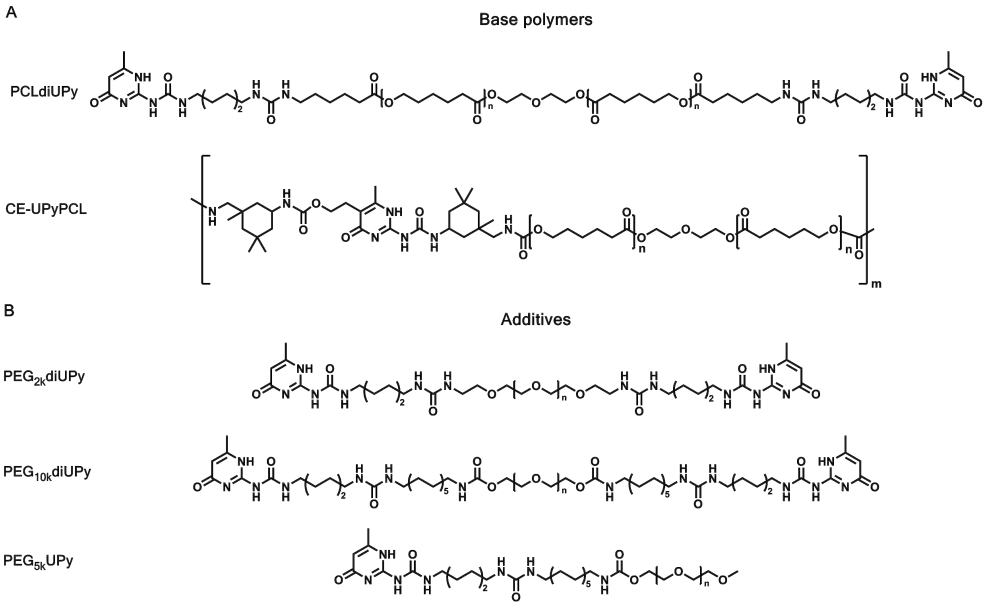

Figure 5.1. A) Structural representation of the base polymers PCLdiUPy and CE-UPyPCL. B) Structural representation of the PEG-based UPy additives PEG2kdiUPy, PEG10kdiUPy and PEG5kUPy.

Our approach to new biomaterials applies an alternative strategy. Using noncovalent supramolecular interactions, based on the self-complementary 2-ureido-4[1H]-pyrimidinone (UPy) moiety[11], we were able to develop modular biomaterials with UPy-modified polycaprolactone (PCLdiUPy) (**Figure 5.1**) as the structural base material.[12–15] To induce bioactive properties in these biomaterials, UPy-peptide conjugates were non-covalently incorporated using the specificity of the UPy-UPy interactions to anchor these additives in the base material. Mollet et al. showed that cell adhesion could be decreased by incorporation of a hydrophilic poly(ethylene glycol) (PEG) based UPy-additive in a UPy-based biomaterial.[15] In this chapter, the functionality of this additive is further explored by testing the adhesion of a variety of cell-types, including endothelial cells, fibroblasts and the myofibroblast-like human vena saphena cells that were used in other studies throughout this thesis. Furthermore, the incorporation in a chain-extended (CE) UPy-polymer as base material is studied, which has improved mechanical properties for *e.g.* vascular replacement therapies compared to PCLdiUPy.[16,17] Moreover, the additive toolbox is extended with two PEG-based UPy-additives of different designs, which have longer PEG-chains (5 kDa and 10 kDa), and an additional alkyl spacer for improved anchoring in the base material (**Figure 5.1**). Cell adhesion assays over 24 hours serve as the main read-out reported in this chapter. In text, these will be related to the surface characterization and more extensive quantification of the cell adhesion as described in the publications related to this chapter.

End-functionalized versus chain-extended UPy-polymer

Human Umbilical Vein Endothelial Cells (HUVEC) and 3T3 cells that were cultured on solution-cast films of PCLdiUPy show a spread-out morphology and exhibit actin-stress fibers (**Figure 5.2**). However, the 3T3 fibroblasts adhere in larger numbers compared to the endothelial cells.[16] The number of adhered cells significantly decreases upon incorporation of PEG_{2k}diUPy in the polymer film, and the cells show a less spread morphology and no defined stress-fibers compared to the pristine material.

Interestingly, when HUVECs and 3T3 cells are cultured for up to 7 days on these surfaces, the effect of the PEG_{2k}diUPy in the CE-UPyPCL is lost, and the cells that did adhere grow

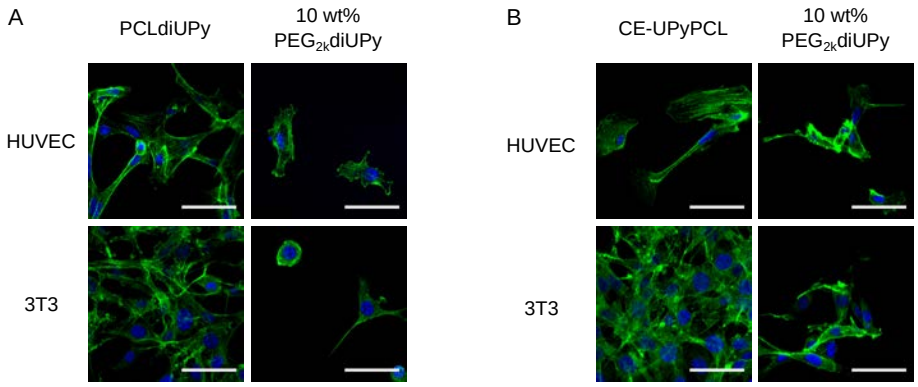

Figure 5.2. A) Fluorescence micrographs of HUVECs and 3T3s cultured on solution-cast films of PCLdiUPy with 10 wt% PEG2kdiUPy for 24 hours. B) Fluorescence micrographs of HUVECs and 3T3s cultured on solution-cast films of CE-UPyPCL with 10 wt% PEG2kdiUPy for 24 hours. The actin cytoskeleton is presented in green, and nuclei in blue. Scale bars represent 50 µm.

to cover the surface. These results are in line with significant erosion of the PEG_{2k}diUPy from the CE-UPyPCL.[16] In the PCLdiUPy, this effect is less pronounced for the HUVECs, whereas the remaining 3T3 cells barely expand.[16]

The PCLdiUPy base material is used in our group for the initial testing of practically all UPy-based additives. The characteristic self-assembly of the UPy-moieties into fibrous structures is a well-established platform to test the effect of additive incorporation on the assembly process, which can be visualized through *e.g.* atomic force microscopy.[13] However, the resulting supramolecular thermoplastic material is quite brittle, when compared to classic thermoplastic elastomers and therefore less well suited for applications such as vascular grafts.[18] The chain-extended UPy-based polymers of a $(AB)_n$ design, such as the CE-UPyPCL as used in this study offer better mechanical stability, but lack the defined assembly that is seen in PCLdiUPy, even when the sterically unfavorable isoforon moiety is not present the structure.[19] Moreover, when a UPy-peptide conjugate was incorporated in a CE-UPy polymer, amorphous phase separation of this additive was clearly visible in AFM phase images.[19] Incorporation of the hydrophilic PEG_{2k}diUPy, which shows self-assembly into fibrous structures on its own, either results in stabilization of the assembly of the CE-UPy polymer or phase separates from the CE-UPy-polymer.[16]

Considering these results, the formulation of non-cell adhesive materials is feasible with both end-functionalized PCLdiUPy and chain extended CE-UPyPCL in combination with PEG_{2k}diUPy. However, the nature of the base material determines here how effective and robust this functionalization is in long-term cell adhesion assays.[16]

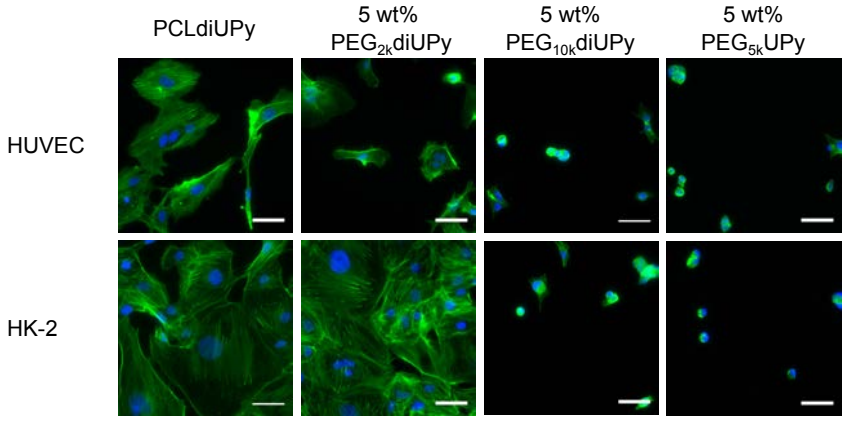

Figure 5.3. Fluorescence micrographs of HUVECs and HK-2 cells cultured on spincoated films of PCLdiUPy with 5 wt% PEG2kdiUPy and PEG5kUPy for 24 hours. The actin cytoskeleton is presented in green, and nuclei in blue. Scale bars represent 50 µm.

Influence of PEG-UPy additive design

On spin-coated surfaces, for which the protein adsorption was quantified using quartz-crystal microbalance with dissipation monitoring (QCM-D), the adhesion of HUVEC endothelial and HK-2 epithelial cells was investigated. The concentration of UPy-PEG additives was reduced from 10 wt% to 5 wt% compared to the solution-cast surfaces

described above. The endothelial and epithelial cells are able to spread on the pristine PCLdiUPy, and both express actin stress fibers (**Figure 5.3**). Similar to the solution-cast surfaces and when compared to the 3T3 fibroblasts, less endothelial cells adhere compared to the epithelial HK-2 cells. The incorporation of 5 % PEG_{2k}diUPy resulted in a decrease in cell spreading for the endothelial cells, whereas the HK-2 cells adhere and spread comparable to pristine. Moreover, the 6-fold decrease in concentration of the PEG_{2k}diUPy compared to previous study with kidney epithelial cells by Mollet et al. resulted in surfaces that had no significant non-cell adhesive properties.[15]

The bi-functional PEG_{10k}diUPy additive has a design where the PEG-length is longer compared to the PEG_{2k}diUPy, and additional alkyl spacers are incorporated in between the PEG and the UPy, to provide proper anchorage in the base material. The mono-functional PEG_{5k}UPy additive is in principle half the PEG_{10k}diUPy, where only one UPy-moiety is combined with a longer PEG-chain and the additional alkyl spacer. Cell-spreading and overall adhesion, as evident by the quantification of surface coverage[20], is significantly reduced upon incorporation of 5 wt% of PEG_{10k}diUPy and PEG_{5k}UPy. Since the amount of PEG that is incorporated for 5 wt% PEG_{10k}diUPy ánd PEG_{5k}UPy is only 1.2 times that of PEG_{2k}diUPy, the design of the molecule, with the increased alkyl spacer and the length of the PEG-chain determines the non-cell adhesive properties. The amount of PEG incorporated for the PEG_{5k}UPy and PEG_{10k}diUPy is also significantly lower than the 30 wt% that was required in the previously mentioned study by Mollet et al.[15] In this study, the morphology of the exposed PEG chains, through attachment on only one side or on either side, has no clear effect on anti-fouling properties, contrasting to the work presented in **Chapter 3** in this thesis.

Generally, the increased hydrophilicity of a PEG-modified surface is correlated to anti-fouling properties, in accordance with the hypothesis that such functionalization strategies are functionally antifouling due to the formation of a stable hydrated layer.[5] For the spin-coated surfaces, no significant difference in hydrophilicity was observed between the mixtures of PCLdiUPy with PEG_{2k}diUPy and PEG_{10k}diUPy,[20] even though a distinct difference in non-cell adhesive properties is evident on films made from the same mixtures. This suggests that an increased hydrophilicity of our surfaces may indicate the presence of PEG, but cannot be used to suggest antifouling properties of such materials.

Pape et al. quantified the protein adsorption of the first three proteins from the Vroman series, which are the first proteins to normally adsorb from blood,[21] on the spin-coated films using quartz crystal microbalance with dissipation monitoring.[20] Since cell-adhesion is presumed to be preceded by aspecific protein adsorption to biomaterials, negating protein adsorption would result in non-cell adhesive surfaces. However, this does not necessarily hold the other way around, since in this study the distinct correlation between protein adsorption and cell adhesion was hard to make; only the adsorption of y-globulin was significantly decreased on surfaces that also resisted cell adhesion, whereas no significant differences were found for albumin, fibrinogen and a mixture of albumin, y-globulin and fibrinogen. These results showed that non-cell adhesive behavior cannot per definition be correlated with a possible reduction in protein adsorption.[20]

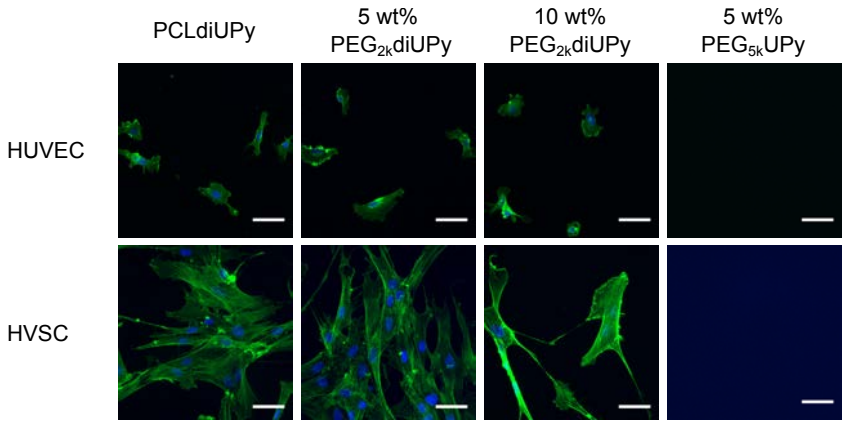

Figure 5.4. Fluorescence micrographs of HUVECs and HVSCs cultured on solution-cast films of PCLdiUPy with 5 and 10 wt% PEG2kdiUPy and 5 wt% PEG5kUPy. The actin cytoskeleton is presented in green, and nuclei in blue. Scale bars represent 50 µm.

Perspective

Cell-adhesive properties of films made by solution-casting the polymeric mixtures of PCLdiUPy with 5 and 10 wt% PEG_{2k}diUPy and 5 wt% PEG_{5k}UPy were additionally examined with HVSCs and HUVECs, to be able to compare these results to other work in this thesis and the spin-coated surfaces from this chapter respectively. Solution-casting from organic solvent rather than spin-coating ensues longer drying times, which gives the mixtures more time to phase separate, as is seen in atomic force microscopy images of similar films.[22] The adhesion of both HVSCs and HUVECs is not significantly decreased upon the incorporation of 5 wt% PEG_{2k}diUPy, similar to the spin-coated surfaces (**Figure 5.4**). Spreading and adhesion does decrease when 10 wt% of the PEG_{2k}diUPy is incorporated, which is in line with the results shown in figure 5.2. Cell-adhesion is drastically decreased for the films cast from the mixture of PCLdiUPy with PEG_{5k}UPy, for both the endothelial cells and myofibroblasts.

These results indicate that, despite the difference in processing and apparent morphology of the films, the non-cell adhesive properties are similar for these two processing techniques. There is a difference in adhesive properties between different cell-types. The endothelial cells studied here tend to adhere less, and are affected more easily when additives are incorporated. The HVSC cells appear to be as adhesive as both the HK-2 epithelial cells and 3T3 mouse-fibroblasts, and therefore are a suitable candidate to use as for the assessment of non-cell adhesive surface properties of our biomaterials.

Conclusion

Adhesion of cells from a variety of sources on surfaces made from polymeric mixtures of two UPy-based base polymers and three PEG-based UPy additives was described in this chapter. The non-cell adhesive properties found in PCLdiUPy can be translated to the CE-UPyPCL, however, these properties are not retained over longer culture periods. The bifunctional PEG_{2k}diUPy requires increased concentrations to reduce cell-adhesion from all sources. The incorporation of 5wt% PEG_{5k}UPy and PEG_{10k}diUPy additives resulted in non-

cell adhesive films, even though the anti-fouling properties were not evident on protein-level. The additional alkyl-spacer in the PEG_{5k}UPy and PEG_{10k}diUPy, which was stipulated to improve anchoring in the base material, might facilitate better anchoring of these additives also in the mechanically more favorable chain-extended UPy-materials. Therefore, the retention of these additives in CE-UPyPCL and the non-cell adhesive properties of the mixtures could be an interesting topic for future research. Moreover, the adhesive character of the HVSCs used throughout this thesis makes them a good candidate for the exploration of non-cell adhesive properties in biomaterials.

Experimental section

Materials
The syntheses of PCLdiUPy[15], CE-UPyPCL[18], PEG_{2k}diUPy[15], PEG_{5k}UPy[23], and PEG_{10k}diUPy[24] have been descirbed previously.

Preparation of polymeric thin films
For results in figure 5.2: Drop cast supramolecular UPy-polymer surfaces were obtained via mixing of UPy-modified PCL polymers with UPy-PEG at different weight ratios. CE-UPyPCL and PCLdiUPy were dissolved in hexafluoroisopropanol (HFIP , Acros Organics) at 10% w/v by stirring at room temperature for 16-24 h. PEG_{2k}diUPy was added to PCLdiUPy and CE-UPyPCL at a w/w ratio of 90:10 base polymer:additive. Each film contained 5 mg UPy-polymer and was cast from a volume of 50 µL 10% w/v polymer solution and dried overnight at room temperature followed by an additional 24h in vacuo at 40 °C. Substrates were cast on 13 mm round glass coverslips and sterilized under UV for 30-60 minutes prior to the cell adhesion assay.

For results in figure 5.3: Polymer solutions were prepared at a concentration of 20 mg mL^{-1} in HFIP. For the mixtures, 5 vol% of the additive polymer solution was added to 95 vol % of PCLdiUPy. This results in a 5:95 wt% additive:PCLdiUPy mixtures, corresponding to 5 and 2.45 mol % for PEG_{2k}diUPy and PEG_{5k}UPy respectively. Samples were prepared by spin-coating 100 µL of a 20 mg mL^{-1} solution of the polymers in HFIP at 5000 rpm for 30 s on glass coverslips with a diameter of 13 mm. The samples were left to dry for 1 h at room temperature before continuing the experiments. The coverlips coated with the thin films were mounted in Minusheet tissue carriers with 13 mm o.d. (Minucells and Minutissue-Vertriebs GmbH) and then sterilized under UV for approximately 1 hour.

For results in figure 5.4: Polymer solutions were prepared at a concentration of 20 mg mL^{-1} in HFIP. For the mixtures, 5 and 10 vol% of the additive solutions were added to 95 and 90 vol% of PCLdiUPy respectively. This results in 5:95 and 10:90 additive:PCLdiUPy mixtures. 40-50 µL solution was cast on 14 mm glass coverslips, after which the samples were dried to the air for 1-2 hours with subsequent overnight drying in vacuo. The solution-cast films were secured in adapted Transwell inserts (Corning) as described before[25,26] and sterilized under UV for 15 minutes.

Cell culture
Human umbilical vein endothelial cells (HUVEC, Lonza) were cultured in endothelial growth medium (Lonza and PromoCell, endothelial basal medium supplemented with endothelial growth factors, and additional Pen/Strep for the supplemented PromoCell medium). Culture flasks were coated with 0.1% gelatin in PBS for approximately 15 minutes at 37 °C prior to cell seeding. HUVECs were passaged before reaching 80% confluency, and used for experiments up to passage 6. Mouse fibroblasts (NIH/3T3) were cultured in Dulbecco's modified eagle medium (DMEM, Gibco) supplemented with 10% v/v fetal bovine serum (FBS, Greinier Bio) and 1% penicillin/streptomycin (Invitrogen). Proximal epithelial cells from a human kidney (HK-2, ATCC) were cultured in DMEM, supplemented with 10% FBS and 1% penicillin/streptomycin. Human vena saphena cells (HVSCs) were harvested from the human vena saphena magna according to the Dutch guidelines for secondary use materials. HVSCs were expanded in DMEM, supplemented with 10% FBS, 1% glutamax (Gibco) and 1% penicillin/streptomycin. HVSCs were used for experiments up to passage 7. All cells were harvested using trypsin/EDTA (Lonza) for use in experiments.

Cell adhesion assay
For the results in figure 5.2, the coverslips coated with polymeric thin films were placed in standard 24 well culture plates. HUVECs and 3T3s were seeded at 3-3.5 x 10^4 cells cm^{-2} onto the coverslips, while holding down the films with a pipet-tip. For the results in figure 5.3, 62 µL from a 2.6 x 10^5 cells mL^{-1} HUVEC and HK-2 cell suspension was pipetted onto the exposed surface of the coverslips, and cells were left to adhere for 1.5 hours, before adding 500 µL culture medium on top of the cells. For the results in figure 5.4 HUVECs and HVSCs were seeded at 25,000 cells cm^{-2} in 500 µL on the inside of the inserts, and 1 mL cell-free growth medium was added outside the insert after establishing the inserts did not leak immediately.

Cells were cultured for 24 hours at 37 °C and 5% CO_2, after which non adherent cells were aspirated and the surfaces were washed with PBS and subsequently fixated in 3.7% formaldehyde. The actin-cytoskeleton of the cells was stained with ATTO-488 conjugated phalloidin, and nuclei were counterstained with 4',6-diamidino-2-phenylindole (DAPI). Stained samples were visualized with a confocal laser scanning microscope (results in figure 5.2: Zeiss LSM510 META NLO) or an epifluorescence microscope (results in figure 5.3: Zeiss Axiovert 200M, results in figure 5.4: Leica DMi8s).

References

(1) Wei, Q.; Becherer, T.; Angioletti-Uberti, S.; Dzubiella, J.; Wischke, C.; Neffe, A. T.; Lendlein, A.; Ballauff, M.; Haag, R. Protein Interactions with Polymer Coatings and Biomaterials. *Angew. Chem., Int. Ed.* **2014**, *53*, 8004–8031.

(2) Ostuni, E.; Chapman, R. G.; Liang, M. N.; Meluleni, G.; Pier, G.; Ingber, D. E.; Whitesides, G. M. Self-Assembled Monolayers That Resist the Adsorption of Cells. *Langmuir* **2001**, *17*, 6336–6343.

(3) Ostuni, E.; Chapman, R. G.; Holmlin, R. E.; Takayama, S.; Whitesides, G. M. A Survey of Structure-Property Relationships of Surfaces That Resist the Adsorption of Protein. *Langmuir* **2001**, *17*, 5605–5620.

(4) Banerjee, I.; Pangule, R. C.; Kane, R. S. Antifouling Coatings: Recent Developments in the Design of Surfaces That Prevent Fouling by Proteins, Bacteria, and Marine Organisms. *Adv. Mater.* **2011**, *23*, 690–718.

(5) Chen, S.; Li, L.; Zhao, C.; Zheng, J. Surface Hydration: Principles and Applications toward Low-Fouling/nonfouling Biomaterials. *Polymer* **2010**, *51*, 5283–5293.

(6) Hucknall, A.; Rangarajan, S.; Chilkoti, A. In Pursuit of Zero: Polymer Brushes That Resist the Adsorption of Proteins. *Adv. Mater.* **2009**, *21*, 2441–2446.

(7) Surman, F.; Riedel, T.; Bruns, M.; Kostina, N. Y.; Sedláková, Z.; Rodriguez-Emmenegger, C. Polymer Brushes Interfacing Blood as a Route toward High Performance Blood Contacting Devices. *Macromol. Biosci.* **2015**, *15*, 636–646.

(8) Zhang, Z.; Zhang, M.; Chen, S.; Horbett, T. A.; Ratner, B. D.; Jiang, S. Blood Compatibility of Surfaces with Superlow Protein Adsorption. *Biomaterials* **2008**, *29*, 4285–4291.

(9) Harrison, R. H.; Steele, J. A. M.; Chapman, R.; Gormley, A. J.; Chow, L. W.; Mahat, M. M.; Podhorska, L.; Palgrave, R. G.; Payne, D. J.; Hettiaratchy, S. P.; et al. Modular and Versatile Spatial Functionalization of Tissue Engineering Scaffolds through Fiber-Initiated Controlled Radical Polymerization. *Adv. Funct. Mater.* **2015**, *25*, 5748–5757.

(10) Kostina, N. Y.; Pop-Georgievski, O.; Bachmann, M.; Neykova, N.; Bruns, M.; Michálek, J.; Bastmeyer, M.; Rodriguez-Emmenegger, C. Non-Fouling Biodegradable Poly(ϵ-

Caprolactone) Nanofibers for Tissue Engineering. *Macromol. Biosci.* **2016**, *16*, 83–94.
(11) Sijbesma, R. P.; Beijer, F. H.; Brunsveld, L.; Folmer, B. J.; Hirschberg, J. H.; Lange, R. F.; Lowe, J. K.; Meijer, E. W. Reversible Polymers Formed from Self-Complementary Monomers Using Quadruple Hydrogen Bonding. *Science* **1997**, *278*, 1601–1604.
(12) Dankers, P. Y. W.; Harmsen, M. C.; Brouwer, L. A.; van Luyn, M. J. A.; Meijer, E. W. A Modular and Supramolecular Approach to Bioactive Scaffolds for Tissue Engineering. *Nat. Mater.* **2005**, *4*, 568–574.
(13) Wisse, E.; Spiering, a. J. H.; Dankers, P. Y. W.; Mezari, B.; Magusin, P. C. M. M.; Meijer, E. W. Multicomponent Supramolecular Thermoplastic Elastomer with Peptide-Modified Nanofibers. *J. Polym. Sci. Part A: Polym. Chem.* **2011**, *49*, 1764–1771.
(14) Dankers, P. Y. W.; Boomker, J. M.; Der Vlag, A. H. Van; Smedts, F. M. M.; Harmsen, M. C.; Van Luyn, M. J. a. The Use of Fibrous, Supramolecular Membranes and Human Tubular Cells for Renal Epithelial Tissue Engineering: Towards a Suitable Membrane for a Bioartificial Kidney. *Macromol. Biosci.* **2010**, *10*, 1345–1354.
(15) Mollet, B. B.; Comellas-Aragonès, M.; Spiering, A. J. H.; Söntjens, S. H. M.; Meijer, E. W.; Dankers, P. Y. W. A Modular Approach to Easily Processable Supramolecular Bilayered Scaffolds with Tailorable Properties. *J. Mater. Chem. B* **2014**, *2*, 2483–2493.
(16) Van Almen, G. C.; Talacua, H.; Ippel, B. D.; Mollet, B. B. B.; Ramaekers, M.; Simonet, M.; Smits, A. I. P. M.; Bouten, C. V. C.; Kluin, J.; Dankers, P. Y. W. Development of Non-Cell Adhesive Vascular Grafts Using Supramolecular Building Blocks. *Macromol. Biosci.* **2016**, *16*, 350–362.
(17) Muylaert, D. E. P.; van Almen, G. C.; Talacua, H.; Fledderus, J. O.; Kluin, J.; Hendrikse, S. I. S.; van Dongen, J. L. J.; Sijbesma, E.; Bosman, A. W.; Mes, T.; et al. Early in-Situ Cellularization of a Supramolecular Vascular Graft Is Modified by Synthetic Stromal Cell-Derived Factor-1α Derived Peptides. *Biomaterials* **2016**, *76*, 187–195.
(18) Dankers, P. Y. W.; van Leeuwen, E. N. M.; van Gemert, G. M. L.; Spiering, A. J. H.; Harmsen, M. C.; Brouwer, L. A.; Janssen, H. M.; Bosman, A. W.; van Luyn, M. J. A.; Meijer, E. W. Chemical and Biological Properties of Supramolecular Polymer Systems Based on Oligocaprolactones. *Biomaterials* **2006**, *27*, 5490–5501.
(19) Bonito, V.; Smits, A. I. P. M.; Goor, O. J. G. M.; Ippel, B. D.; Driessen-Mol, A.; Münker, T. J. A. G.; Bosman, A. W.; Mes, T.; Dankers, P. Y. W.; Bouten, C. V. C. Modulation of Macrophage Phenotype and Protein Secretion via Heparin-IL-4 Functionalized Supramolecular Elastomers. *Acta Biomater.* **2018**, *71*, 1–23.
(20) Pape, A. C. H.; Ippel, B. D.; Dankers, P. Y. W. Cell and Protein Fouling Properties of Polymeric Mixtures Containing Supramolecular Poly(ethylene Glycol) Additives. *Langmuir* **2017**, *33*, 4076–4082.
(21) Leonard, E. F.; Vroman, L. Is the Vroman Effect of Importance in the Interaction of Blood with Artificial Materials? *J. Biomater. Sci. Polym. Ed.* **1991**, *3*, 95–107.
(22) Pape, A. C. H. Ureidopyrimidinone-Based Supramolecular Networks for Biomedical Applications, Technische Universiteit Eindhoven, 2015.
(23) Kieltyka, R. E.; Pape, A. C. H.; Albertazzi, L.; Nakano, Y.; Bastings, M. M. C.; Voets, I. K.; Dankers, P. Y. W.; Meijer, E. W. Mesoscale Modulation of Supramolecular Ureidopyrimidinone-Based Poly(ethylene Glycol) Transient Networks in Water. *J. Am. Chem. Soc.* **2013**, No. 135, 11159–11164.
(24) Dankers, P. Y. W.; Hermans, T. M.; Baughman, T. W.; Kamikawa, Y.; Kieltyka, R. E.; Bastings, M. M. C.; Janssen, H. M.; Sommerdijk, N. a J. M.; Larsen, A.; Van Luyn, M. J.

a; et al. Hierarchical Formation of Supramolecular Transient Networks in Water: A Modular Injectable Delivery System. *Adv. Mater.* **2012**, *24*, 2703–2709.

(25) Ippel, B. D.; Keizer, H. M.; Dankers, P. Y. W. Supramolecular Antifouling Additives for Robust and Efficient Functionalization of Elastomeric Materials: Molecular Design Matters. *Adv. Funct. Mater.* **2019**, *29*, 1805375.

(26) Zaccaria, S.; van Gaal, R. C.; Riool, M.; Zaat, S. A. J.; Dankers, P. Y. W. Antimicrobial Peptide Modification of Biomaterials Using Supramolecular Additives. *J. Polym. Sci. Part A: Polym. Chem.* **2018**, *56*, 1926–1934.

6

Supramolecular additive initiated controlled atom transfer radical polymerization of zwitterionic brushes on ureido-pyrimidinone-based biomaterial surfaces

Abstract

Surface-initiated controlled radical polymerization is a popular technique for the modification of biomaterials with, for example, antifouling polymers. Here we report on the functionalization of a supramolecular biomaterial with zwitterionic poly(sulfobetaine methacrylate) via atom transfer radical polymerization from a macro-initiator additive, which is embedded in the hard-phase of the ureidopyrimidinone-based material. Poly(sulfobetaine methacrylate) was successfully polymerized from these surfaces, and the polymerized sulfobetaine content, with corresponding antifouling properties, depended on both the macro-initiator additive concentration and polymerization time. Furthermore, the polymerization from the macro-initiator additive was successfully translated to functional electrospun scaffolds, showing the potential for this functionalization strategy in supramolecular material systems.

The content of this chapter is based on:

Bastiaan D. Ippel*, Muhabbat I. Komil*, Paul A.A. Bartels, Roy J.E.A. Boonen, Maarten M.J. Smulders, Patricia Y.W. Dankers, *Supramolecular additive initiated controlled radical polymerization of zwitterionic brushes on ureidopyrimidinone-based biomaterial surface,* submitted

Introduction

Antifouling functionalization strategies are of interest for a variety of applications, ranging from the prevention of biofouling in marine environments to the restriction of fouling of blood components in vascular grafts. Hydrophilic surface functionalization is a well-established method to decrease undesired fouling for biomaterials[1,2] and is hypothesized to be effective through the formation of a thin, but stable hydrated layer that serves as a barrier between the material and the environment.[3] In recent years, surface functionalization with zwitterionic polymers has gained more traction for the purpose of generating antifouling properties.[4] Their ability to repel for instance protein adsorption exceeds that of classic hydrophilic polymers such as poly(ethylene glycol) (PEG) through a stronger interaction between zwitterions and water molecules.[5,6] Monomers with intramolecular opposing charges on which such polymers are based include carboxybetaine, sulfobetaine and phosphorylcholine derivatives.[4] The functioning of zwitterionic layers depends on the design of the zwitterionic moiety in terms of potential charge and separation of the charges, the overall polymer morphology and molecular weight, and functionalization density.[7,8]

Several controlled polymerization strategies can be applied to functionalize biomaterial surfaces with zwitterionic polymers, among which radical polymerization techniques such as surface-initiated atom transfer radical polymerization (SI-ATRP) can yield highly antifouling layers.[1,9,10] Furthermore, surface-initiated controlled radical polymerization (SI-CRP) allows for the precise control over the molecular weight and polymer morphology, as well as grafting density.[11,12]

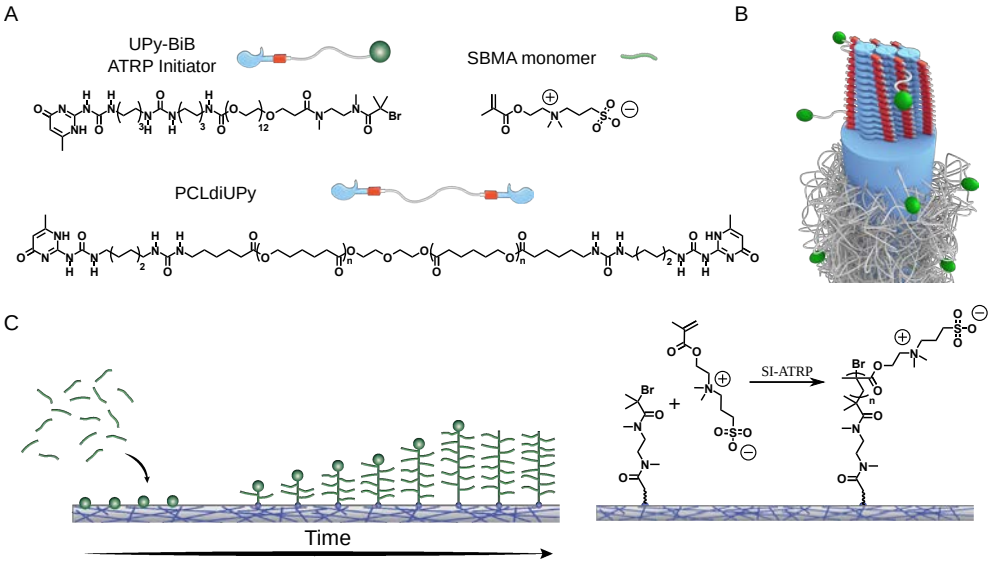

Figure 6.1. Schematic overview of the approach used in this study. A) Structural and graphical representations of the PCLdiUPy supramolecular base material, the UPy-BiB macro-initiator additive and the SBMA monomer. B) Schematic representation of fibrous hard-phase formed through UPy-dimerization and assembly. C) Schematic representation of SI-ATRP with SBMA from the UPy-BiB initiator additive.

Methods for SI-CRP are commonly developed on model substrates such as silica or flat and thin polymer layers. Availability of a highly reactive initiating group on the surface of these materials is a prerequisite. Initiators can be simply covalently conjugated to a surface[13–15] or attached through catechol-mediated chemistry.[16,17] Both these methods can be applied to functional constructs such as filtration membranes and biological scaffolds,[18–23] but require extra processing steps after fabrication prior to polymerization. Inclusion of additives with the initiating groups before fabrication, in a similar fashion to formulation of everyday polymeric materials, can overcome this need for extra post-fabrication modification of the material.

Zwitterionic amphiphilic additives, where a macromolecular hydrophobic block facilitates anchoring in the base material through hydrophobic interactions, have been previously used to directly incorporate zwitterionic functionality.[24–29] In a comparable approach macromolecular additives functionalized with initiating groups were mixed with base polymers prior to fabrication into porous membranes.[30–32] From the available initiators at the surface of the membranes or electrospun scaffolds, antifouling polymers were polymerized, thereby retaining the control over the brush properties.[33] For biomaterial development, we propose that the interactions between the structural material and the additive should be managed with care. Additional interactions, such as hydrogen bonding, introduce a higher degree of specificity. Previously, hydrogen-bonded supramolecular materials were specifically functionalized with additives for antifouling properties[34–37], antimicrobial activity[38], additional bioactivity[36,39–41] and post-functionalization.[42,43] Here, we use the quadruple hydrogen bonding of the ureidopyrimidinone (UPy) moiety to facilitate the incorporation of a macroinitiator for SI-ATRP, to increase the functionalization potential of this class of materials.

A newly synthesized UPy-ATRP macro-initiator additive that contains a tertiary bromide (UPy-BiB) was mixed with UPy-modified polycaprolactone (PCLdiUPy) (**Figure 6.1**). Thin films were cast for initial screening of the reactivity of the mixtures with the macromolecular initiator. Sulfobetaine methacrylate (SBMA) monomers were polymerized by means of SI-ATRP from the additive that was embedded in the hard-phase of the constructs (**Figure 6.1**). The surfaces were characterized with water contact angle measurements (WCA), X-ray photoelectron spectroscopy (XPS) and atomic force microscopy (AFM), followed by functional cell adhesion assays. Furthermore, functional porous scaffolds were fabricated from the material mixtures with the UPy-BiB additive via electrospinning, to demonstrate applicability of the approach described here.

Surface characterization

Surfaces were prepared by casting solutions of mixtures of PCLdiUPy and the UPy-BiB macro-initiator additive on glass coverslips to investigate the influence of the incorporation of the UPy-BiB additive on the surface properties. The surface morphology of the solution-cast films was investigated with AFM. In the phase diagrams, where brighter domains indicate a harder phase, the fibrous structure resulting from the self-assembly of the UPy moieties was clearly visible (**Figure 6.2**).[44–46] This fibrous morphology was not altered by incorporation of up to 10% UPy-BiB additive, except for only a few small bright spots. The surfaces without initiator additive were exposed to the polymerization reaction mixture

for 3, 6, and 24 hours, after which the surfaces were thoroughly washed and dried before analysis. Little aspecific adsorption of components from the polymerization reaction mixture was observed, which was evident from the small increase in the number of brighter domains on the surfaces that were present over the exposure time (**Figure 6.2**, **Figure 6.3**). After 3 hours of grafting from the supramolecular UPy-BiB additive, a concentration dependent presence of brighter domains was observed, indicative of SBMA presence and therefore successful polymerization (**Figure 6.2**, **Figure 6.3**). For 5 and 10 mol% additive, these domains increased in size across the surface upon further reaction to 6 hours, whereas for 1 mol% additive, a minimal difference was observed. When the polymerization was run for up to 24 hours, the concentration dependent increase was no longer apparent. In the background, the fibrous morphology of the PCLdiUPy base material was still clearly visible in all samples. The most astonishing observation from these AFM images was that the brighter pSBMA domains originated from the hard-phase in the base material, as observed

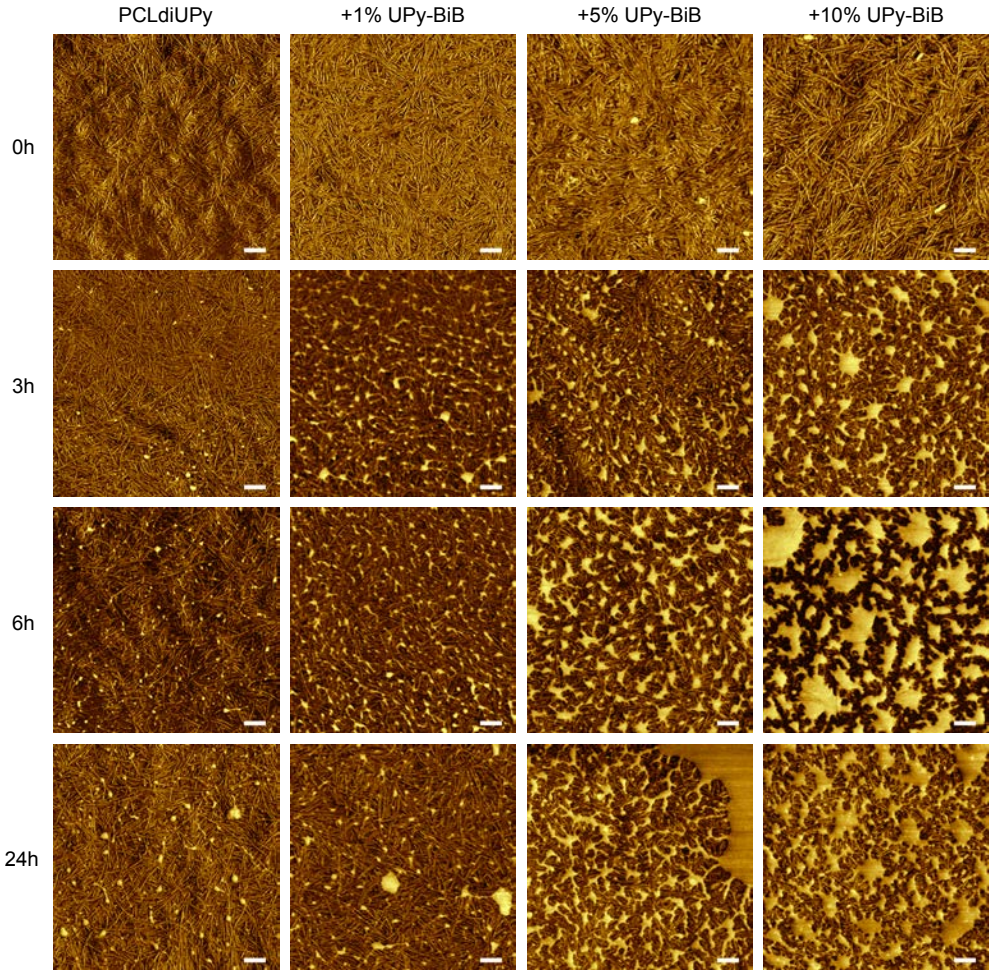

Figure 6.2. AFM phase micrographs of solution-cast films of PCLdiUPy with 0, 1, 5, and 10 % UPy-BiB macro-initiator additive before and after 3, 6, and 24 hours of polymerization on the surfaces. Scale bars indicate 100 nm.

from the zoomed in images (**Figure 6.3**). This confirmed that the initiator additive was well incorporated the UPy-based assemblies and that the polymerization reaction occurred from the hard-segments of this supramolecular thermoplastic elastomer.

In previous studies using SI-ATRP for the functionalization with sulfobetaine polymers, a brush thickness of ≥ 20 nm has been reported sufficient for antifouling properties.[15,47,48] From the height images recorded with AFM, the height of the pSBMA domains that were observed was quantified (**Figure 6.3**, **Figure 6.4**). Even though the assessment of the height was relatively inaccurate due to the inherent roughness of the solution-cast surfaces (**Table 6.1**), the thickness of the pSBMA domains did not exceed the 20 nm in general, for all UPy-BiB concentrations and polymerization times. Instead a thickness slightly over 10 nm could be achieved for the samples.

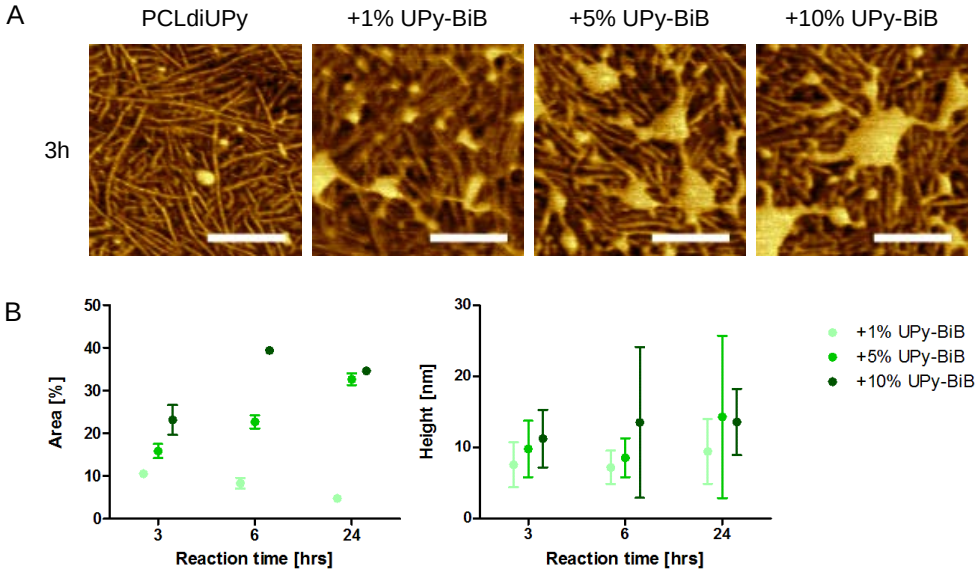

Figure 6.3. A) Zoomed cutouts of AFM phase micrographs from the 3 hour reaction time samples. Scale bars indicate 100 nm. B) Percentage of the solution-cast surface covered with SBMA domains, and the height of these domains. Data is represented as mean ± SD.

The presence of zwitterionic SBMA on the surface of the biomaterials was evident from an emerging sulfur signal and an additional quaternary nitrogen signal in the XPS spectra (**Figure 6.5**, **Table 6.2**). For increasing concentrations and polymerization reaction times, the contributions of the extra nitrogen and sulfur components also increased. A surface of pure pSBMA would result in a theoretical sulfur and quaternary nitrogen concentration of approximately 5.6%. The concentrations observed on the pSBMA grafted biomaterials were significantly lower (Table S2). This could suggest that the surface coverage was indeed not complete, or the thickness of polymerized pSBMA does not exceed the penetration depth of the radiation in the XPS measurements. Furthermore, the determined quaternary nitrogen component was generally lower than that for the sulfur species. Interestingly though, the reactive tertiary bromide is retained more with increasing polymerization time and thereby amount of pSBMA (**Table 6.2**). A hypothetical explanation for the retention of

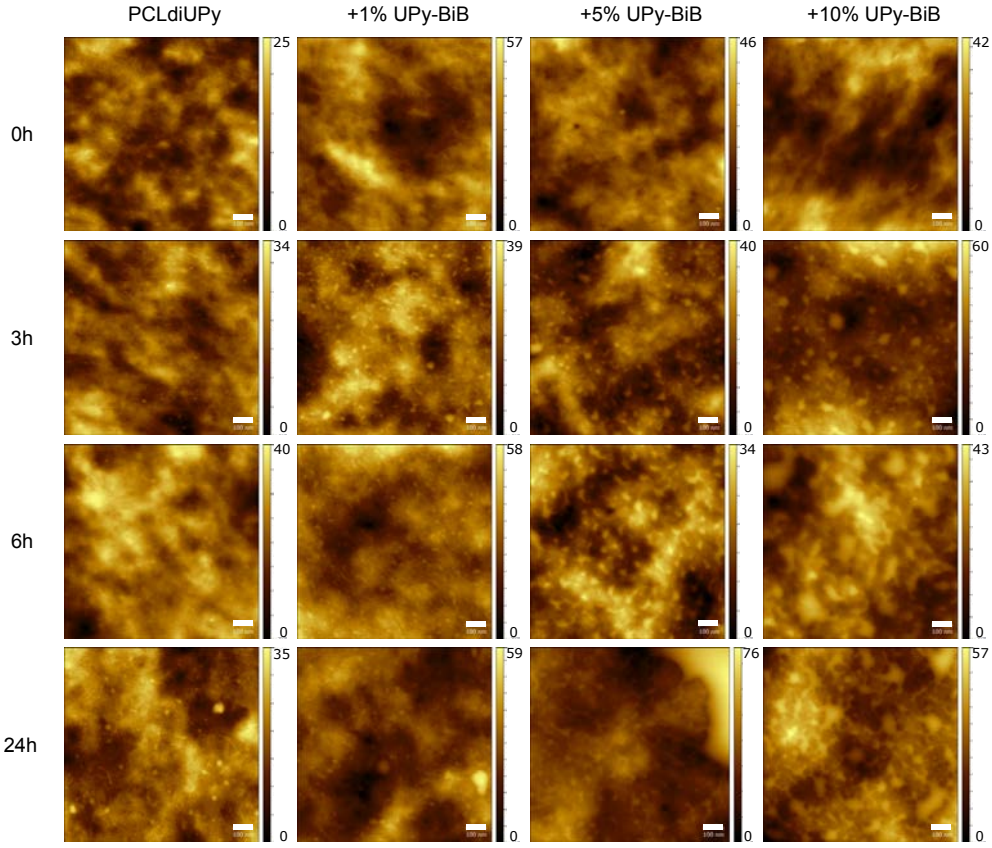

Figure 6.4. AFM height images recorded in tapping mode in air of solution-cast films of PCLdiUPy with 0, 1, 5, and 10% UPy-BiB additive before and after 3, 6, and 24 hours of polymerization on the surface. Scale bars represent 100 nm.

Table 6.1. Root Mean Square (RMS) roughness of solution-cast films.

	PCLdiUPy [nm]	**+1% UPy-BiB** [nm]	**+5% UPy-BiB** [nm]	**+10% UPy-BiB** [nm]
0h	4.6 ± 1.4	8.7 ± 0.8	6.3	5.1 ± 0.1
3h	4.5 ± 0.4	7.7 ± 2.3	7.5 ± 1.6	8.2 ± 0.8
6h	5.6 ± 1.0	7.6 ± 0.4	6.0 ± 0.2	7.1 ± 0.2
24h	5.8 ± 0.5	7.2 ± 1.6	11.1 ± 1.5	7.5 ± 0.1

the bromide could be that the chain-end folds back into the polymer layer, where it is less accessible for elimination. It's worthwhile to note that the presence of the bromide can facilitate secondary functionalization approaches.[49]

The macro-scale hydrophilicity of the surface was measured by means of WCA measurements, where a decrease in contact angle indicated the presence of hydrophilic pSBMA at the surface of the films. The addition of the UPy-BiB additive had no significant effect on the hydrophilicity of the surfaces (**Figure 6.5**). Exposure to the polymerization

reaction mixture decreased the contact angle only slightly on the films without UPy-BiB, going from 76 ± 1 ° to 71 ± 1 ° for subsequent polymerization reaction times. For films modified with the UPy-BiB additive, the contact angle decreased both with 3 and 6 hour polymerization reaction time, and increasing additive concentration. However, contact angles of below 20 °, reported for completely covered surfaces,[50,51] were not reached, which could result from incomplete SBMA surface coverage. For the films with 1, 5, and 10% UPy-BiB, the contact angles were again slightly higher after the 24 hour reaction times compared to the 6 hour samples.

The observations from AFM, WCA and XPS measurements all indicate an increased efficacy in polymerization with increasing UPy-BiB additive concentrations up to 6 hours of reaction time. However, for 24 hours of reaction time, these measurements show no clear increase in polymerization efficacy compared to the 6 hour time point. Due to extended polymerization times, the presence of longer and more water-soluble polymer chains may result in increased erosion from the supramolecular surface during the polymerization reaction and the subsequent washing steps.

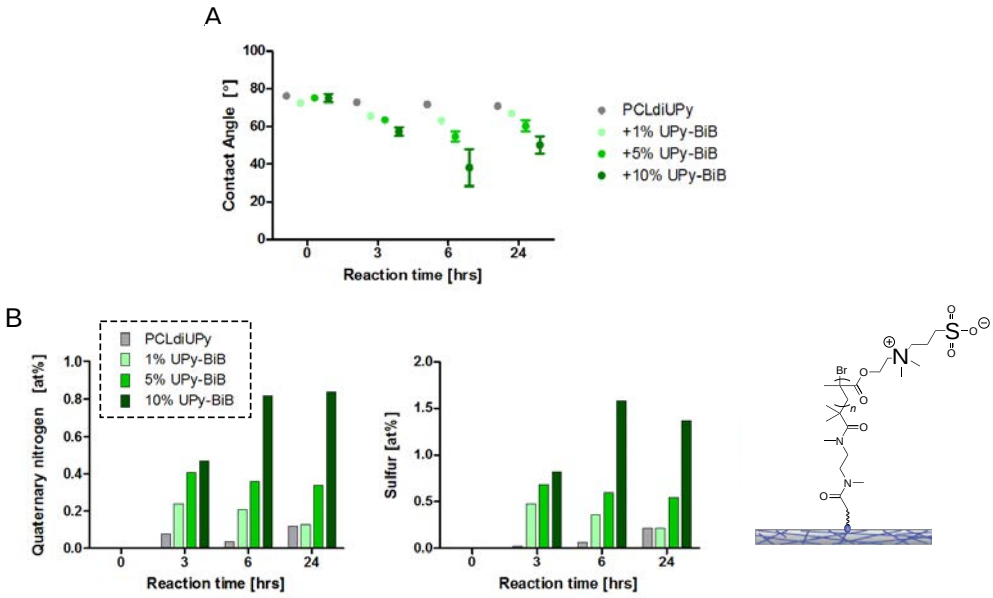

Figure 6.5. A) Water contact angles measured on solution-cast films with 0, 1, 5, and 10% UPy-BiB before and after 3, 6, and 24 hours of polymerization on the surface. Data are represented as mean ± SD. B) Contribution of quaternary nitrogen and sulfur components, which are unique for the SBMA, calculated from XPS spectra of the solution-cast films.

Cell adhesion on surfaces modified with zwitterionic polymers

To probe the functionality of the SBMA-functionalized surfaces, cell adhesion was assessed. Human Vena Saphena Cells (HVSC) were cultured on the pristine solution-cast surfaces with 0, 1, 5 and 10% UPy-BiB and after 3, 6 and 24 hours of polymerization of SBMA. The

presence of 1, 5 and 10% UPy-BiB alone did not influence cell adhesion, as the HVSCs adhered and spread similarly to the PCLdiUPy surface without additive (**Figure 6.6**). The surfaces without the UPy-BiB additive that were exposed to the SI-ATRP reaction conditions for 3, 6 and 24 hours showed no distinct decrease in cell adhesive properties, which indicates that neither the exposure to the polymerization reaction mixture, nor the presence of aspecific adsorbed pSBMA affects cell adhesion. For the films with 1% UPy-BiB the SBMA that was reacted to the surface had no significant effect on the adhesion and spreading of the HVSCs. After 3 hours of SI-ATRP reaction, the presence of pSBMA on the surface of the films with 5% UPy-BiB did not negatively influence cell adhesion. However, after 6 hours reaction time, a striking decrease in the adhesion of the HVSCs was observed here. Patches of cells were interchanged with clusters of rounded cells on these surfaces. For the surfaces with 10% UPy-BiB the cell adhesion decreased significantly already at 3 hours reaction time, which was amplified after 6 hours. However, the surfaces that have been used for the polymerization reaction for 24 hours, showed an increase in amount and variability of cell adhesion.

These results show that the pSBMA reacted from the UPy-BiB additive is functional to the extent where cell adhesion is significantly decreased. However, increased reaction time did not necessarily result in increased antifouling properties, which indicates that a critical pSBMA polymer chain length should not be exceeded.

Mechanistic insight in the surface-initiated polymerization is essential for further understanding of the process. The detected amount of SBMA increased accordingly with the UPy-BiB additive concentration. Also, the increase in surface area occupied by SBMA

Table 6.2. Atomic surface composition of solution-cast films with 0, 1, 5, and 10 mol% UPy-BiB before and after exposure to the SI-ATRP reaction conditions for 3, 6, and 24 hour.

		Surface composition [at%]					
		C	**O**	**N**	**N+**	**S**	**Br**
PCLdiUPy	0h	74.45	22.17	3.38	0.00	0.00	0.00
	3h	75.20	20.67	4.00	0.08	0.03	0.00
	6h	76.64	19.60	3.65	0.04	0.07	0.00
	24h	75.36	20.48	3.80	0.12	0.23	0.00
+1% UPy-BiB	0h	74.72	21.30	3.95	0.00	0.03	0.00
	3h	74.23	21.36	3.65	0.24	0.48	0.04
	6h	74.93	20.69	3.75	0.21	0.36	0.04
	24h	74.81	20.82	4.02	0.13	0.22	0.00
+5% UPy-BiB	0h	73.81	22.23	3.85	0.00	0.07	0.03
	3h	73.15	22.21	3.41	0.41	0.69	0.11
	6h	74.87	20.64	3.42	0.36	0.60	0.10
	24h	73.48	22.31	3.24	0.34	0.55	0.07
+10% UPy-BiB	0h	74.23	21.16	4.46	0.00	0.07	0.08
	3h	71.38	23.78	3.37	0.47	0.82	0.16
	6h	70.76	23.66	2.97	0.82	1.58	0.22
	24h	72.21	22.23	3.23	0.84	1.37	0.12

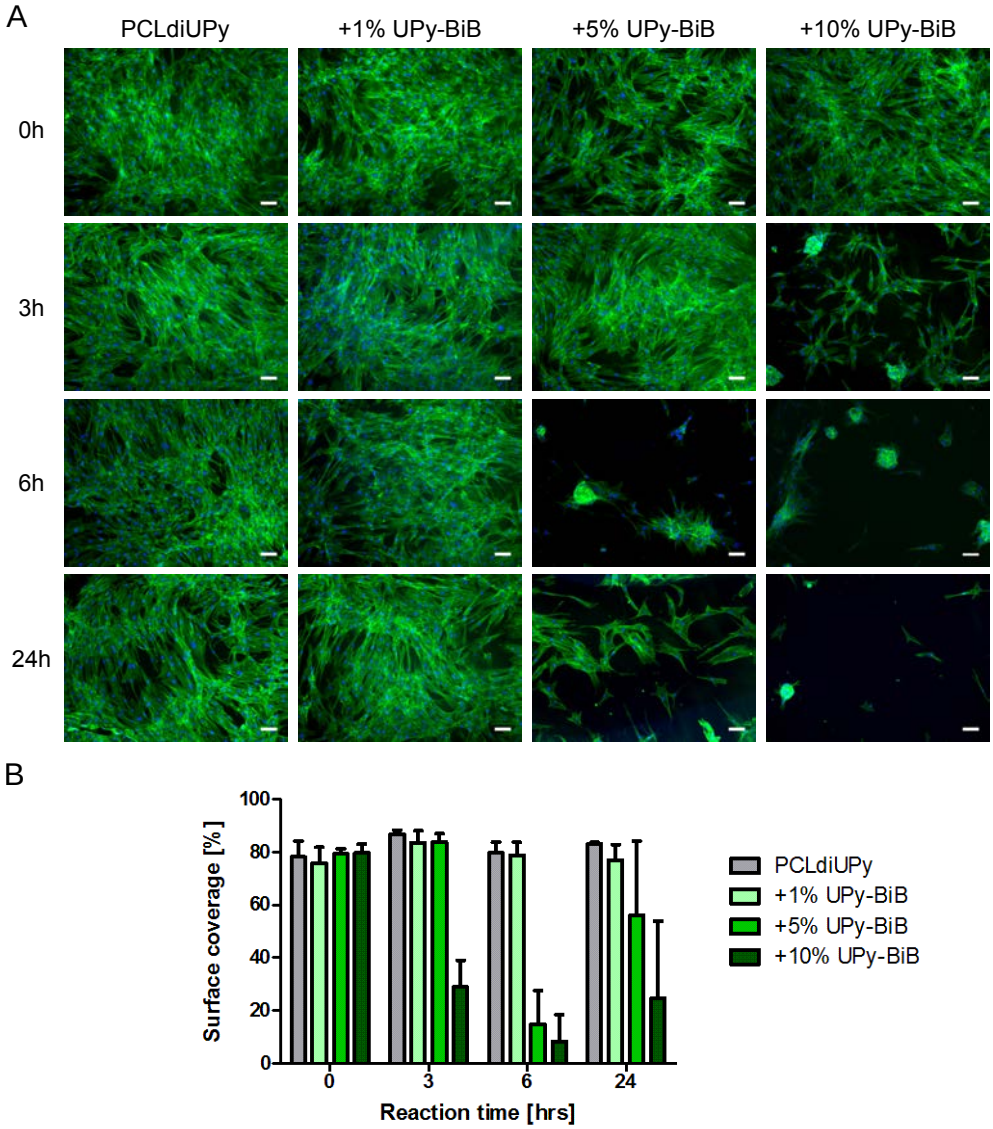

Figure 6.6. A) Fluorescence micrographs of HVSCs cultured for 24 hours on PCLdiUPy based solution-cast films, with 0, 1, 5, and 10% UPy-BiB, before and after 3, 6, and 24 hour polymerization reaction on the surface. Actin cytoskeleton is depicted in green and nuclei in blue. Scale bars represent 100 µm. B) Quantified surface coverage for the HVSCs on the solution-cast films. Data is represented as mean ± SD.

associated domains followed this trend. However, it would be particularly interesting to evaluate the amount of actual initiation sites for polymerization, and whether or not those correlate to the UPy-BiB concentrations and amount of detected pSBMA. From the AFM images of the solution-cast films it could be deduced that there might be localized points of initiation, since, especially with increasing polymerization times, the surfaces are characterized by separated domains of pSBMA. A certain spacing between initiation points

may be more preferable for the SI-ATRP reaction to occur. Furthermore, the assessment of the length of the UPy-pSBMA polymers within these domains would provide important information on the polymerization efficiency and chain-length. However quantification of the pSBMA size was practically not feasible, because of the small absolute amount of UPy-pSBMA in these small 2D samples, and the difficult quantification of molecular weight of zwitterionic polymer brushes on our non-ideal biomaterial surfaces.

Functionality of post-modified electrospun scaffolds

To further study the applicability of this post-functionalization polymerization strategy initiated from the hard-phase in a supramolecular thermoplastic elastomer, the mixture of 10% UPy-BiB additive and PCLdiUPy was electrospun into fibrous scaffolds. The scaffolds with and without 10% UPy-BiB additive had comparable morphologies and a fiber diameter of 0.36 ± 0.15 μm, and 0.46 ± 0.23 μm respectively (**Figure 6.7**). The hydrophilicity was similar for the scaffolds with and without additive (data not shown). The SI-ATRP reaction was performed on the electrospun scaffolds for 24 hours, since the relative surface area of the fibrous construct is significantly higher compared to 2D solution-cast substrates. After polymerization, the hydrophilicity of the scaffolds decreased significantly for both the scaffolds with and without 10% UPy-BiB additive, but was not determinable due to fast wetting of the microporous samples. The fiber diameter of the reacted samples increased slightly to 0.43 ± 0.15 μm and 0.58 ± 0.24 μm for the scaffolds with and without UPy-BiB, respectively. However, quantification was hampered by the presence of apparently fused fibers after the subsequent washing and drying procedures. Remarkably, the scaffolds with UPy-BiB additive that were reacted for 24 hours charged significantly faster whilst measuring with scanning electron microscopy. The XPS measurements on the scaffolds revealed presence of the quaternary nitrogen and sulfur components in the scaffolds with and without UPy-BiB that were exposed to the SI-ATRP reaction mixture. More SBMA appeared to be present in the scaffolds without initiator additive (**Figure 6.7**, **Table 6.3**). Moreover, little residual copper was detected on the scaffolds (<1 at%, **Table 6.3**), which was not observed on the solution-cast samples. The presence of physisorbed SBMA and copper indicate that in future experiments washing procedures must be further optimized.

The functional antifouling properties of the SBMA post-modified scaffolds were assessed with a cell adhesion assay. HVSCs were cultured for 24 hours on the scaffolds, which adhered and spread on the pristine scaffolds (**Figure 6.7**). The adhesion of the fibroblast-like cells was significantly decreased on the scaffolds with UPy-BiB that were reacted for 24 hours, whereas the decrease in cell adhesion was less defined for the scaffolds without UPy-BiB additive. This shows that, even though the XPS measurements implied increased SBMA presence on the scaffolds without UPy-BiB, compared to the scaffolds with UPy-BiB,

Table 6.3. Surface composition of electrospun scaffolds.

	Surface composition [at %]						
	C	**O**	**N**	**N+**	**S**	**Br**	**Cu**
PCLdiUPy 0h	75.16	20.68	4.16	0.00	0.00	0.00	0.00
PCLdiUPy 24h	67.58	26.41	2.07	1.13	2.00	0.00	0.81
10% UPy-BiB 0h	74.59	20.89	4.48	0.00	0.00	0.03	0.00
10% UPy-BiB 24h	70.63	24.07	2.91	0.72	1.20	0.09	0.38

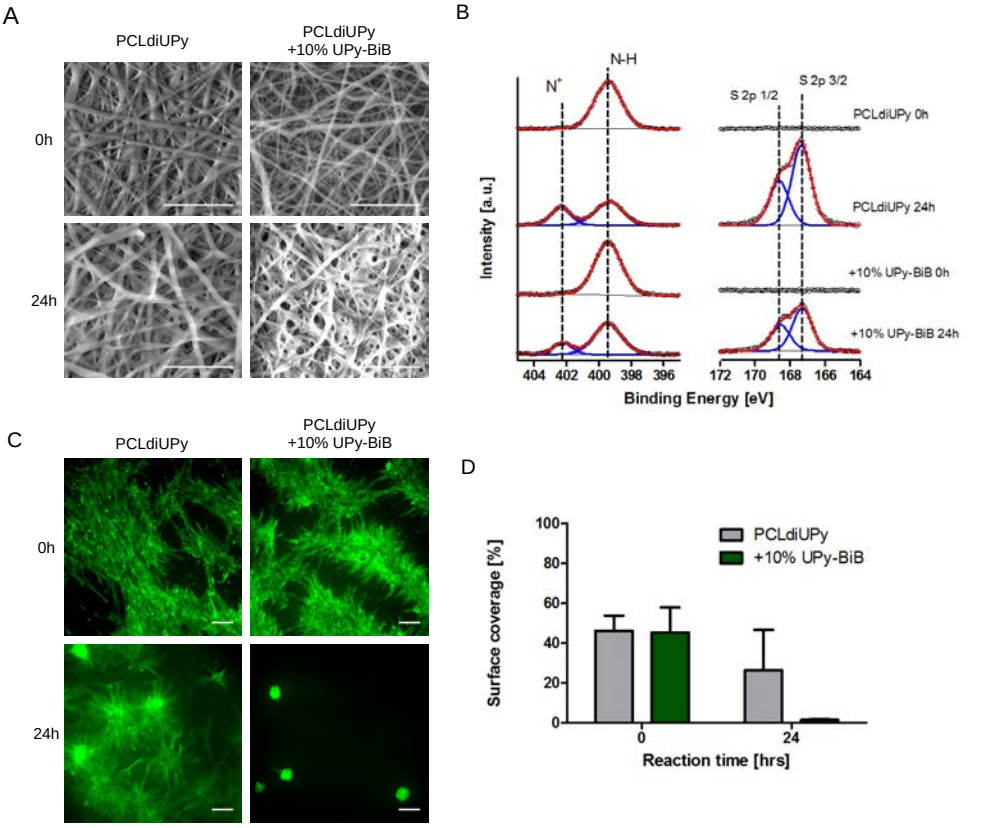

Figure 6.7. A) Scanning electron micrographs of electrospun scaffolds of PCLdiUPy with 0 and 10 mol% UPy-BiB, before and after 24 hour reaction. Scale bars indicate 10 µm. B) XPS spectra focused on nitrogen and sulfur signals. The data are represented in black, the modelled components by blue lines and the total fit by the red line. Dashed lines indicate the location of characteristic contributions in the spectra. C) Fluorescence micrographs of HVSCs cultured for 24 hours on the electrospun scaffolds used for the SI-ATRP reaction. Actin cytoskeleton is depicted in green, scale bars indicate 100 µm. D) Quantified surface coverage for the HVSCs on the electrospun scaffolds. Data is represented as mean ± SD.

the functional antifouling properties of the polymerized UPy-pSBMA are clearly superior.

General discussion

One interesting observation from both solution-cast films and electrospun scaffolds, was the apparent improved stability of the tertiary bromide on the polymerized pSBMA molecules, compared to the UPy-BiB initiator. In previous reports, the bromide signal is not present after polymerization, where reported tertiary bromide concentrations prior to reacting range from 0.81 to 1.9.[16,52,53] Due to the non-covalent nature of the incorporation of the UPy-pSBMA after polymerization, stability of the post-functionalized substrates should be subject of future studies. The polymerization reaction time of 24 hours is particularly long, compared to literature.[15] In the current setup, a color change in the polymerization reaction mixture indicated full oxidation of the copper catalyst, between the 6 and 24 hour time points. Therefore, future efforts should focus on shorter polymerization times to have

better control over the polymer brush dispersity and polymer chain-end livingness.

Conclusion and outlook

For the first time, the successful ATRP of zwitterionic SBMA monomers from a macro-initiator additive incorporated in the hard-phase of a supramolecular elastomeric material is reported here. Surface analysis by AFM, XPS and WCA measurements, as well as cell adhesion assays, show an initiator concentration and reaction time dependent polymerization efficacy. Cell adhesion was decreased significantly for surfaces with 5 and 10 mol% UPy-BiB additive and 6 hours reaction time. The non-cell adhesive properties could be translated to a functional electrospun scaffold with 10 mol% UPy-BiB. These results serve as a first step towards the fabrication of scaffolds or membranes that can be functionally post-modified via polymerization through the simple inclusion of a macro-initiator additive in the hard-phase of the structural base material.

The electrospun scaffolds post-modified with zwitterionic polymers offer many possibilities, mostly due to the properties of the zwitterionic compounds. The responsivity to varying salt concentrations could be employed to tune the porosity of the scaffolds reversibly[27]. Additionally, the interesting UCST behavior of pSBMA can give similar switchable properties.[54]

Moreover, a popular approach featuring antifouling materials involves further modification with specific bioactive moieties.[55] This could be achieved through the reaction of bioactive moieties to reactive monomers that were co-polymerized during the modification with the antifouling layer,[53] or by end-functionalizing the antifouling brush, making use of the reactive nature of the halide-capped polymer ends.[56]

Additionally, the presence of copper in the electrospun scaffolds after washing indicates that greener radical polymerization strategies such as activators regeneration ATRP methods where significantly lower amounts of copper are used, may be worth investigating, especially for biomedical applications.[57–64]

Experimental section

Materials

Unless stated otherwise, all reagents were used without further purification. Copper(I) chloride (CuCl, ≥99.99%) copper(II) chloride ($CuCl_2$, 97%) and 2,2′-bipyridyl (bpy, ≥99%) were obtained from Sigma-Aldrich. 2-(*N*-3-Sulfopropyl-*N,N*-dimethyl ammonium)ethyl methacrylate (SBMA, ≥98%) was obtained from Merck. The UPy-BiB additive was kindly synthesized and provided by Muhabbat Komil. UPy-modified polycaprolactone (PCLdiUPy) was purchased from SyMO-Chem. Copper(I) chloride (≥98%) was purified by vigorous stirring in acetic acid three times, washed with ethanol multiple times and dried under vacuum overnight.[62]

Chloroform (>99.8%), diethyl ether (DEE, >99.5%), dichloromethane (DCM, >99.9%), *N,N*-dimethylformamide (DMF, >99.8%), dioxane (>99.8%), ethanol (EtOH, >99.9%), ethyl acetate (>99.8%), heptane (>95%) and methanol (>99.8%) were purchased from Biosolve. 1,1,1,3,3,3-hexafluoroisopropanol (HFIP, >99%) was obtained from Sigma-Aldrich and Fluorochem.

Preparation of polymer films

PCLdiUPy (molecular weight of 2650 g mol^{-1}) and the additive UPy-BiB were dissolved

separately in HFIP at concentrations of 7.55 mM, each. The solutions were stirred overnight at room temperature in the dark. The conditions 1, 5, and 10 mol% UPy-BiB were mixed in molar ratios PCLdiUPy:UPy-BiB of 99:1, 95:5, and 90:10 in separate vials. In a large glass petri dish equipped with a cover, the solutions were cast (50 µL) on ø14 mm glass cover slips. The films were allowed to dry covered in the petri dish for 1 hour and subsequently air-dried overnight. Prior to characterizations the films were dried in vacuo overnight.

Preparation of electrospun scaffolds

PCLdiUPy and PCLdiUPy + 10% UPy-BiB were dissolved in HFIP at a total concentration of 340 mg mL^{-1}. Solutions were stirred overnight at room temperature. The electrospun constructs were prepared on a climate controlled electrospinning setup by IME technologies (Geldrop, Netherlands). A cylindrical mandrel rotating at 100 rpm with a diameter of 21 mm, covered in aluminium foil was used to collect the polymer fibers. A voltage of 18 kV, + 17 kV on the needle and -1 kV on the rotating mandrel, was applied over a distance of 12 cm between needle and collector. Temperature was set at 23 °C and relative humidity at 30%. The polymer solutions were fed through a nozzle (ø 0.8 mm) with a rate of 25 µL min^{-1} and 15 µL min^{-1} for PCLdiUPy and PCLdiUPy+10% UPy-BiB respectively. The aluminium foil, covered with the electrospun scaffold was removed from the mandrel and dried overnight in vacuum. Using a biopsy punch (Kai Medical), 8 mm circular discs were cut from the scaffold and used for polymerization and further analyses.

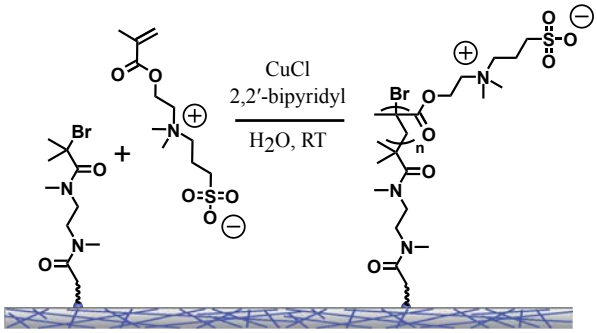

Scheme 6.1: Reaction conditions for SI-ATRP of SBMA from UPy-BiB functionalized surfaces.

Surface-initiated atom transfer radical polymerization (Scheme 6.1)

The polymerization stock solution was prepared as follows: CuCl (2.60 mg, 0.03 mmol, 1 eq.), $CuCl_2$ (31.78 mg, 0.24 mmol, 9 eq.) and bpy (90.24 mg, 0.58 mmol, 22 eq.) were weighed in a 10 mL Schlenk flask equipped with a septum and a magnetic stirring bar. The flask was sealed and deoxygenated by argon flow for 30 minutes. Deoxygenated milliQ (2.60 mL) was transferred to the catalyst/ligand mixture and further deoxygenated by argon flow until fully dissolved by stirring. The catalyst/ligand/solvent mixture was transferred to deoxygenated sulfobetaine methacrylate (1.47 g, 5.25 mmol, 200 eq.) in a separate 10 mL Schlenk flask equipped with a septum and a magnetic stirring bar. The polymerization mixture was further deoxygenated for 15 minutes, and used for the polymerization immediately.

For each polymerization condition, 10 solution-cast polymer films were immobilized in adapted 12-well Transwell inserts, from which the membrane was removed and custom made poly(ether ether ketone) (PEEK) rings were used to mount the samples. The polymer films were degassed under a funnel with heavy argon flow for 30 minutes. The polymerization was initiated by transferring the polymerization mixture (200 µL) from the stock solution to each Transwell insert under exclusion of air. The polymerization was carried out at room temperature, under moderate argon flow. The polymerization was stopped by exposing the reaction mixture to air. The polymerization mixture was removed,

and each polymer film was washed with milliQ (0.5 mL) three times. Subsequently, the polymer films were removed from the inserts and thoroughly washed three times with milliQ (1 mL), and air-dried for several hours. Prior to characterization techniques the films were dried in vacuo overnight. For the electrospun scaffolds, 10 samples were immobilized in similarly adapted 24-well Transwell inserts. The same polymerization conditions were applied as for solution-cast films. Post-polymerization, the samples were washed by submerging the scaffolds in milliQ (3 mL) three times, or until the strong catalyst color was imperceptible. Prior to characterization the scaffolds were dried in vacuo overnight.

Water Contact Angle Measurements
Static water contact angles were measured using a DataPhyisics OCA 30 goniometer at room temperature. Droplets of 2 µL were applied on the surface and the contact angle was measured using SCA20 software (v4.1.13) at the polymer-air-water interfaces 5 seconds after depositing the droplet.

Scanning Electron Microscopy
Electrospun scaffolds were analyzed using a FEI Quanta 600 scanning electron microscope and Xt Microscope control software. Images were recorded in low vacuum (~0.6 mbar) with water vapor, of samples fixed on metal stubs with adhesive carbon conductive tape. Secondary and backscattered electrons were detected with an accelerating voltage of 10 kV and a working distance of 10 mm. Compound images were constructed by overlaying the resulting images from both detectors.

Atomic Force Microscopy
A Digital Instruments Multimode and a Dimension 3100 with Nanoscope III controllers were used to probe the surfaces of the solution-cast films. Silicon cantilever tips with a typical tip radius of 7 nm were used to record phase and height images in the tapping mode regime at room temperature. Images were processed using Gwyddion software (version 2.43). The percentage of the surface covered by SBMA domains was determined from two 1 × 1 µm phase images, and the height of the domains from 40 measurements per condition using ImageJ (NIH, version 1.48).

X-ray photoelectron spectroscopy
XPS was performed using a Thermo Scientific K-Alpha spectrometer equipped with a monochromatic, small-spot X-ray source, and a 180° double focusing hemispherical analyzer with a 128-channel detector. Spectra were obtained using an aluminium anode (Al Kα, 1486.7 eV, 72 W). Survey scans were measured at a pass energy of 200 eV and region scans at a pass energy of 50 eV. Analysis and quantification of the spectra were performed using CasaXPS software (version 2.3.18).

Cell culture and adhesion assay
Human vena saphena cells were harvested from the human vena saphena magna according to the Dutch guidelines for secondary use of materials. HVSCs were expanded in culture medium, which consisted of Dulbecco's modified Eagle medium (DMEM, Gibco) supplemented with 10% fetal bovine serum (FBS), 1% glutamax (Gibco), and 1% penicillin/streptomycin, and used for experiments up to passage 7.

The solution-cast polymer films on glass were secured in adapted 12 well Transwell inserts (Corning), from which the membrane was removed and custom made PEEK rings were used to mount the samples. Samples were sterilized under UV for 15 minutes. An 8 mm biopsy punch (Kai Medical) was used to prepare circular samples from the electrospun constructs. These were mounted in similarly adapted 24 well Transwell inserts and sterilized under UV on both sides for 15 minutes. Cells were harvested from the culture flasks using trypsin/EDTA and seeded at a concentration of 25 000 cells cm^{-2} on the solution-cast films and 60 000 cells cm^{-2} on the scaffold samples. After 24 hours culture, non-adherent cells were aspirated and the samples were washed twice with PBS prior to fixation in 3.7% formaldehyde. The actin cytoskeleton was stained with phalloidin-ATTO488, and nuclei were stained with 4',6-diamidino-2-phenylindole (DAPI). Samples were visualized using a Zeiss Axiovert 200M.

References

(1) Wei, Q.; Becherer, T.; Angioletti-Uberti, S.; Dzubiella, J.; Wischke, C.; Neffe, A. T.; Lendlein, A.; Ballauff, M.; Haag, R. Protein Interactions with Polymer Coatings and Biomaterials. *Angew. Chem., Int. Ed.* **2014**, *53*, 8004–8031.

(2) Ippel, B. D.; Dankers, P. Y. W. Introduction of Nature's Complexity in Engineered Blood-Compatible Biomaterials. *Adv. Healthcare Mater.* **2018**, *7*, 1700505.

(3) Chen, S.; Li, L.; Zhao, C.; Zheng, J. Surface Hydration: Principles and Applications toward Low-Fouling/nonfouling Biomaterials. *Polymer* **2010**, *51*, 5283–5293.

(4) Schlenoff, J. B. Zwitteration: Coating Surfaces with Zwitterionic Functionality to Reduce Nonspecific Adsorption. *Langmuir* **2014**, *30*, 9625–9636.

(5) Jiang, S.; Cao, Z. Ultralow-Fouling, Functionalizable, and Hydrolyzable Zwitterionic Materials and Their Derivatives for Biological Applications. *Adv. Mater.* **2010**, *22*, 920–932.

(6) Chen, W.-L.; Cordero, R.; Tran, H.; Ober, C. K. 50th Anniversary Perspective : Polymer Brushes: Novel Surfaces for Future Materials. *Macromolecules* **2017**, *50*, 4089–4113.

(7) Banerjee, I.; Pangule, R. C.; Kane, R. S. Antifouling Coatings: Recent Developments in the Design of Surfaces That Prevent Fouling by Proteins, Bacteria, and Marine Organisms. *Adv. Mater.* **2011**, *23*, 690–718.

(8) Shao, Q.; Jiang, S. Molecular Understanding and Design of Zwitterionic Materials. *Adv. Mater.* **2015**, *27*, 15–26.

(9) Edmondson, S.; Osborne, V. L.; Huck, W. T. S. Polymer Brushes via Surface-Initiated Polymerizations. *Chem. Soc. Rev.* **2004**, *33*, 14.

(10) Yuan, L.; Yu, Q.; Li, D.; Chen, H. Surface Modification to Control Protein/Surface Interactions. *Macromol. Biosci.* **2011**, *11*, 1031–1040.

(11) Krishnamoorthy, M.; Hakobyan, S.; Ramstedt, M.; Gautrot, J. E. Surface-Initiated Polymer Brushes in the Biomedical Field: Applications in Membrane Science, Biosensing, Cell Culture, Regenerative Medicine and Antibacterial Coatings. *Chem. Rev.* **2014**, *114*, 10976–11026.

(12) Barbey, R.; Lavanant, L.; Paripovic, D.; Schüwer, N.; Sugnaux, C.; Tugulu, S.; Klok, H. Polymer Brushes via Surface-Initiated Controlled Radical Polymerization: Synthesis, Characterization, Properties, and Applications. *Chem. Rev.* **2009**, *109*, 5437–5527.

(13) Wei, Y.; Zhang, J.; Feng, X.; Liu, D. Bioactive Zwitterionic Polymer Brushes Grafted from Silicon Wafers via SI-ATRP for Enhancement of Antifouling Properties and Endothelial Cell Selectivity. *J. Biomater. Sci. Polym. Ed.* **2017**, *28*, 2101–2116.

(14) Zhang, Z.; Chen, S.; Jiang, S. Dual-Functional Biomimetic Materials: Nonfouling Poly(carboxybetaine) with Active Functional Groups for Protein Immobilization. *Biomacromolecules* **2006**, *7*, 3311–3315.

(15) van Andel, E.; Lange, S. C.; Pujari, S. P.; Tijhaar, E. J.; Smulders, M. M. J.; Savelkoul, H. F. J.; Zuilhof, H. Systematic Comparison of Zwitterionic and Non-Zwitterionic Antifouling Polymer Brushes on a Bead-Based Platform. *Langmuir* **2019**, *35*, 1181–1191.

(16) Kuang, J.; Messersmith, P. B. Universal Surface-Initiated Polymerization of Antifouling Zwitterionic Brushes Using a Mussel-Mimetic Peptide Initiator. *Langmuir* **2012**, *28*, 7258–7266.

(17) Fan, X.; Lin, L.; Dalsin, J. L.; Messersmith, P. B. Biomimetic Anchor for Surface-Initiated Polymerization from Metal Substrates. *J. Am. Chem. Soc.* **2005**, *127*, 15843–15847.

(18) Surman, F.; Riedel, T.; Bruns, M.; Kostina, N. Y.; Sedláková, Z.; Rodriguez-Emmenegger, C. Polymer Brushes Interfacing Blood as a Route toward High Performance Blood Contacting

Devices. *Macromol. Biosci.* **2015**, *15*, 636–646.

(19) Kostina, N. Y.; Pop-Georgievski, O.; Bachmann, M.; Neykova, N.; Bruns, M.; Michálek, J.; Bastmeyer, M.; Rodriguez-Emmenegger, C. Non-Fouling Biodegradable Poly(ϵ-Caprolactone) Nanofibers for Tissue Engineering. *Macromol. Biosci.* **2016**, *16*, 83–94.

(20) Gualandi, C.; Vo, C. D.; Focarete, M. L.; Scandola, M.; Pollicino, A.; Di Silvestro, G.; Tirelli, N. Advantages of Surface-Initiated ATRP (SI-ATRP) for the Functionalization of Electrospun Materials. *Macromol. Rapid Commun.* **2013**, *34*, 51–56.

(21) Yue, W. W.; Li, H. J.; Xiang, T.; Qin, H.; Sun, S. D.; Zhao, C. S. Grafting of Zwitterion from Polysulfone Membrane via Surface-Initiated ATRP with Enhanced Antifouling Property and Biocompatibility. *J. Memb. Sci.* **2013**, *446*, 79–91.

(22) Liu, P.; Huang, T.; Liu, P.; Shi, S.; Chen, Q.; Li, L.; Shen, J. Zwitterionic Modification of Polyurethane Membranes for Enhancing the Anti-Fouling Property. *J. Colloid Interface Sci.* **2016**, *480*, 91–101.

(23) Yuan, H.; Qian, B.; Zhang, W.; Lan, M. Protein Adsorption Resistance of PVP-Modified Polyurethane Film Prepared by Surface-Initiated Atom Transfer Radical Polymerization. *Appl. Surf. Sci.* **2016**, *363*, 483–489.

(24) Sun, Q.; Su, Y.; Ma, X.; Wang, Y.; Jiang, Z. Improved Antifouling Property of Zwitterionic Ultrafiltration Membrane Composed of Acrylonitrile and Sulfobetaine Copolymer. *J. Memb. Sci.* **2006**, *285*, 299–305.

(25) Wang, L.; Su, Y.; Zheng, L.; Chen, W.; Jiang, Z. Highly Efficient Antifouling Ultrafiltration Membranes Incorporating Zwitterionic poly([3-(Methacryloylamino)propyl]-dimethyl(3-Sulfopropyl) Ammonium Hydroxide). *J. Memb. Sci.* **2009**, *340*, 164–170.

(26) Li, J. H.; Li, M. Z.; Miao, J.; Wang, J. Bin; Shao, X. S.; Zhang, Q. Q. Improved Surface Property of PVDF Membrane with Amphiphilic Zwitterionic Copolymer as Membrane Additive. *Appl. Surf. Sci.* **2012**, *258*, 6398–6405.

(27) Zhao, Y.-F.; Zhang, P.-B.; Sun, J.; Liu, C.-J.; Zhu, L.-P.; Xu, Y.-Y. Electrolyte-Responsive Polyethersulfone Membranes with Zwitterionic Polyethersulfone-Based Copolymers as Additive. *J. Memb. Sci.* **2016**, *510*, 306–313.

(28) Fang, L.-F.; Jeon, S.; Kakihana, Y.; Kakehi, J.; Zhu, B.-K.; Matsuyama, H.; Zhao, S. Improved Antifouling Properties of Polyvinyl Chloride Blend Membranes by Novel Phosphate Based-Zwitterionic Polymer Additive. *J. Memb. Sci.* **2017**, *528*, 326–335.

(29) Kaner, P.; Rubakh, E.; Kim, D. H.; Asatekin, A. Zwitterion-Containing Polymer Additives for Fouling Resistant Ultrafiltration Membranes. *J. Memb. Sci.* **2017**, *533*, 141–159.

(30) Rodda, A. E.; Ercole, F.; Glattauer, V.; Nisbet, D. R.; Healy, K. E.; Dove, A. P.; Meagher, L.; Forsythe, J. S. Controlling Integrin-Based Adhesion to a Degradable Electrospun Fibre Scaffold via SI-ATRP. *J. Mater. Chem. B* **2016**, *4*, 7314–7322.

(31) Duque-Sánchez, L.; Brack, N.; Postma, A.; Pigram, P. J.; Meagher, L. Optimisation of Grafting of Low Fouling Polymers from Three-Dimensional Scaffolds: Via Surface-Initiated Cu(0) Mediated Polymerisation. *J. Mater. Chem. B* **2018**, *6*, 5896–5909.

(32) Harrison, R. H.; Steele, J. A. M.; Chapman, R.; Gormley, A. J.; Chow, L. W.; Mahat, M. M.; Podhorska, L.; Palgrave, R. G.; Payne, D. J.; Hettiaratchy, S. P.; et al. Modular and Versatile Spatial Functionalization of Tissue Engineering Scaffolds through Fiber-Initiated Controlled Radical Polymerization. *Adv. Funct. Mater.* **2015**, *25*, 5748–5757.

(33) Duque Sánchez, L.; Brack, N.; Postma, A.; Pigram, P. J.; Meagher, L. Surface Modification of Electrospun Fibres for Biomedical Applications: A Focus on Radical Polymerization Methods. *Biomaterials* **2016**, *106*, 24–45.

(34) Pape, A. C. H.; Ippel, B. D.; Dankers, P. Y. W. Cell and Protein Fouling Properties of Polymeric Mixtures Containing Supramolecular Poly(ethylene Glycol) Additives. *Langmuir* **2017**, *33*, 4076–4082.

(35) Van Almen, G. C.; Talacua, H.; Ippel, B. D.; Mollet, B. B. B.; Ramaekers, M.; Simonet, M.; Smits, A. I. P. M.; Bouten, C. V. C.; Kluin, J.; Dankers, P. Y. W. Development of Non-Cell Adhesive Vascular Grafts Using Supramolecular Building Blocks. *Macromol. Biosci.* **2016**, *16*, 350–362.

(36) Mollet, B. B.; Comellas-Aragonès, M.; Spiering, A. J. H.; Söntjens, S. H. M.; Meijer, E. W.; Dankers, P. Y. W. A Modular Approach to Easily Processable Supramolecular Bilayered Scaffolds with Tailorable Properties. *J. Mater. Chem. B* **2014**, *2*, 2483–2493.

(37) Ippel, B. D.; Keizer, H. M.; Dankers, P. Y. W. Supramolecular Antifouling Additives for Robust and Efficient Functionalization of Elastomeric Materials: Molecular Design Matters. *Adv. Funct. Mater.* **2019**, *29*, 1805375.

(38) Zaccaria, S.; van Gaal, R. C.; Riool, M.; Zaat, S. A. J.; Dankers, P. Y. W. Antimicrobial Peptide Modification of Biomaterials Using Supramolecular Additives. *J. Polym. Sci. Part A: Polym. Chem.* **2018**, *56*, 1926–1934.

(39) Dankers, P. Y. W.; Harmsen, M. C.; Brouwer, L. A.; van Luyn, M. J. A.; Meijer, E. W. A Modular and Supramolecular Approach to Bioactive Scaffolds for Tissue Engineering. *Nat. Mater.* **2005**, *4*, 568–574.

(40) Spaans, S.; Fransen, P. P. K. H.; Ippel, B. D.; de Bont, D. F. A.; Keizer, H. M.; Bax, N. A. M. A. M.; Bouten, C. V. C.; Dankers, P. Y. W. Supramolecular Surface Functionalization via Catechols for the Improvement of Cell–material Interactions. *Biomater. Sci.* **2017**, *5*, 1541–1548.

(41) Muylaert, D. E. P.; van Almen, G. C.; Talacua, H.; Fledderus, J. O.; Kluin, J.; Hendrikse, S. I. S.; van Dongen, J. L. J.; Sijbesma, E.; Bosman, A. W.; Mes, T.; et al. Early in-Situ Cellularization of a Supramolecular Vascular Graft Is Modified by Synthetic Stromal Cell-Derived Factor-1α Derived Peptides. *Biomaterials* **2016**, *76*, 187–195.

(42) Goor, O. J. G. M.; Brouns, J. E. P.; Dankers, P. Y. W. Introduction of Anti-Fouling Coatings at the Surface of Supramolecular Elastomeric Materials via Post-Modification of Reactive Supramolecular Additives. *Polym. Chem.* **2017**, *8*, 5228–5238.

(43) Goor, O. J. G. M.; Keizer, H. M.; Bruinen, A. L.; Schmitz, M. G. J.; Versteegen, R. M.; Janssen, H. M.; Heeren, R. M. A.; Dankers, P. Y. W. Efficient Functionalization of Additives at Supramolecular Material Surfaces. *Adv. Mater.* **2017**, *29*, 1604652.

(44) Kautz, H.; van Beek, D. J. M.; Sijbesma, R. P.; Meijer, E. W. Cooperative End-to-End and Lateral Hydrogen-Bonding Motifs in Supramolecular Thermoplastic Elastomers. *Macromolecules* **2006**, *39*, 4265–4267.

(45) Appel, W. P. J.; Meijer, E. W.; Dankers, P. Y. W. Enzymatic Activity at the Surface of Biomaterials via Supramolecular Anchoring of Peptides: The Effect of Material Processing. *Macromol. Biosci.* **2011**, *11*, 1706–1712.

(46) Appel, W. P. J.; Portale, G.; Wisse, E.; Dankers, P. Y. W.; Meijer, E. W. Aggregation of Ureido-Pyrimidinone Supramolecular Thermoplastic Elastomers into Nanofibers: A Kinetic Analysis. *Macromolecules* **2011**, *44*, 6776–6784.

(47) Nguyen, A. T.; Baggerman, J.; Paulusse, J. M. J.; van Rijn, C. J. M.; Zuilhof, H. Stable Protein-Repellent Zwitterionic Polymer Brushes Grafted from Silicon Nitride. *Langmuir* **2011**, *27*, 2587–2594.

(48) Blaszykowski, C.; Sheikh, S.; Thompson, M. A Survey of State-of-the-Art Surface Chemistries to Minimize Fouling from Human and Animal Biofluids. *Biomater. Sci.* **2015**, *3*, 1335–1370.

(49) Zoppe, J. O.; Ataman, N. C.; Mocny, P.; Wang, J.; Moraes, J.; Klok, H.-A. Surface-Initiated

Controlled Radical Polymerization: State-of-the-Art, Opportunities, and Challenges in Surface and Interface Engineering with Polymer Brushes. *Chem. Rev.* **2017**, *117*, 1105–1318.

(50) Cheng, N.; Brown, A. A.; Azzaroni, O.; Huck, W. T. S. Thickness-Dependent Properties of Polyzwitterionic Brushes. *Macromolecules* **2008**, *41*, 6317–6321.

(51) Emmenegger, C. R.; Brynda, E.; Riedel, T.; Sedlakova, Z.; Houska, M.; Alles, A. B. Interaction of Blood Plasma with Antifouling Surfaces. *Langmuir* **2009**, *25*, 6328–6333.

(52) Fan, X.; Lin, L.; Dalsin, J. L.; Messersmith, P. B. Biomimetic Anchor for Surface-Initiated Polymerization from Metal Substrates. **2005**, No. 9, 15843–15847.

(53) Lange, S. C.; van Andel, E.; Smulders, M. M. J.; Zuilhof, H. Efficient and Tunable Three-Dimensional Functionalization of Fully Zwitterionic Antifouling Surface Coatings. *Langmuir* **2016**, *32*, 10199–10205.

(54) Azzaroni, O.; Brown, A. A.; Huck, W. T. S. UCST Wetting Transitions of Polyzwitterionic Brushes Driven by Self-Association. *Angew. Chem., Int. Ed.* **2006**, *45*, 1770–1774.

(55) Baggerman, J.; Smulders, M. M. J.; Zuilhof, H. Romantic Surfaces: A Systematic Overview of Stable, Biospecific, and Antifouling Zwitterionic Surfaces. *Langmuir* **2019**, *35*, 1072–1084.

(56) Huang, C. J.; Brault, N. D.; Li, Y.; Yu, Q.; Jiang, S. Controlled Hierarchical Architecture in Surface-Initiated Zwitterionic Polymer Brushes with Structurally Regulated Functionalities. *Adv. Mater.* **2012**, *24*, 1834–1837.

(57) Matyjaszewski, K.; Hongchen, D.; Jakubowski, W.; Pietrasik, J.; Kusumo, A. Grafting from Surfaces For "everyone": ARGET ATRP in the Presence of Air. *Langmuir* **2007**, *23*, 4528–4531.

(58) Hong, D.; Hung, H. C.; Wu, K.; Lin, X.; Sun, F.; Zhang, P.; Liu, S.; Cook, K. E.; Jiang, S. Achieving Ultralow Fouling under Ambient Conditions via Surface-Initiated ARGET ATRP of Carboxybetaine. *ACS Appl. Mater. Interfaces* **2017**, *9*, 9255–9259.

(59) Wang, M.; Yuan, J.; Huang, X.; Cai, X.; Li, L.; Shen, J. Grafting of Carboxybetaine Brush onto Cellulose Membranes via Surface-Initiated ARGET-ATRP for Improving Blood Compatibility. *Colloids Surf., B* **2013**, *103*, 52–58.

(60) Jakubowski, W.; Matyjaszewski, K. Activators Regenerated by Electron Transfer for Atom-Transfer Radical Polymerization of (Meth)acrylates and Related Block Copolymers. *Angew. Chem., Int. Ed.* **2006**, *45*, 4482–4486.

(61) Min, K.; Gao, H.; Matyjaszewski, K. Use of Ascorbic Acid as Reducing Agent for Synthesis of Well-Defined Polymers by ARGET ATRP. *Macromolecules* **2007**, *40*, 1789–1791.

(62) Konkolewicz, D.; Magenau, A. J. D.; Averick, S. E.; Simakova, A.; He, H.; Matyjaszewski, K. ICAR ATRP with Ppm Cu Catalyst in Water. *Macromolecules* **2012**, *45*, 4461–4468.

(63) Konkolewicz, D.; Krys, P.; Góis, J. R.; Mendonça, P.V.; Zhong, M.; Wang, Y.; Gennaro, A.; Isse, A. A.; Fantin, M.; Matyjaszewski, K. Aqueous RDRP in the Presence of Cu0: The Exceptional Activity of CuI Confirms the SARA ATRP Mechanism. *Macromolecules* **2014**, *47*, 560–570.

(64) Pan, X.; Malhotra, N.; Simakova, A.; Wang, Z.; Konkolewicz, D.; Matyjaszewski, K. Photoinduced Atom Transfer Radical Polymerization with Ppm-Level Cu Catalyst by Visible Light in Aqueous Media. *J. Am. Chem. Soc.* **2015**, *137*, 15430–15433.

(65) De Feijter, I.; Goor, O. J. G. M.; Hendrikse, S. I. S.; Comellas-Aragonès, M.; Söntjens, S. H. M.; Zaccaria, S.; Fransen, P. P. K. H.; Peeters, J. W.; Milroy, L. G.; Dankers, P. Y. W. Solid-Phase-Based Synthesis of Ureidopyrimidinone-Peptide Conjugates for Supramolecular Biomaterials. *Synlett* **2015**, *26*, 2707–2713.

(66) Keller, R. N.; Wrcoff, H. D.; Marchi, L. E. Copper(I) Chloride. In *Inorganic Syntheses*; 1946; Vol. I, pp 1–4.

7

Impact of additives on mechanical properties of supramolecular electrospun scaffolds

Abstract

Modification with supramolecular additives is used to alter the properties of elastomeric materials, rendering these anti-fouling, specifically cell-adhesive, or suitable for further post-functionalization. Often, the additive containing materials are processed into functional scaffolds using electrospinning for mechanically challenging applications. Under these conditions, the mechanical properties of the scaffold are unequivocally important. Here, the effect of supramolecular additive functionalization on mechanical behavior of electrospun scaffolds was investigated for one model supramolecular filler and three previously developed antifouling additives. Results indicated that the filler additive had no effect on the mechanical properties of the bulk material, whereas the mechanical properties were slightly decreased following the addition of the additives compared to the pristine elastomeric PCL-BU base material.

The content of this chapter is based on:

Bastiaan D. Ippel, Eline E. van Haaften, Carlijn V.C. Bouten, Patricia Y.W. Dankers, *Impact of additives on mechanical properties of supramolecular electrospun scaffolds*, (in preparation)

Introduction

Supramolecular biomaterials can be functionalized by modular incorporation of additives, to formulate materials with antifouling and specific cell-adhesive properties, and with groups that allow for post-functionalization. The properties of the functionalized materials were initially studied on thin films, which were either solution-cast or spin-coated. In **Chapters 3** and **6** the translational step towards functional biomaterials was made through processing of the studied materials into electrospun scaffolds. In general, the mechanical properties of functional, load-bearing scaffolds fabricated with electrospinning, such as vascular grafts, are particularly important for proper functioning.

Hydrogen bonded thermoplastic elastomers, such as polyurethane, poly(urethane urea), or polyurea, are regularly used in biomedical applications, such as cardiac patches[1], heart valves[2], and vascular grafts.[3,4] The unique mechanical properties of these materials arise from their molecular composition, where macromolecular soft-blocks with rubber-like properties are alternated with hard-blocks capable of crystallization, e.g. through hydrogen-bonding.[5] These two components have the tendency to phase-separate on the nano-scale, and in the case where the hard-block is comprised of well-defined hydrogen bonding units, intriguingly form fibrous hard-segments.[6,7] Past investigations have tried to elucidate the molecular reorganization of hydrogen-bonded fibrous thermoplastic elastomers during elongation.[7,8] The orientation of the fibrous hard-phase is generally isotropic following solution-casting, as seen in atomic force microscopy phase images (example in **Figure 7.1B**). Upon stretching, the hard-segments orient in the direction of the applied strain. When the yield-point is exceeded, the hard-segments fracture and their orientation transgresses to the direction perpendicular to the strain.[7,8]

Previously, the supramolecular functionalization strategy based on molecular recognition by bisurea additives, has been used to tune the mechanical properties of bisurea-based thermoplastic elastomers.[9] Through incorporation of a small molecular filler, which was shown to co-assemble with the bisurea phase in the poly(caprolactone)-bisurea (PCL-BU) base material up to approximately 25 mol%, the ratio of hard-block to soft-block was altered in a supramolecular fashion. This resulted in an approximately twofold increased Young's modulus, without a clear loss in ultimate tensile strength.[9] Higher concentrations of filler additive resulted in two distinct hard-segment domains. Below this threshold, similar strain-induced orientation of the fibrous hard-segments is observed compared to the unmodified base material.[10] Hard-segments consisting of solely filler, that form with increased bisurea-filler concentration, do not orient with the hard-phase of the base material, as little interaction forces them to.[10]

However, when these materials are processed into electrospun scaffolds, another order of complexity is introduced in the mechanical behaviour. The mechanical properties of electrospun scaffolds are not only determined by the bulk material properties, but also by microscale scaffold properties, such as fiber diameter, fiber structure, fiber distribution, and fiber interconnectivity (**Figure 7.1C**).[11,12] Biaxial deformation of isotropically distributed electrospun fibers results in stretching of the fibers, until the fiber-fiber crosslinks are strained at higher strains.[13] With uniaxial elongation, additional alignment of the fibers occurs. This shows that several principles play important roles in the mechanical behaviour

in physiologically relevant strain-regimes.[14]

Since supramolecular functionalization has been used to change the bulk mechanical properties of bisurea-based thermoplastic elastomers, it is extremely relevant to investigate the influence of functional additives on the mechanical performance of electrospun fibrous scaffolds for load-bearing applications. Therefore, in this chapter the properties of supramolecular electrospun scaffolds functionalized with the antifouling oligo(ethylene glycol) (OEG)-based bisurea additives described in **Chapter 3**, and the bisurea-filler (BF)

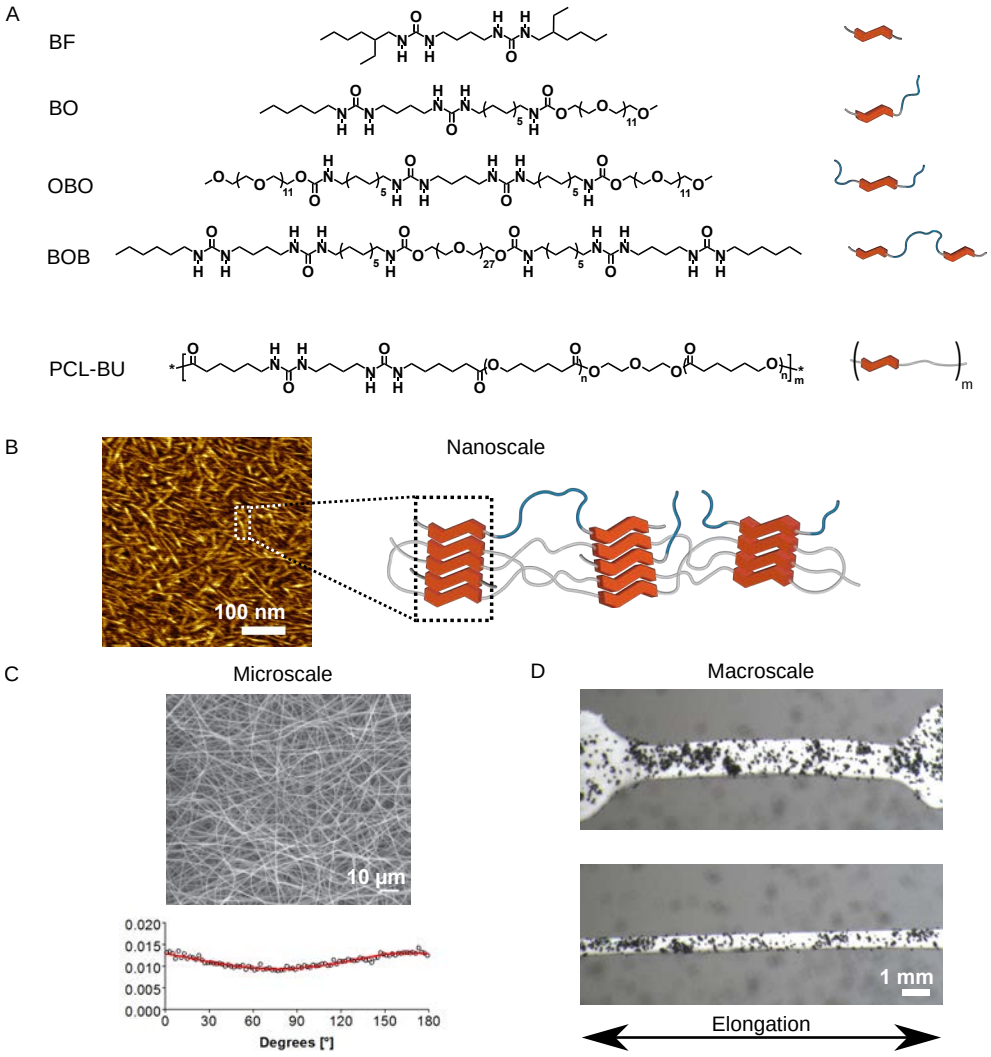

Figure 7.1. Multi-scale overview of study A) Structural representation of bisurea additives and the PCL-BU base polymer used in this chapter. B) Atomic force microscopy phase image with fibrous hard-segments attributed to the bisurea-assembly. Scale bar indicates 100 nm. C) Example of scanning electron micrograph of electrospun PCL-BU scaffold (scale bar indicates 10 µm) and the fiber orientation analysis of an electrospun scaffold. D) Dogbone shaped sample for tensile testing coated with graphite for strain analysis, before and during elongation.

as a model compound, were studied (**Figure 7.1A**) and compared to pristine controls. Considering that fiber diameter and orientation directly influence the mechanical properties of electrospun scaffolds[15,16], we fabricated electrospun scaffolds with similar fiber diameters and isotropic fiber distributions in this study. To determine if the bisureas from the additives are incorporated in the same hard-segments as those from the TPE base material, the thermal properties of the functionalized materials were assessed with differential scanning calorimetry (DSC). Finally, the mechanical properties of the electrospun scaffolds were measured with uniaxial tensile testing.

Efficacy of bisurea-filler additive in electrospun scaffolds

Firstly, the effect on mechanical properties of the BF additive was investigated in both thick films and electrospun scaffolds at concentrations of 5, 10, and 25 mol% additive. For this additive, the mechanical properties of the composite material are affected if one bisurea hard-phase is formed, which was the case for < 25 mol% in previously reported literature.[9] In that case, a single melting peak associated with the crystalline bisurea domain was observed with DSC. In the thermogram of both the films and electrospun scaffolds a single peak was observed (**Figure 7.2**), for which the melting temperature decreased slightly with increasing BF concentration (**Table 7.1**). However, the melting peak of the pure BF additive overlapped with that of the bisurea in the PCL-BU, which hampers the determination of segregated hard-phases as in Wisse et al.[9] Remarkably, the enthalpy decreased slightly for the films with increasing BF concentration, whereas it increased somewhat for the electrospun scaffolds with increasing BF concentration, which could indicate minor differences in the crystallinity of the hard-phases.

Table 7.1. Melting temperatures and melting enthalpy for the films and electrospun scaffolds of PCL-BU with 5, 10, and 25 mol% BF additive.

	PCL-BU	5% BF	10% BF	25% BF	100% BF
			Films		
Melting temperature [°C]	121.5	120.2	120.6	117.0	117.7
Melting enthalpy [J g^{-1}]	11.1	11.5	10.7	10.1	19.4
			Scaffolds		
Melting temperature [°C]	121.0	121.5	120.3	117.2	
Melting enthalpy [J g^{-1}]	11.9	12.1	13.2	13.6	

Prior to mechanical testing, the morphology of the scaffolds was characterized using scanning electron microscopy and subsequent image analysis. The fiber diameters for the electrospun scaffolds were comparable at approximately 0.6-0.7 um (**Table 7.2**). Using a previously reported method, the degree of (an)isotropy of the electrospun fibers was quantified.[17] Using this method, the fiber directionality histograms obtained after image analysis were fit with a Gaussian distribution on top of a baseline, where the portion below the baseline is considered the isotropic fraction. For these electrospun scaffolds the approximated anisotropic fraction was low with broad peaks (**Figure 7.3**, **Table 7.2**), and therefore these scaffolds could be considered sufficiently isotropic. The combined similarity of fiber diameter and isotropy substantiated the assumption that these scaffolds also had similar porosity.

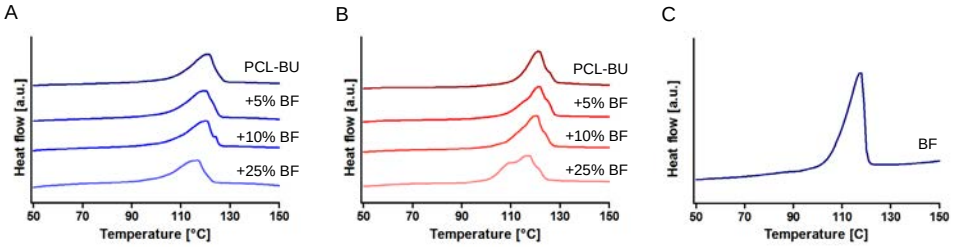

Figure 7.2. Thermograms of the first heating run of A) films of PCL-BU with 5, 10 and 25 % BF additive, B) electrospun scaffolds of PCL-BU with 5, 10, and 25 mol% BF additive, and the second heating run of the pure BF additive. Endotherm processes appear as peaks.

Interestingly, the Young's modulus did not increase for the films with increasing BF additive concentration (**Figure 7.3**), in contrast to the results reported by Wisse et al..[9] Compared to these earlier reported results, the Young's modulus of the pristine PCL-BU films measured in the current study was significantly higher, whereas the amount of hard segments was lower due to an increased soft-block length (PCL, M_n=2 kg mol^{-1} in this study[18] compared to M_n=1.4 kg mol^{-1} in Wisse et al.[9]). The moduli determined for the electrospun scaffolds were roughly one order of magnitude lower than for the films, which could be explained from the porosity of the scaffolds and deformation mechanisms involved in changing scaffold microstructure. Upon incorporation of BF additive, the stiffness of the scaffolds decreased 10-25 %, although no BF concentration-dependence was observed.

Table 7.2. Morphological properties of the electrospun scaffolds of PCL-BU with 5, 10, and 25% of the BF model compound.

	PCL-BU	+5% BF	+10% BF	+25% BF
Fiber diameter [µm]	0.6 ± 0.2	0.6 ± 0.2	0.7 ± 0.2	0.7 ± 0.2
Anisotropic fraction [-]	0.14	0.28	0.22	0.06
Peak σ [°]	35	41	36	22

Scaffolds functionalized with antifouling additives

The electrospun scaffolds functionalized with the antifouling additives were characterized in a similar fashion with DSC. The melting temperature of the bisurea only varies a few degrees upon functionalization with the three OEG-based additives (**Figure 7.4, Table 7.3, Table 7.4**). Interestingly, the melting temperatures for the pure additives are substantially higher. The absence of these additional peaks in the thermograms of the functionalized scaffolds indicates that the bisurea motifs of the additives are incorporated in the hard phase of the PCL-BU base material. The increased temperature of the bisurea additives, along with a clear melting transition that is not necessarily wider compared to PCL-BU, indicates nice assembly of the larger hard-segments with additional hydrogen bonding urethane groups in these additives.[19] The different melting temperatures for the three additives can also be attributed to the slightly different composition of the hydrophobic parts in the additives. The negative (i.e. exothermic) peak that is observed for the scaffold with 10% BOB additive might be related to degradation of the material, as little to no crystallinity is observed in this region in subsequent heating runs. The fiber diameter in these scaffolds ranges from

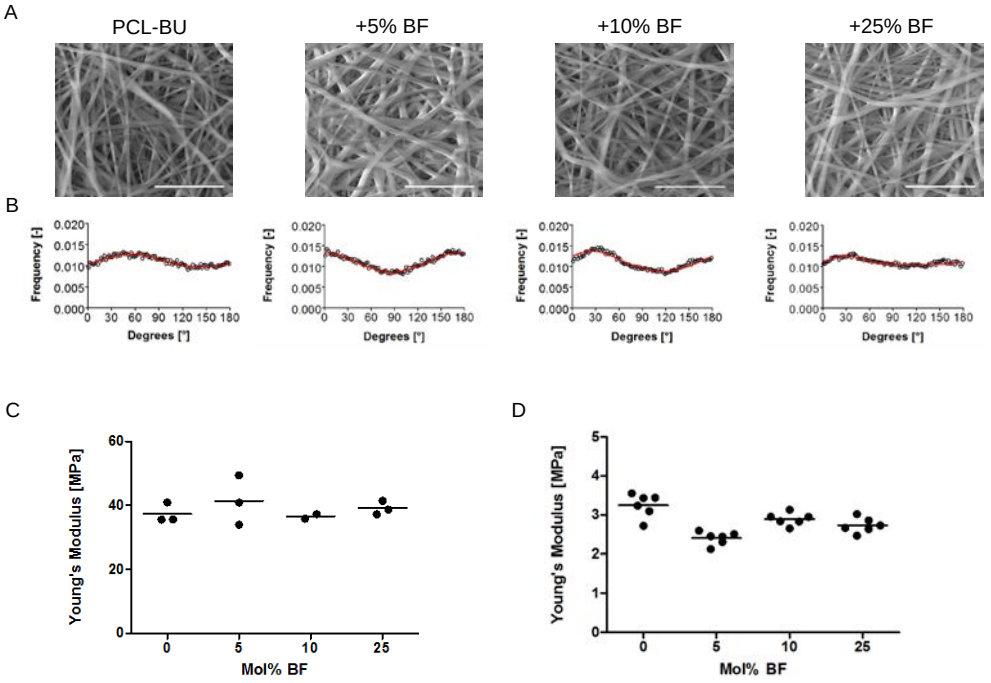

Figure 7.3. A) Scanning Electron Micrographs of electrospun scaffolds of PCL-BU with 5, 10, and 25% of the BF additive. Scale bars indicate 10 µm. B) Fiber distributions for the electrospun scaffolds. Open circles represent the data, and the red line represents the fit. C) Young's moduli of films (determined between 0 and 5% stretch) of PCL-BU with 0, 5, 10, and 25% BF additive. D) Young's moduli (determined between 0 and 20% stretch) of electrospun scaffolds of PCL-BU with 0, 5, 10, and 25% BF additive.

0.7 ± 0.1 µm to 0.8 ± 0.1 µm and can therefore be considered similar for the purpose of these experiments (**Table 7.5**). Moreover, the overall morphology and isotropic properties of the scaffolds are comparable (**Figure 7.5, Table 7.5**). The stiffness of the electrospun scaffolds decreases slightly upon functionalization with either one of the three OEG-based additives, approximately to the same extent was observed for the model BF compound (**Figure 7.5**). Interestingly, a slight strain-stiffening trend can be observed in the tensile test up to 100% strain, which is typically observed for biopolymer materials.[20]

Combining the data on mechanical testing of electrospun scaffolds of PCL-BU modified with the BF model compound and with the antifouling OEG-based additives indicates that incorporation of a supramolecular additive can result in a slight decrease in initial modulus of the electrospun scaffolds. For the BF additive, this cannot be related to a change in mechanical properties of the bulk material, which was unexpectedly not affected by filler incorporation, as was earlier reported.[9] Therefore, the observed decrease in modulus of the electrospun scaffolds, which have apparent similar morphologies, must have a cause in a different aspect of the scaffold properties.

Other studies have reported on the mechanical properties of electrospun scaffolds with changing chemical composition. In a study by Ye et al., electrospun scaffolds were fabricated from a PCL-based poly(urethane urea), that had increasing sulfobetaine content

incorporated in the polymer backbone, and corresponding increasing hard-phase:soft-phase ratios. The initial modulus of the bulk material did not change up to 50% sulfobetaine content when measured in dry conditions, and decreased slightly when measured in wet conditions. The initial modulus of their electrospun scaffolds also decreased considerably with increasing sulfobetaine content, which illustrates the effect chemical adaptations can have on electrospun scaffold properties.[21]

The degree of fiber-fiber interactions in electrospun scaffolds has been shown to affect mechanical behavior.[13] Electrospinning with different material composition may need different spinning condition and may result in different spinning outcomes and thereby a change in fiber-fiber interactions, which would not be obvious in the optical characterization implemented here. Furthermore, a change in surface chemistry of the fibers, which was present at least for the scaffolds modified with OEG-based additives (**Chapter 3**), can also result in changed fiber-fiber interactions. However, decreased interactions between the fibers was not expected in particular for the BF additive, because of an expected limited effect on surface chemistry. Besides the fiber-fiber interactions, the overall porosity of the scaffold might be influenced by the incorporation of additives. Now, based on the similarities in fiber diameter and isotropy the porosity was also assumed to be similar. Yet, changes in porosity would influence the true stress in the material. An increased porosity for the additive modified scaffolds would explain the decrease in initial stiffness. Therefore,

Table 7.3. Melting temperatures and melting enthalpy of the bisurea-melt in the first heating cycle for the electrospun scaffolds of PCL-BU with 10% of the BO, OBO, and BOB additive.

	PCL-BU	10% BO	10% OBO	10% BOB
Melting temperature [°C]	117.0	120.5	116.1	119.6
Melting enthalpy [J g^{-1}]	8.5	7.3	11.6	5.6

Table 7.4. Melting temperature and melting enthalpy of the bisurea melt in the second heating cycle for the pure BO, OBO, and BOB additive.

	BO	OBO	BOB
Melting temperature [°C]	157.9	130.3	152.5

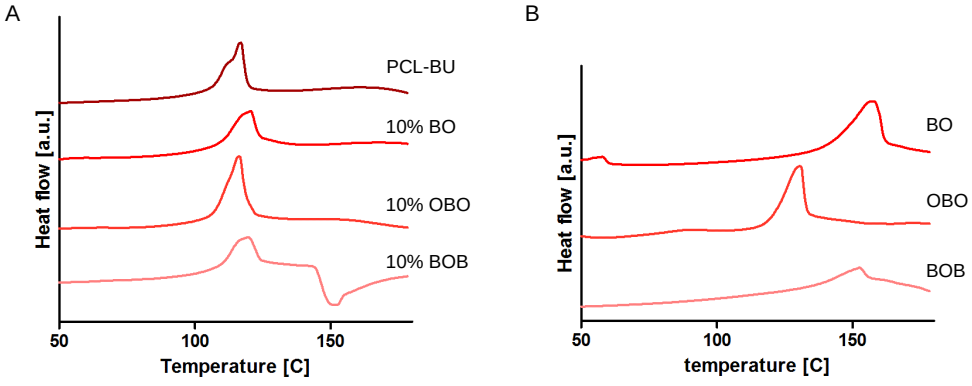

Figure 7.4. A) Thermogram of first heating run of electrospun scaffolds of PCL-BU with 10% BO, OBO and BOB additive. Endotherm processes appear as peaks. B) Second heating run of pure BO, OBO and BOB additive. Endotherm processes appear as peaks.

Table 7.5. Morphological properties of the electrospun scaffolds of PCL-BU with 10% BO, OBO, and BOB additive.

	PCL-BU	+10% BO	+10% OBO	+10% BOB
Fiber diameter [µm]	0.7 ± 0.1	0.8 ± 0.1	0.8 ± 0.1	0.7 ± 0.1
Anisotropic fraction	0.23	0.20	0.18	0.19
Peak σ [°]	36	19	35	31

porosity should be determined accurately in future efforts.[22]

The choice for thermoplastic elastomers with defined hard-blocks such as the PCL-BU studied here follows from their enhanced mechanical properties compared to TPEs with less defined hard-segments.[8] This was attributed to an increased nanoscale segregation of the hard and soft phases, in combination with increased crystallinity. The comparable melting transitions observed here for films of PCL-BU and scaffolds (**Figure 7.2**) suggest that similar degrees of crystallinity are obtained, which would point towards the same amount of segregation between soft and hard phase. However, the mechanical behavior under tensile deformation of the bulk material involves reorientation of the fibrous hard phase from isotropic to anisotropic, parallel to the strain directions. For other polymeric electrospun fibers, orientation of the polymer chains parallel to the fiber direction is observed.[11] Furthermore, in supramolecular TPE electrospun fibers evidence from

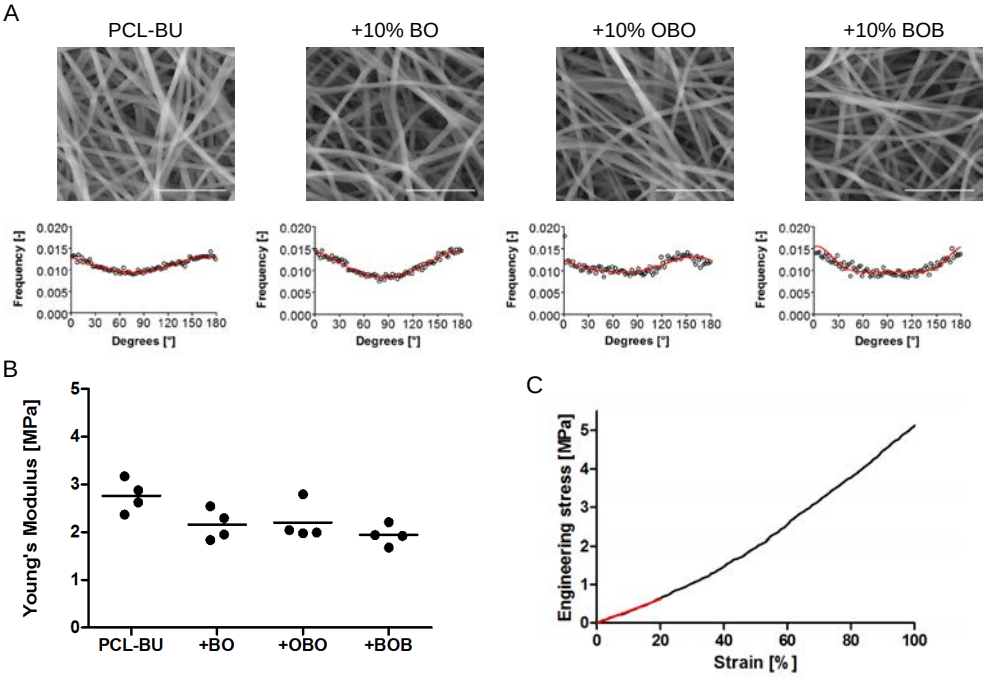

Figure 7.5. A) Top row: Scanning Electron Micrographs of electrospun scaffolds of PCL-BU with 10% BO, OBO, and BOB additive. Scale bars indicate 10 µm. Bottom row: Fiber distributions for the electrospun scaffolds. Open circles represent the data, and the red line represents the fitted distribution. B) Young's modulus of electrospun scaffolds of PCL-BU with 10% BO, OBO, and BOB additive. C) Representative engineering stress-strain curve for electrospun scaffold, up to 100% strain. The Young's modulus is determined from slope of the red fitted line.

wide angle X-ray scattering and atomic force microscopy measurements points towards the presence of nanofibers, similar to those seen in solution-cast films.[23] These findings, in combination with the comparable degree of bisurea hard-phase crystallinity in the electrospun scaffolds may indicate a molecular hard-segment conformation with alignment already perpendicular to the fiber direction, which would correspond to a bulk material beyond the yield point. It would be particularly interesting to more closely investigate the molecular conformation of the bisurea-based TPEs in electrospun fibers with X-ray diffraction methods under strain, in a similar fashion as for the bulk materials, to get a more fundamental understanding of the nano-scale processes that are involved in deformation of supramolecular electrospun scaffolds. Furthermore, the opportunity to probe strain at a molecular level using mechanically sensitive additives can be used in a complimentary fashion.[24–26] Additionally, numerical modelling efforts may result in increased understanding of the principles involved in these complex, multi-scale questions.[15,27]

Conclusion

In this chapter we have shown that despite a lack of change in bulk mechanical properties, the initial modulus of electrospun scaffolds can be affected due to supramolecular additive modification. The decrease in initial stiffness was similar for the four additives studied here, and was independent of model additive concentration. These results show that the combination of supramolecular modification and processing into complex 3D shapes with electrospinning is a multi-scale problem that requires more in depth understanding. Furthermore, in designing functional biomaterial constructs, care should be taken with the –albeit minor – effect of the functionalization on mechanical properties of the electrospun scaffolds.

Experimental section

Materials

The (2-ethylhexyl)$_2$-U4U (Bisurea filler, BF)[9], antifouling additives (BU-OEG, BU-OEG-BU, and OEG-BU-OEG),[28] and PCL-BU[9,18] were synthesized by SyMO-Chem as described previously.

Fabrication of electrospun scaffolds

Solutions were prepared by dissolving mixtures of PCL-BU with 10 mol% additives in hexafluoroisopropanol (HFIP, Fluorochem) at 12% w/w. The molar ratio PCL-BU:additive of 90:10 was determined with respect to the molecular weight of a single repeating unit of PCL-BU, as depicted in figure 7.1. The solutions were mixed overnight at room temperature with a magnetic stirrer. The electrospun scaffolds were prepared in a climate controlled electrospinning setup by IME technologies (Geldrop, Netherlands). A cylindrical mandrel rotating at 500 rpm with a diameter of 18-21 mm, covered in aluminium foil was used to collect the polymer fibers. A voltage of 25 kV, +24 kV on the needle and -1 kV on the collector, was applied over a distance of 20 cm between needle and rotating mandrel. The temperature was controlled at 23 °C and relative humidity at 30%. Using a flow rate of 15 µL min^{-1} for the pristine PCL-BU, and 20 µL min^{-1} for the mixtures with additive, the polymer solutions were fed through a needle with an inner diameter of 0.8 mm. The needle scanned a distance of 60 – 80 mm, at a speed of 12 mm s^{-1}. The electrospun scaffolds were removed from the mandrel with the aluminium foil and dried overnight in vacuum.

Preparation of films

The solution that was left over after electrospinning was evaporated and re-dissolved at approximately 100 mg mL^{-1} in HFIP by stirring overnight at room temperature. The solutions were then poured in rectangular Teflon molds measuring 2 cm by 4 cm and solvent was evaporated overnight.

Differential Scanning Calorimetry
DSC measurements were performed on a DSC Q2000 (TA Instruments). Using a 5 mm biopsy punch (Kai Medical), samples were cut from the electrospun scaffolds and films. These samples, and pure additive, were placed in Tzero aluminium pans to be weighed and hermetically sealed. The samples cut from the electrospun scaffolds and films were subjected to three heating/cooling cycles from -70°C to 160°C, and the pure additives to three heating/cooling cycles from -70 °C to 180 °C. The data was analyzed and quantified using Universal Analysis Software (TA Instruments, V4.5A).

Scanning electron microscopy
The electrospun scaffolds were visualized using a FEI Quanta 600 scanning electron microscope with Xt Microscope control software. Images of samples immobilized on metal stubs with adhesive carbon conductive tape were recorded in low vacuum (~0.6 mbar) with the presence of water vapor. Secondary electrons were detected with an accelerating voltage of 10 kV and a working distance of 10 mm.

Morphological characterization of scaffolds
Average fiber diameters were determined from >45 individual fibers from 3 SEM images using ImageJ software (NIH, version 1.48). The fiber distributions were determined using a custom-made MatLab (Mathworks, 2017b) script. In short, fiber orientations were calculated based on the vesselness measure as described by Frangi et al.[29] on three SEM images per scaffold. Subsequently, the degree of anisotropy was calculated using previously developed software.[17] Average sample thickness was determined using a Keyence VHX-500FE. To this end, samples cut from the films and scaffolds were placed in between two glass microscopy slides, to be able to make cross-sectional images. Thickness of the films was approximately 150 µm, and the thickness for the scaffolds ranged from 120 to 160 µm, and 200 to 250 µm for the scaffolds with BF additive and BU-OEG additives, respectively.

Mechanical Characterization
Dogbone shaped samples (width of narrow section approximately 14 mm) of the films and electrospun scaffolds were cut using a Zwick (ZCP 020) manual cutting press and patterned with graphite prior to testing. Uniaxial tensile tests were performed on a CellScale Tensile setup, using a 5N loadcell. Strains in the loading direction were computed from images recorded during the measurement using digital image correlation in Labjoy software (Cellscale). Engineering stress-strain curves were calculated, where a cross-sectional area based on 0 % porosity and an average sample thickness per experimental group was used for both films and scaffolds. For the films, the initial elastic modulus was determined in the region from 0 to 5 % strain and for the scaffolds in the region from 0 to 20 % strain.

References

(1) Gu, X.; Matsumura, Y.; Tang, Y.; Roy, S.; Hoff, R.; Wang, B.; Wagner, W. R. Sustained Viral Gene Delivery from a Micro-Fibrous, Elastomeric Cardiac Patch to the Ischemic Rat Heart. *Biomaterials* **2017**, *133*, 132–143.

(2) Kluin, J.; Talacua, H.; Smits, A. I. P. M. P. M.; Emmert, M. Y.; Brugmans, M. C. P.; Fioretta, E. S.; Dijkman, P. E.; Söntjens, S. H. M.; Duijvelshoff, R.; Dekker, S.; et al. In Situ Heart Valve Tissue Engineering Using a Bioresorbable Elastomeric Implant – From Material Design to 12 Months Follow-up in Sheep. *Biomaterials* **2017**, *125*, 101–117.

(3) Seifalian, A. M.; Salacinski, H. J.; Tiwari, A.; Edwards, A.; Bowald, S.; Hamilton, G. In Vivo Biostability of a Poly(carbonate-Urea)urethane Graft. *Biomaterials* **2003**, *24*, 2549–2557.

(4) Hong, Y.; Ye, S. H.; Nieponice, A.; Soletti, L.; Vorp, D. A.; Wagner, W. R. A Small Diameter, Fibrous Vascular Conduit Generated from a Poly(ester Urethane)urea and Phospholipid Polymer Blend. *Biomaterials* **2009**, *30*, 2457–2467.

(5) Spontak, R. J.; Pate, N. P. Thermoplastic Elastomers : Fundamentals and Applications. **2000**, *5*, 334–341.

(6) Koevoets, R. A.; Versteegen, R. M.; Kooijman, H.; Spek, A. L.; Sijbesma, R. P.; Meijer, E. W. Molecular Recognition in a Thermoplastic Elastomer. *J. Am. Chem. Soc.* **2005**, *127*, 2999–3003.

(7) Sauer, B. B.; Mclean, R. S.; Gaymans, R. J.; Niesten, M. C. J. E. Crystalline Morphologies in Segmented Copolymers with Hard Segments of Uniform Length. **2003**, 1783–1792.

(8) Versteegen, R. M.; Kleppinger, R.; Sijbesma, R. P.; Meijer, E. W. Properties and Morphology of Segmented Copoly(ether Urea)s with Uniform Hard Segments. *Macromolecules* **2006**, *39*, 772–783.

(9) Wisse, E.; Govaert, L. E.; Meijer, H. E. H.; Meijer, E. W. Unusual Tuning of Mechanical Properties of Thermoplastic Elastomers Using Supramolecular Fillers. *Macromolecules* **2006**, *39*, 7425–7432.

(10) Wisse, E.; Spiering, A. J. H.; Pfeifer, F.; Portale, G.; Siesler, H. W.; Meijer, E. W. Segmental Orientation in Well-Defined Thermoplastic Elastomers Containing Supramolecular Fillers. *Macromolecules* **2009**, *42*, 524–530.

(11) Baji, A.; Mai, Y. W.; Wong, S. C.; Abtahi, M.; Chen, P. Electrospinning of Polymer Nanofibers: Effects on Oriented Morphology, Structures and Tensile Properties. *Compos. Sci. Technol.* **2010**, *70*, 703–718.

(12) Amoroso, N. J.; Amore, A. D.; Hong, Y.; Wagner, W. R.; Sacks, M. S. Elastomeric Electrospun Polyurethane Scaffolds : The Interrelationship Between Fabrication Conditions , Fiber Topology , and Mechanical Properties. **2011**, 106–111.

(13) Stella, J. A.; Wagner, W. R.; Sacks, M. S. Scale-Dependent Fiber Kinematics of Elastomeric Electrospun Scaffolds for Soft Tissue Engineering. *J. Biomed. Mater. Res., Part A* **2009**, *93A*, 1032–1042.

(14) van Haaften, E.; Bouten, C.; Kurniawan, N. Vascular Mechanobiology: Towards Control of In Situ Regeneration. *Cells* **2017**, *6*, 19.

(15) Argento, G.; Simonet, M.; Oomens, C. W. J.; Baaijens, F. P. T. Multi-Scale Mechanical Characterization of Scaffolds for Heart Valve Tissue Engineering. *J. Biomech.* **2012**, *45*, 2893–2898.

(16) Kwon, I. K.; Kidoaki, S.; Ã, T. M. Electrospun Nano- to Microfiber Fabrics Made of Biodegradable Copolyesters : Structural Characteristics , Mechanical Properties and Cell Adhesion Potential. **2005**, *26*, 3929–3939.

(17) van Haaften, E. E.; Wissing, T. B.; Rutten, M. C. M.; Bulsink, J. A.; Gashi, K.; van Kelle, M. A. J.; Smits, A. I. P. M.; Bouten, C. V. C.; Kurniawan, N. A. Decoupling the Effect of Shear Stress and Stretch on Tissue Growth and Remodeling in a Vascular Graft. *Tissue Eng., Part C* **2018**, *24*, 418–429.

(18) Duijvelshoff, R.; van Engeland, N.; Gabriels, K.; Söntjens, S.; Smits, A.; Dankers, P.; Bouten, C. Host Response and Neo-Tissue Development during Resorption of a Fast Degrading Supramolecular Electrospun Arterial Scaffold. *Bioengineering* **2018**, *5*, 61.

(19) Wisse, E.; Spiering, A. J. H.; van Leeuwen, E. N. M.; Renken, R. A. E.; Dankers, P. Y. W.; Brouwer, L. A.; van Luyn, M. J. A.; Harmsen, M. C.; Sommerdijk, N. A. J. M.; Meijer, E. W. Molecular Recognition in Poly(ε-Caprolactone)-Based Thermoplastic Elastomers. *Biomacromolecules* **2006**, *7*, 3385–3395.

(20) Storm, C.; Pastore, J. J.; MacKintosh, F. C.; Lubensky, T. C.; Janmey, P. A. Nonlinear Elasticity in Biological Gels. *Nature* **2005**, *435*, 191–194.

(21) Ye, S.; Hong, Y.; Sakaguchi, H.; Shankarraman, V.; Luketich, S. K.; D'Amore, A.; Wagner, W. R. Nonthrombogenic, Biodegradable Elastomeric Polyurethanes with Variable Sulfobetaine Content. *ACS Appl. Mater. Interfaces* **2014**, *6*, 22796–22806.

(22) Maire, E. Characterization of Porosity , Structure , and Mechanical Properties of Electrospun SiOC Fiber Mats. **2015**, 4221–4231.

(23) Mollet, B. B.; Bogaerts, I. L. J.; van Almen, G. C.; Dankers, P.Y.W. A Bioartificial Environment for Kidney Epithelial Cells Based on a Supramolecular Polymer Basement Membrane Mimic and an Organotypical Culture System. *J. Tissue Eng. Regen. Med.* **2017**, *11*, 1820–1834.

(24) Karthikeyan, S.; Sijbesma, R. P. Probing Strain in Thermoplastic Elastomers Using Fluorescence Resonance Energy Transfer. *Macromolecules* **2009**, *42*, 5175–5178.

(25) Filonenko, G. A.; Lugger, J. A. M. M.; Liu, C.; Heeswijk, E. P. A. Van; Hendrix, M. M. R. M. R. M.; Weber, M.; Christian, M.; Hensen, E. J. M. M.; Sijbesma, R. P.; Pidko, E. A.; et al. Tracking Local Mechanical Impact in Heterogeneous Polymers with Direct Optical Imaging. *Angew. Chem., Int. Ed.* **2018**, *57*, 16385–16390.

(26) Filonenko, G. A.; Khusnutdinova, J. R. Dynamic Phosphorescent Probe for Facile and Reversible Stress Sensing. *Adv. Mater.* **2017**, *29*, 1–6.

(27) D'Amore, A.; Amoroso, N.; Gottardi, R.; Hobson, C.; Carruthers, C.; Watkins, S.; Wagner, W. R.; Sacks, M. S. From Single Fiber to Macro-Level Mechanics: A Structural Finite-Element Model for Elastomeric Fibrous Biomaterials. *J. Mech. Behav. Biomed. Mater.* **2014**, *39*, 146–161.

(28) Ippel, B. D.; Keizer, H. M.; Dankers, P. Y. W. Supramolecular Antifouling Additives for Robust and Efficient Functionalization of Elastomeric Materials: Molecular Design Matters. *Adv. Funct. Mater.* **2019**, *29*, 1805375.

(29) Frangi, A. F.; Niessen, W. J.; Vincken, K. L.; Viergever, M. A. Multiscale Vessel Enhancement Filtering. In *Medical Image Computing and Computer-Assisted Intervention*; Springer Berlng Heidelberg, 1998; pp 130–137.

8

General discussion and future directions

Introduction

Functionalization of supramolecular elastomeric materials, based on both ureidopyrimidinone (UPy) and bisurea motifs, has been described in this thesis. Mixtures with antifouling additives, bioactive additives, and with reactive groups for post-functionalization were prepared and analyzed with various methods. These studies gave new handles for the optimal design for oligo(ethylene glycol) (OEG) based antifouling additives (**Chapter 3**), the efficacy of combinatorial functionalization with antifouling additives and bisurea-peptide conjugates (**Chapter 4**), the non-cell adhesive properties of formulations with UPy-poly(ethylene glycol) (UPy-PEG) additives and varying base polymers (**Chapter 5**), the exploration of supramolecular hard-phase initiated controlled radical polymerization (**Chapter 6**), and the influence of supramolecular additives on the mechanical properties of functional electrospun scaffolds (**Chapter 7**).

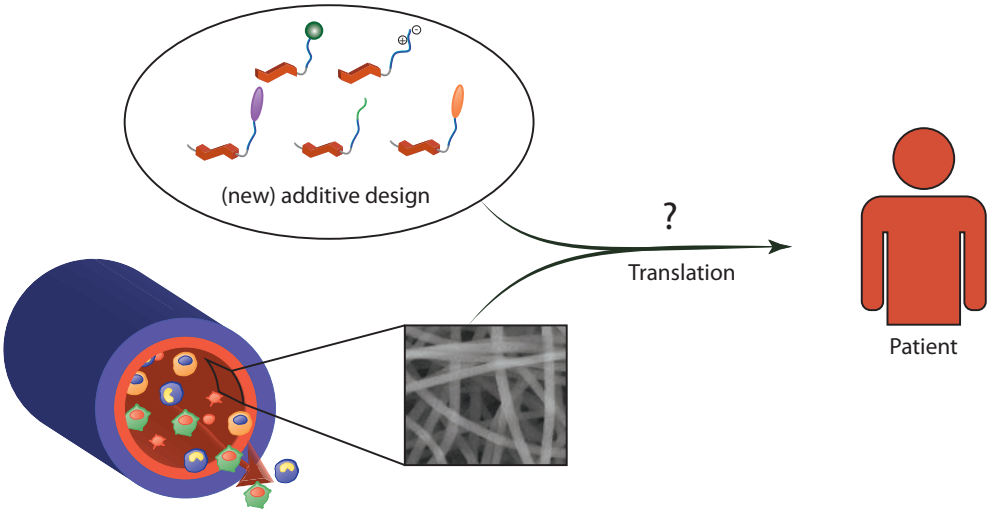

Figure 8.1. Contents of final chapter. First, preliminary results for new additives are reported, followed by the review of molecular design of our supramolecular additives. Finally, the translation of biomaterial development for vascular grafts towards clinical application is discussed.

The content of this final chapter is threefold, as schematically depicted in **Figure 8.1.** First, an overview is presented of preliminary studies with alternative bisurea additives (**Figure 8.2**), with functional end-groups that would bestow biomaterials with antifouling properties and new post-functionalization possibilities. The characterization of materials functionalized with these new additives provides further insights that may advance our understanding of supramolecular functionalization. Second, the molecular design of supramolecular additives, which has been shown to be particularly important in supramolecular functionalization strategies, is discussed, with implications for future research directions. Finally, the relevance of the results for vascular (access) grafts as well as opportunities and challenges for the steps towards clinical application of the next generation of vascular (access) grafts will be discussed.

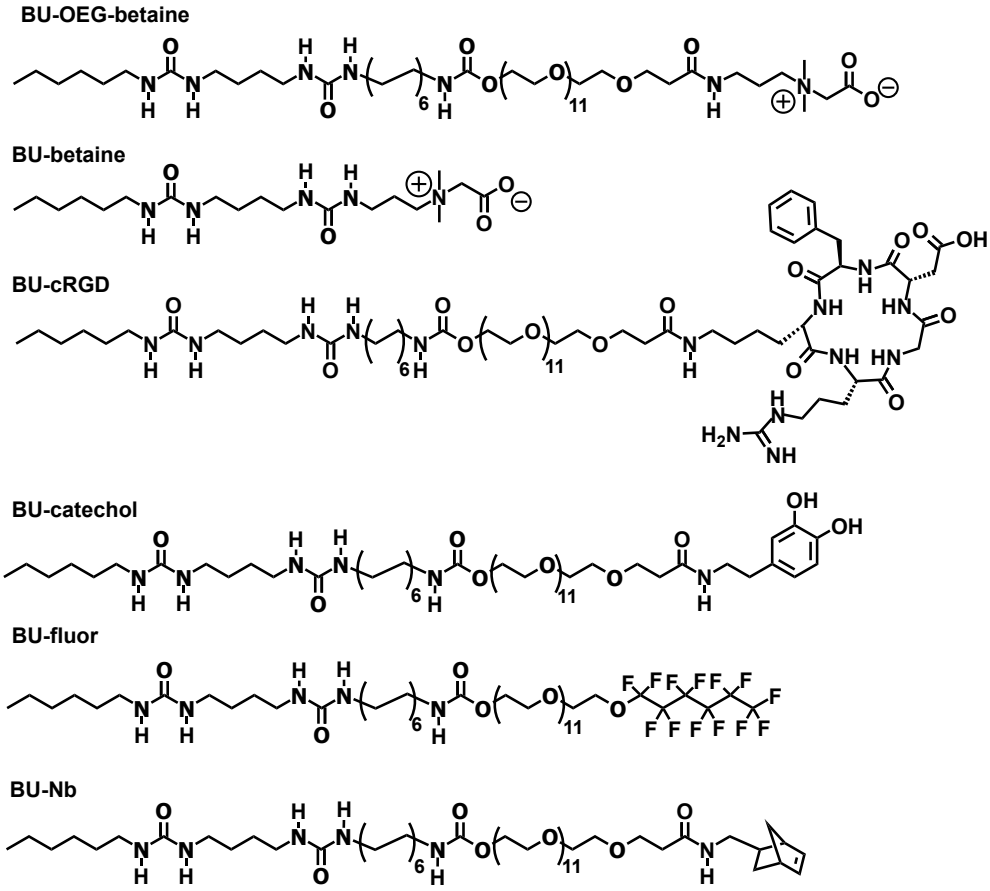

Figure 8.2. Structural representation of the additional bisurea additives of which the functionality is explored in this chapter.

Alternative bisurea additives

Supramolecular functionalization with zwitterionic bisurea-additive

The functionalization of elastomeric materials with supramolecular antifouling additives was described in chapter 3.[1] Three oligo(ethylene glycol)-based bisurea additives were studied in the PCL-BU base material. Besides functionalization with hydrophilic moieties, zwitterionic functional groups have been used for the fabrication of antifouling materials.[2–4] Due the different nature through which zwitterionic layers bind water compared to hydrophilic non-charged molecules (electrostatic and hydrogen bonding respectively) it is argued that the hydration layer is even more stable.[3] A popular approach for zwitteration is through surface initiated polymerization, where zwitterionic polymers are grafted from a biomaterial surface.[5] However, non-covalent incorporation of zwitterionic additives has been reported previously, with either random zwitterionic copolymers,[6,7] or A-B type block-copolymers consisting of a macromolecular part A that provides anchoring in the base material and where B is a zwitterionic polymer.[8–10] Here, we set the first step towards

modular incorporation of a small, supramolecular zwitterionic additive in our defined supramolecular base material, where anchoring in the base material is provided by the highly-directional hydrogen bonding bisurea moiety. A zwitterionic moiety was conjugated directly to a bisurea (BU-betaine, **figure 8.2**) and on the end of a oligo(ethylene glycol) (OEG) 12 linker (BU-OEG-betaine), similar to the way bioactive peptides have been conjugated to the bisurea in Chapter 4. Antifouling properties were studied through a cell adhesion assay using human vena saphena cells (HVSC), which allows for comparison with antifouling properties of solution-cast films found in this thesis, and directly compared to the BU-OEG additive that was described in chapter 3.

Adhesion of HVSCs on solution-cast films of PCL-BU with 0.5, 1, 2, and 4 mol% of BU-OEG, BU-OEG-betaine, and BU-betaine is shown in **Figure 8.3.** Matching the results reported in chapter 3, adhesion of HVSCs on surfaces functionalized with 0.5 and 1 mol% BU-OEG is not affected compared to pristine; cells spread and cover essentially the entire biomaterial surface. With 2 mol% BU-OEG, less cells are present, but these still show a spread morphology, whereas for 4 mol% BU-OEG cell adhesion is significantly decreased. Interestingly, the cell adhesion on surfaces with BU-OEG-betaine shows a different trend, with less pronounced antifouling properties. Only at 4 mol% BU-OEG-betaine adhesion of HVSCs is slightly decreased. No effect on cell-adhesive properties is observed in the range of 0.5 to 4 mol% for the BU-betaine additive.

In early investigative studies for functionalized surfaces that can repel fouling, single-component self-assembled monolayers were also investigated, where zwitterionic end-groups showed relatively good antifouling properties, compared to OEG_3 terminated surfaces.[11] Here, a carboxybetaine with a methylene spacer between the charged quaternary nitrogen and carboxylic acid groups was used. The length of the spacer between the charged groups has been shown to be important for antifouling properties of carboxybetaineacrylamide based zwitterionic polymers and was comparable for an ethylene and a methylene spacer, but increased compared to a propylene spacer.[12] Nevertheless, in most biomaterial functionalization strategies where zwitterions were applied as antifouling component, polymerized zwitterions, e.g. through radical polymerization of methacrylated

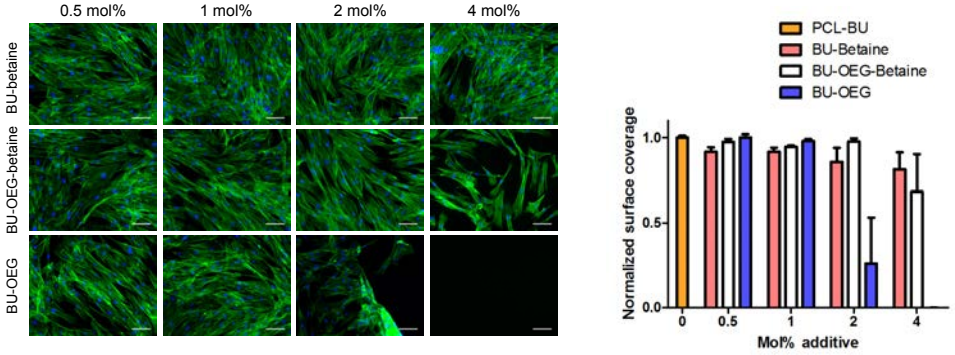

Figure 8.3. A) Fluorescence micrographs of HVSCs cultured on solution-cast surfaces of PCL-BU with 0.5, 1, 2, and 4% additive. Actin cytoskeleton is presented in green, and nuclei in blue. Scale bar represents 100 µm. B) Surface of the solution-cast films that is covered by the HVSCs, normalized to pristine PCL-BU. Data is represented as mean ± SD.

zwitterions, are used.[4,5] Moreover, the modular incorporation of supramolecular additives relies on the presentation at the surface of the functional groups of these additives for functional surfaces. We have observed an enhanced presence of additives at the surface of our biomaterials, attributed there to the presence of a PEG-linker.[13] The absence of such a linker, in combination with the smaller capacity of a single betaine to form a hydration could explain the negligible effect on cell adhesion for the BU-betaine additive.

The BU-OEG-betaine shows an increased cell adhesion compared to the BU-OEG additive. The additional zwitterionic group was not expected to decrease the antifouling properties of this additive design. Since in two dimensional structures the antifouling properties induced by incorporation of OEG-based bisurea additives seems to be determined by the OEG-content, the structure of the BU-OEG-betaine could result in less exposed OEG at the surface of the films when compared to BU-OEG. The amide bond that links the OEG and the betaine in this additive could be able to form additional hydrogen bonds that might intercalate in the bisurea-bisurea assemblies, thereby 'looping' the betaine into the material bulk and limiting the exposure of OEG at the surface of these films.

All-in-all, these results indicate that the supramolecular incorporation of these zwitterionic additives does not result in sufficient surface exposure of the zwitterionic functional groups to induce antifouling properties. Moreover, the design of the zwitterionic component in supramolecular additives could be improved for enhanced antifouling properties, for instance through the use of a polymeric zwitterion, with an optimized zwitterionic monomer design.

Influence of polymer backbone on functional additive presentation

In Chapter 3, the functionality of three antifouling OEG-bisurea additives was described (BO, OBO, and BOB). Solution-cast films composed of these additives in thermoplastic elastomeric (TPE) base materials, with either polycaprolactone (PCL-BU) or polycarbonate (PC-BU) soft-blocks were studied. The efficacy of non-cell adhesive functionalization was similar for the three additives in the two materials with different soft-block. However, nano-scale phase separation and self-assembly of supramolecular TPEs is known to be affected by the physiochemical properties of the soft-segment.[14,15] Moreover, one can imagine that the result from co-formulation of additives with different supramolecular TPEs relies on complex processes where interactions between the supramolecular motif of the additive and the base material and their respective functional group and soft-segment all play a role. Therefore we systematically studied the effect of the polymeric backbone on the presentation of two bioactive additives, from which a section of the results related to bisurea-based materials is shown here. The first additive has a functional catechol moiety (BU-catechol), which was previously conjugated to a UPy-group where both improved cell-material interactions[14] and neglible effect on cell-adhesion[16] were observed. The second additive is a bisurea-cyclic RGD conjugate (BU-cRGD) that is known to influence human epithelial cell adhesion. The surface of thin films cast from mixtures of either PCL-BU or PC-BU with the BU-catechol or BU-cRGD additive was characterized with atomic force microscopy and water contact angle measurements. Adhesion of human kidney epithelial cells served as a functional read-out for cellular response to these biomaterials.

The surface morphology of the solution-cast films of PCL-BU and PC-BU with the

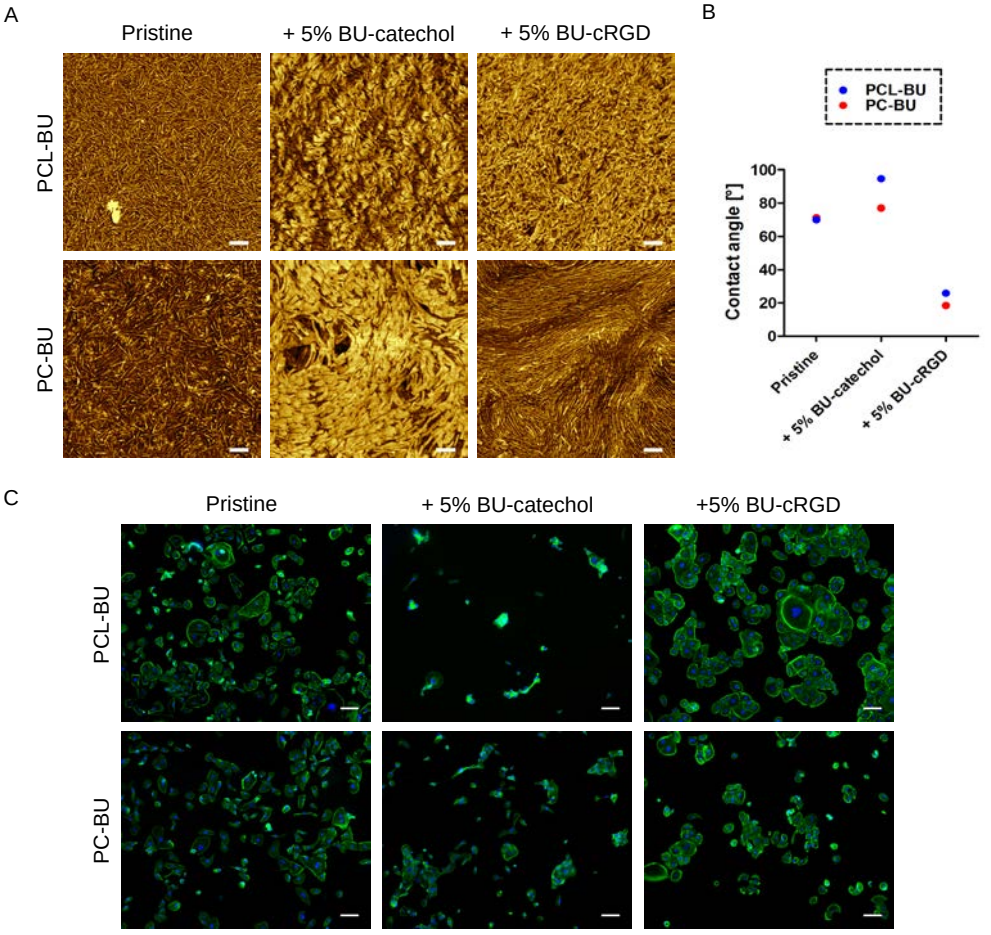

Figure 8.4. A) Atomic force microscopy phase images of solution-cast films of PCL-BU and PC-BU with 5% of the BU-catechol and BU-cRGD additives. Scale bars indicate 100 nm. B) Water contact angles measured on solution-cast films of PCL-BU and PC-BU with 5% of the BU-catechol and BU-cRGD additives. Data is presented as mean ± SD. C) Fluorescence micrographs of HK-2 cells cultured on the solution-cast films of PCL-BU and PC-BU with 5% BU-catechol and BU-cRGD additive. Actin cytoskeleton is stained in green and nuclei in blue. Scale bars represent 100 µm.

addition of either 5 mol% BU-catechol or 5 mol% BU-cRGD was analyzed with atomic force microscopy. In the phase images of the pristine materials, the characteristic fibrous morphology is observed for PCL-BU, whereas for PC-BU the hard-phase fibers appear shorter and less abundant (**Figure 8.4**). Upon incorporation of both the BU-catechol and the BU-cRGD additives, striking differences in surface morphology can be observed. For 5 mol% BU-catechol, the surface of the solution-cast film appears to be covered with non-fibrous platelet-like structures. For the PC-BU base material, these platelets are also present, but appear more fibrous in nature. Presence of BU-cRGD in the mixture with PCL-BU is evident from the small, fibrillary structures that were previously seen for other bisurea-peptide additives in PCL-BU (Chapter 6). In PC-BU, the morphology is drastically different, with longer, flowing fibrous structures. The macroscale hydrophilic

properties change accordingly with the additives. The BU-catechol functionalization results in an increased contact angle indicative of a more hydrophobic surface, and the BU-cRGD decreases the contact-angle leading to significantly more hydrophilic surfaces. The functionalization with BU-catechol had an adverse effect on the adhesion of the HK-2 cells, compared to pristine material (**Figure 8.4C**). This was more pronounced in PCL-BU compared to PC-BU. This negative effect may be the result of the protein mediated functioning of catechol-modified biomaterials. The incorporation of BU-cRGD had a limited effect on cell adhesion and spreading of the epithelial cells, with slightly improved spreading on PCL-BU functionalized surfaces and decreased spreading on PC-BU surfaces.

These results show that slight variations in the chemical structure of the soft-segment of the bisurea TPEs drastically changes the presentation of bisurea additives, even though evidence of these changes may not be evident on a larger scale. Furthermore, the introduced functionality through additive incorporation in one supramolecular is not necessarily translated to another supramolecular system with similarities in terms of meso-scale assembly, by simple conjugation of the functional moiety to the respective supramolecular motifs.

Fluorinated bisurea additive for hydrophobic surface functionalization

The fluoropolymer polytetrafluoroethylene (PTFE) is a popular material for the fabrication of blood-contacting material, such as vascular grafts, due to its inert properties. However, the hydrophobic nature of the polymer can lead to unwanted protein adsorption and platelet adhesion, eventually leading to thrombus formation.[17,18] Interestingly, the hydrophobic nature of fluorinated molecules has also been exploited for antifouling properties.[19–21] In combination with intricately designed nano-scale patterns, surfaces with extreme fluid repelling properties have been developed.[22] However, the application of such surfaces is hampered by the functionality dependence on the combination of surface morphology, roughness and wettability.[22,23] Here, we introduce a fluorinated bisurea additive (BU-fluor) (**Figure 8.2**), for hydrophobic surface functionalization. The combinatorial modification of PCL-BU with the hydrophilic BO additive described in chapter 3 is studied on solution-cast films with atomic force microscopy (AFM) and water contact angle measurements.

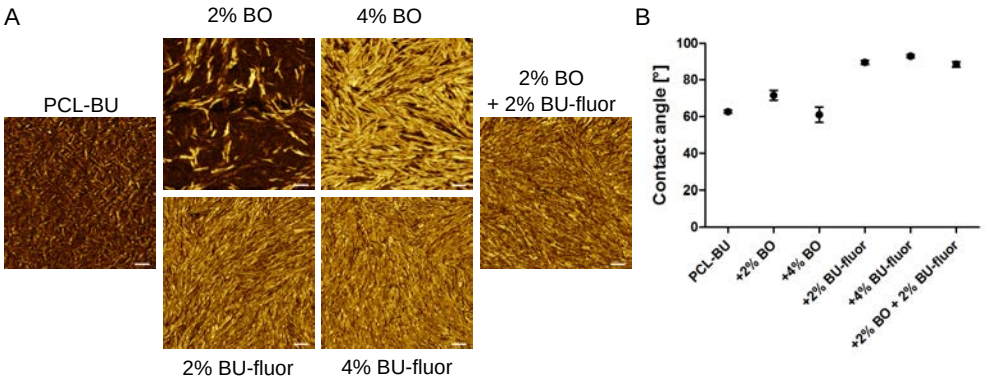

Figure 8.5. A) Atomic force microscopy phase diagrams of solution-cast films of PCL-BU with 2 and 4 mol% BO and BO-fluor, and the combination of 2 mol% BO and BO-fluor. Scale bars indicate 100 nm. B) Water contact angle measured on the solution-cast films. Data is represented as mean ± SD.

AFM phase images show the characteristic fibrous structure for pristine PCL-BU (**Figure 8.5A**) Upon incorporation of 2 mol% BO, elongated brighter yellow structures, attributed to crystalline OEG, are observed, which increase in number significantly for 4 mol% BO. In the background, the fibrous structure of PCL-BU is still visible for 2 mol% BO. With 2 mol% BU-fluor, the surface is already saturated with sharp platelet-like domains, which remain for 4% BU-fluor. The bulkier fluorinated end-group therefore results in increased surface presentation of this particular additive. Both the BO and BU-fluor modified surfaces are relatively fibrous in nature. The surface with a combination of 2% BO and 2% BU-fluor more closely resembles the BU-fluor functionalized surfaces, than the surface with BO. The water contact angle for BO-functionalized PCL-BU increases slightly for 2% BO and then decreases for 4% BO. The surfaces with 2 and 4% BU-fluor, equally so for the combination with 2% BO, show an increased contact angle, indicative of increased hydrophobic properties. These results indicate that the BU-fluor additive incorporation, both with and without BO results in the presence of the fluorinated end-group of the BU-fluor additive at the surface of these films. In the combinatorial functionalization this effect could be aided by the OEG-linker that is present in the BU-fluor additive, as suggested previously.[24] Decreased concentrations of the BU-fluor additive, in combination with 2% BO could provide more insight in the interactions between these two additives in a self-assembled elastomeric system. Moreover, cell-adhesion assays may provide information on the efficacy of hydrophobic surface functionalization strategies in supramolecular materials for antifouling properties.

Towards patterned supramolecular surfaces

The modification of supramolecular biomaterials with functional additives relies on self-assembly for the presentation of the functional groups at the surface. An increased concentration of additives at the surface compared to the bulk of the material has been seen,[13] however the distribution of the additive over the surface is random. Topographical organization is important for tissue function[25], and patterned biomaterials have been shown to direct cellular behavior in terms of survival[26], orientation,[27] migration,[28] and sprouting.[29] Using a bisurea-norbornene additive (BU-Nb, Figure 8.2), the first steps towards topographical control over the presentation of bioactive moieties at the surface of supramolecular biomaterials are explored. The norbornene moiety is proposed to be used to decorate the surface of elastomeric films via photo-activated thiol-ene click-chemistry (Figure 8.7A), with thiolated bioactive molecules.[30,31] First the properties, i.e., surface morphology, hydrophilicity, and cell-adhesive properties of solution-cast films with 1, 5, and 10% of the BU-Nb additive were assessed. Next, preliminary results based on surface matrix-assisted laser desorption/ionization-time-of-flight mass spectrometry (MALDI-ToF MS) and a cell adhesion measurements are shown for the surface modification with a thiolated RGD peptide, as a first step towards patterned bioactive supramolecular surfaces.

The incorporation of 1% BU-Nb results in a surface morphology comparable to pristine PCL-BU, with fibrous hard-segments clearly visible in light yellow (Figure 8.6A). The surface cast from the mixture with 5 % BU-Nb shows abundant elongated brighter yellow domains, which cover the entire surface at 10% additive concentration. In the background, the fibrous morphology of the PCL-BU base material is still visible. The contact angle for the surfaces with 0 and 1% BU-Nb is comparable, measuring 70 ± 2° and 69 ± 3° , respectively (Figure

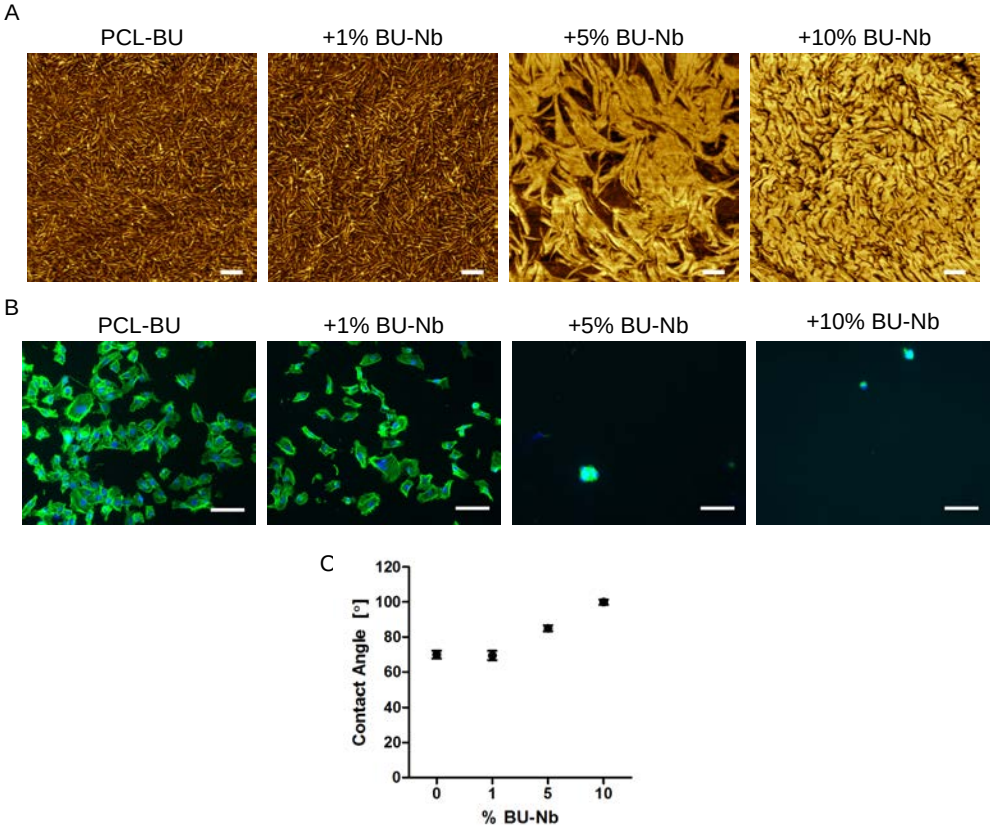

Figure 8.6. A) Atomic force microscopy phase diagrams of solution-cast films of PCL-BU with 1 and 5 mol% BU-Nb additive. Scale bars indicate 100 nm. B) Fluorescence micrographs of HK-2 cells cultured for 24 hours on the solution-cast films. Actin cytoskeleton is depicted in green and nuclei in blue. Scale bars indicate 100 µm. C) Water contact angles measured on the solution-cast films. Data is represented as mean ± SD.

8.6C). With increased BU-Nb concentration, the contact angle also increases. This indicates that the surface properties become predominantly more hydrophobic, which could be due to the presence of the hydrophobic norbornene moiety. Interestingly, the adhesion of human epithelial kidney cells (HK-2) is significantly reduced on the surfaces with 5 and 10% BU-Nb (Figure 8.6B). This compares to the adhesion of these cells on the surfaces with BU-catechol described previously in this chapter.

Surface MALDI-ToF MS measurements of the materials with 0, 1, 5 and 10 % BU-Nb confirm the presence of the additive (1192 m/z) at the surface (**Figure 8.7B**). Moreover, after incubating the 5 and 10% norbornene functionalized surfaces with a thiolated RGD peptide (CGGRGDS) for 20 minutes with UV irradiation (365 nm, 10 mW cm^{-2}), the expected mass of the BU-Nb-RGD product is detected (1840 m/z), indicative of occurrence of the reaction (**Figure 8.7**). Furthermore, the adhesion of HK-2 cells is improved on solution-cast surfaces with 4 % BU-Nb with the same reaction conditions (**Figure 8.7**). Interestingly though, the samples that were not exposed to UV light also show evidence of reaction in terms of cell-adhesion (**Figure 8.7**) and presence of the BU-Nb-RGD product (measured

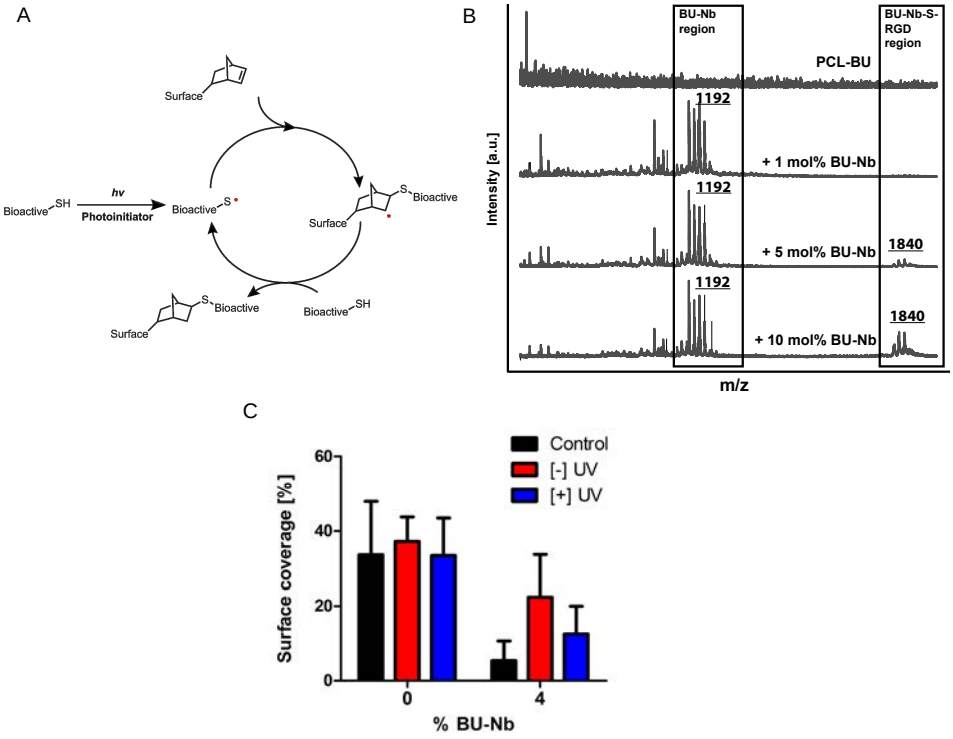

Figure 8.7. A) Schematic representation of the light-induced light-mediated thiol-ene click reaction between a norbornene and a thiol. B) Surface MALDI-ToF MS spectra of BU-Nb functionalized thin films after reacting with the thiolated RGD peptide. Regions for the mass of the BU-Nb additive and the BU-Nb-RGD product are indicated. C) Quantified surface coverage of HK-2 cells cultured for 24 hours on surfaces with 4% BU-Nb after reacting with the thiolated RGD peptide. Data is represented as mean ± SD.

with MALDI-ToF MS, data not shown).

These results show that the norbornene functionalized supramolecular elastomeric materials are reactive and a thiolated peptide can be conjugated to the surface. The photo-activation and efficiency of the reaction should be studied in more detail for more control and the possibility to move towards light-mediated patterning methods.

On the design of bisurea-additives

Preparation relies on supramolecular assembly.

The results in this thesis show that the supramolecular functionalization of our biomaterials is facile and can be performed in an accessible modular fashion. Moreover, extensive opportunities arise with the combination of additives with different intended functionalities. However, the actual control over surface properties and the presentation of the functional groups on the supramolecular additives remains limited. The incorporation of the additives, as elaborately described, relies on the non-covalent and reversible interactions between the supramolecular motifs of the base material and the additives, which are the hydrogen bonding bisurea and UPy moieties in particular in this thesis. Many factors besides

changes in molecular structure can influence the assembly process, and consequently the presentation of the functional groups of additives.[32] Processing into solution-cast films and electrospinning has been performed in a climate-controlled environment, and samples were stored in a desiccator to eliminate some variability. Nevertheless, within these perimeters, the detailed surface characterization we have performed sometimes reveals varying morphologies and properties with the same preparation conditions, as for example with the same concentration BU-OEG and BU-RGD additives.

Value of detailed surface characterization

The combination of surface characterization and determination of functionality was intended to give insights in the structure-property relationships of our functionalized supramolecular biomaterials. However, the correlation between observations on the material level with AFM and XPS and functionality on cell-level is non-trivial; the results described in **Chapter 3** showed evidence for an increased presence of OEG with increasing BU-OEG-BU and OEG-BU-OEG additive concentration, which matched with a decrease in cell adhesive properties. Yet such measurements could not be used to predict non-cell adhesiveness of our supramolecular biomaterials in the future. In **Chapter 4**, the presence of bisurea-peptides was evident, but could not be correlated to functional presentation of the peptides. Furthermore, macroscale properties such as hydrophilicity of the functionalized materials can indicate presence of a functional group, but are not indicative of functionality. Additionally, the surface characterization with e.g. AFM, XPS and WCA measurements are performed in dry and ambient conditions. With AFM measurements, the bisurea additives with OEG linkers are present in a crystalline fashion at the surface of the materials. Investigating the surface morphology in wet and or physiological conditions with AFM could provide more insight in a relevant biological environment.

This indicates that the way we characterize our surfaces and materials can be optimized to further study structure-property relationships for increased understanding and to aid in the design of new supramolecular additives.

Future bioactive additive design: Bisurea and UPy compared

In early work with bioactive supramolecular additives, the functional moiety, e.g. peptide, was directly conjugated to the UPy-group.[33,34] In the following development of UPy-additives, firstly an additional C_6-Urea was introduced, which improved incorporation in the PCLdiUPy base material, attributed to the matching chemical structure.[15,35] For combinatorial functionalization with the PEG_{2k}diUPy additive, an additional short OEG_5 linker was introduced to facilitate presentation in the presence of a hydrated PEG-layer.[24] In following studies, these alkyl and OEG spacers could be used to tune the amphiphilic properties of UPy-peptide conjugates[36], and have been used in UPy-additives since, also in **Chapter 6** of this thesis.[13,16,37–39] Moreover, the short OEG spacers do not inhibit cell-adhesion alone[14] or end-functionalized with a catechol[14] or reactive tetrazine moiety[40] as compared to the longer PEG_{5k}UPy that does.[41]

In the translation to recent bisurea-based bioactive additives, which are featured prominently in this thesis, a C_6-Urea-C_4-Urea-C_{12}-Urethane-OEG_{12}-X design is used, where

X represents the functional moiety, which comprises both the additional alkyl spacer and urethane linker, and the OEG spacer. Interestingly, the BU-OEG additive without functional moiety inhibited cell adhesion at 4 mol% in PCL-BU (**Chapter 3**).[1] As described above, bisurea additives of this design with catechol and reactive norbornene functional groups also decrease cell adhesive properties of the biomaterials, and activity of bisurea-peptide conjugates was unpredictable (**Chapter 4**). Additionally, the slight variation in molecular structure through substitution of the functional group results in drastically different surface morphologies. Especially in the case of bisurea-peptide additives, it would be interesting to study if this relates to the possibility of the additive to form supramolecular assemblies on their own.

Surely, the design of bioactive bisurea additives can yet be improved upon, where a reduction of the OEG-linker may decrease the tendency to formulate non-cell adhesive materials, whilst at the same time retaining the additives in the base material.

Furthermore, since the interaction with the base material ensures the effectivity of the assembly and incorporation of additives, the composition of the soft-segment in the base material, apart from the supramolecular bisurea or UPy-moiety could provide a platform to improve said incorporated additive. The results from the direct comparison between the PC-BU and PCL-BU base material illustrate the influence of the soft-segment, but the exact mechanisms are not yet understood.

Besides contributing to effective supramolecular additive incorporation, the properties of the soft-segment of the elastomeric base may provide tools for other purposes besides mechanical strength and susceptibility to degradation. Through the engineering of supramolecular thermoplastic elastomers with soft-blocks that have additional functionality, an additional approach for supramolecular functionalization could be utilized.

Improving understanding of the antifouling properties of BU-OEG additives

In **Chapter 3** we showed that the design of supramolecular antifouling additives has a big impact on the functionality of the functionalized material, especially when processed into electrospun scaffolds. There, we suggested that the looped conformation of the hydrophilic OEG induced increased hydration of the brushes, which is known to influence antifouling properties.[3,42] However, we have not presented direct proof to substantiate this statement. Future research with other techniques could elucidate the interesting diverse properties of these materials with supramolecular antifouling additives. We have explored the use of quartz crystal microbalance with dissipation monitoring (QCM-D) to study the hydration of these material mixtures, where the formation of a hydrated layer would result in an increase of mass and a change of the visco-elastic properties of the surfaces. First results for the detection of the hydrated layers were promising when spin-coated layers of cell-adhesive PCL-BU and non-cell adhesive PCL-BU + 8 mol% BOB were compared (data not shown). However, reproducibility issues necessitate further optimization. Other techniques that would allow for the characterization of the interaction of water with the functionalized supramolecular materials include DSC and Raman spectroscopy, which offer the tools to distinguish different states of water upon interaction with materials.[43–45]

Making bisurea hydrogels

The interaction of the amphiphilic bisurea-additives with water can also be exploited in more dilute systems. Bisurea-based supramolecular assemblies have been used in the past to formulate particles and hydrogels[46–48] Interestingly, the bola-amphiphilic OBO additive forms fibrous structures in water, and would therefore be an interesting candidate for hydrogel formation (**Figure 8.8**). Furthermore, such assemblies in aqueous environments could be functionalized with additives in a similar fashion as has been explored for BTA, peptide-amphiphiles, or UPy-based systems.[49]

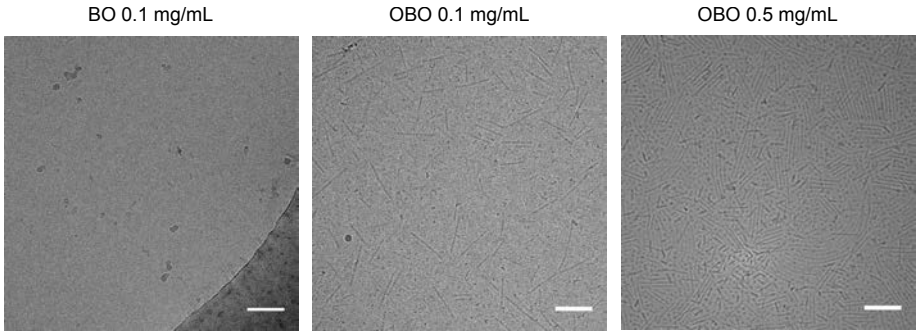

Figure 8.8. Cryogenic transmission electron micrographs of BO and OBO in water. Scale bars indicate 100 nm.

Translation and valorization

The BU-OEG-BU additive efficiently reduced cell adhesion on solution-cast films and electrospun scaffolds with PCL-BU and PC-BU as structural base material. Furthermore, protein adsorption was decreased on the PCL-BU based scaffolds with BU-OEG-BU. One aspect that was not covered in this thesis, which is relevant with respect to the translation to vascular graft development, is the more practical assessment of blood-compatibility. We have assumed that the decrease in cell adhesion and protein adsorption would coincide with reduced thrombogenicity.[50] However, in vitro testing of blood-compatibility of our functionalized and processed biomaterials could aid in their development. Promisingly, the pristine PCL-BU and PC-BU show intrinsic thrombin generation profiles upon contact activation, in the same range as commercial shunt materials, when measured using a calibrated automated thrombogram (**Figure 8.9**).[51]

The following step to test the efficiency of antifouling functionalisation, would be through *in vivo* examination. In collaboration with partners from the University Medical Center in Utrecht, this material could be tested in an abdominal aorta interposition model in rats. By choice, the fiber diameter of the electrospun scaffolds described in **Chapter 3** was below 1 µm to prevent cellular infiltration for ease of analysis. However, for application in vascular grafts purposed for in situ tissue engineering, a more porous scaffold is required, which is generally acquired by an increased fiber diameter. Moreover, the design of the small diameter vascular grafts for in vivo testing features a luminal diameter of 1.4 mm, and a wall thickness of approximately 300 µm.

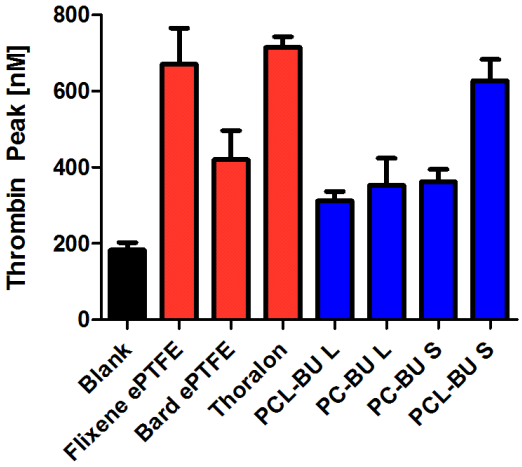

Figure 8.9. Thrombin peak for the commercial graft samples and electrospun bisurea-based TPEs. Data is represented as mean ± SD.

Through changes in the solvent system and electrospinning conditions (**Table 8.1**) scaffolds with a fiber diameter of 3.4 ± 0.4 µm were produced (**Figure 8.10**). Unexpectedly, removing the graft from the mandrel proved to be a tough challenge. Hence we tested methods for graft removal. The method that provided grafts with the best features as based on visual inspection, comprises the use of a sodium alginate coated mandrel as collector, subsequent freezing of the scaffold on the mandrel in water, removal of the mandrel, and freeze drying of the scaffold to remove excess water. However, the presence of residual alginate raised concerns for increased thrombogenicity of the luminal surface of the vascular grafts. Therefore, future efforts should focus on the development of methods for easy graft removal, where no effect on surface chemistry of the remaining material is expected.

Towards the next generation of vascular access grafts

The end-goal of all medical device development, including that of vascular (access) grafts, is application in a clinical setting. The road towards clinical application is time-consuming and expensive and involves rigorous testing and evaluation of safety before approval is

Table 8.1. Comparison of electrospinning conditions for the PC-BU with 10 mol% BOB scaffolds as described in chapter 3, and for the fabrication of small diameter vascular grafts with increased fiber size.

	Solvent	Conc.	Flow rate	V	Mandrel diameter	WD	Mandrel rotation	Climate	GS
Sheets	HFIP	12% w/w	20 µL min^{-1}	24(-1) kV	>18 mm	24 cm	500 rpm	T: 23 °C H: 30%	~
Grafts	$CHCl_3$:AA 95:5 v/v	16% w/w	40 µL min^{-1}	24(-1) kV	1.4 mm	11 cm	500 rpm	T: 23 °C H: 50%	$CHCl_3$ 35 ml min^{-1}

HFIP: Hexafluoroisopropanol, CHCL3: Chloroform, AA: Acetic Acid, Conc.: Concentration, V: Voltage, WD: Working Distance, GS: Gas Shielding

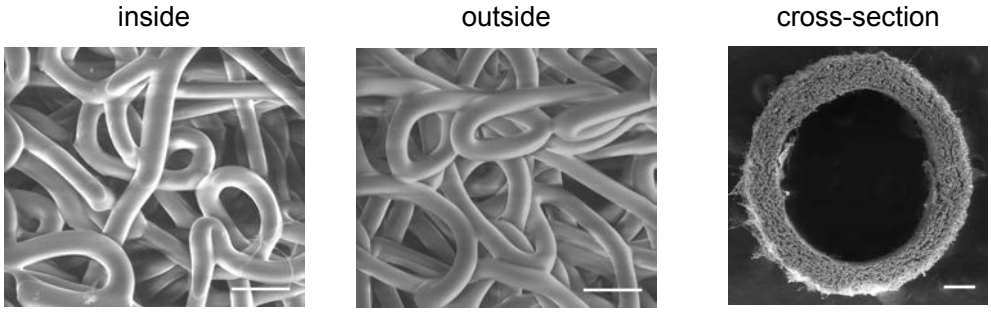

Figure 8.10. Scanning electron micrographs of small diameter electrospun vascular graft. Scale bars represent 10 µm for the inside and outside image and 250 µm for the cross-section.

procured.[52] Therefore, relatively simple approaches may find the way to the clinic faster. However, as was highlighted in **Chapter 2**, the trend in blood-compatible biomaterials development shifts towards increased complexity rather than simplicity, in an effort to mimic the dynamics of endothelial cell-mediated hemostasis. With respect to the tissue engineering approach, biomaterial-independent factors such as patient-to-patient variability and co-morbidities might actually necessitate more complex and instructive biomaterials to properly steer *de novo* tissue formation. It is also imperative that future efforts will not only be evaluated in healthy (animal) models, but also in *in vitro* or *in vivo* (disease) models that capture the disrupted environment present in patients.

In this thesis, functionalization strategies based on small supramolecular additives were shown to improve control over cell-biomaterial interactions. Importantly, it was shown that the supramolecular materials platform allows for versatile and combinatorial approaches for bioactivation of biomaterial scaffolds. However, the interactions that were tuned were still one-directional, where in nature, cells communicate in a dynamic reciprocal fashion with their extracellular environment. In future, such dynamic interactions are proposed to be incorporated in vascular biomaterials, to give the cells of the patient - depending on the specific requirements - the proper stimuli, and thereby guide *in situ* generation of vascular tissue.

Acknowledgements

Ronald van Gaal is gratefully acknowledged for the culture of the HK-2 cells and WCA measurements. Researchers from SyMO-CHEM B.V. are acknowledged for the synthesis of the BU-fluor, BU-betaine, BU-cRGD and BU-OEG-betaine additives. Peter-Paul K.H. Fransen is acknowledged for the synthesis of the BU-catechol. Maaike Schotman is acknowledged for the cryogenic TEM measurements. Izy Janssens is acknowledged for the synthesis of the BU-Nb additive, and the experimental work revolving around this additive. Rachel Toorop is acknowledged for providing the commercial vascular graft samples. Henri Spronk and Rene van Oerle are acknowledged for collaboration with the CAT measurements.

Experimental section

Materials and instrumentation
Unless stated otherwise, all used solvents and chemicals were purchased from Biosolve. PCL-BU, and the BU- COOH synthon were synthesized by SyMO-Chem BV (Eindhoven, the Netherlands).

N,N'-diisopropylethylamine (DIPEA) and Irgacure D-2959 (I2959) were purchased from Sigma-Aldrich. 5-norbornene-2-methylamine and lithium phenyl-2,4,6-trimethylbenzoylphosphinate (LAP) were purchased from TCI chemicals. Piperidine was purchased from Carlo Erba Reagents and dichloromethane (DCM) was used from Cambridge Isotope Laboratory.

HPLC-PDA/ESI-MS analyses were performed using a Shimadzu LC-10 AD VP series HPLC coupled to a diode array detector (Finnigan Surveyor PDA Plus detector, Thermo Electron Corporation) and an ion-trap (LCQ Fleet, Thermo Scientific). 1H-NMR data were recorded on a Bruker Cryomagnet for NMR spectroscopy (400 MHz) at room temperature. Proton experiments were reported in parts per million (ppm) downfield of TMS. The 1H-NMR data are abbreviated as the following: chemical shift, multiplicity (s = singlet, d = doublet, t = triplet, q = quartet, m = multiplet) and integration.

Synthesis of bisurea-norbornene
BU-COOH (101 mg, 93 mmol) was stirred in 10 mL dimethylformamide (DMF) until dissolved, followed by addition of *N,N,N',N'*-Tetramethyl-*O*-(1H-benzotriazol-1-yl)uronium hexafluorophosphate (HATU) (51 mg, 134.1 mmol) in 1 mL DMF and DIPEA (80.1 mL, 460 mmol). After stirring for 30 minutes at room temperature, 5-norbornene-2-methylamine (23.6 mL, 184 mmol) in 1 mL DMF was added to the mixture. The reaction mixture was stirred for 24 hours at room temperature under Argon. The mixture was dropwise added to 40 mL of cold di-ethyl ether in which it precipitated. The solid was dried with N_2, yielding a light orange solid (90 mg, 89%). ^{1}H NMR (399 MHz, Chloroform-*d*) δ 6.22 – 5.89 (m, 2H), 5.40 (d, *J* = 62.2 Hz, 1H), 4.19 (s, 2H), 3.62 (d, *J* = 27.0 Hz, 62H), 3.38 (s, 3H), 3.13 (s, 11H), 2.99 (s, 1H), 2.86 (d, *J* = 29.9 Hz, 3H), 2.45 (s, 2H), 2.25 (s, 1H), 1.84 (s, 1H), 1.47 (s, 12H), 1.29 (s, 25H), 0.89 (s, 3H), 0.56 (s, 1H). R: ν = 3322, 2923, 2852, 1680, 1616, 1575, 1539, 1477, 1467, 1344, 1311, 1269, 1235, 1145, 1105, 1060, 963, 842, 782, 723, 631, 584, 558 cm^{-1}. LC-MS (ESI), calc. m/z 1191.60, found: $[M+H]^+$, 1191.83 m/z and $[M+2H]^+$, 596.67.

Synthesis of CGGRGDS
The CGGRGDS (Cys-Gly-Gly-Arg-Gly-Asp-Ser) was synthesized on a Rink-amide resin through Fmoc-based solid phase peptide synthesis (100 umol scale). The resin was swollen in Dimethyl formamide (DMF, 4 mL) for 30 minutes prior to the first coupling. After swelling, DMF is drained from resin. The resin is deprotected 2 times with 20 v% piperidine in 80 v% DMF (6 mL, 10 min) and subsequently washed 5 times with DMF (4 mL, 30 sec). The amino acid (100mM, 4mL) was coupled 2 times to the resin in the presence of HCTU (200mM, 2mL) and diisopropylethylamine (DIPEA, 800mM, 2 mL) for 10 minutes, followed by washing 5 times with DMF (4 mL, 30 sec). The process was repeated until all amino acids were coupled. The final peptide was deprotected 2 times using 20 vol% piperidine in 80 vol% DMF (6 mL, 10 min) and washed 5 times with DMF (4 mL, 30 sec). Subsequently the resin was washed 3 times with DCM and 3 times with cold diethyl ether alternately. The peptide was cleaved from the resin by shaking for 2 hours with a cleavage mixture consisting of 92.5 vol% trifluoroacetic acid (TFA), 2.5 vol% milli-Q, 2.5 vol% triisopropylsilane and 2.5 vol% 1,2-ethyldithiol (EDT). The suspension was filtered, and the resin was washed 3 times with DMF. The filtrate was precipitated in cold diethyl ether and centrifuged at 3000 rpm for 5 minutes.

LCMS (ESI), calc. m/z 650.25, found: [M+2H]+ 325.75 m/z and [M+H]+ 650.33 m/z.

Preparation of polymer films
The PCL-BU and additives were dissolved in 1,1,1,3,3,3, hexofluorisopropanol (HFIP, Fluorochem) at a concentration of 7.4 mM – where the molar mass of a single repeating unit is used - , which is equal to 20 mg mL^{-1} for the base polymer. These solutions were mixed in molar ratios additive:PCL-BU of 0.5:99.5, 1:99, 2:98, and 4:96, or additive 1:additive 2:PCL-BU of 2:2:96, for double functionalization, prior to casting 50-60 µL on 13 or 14 mm glass coverslips. The polymer films were air-dried for several hours, before final drying in vacuum overnight.

Cell culture
Human vena saphena cells, which are vascular derived matrix producing myofibroblasts[54] were harvested from the human vena saphena magna according to the Dutch guidelines for secondary use of materials. HVSCs were expanded in culture medium, which consisted of Dulbecco's modified

Eagle medium (DMEM, #41966 Gibco) supplemented with 10% fetal bovine serum, 1% Glutamax (Gibco) and 1% Penicillin/Streptomycin, and used for experiments up to passage 7. Human kidney 2 cells (HK-2, ATCC) were cultured in DMEM supplemented with 10% FBS (Greiner), and 1% penicillin/streptomycin (Invitrogen).

Cell adhesion analysis
Solution-cast films on glass were secured in adapted 12 well Transwell inserts (Corning), from which the membrane was removed and custom made PEEK rings were used to mount the samples. Samples were sterilized under UV on both sides for 15 minutes. Cells were collected from the culture flasks using trypsin and seeded at a concentration of 25,000 cells cm^{-2} and 20,000 cells cm^{-2} on the solution-cast films for HVSCs and HK-2s, respectively. Non-adherent cells were aspirated and samples were washed twice with PBS prior to fixation with 3.7% formaldehyde. The actin cytoskeleton was stained with ATTO 488 conjugated phalloidin and nuclei with DAPI, after removal of the samples from the adapted Transwell inserts. Samples were visualized with a Zeiss Axiovert 200M fluorescence microscope.

Quantification of surface coverage
Surface coverage was quantified by binarizing the fluorescence micrographs of the phalloidin-stained cells on the polymer surfaces in ImageJ (NIH, version X) such that background and cells were black and white respectively. The number of foreground, i.e., the cells, pixels divided by the total number of pixels per image gives the percentage surface coverage. Since this measure can be dependent on seeding density for different experiments, the coverage was normalized for the amount of surface coverage on pristine PCL-BU for the concerning experiment.

AFM
Atomic Force Microscopy was performed on a Digital Instruments Multimode Nanoscope IIIa, and a Digitial Instruments Dimension 3100 Nanoscope IIIa. Phase images of solution-cast films were recorded in the tapping mode regime in air at room temperature using silicon cantilever tips (PPP-NCHR). Images were processed using Gwyddion software (version 2.43).

Water Contact Angle Measurements
An OCA30 machine (DataPhysics), operated with SCA20 software (version 4.1.13), was used to determine static water contact angles on solution-cast films at room temperature. 5 µL Milli-Q water droplets were applied to the surface through a needle and the contact angle was measured at the polymer-air-water interface 5 seconds after deposition of the droplet.

Surface modification of BU-Nb functionalized materials with CGGRGDS
CGGRGDS (4.4 mg, 0.17 µmol), photo initiator (0.07 µg, 6.6 nmol), 0.05 v/v% Triton-X-100 in PBS were dissolved in 8 mL PBS. The solution was bubbled under Argon for 15 minutes. Prior to surface reactions, solution-cast films were secured in adapted 12 well Transwell inserts (Corning). Subsequently, 200 µL of CGGRGDS solution was pipetted onto solution-casted and UV irradiated (365 nm) for 20 minutes under 10 mW cm^{-2}. Finally, the samples were washed 5 times for 10 minutes on a shaker plate with milliQ water. For cell adhesion experiments, the post-modified solution-cast samples were stored in PBS at 4 °C. For water contact angle measurements, the samples were dried overnight in a desiccator containing silica drying beads under vacuum at room temperature.

Surface MALDI-ToF MS
Matrix-assisted laser desorption ionization time-of-flight mass spectrometry was performed on an Autoflex Speed MALDI-MS (Bruker). Samples for surface MALDI-ToF MS experiments were prepared via casting 3 µL polymer solution (prepared similar to the regular solution-cast samples, but at a concentration of 14.8 mM), with 0, 1, 5, and 10 mol% BU-Nb on a MTP 384 polished steel TF target plate. The solution-cast films were incubated with 1.5 or 5 mM CGGRGDS for 20 minutes at RT under 10 mW cm^{-2} UV irradiation followed by washing with milliQ water 5 times. Subsequently, 1 µL α-cyano-4-hydroxycinnamic acid (CHCA) in 49.5/49.5/1 acetonitrile/water/trifluoroacetic acid (v/v/v) was spotted on each surface and dried to the air for 30 minutes. Measurements were performed in positive linear mode (method: 700-2000 Da), 3000 shots per spot and a laser power of 60%.

Cryo-TEM
For Cryo-TEM, solutions of BU-OEG and OEG-BU-OEG were prepared at 0.1 mg mL^{-1} and 0.1 and 0.5 mg mL^{-1} in milliQ, respectively. Vitrified films were prepared in a Vitrobot instrument at 22 °C and at a relative humidity of 100%. 3 μL samples were applied on a Quantifoil grid (R2/2, Quantifoil Micro Tools GmbH), which was surface-plasma treated prior to use (Cressington 208 carbon coater operated at 5 mA for 40 s). Excess sample solution was removed by blotting with filter paper for 3 s at -3 mm. The films were plunged into liquid ethane just above its freezing point. The vitrified films were transferred to a cryoholder Gatan 626) and observed at temperatures below −170 °C in a FEI Titan TEM equipped with a field emission gun operating at 300 kV. Micrographs were recorded at low dose conditions, using a defocus setting of 5 or 10 µm at 24,000 times magnification.

Electrospinning
For the CAT-experiments two types of grafts were prepared, with an intended fiber diameter of ~ 1 µm (marked with an extra 'S') and a fiber diameter of ~ 4 µm (marked with an extra 'L'), from both PCL-BU and polycarbonate-bisurea (PC-BU). For the smaller fibers, both polymers were dissolved at a concentration of 12% w/w in HFIP. For the larger fibers, PCL-BU was dissolved at a concentration of 13% w/w in a 90:10 (v:v) chloroform:HFIP mixture, and PC-BU at a concentration of 23% w/v in a 85:15 (v:v) chloroform:HFIP mixture. The sheets were spun in a climate controlled electrospinning setup with the following settings:

Table 8.2. Electrospinning settings for sheets intended for the CAT-assays.

	Flow rate	Voltage	Mandrel diameter	Working distance	Mandrel rotation	Climate
PCL-BU L	55 µL min^{-1}	16(-1) kV	27 mm	14 cm	200 rpm	T: 23 °C H: 30%
PC-BU L	80 µL min^{-1}	19(-1) kV	27 mm	15 cm	500 rpm	T: 23 °C H: 50%
PCL-BU S	10 µL min^{-1}	24(-1) kV	18 mm	22 cm	2000 rpm	T: 23 °C H: 50%
PC-BU S	10 µL min^{-1}	24(-1) kV	18 mm	22 cm	2000 rpm	T: 23 °C H: 30%

For the tubular grafts, solutions from the mixture of PC-BU and BU-OEG-BU in a 90:10 molar ratio were dissolved by overnight stirring on a heated plate (45 °C). The grafts were electrospun onto alginate coated 1.4 ø mm mandrels with the settings in table 8.1. Critically, the climate chamber doors were closed 10 minutes prior to initiating the spinning procedure. Moreover, in between grafts, the electrospinning needle was replaced by a clean one. After spinning, the grafts were dried overnight in vacuum, whilst still on the mandrel. For removal, the following procedure was followed: the exposed end of the mandrel was inserted through a 1.4 mm hole in the bottom of a 15 mL falcon tube, which was subsequently filled with milliQ water and placed at -30 °C. Once frozen, the end of the mandrel sticking out of the falcon tube was heated for a couple of seconds with warm water, after which the mandrel was gently removed from the graft embedded in ice using pliers. Most of the water was then thawed, after which the grafts were again frozen and freeze dried to remove the last of the water, without collapsing.

Calibrated Automated Thrombogram
Samples with a diameter of 7 mm were punched using a biopsy punch and subsequently glued to the bottom of a 96 well assay plate using surgical glue. The CAT measurement was performed in a fluorimeter (Thermo Fisher). In short, samples were incubated with a mixture of normal platelet poor plasma, a fluorogenic substrate (Thrombinoscope BV), and MP-reagent (Thrombinoscope BV). The formation of thrombin was measured in time, against a calibrated control to obtain the calibrated thrombogram.

Scanning electron microscopy
Electrospun scaffold samples were analyzed using a FEI Quanta 600 scanning electron microscope operated with Xt Microscope control software. Images were recorded in low vacuum (~0.6 mbar) in the presence of water vapor, of samples fixed on metal stubs with adhesive carbon conductive tape. Secondary and backscattered electrons were detected with an accelerating voltage of 10 kV and a working distance of 10 mm. Compound images were constructed by overlaying the resulting images from both detectors.

References

(1) Ippel, B. D.; Keizer, H. M.; Dankers, P. Y. W. Supramolecular Antifouling Additives for Robust and Efficient Functionalization of Elastomeric Materials: Molecular Design Matters. *Adv. Funct. Mater.* **2019**, *29*, 1805375.

(2) Schlenoff, J. B. Zwitteration: Coating Surfaces with Zwitterionic Functionality to Reduce Nonspecific Adsorption. *Langmuir* **2014**, *30*, 9625–9636.

(3) Chen, S.; Li, L.; Zhao, C.; Zheng, J. Surface Hydration: Principles and Applications toward Low-Fouling/nonfouling Biomaterials. *Polymer* **2010**, *51*, 5283–5293.

(4) Wei, Q.; Becherer, T.; Angioletti-Uberti, S.; Dzubiella, J.; Wischke, C.; Neffe, A. T.; Lendlein, A.; Ballauff, M.; Haag, R. Protein Interactions with Polymer Coatings and Biomaterials. *Angew. Chem., Int. Ed.* **2014**, *53*, 8004–8031.

(5) Li, Q.; Imbrogno, J.; Belfort, G.; Wang, X.-L. Making Polymeric Membranes Antifouling Via "grafting From" polymerization of Zwitterions. *J. Appl. Polym. Sci.* **2015**, *132*, 41781-.

(6) Wang, L.; Su, Y.; Zheng, L.; Chen, W.; Jiang, Z. Highly Efficient Antifouling Ultrafiltration Membranes Incorporating Zwitterionic poly([3-(Methacryloylamino)propyl]-dimethyl(3-Sulfopropyl) Ammonium Hydroxide). *J. Memb. Sci.* **2009**, *340*, 164–170.

(7) Sun, Q.; Su, Y.; Ma, X.; Wang, Y.; Jiang, Z. Improved Antifouling Property of Zwitterionic Ultrafiltration Membrane Composed of Acrylonitrile and Sulfobetaine Copolymer. *J. Memb. Sci.* **2006**, *285*, 299–305.

(8) Li, J. H.; Li, M. Z.; Miao, J.; Wang, J. Bin; Shao, X. S.; Zhang, Q. Q. Improved Surface Property of PVDF Membrane with Amphiphilic Zwitterionic Copolymer as Membrane Additive. *Appl. Surf. Sci.* **2012**, *258*, 6398–6405.

(9) Kaner, P.; Rubakh, E.; Kim, D. H.; Asatekin, A. Zwitterion-Containing Polymer Additives for Fouling Resistant Ultrafiltration Membranes. *J. Memb. Sci.* **2017**, *533*, 141–159.

(10) Fang, L.-F.; Jeon, S.; Kakihana, Y.; Kakehi, J.; Zhu, B.-K.; Matsuyama, H.; Zhao, S. Improved Antifouling Properties of Polyvinyl Chloride Blend Membranes by Novel Phosphate Based-Zwitterionic Polymer Additive. *J. Memb. Sci.* **2017**, *528*, 326–335.

(11) Ostuni, E.; Chapman, R. G.; Liang, M. N.; Meluleni, G.; Pier, G.; Ingber, D. E.; Whitesides, G. M. Self-Assembled Monolayers That Resist the Adsorption of Cells. *Langmuir* **2001**, *17*, 6336–6343.

(12) Vaisocherová, H.; Zhang, Z.; Yang, W.; Cao, Z.; Cheng, G.; Taylor, A. D.; Piliarik, M.; Homola, J.; Jiang, S. Functionalizable Surface Platform with Reduced Nonspecific Protein Adsorption from Full Blood Plasma-Material Selection and Protein Immobilization Optimization. *Biosens. Bioelectron.* **2009**, *24*, 1924–1930.

(13) Goor, O. J. G. M.; Keizer, H. M.; Bruinen, A. L.; Schmitz, M. G. J.; Versteegen, R. M.; Janssen, H. M.; Heeren, R. M. A.; Dankers, P. Y. W. Efficient Functionalization of Additives at Supramolecular Material Surfaces. *Adv. Mater.* **2017**, *29*, 1604652.

(14) Spaans, S.; Fransen, P. P. K. H.; Ippel, B. D.; de Bont, D. F. A.; Keizer, H. M.; Bax, N. A. M. A. M.; Bouten, C. V. C.; Dankers, P. Y. W. Supramolecular Surface Functionalization via Catechols for

the Improvement of Cell–material Interactions. *Biomater. Sci.* **2017**, *5*, 1541–1548.

(15) Wisse, E.; Spiering, a. J. H.; Dankers, P. Y. W.; Mezari, B.; Magusin, P. C. M. M.; Meijer, E. W. Multicomponent Supramolecular Thermoplastic Elastomer with Peptide-Modified Nanofibers. *J. Polym. Sci. Part A: Polym. Chem.* **2011**, *49*, 1764–1771.

(16) van Gaal, R. C.; Fedecostante, M.; Fransen, P.-P. K. H.; Masereeuw, R.; Dankers, P. Y. W. Renal Epithelial Monolayer Formation on Monomeric and Polymeric Catechol Functionalized Supramolecular Biomaterials. *Macromol. Biosci.* **2018**, *1800300*, 1800300.

(17) Gabriel, M.; Niederer, K.; Becker, M.; Raynaud, C. M.; Vahl, C. F.; Frey, H. Tailoring Novel PTFE Surface Properties: Promoting Cell Adhesion and Antifouling Properties via a Wet Chemical Approach. *Bioconjugate Chem.* **2016**, *27*, 1216–1221.

(18) Roy-Chaudhury, P.; Kelly, B. S.; Miller, M. A.; Reaves, A.; Armstrong, J.; Nanayakkara, N.; Heffelfinger, S. C. Venous Neointimal Hyperplasia in Polytetrafluoroethylene Dialysis Grafts. *Kidney Int.* **2001**, *59*, 2325–2334.

(19) Brown, P. S.; Bhushan, B. Bioinspired, Roughness-Induced, Water and Oil Super-Philic and Super-Phobic Coatings Prepared by Adaptable Layer-by-Layer Technique. *Sci. Rep.* **2015**, *5*, 1–16.

(20) Brown, P. S.; Bhushan, B. Mechanically Durable, Superomniphobic Coatings Prepared by Layer-by-Layer Technique for Self-Cleaning and Anti-Smudge. *J. Colloid Interface Sci.* **2015**, *456*, 210–218.

(21) Wang, Z.; Zuilhof, H. Self-Healing Superhydrophobic Fluoropolymer Brushes as Highly Protein-Repellent Coatings. *Langmuir* **2016**, *32*, 6310–6318.

(22) Tuteja, A.; Choi, W.; Ma, M.; Mabry, J. M.; Mazzella, S. a; Rutledge, G. C.; McKinley, G. H.; Cohen, R. E. Designing Superoleophobic Surfaces. *Science* **2007**, *318*, 1618–1622.

(23) Deng, X.; Mammen, L.; Butt, H. J.; Vollmer, D. Candle Soot as a Template for a Transparent Robust Superamphiphobic Coating. *Science* **2012**, *335*, 67–70.

(24) Mollet, B. B.; Comellas-Aragonès, M.; Spiering, A. J. H.; Söntjens, S. H. M.; Meijer, E. W.; Dankers, P. Y. W. A Modular Approach to Easily Processable Supramolecular Bilayered Scaffolds with Tailorable Properties. *J. Mater. Chem. B* **2014**, *2*, 2483–2493.

(25) Nguyen, A. T.; Sathe, S. R.; Yim, E. K. F. From Nano to Micro: Topographical Scale and Its Impact on Cell Adhesion, Morphology and Contact Guidance. *J. Phys. Condens. Matter* **2016**, *28*.

(26) S., C. C.; M., M.; S., H.; M., W. G.; E, I. D. Geometric Control of Cell Life and Death. *Science* **1997**, *276*, 1425.

(27) Tamiello, C.; Buskermolen, A. B. C.; Baaijens, F. P. T.; Broers, J. L. V.; Bouten, C. V. C. Heading in the Right Direction: Understanding Cellular Orientation Responses to Complex Biophysical Environments. *Cell. Mol. Bioeng.* **2016**, *9*, 12–37.

(28) Jeon, H.; Koo, S.; Reese, W. M.; Loskill, P.; Grigoropoulos, C. P.; Healy, K. E. Directing Cell Migration and Organization via Nanocrater-Patterned Cell-Repellent Interfaces. *Nat. Mater.* **2015**, *14*, 918–923.

(29) Tiemeijer, L. A.; Frimat, J. P.; Stassen, O. M. J. A.; Bouten, C. V. C.; Sahlgren, C. M. Spatial Patterning of the Notch Ligand Dll4 Controls Endothelial Sprouting in Vitro. *Sci. Rep.* **2018**, *8*, 1–10.

(30) Vega, S. L.; Kwon, M. Y.; Song, K. H.; Wang, C.; Mauck, R. L.; Han, L.; Burdick, J. A. Combinatorial Hydrogels with Biochemical Gradients for Screening 3D Cellular Microenvironments. *Nat. Commun.* **2018**, *9*, 614.

(31) Tasdelen, M. A.; Yagci, Y. Light-Induced Click Reactions. *Angew. Chem., Int. Ed.* **2013**, *52*, 5930–5938.

(32) Appel, W. P. J.; Meijer, E. W.; Dankers, P. Y. W. Enzymatic Activity at the Surface of Biomaterials via Supramolecular Anchoring of Peptides : The Effect of Material Processing a. **2011**, 1706–1712.

(33) Wisse, E.; Spiering, A. J. H.; Pfeifer, F.; Portale, G.; Siesler, H. W.; Meijer, E. W. Segmental Orientation in Well-Defined Thermoplastic Elastomers Containing Supramolecular Fillers. *Macromolecules* **2009**, *42*, 524–530.

(34) Dankers, P. Y. W.; Harmsen, M. C.; Brouwer, L. A.; van Luyn, M. J. A.; Meijer, E. W. A Modular and Supramolecular Approach to Bioactive Scaffolds for Tissue Engineering. *Nat. Mater.* **2005**, *4*, 568–574.

(35) Dankers, P. Y. W.; Boomker, J. M.; Huizinga-van der Vlag, A.; Wisse, E.; Appel, W. P. J.; Smedts, F. M. M.; Harmsen, M. C.; Bosman, A. W.; Meijer, W.; van Luyn, M. J. A. Bioengineering of Living Renal Membranes Consisting of Hierarchical, Bioactive Supramolecular Meshes and Human Tubular Cells. *Biomaterials* **2011**, *32*, 723–733.

(36) De Feijter, I.; Goor, O. J. G. M.; Hendrikse, S. I. S.; Comellas-Aragonès, M.; Söntjens, S. H. M.; Zaccaria, S.; Fransen, P. P. K. H.; Peeters, J. W.; Milroy, L. G.; Dankers, P. Y. W. Solid-Phase-Based Synthesis of Ureidopyrimidinone-Peptide Conjugates for Supramolecular Biomaterials. *Synlett* **2015**, *26*, 2707–2713.

(37) Spaans, S.; Fransen, P. P. K. H.; Ippel, B. D.; De Bont, D. F. A.; Keizer, H. M.; Bax, N. A. M.; Bouten, C. V. C.; Dankers, P. Y. W. Supramolecular Surface Functionalization: Via Catechols for the Improvement of Cell-Material Interactions. *Biomater. Sci.* **2017**, *5*.

(38) Zaccaria, S.; van Gaal, R. C.; Riool, M.; Zaat, S. A. J.; Dankers, P. Y. W. Antimicrobial Peptide Modification of Biomaterials Using Supramolecular Additives. *J. Polym. Sci. Part A: Polym. Chem.* **2018**, *56*, 1926–1934.

(39) Muylaert, D. E. P.; van Almen, G. C.; Talacua, H.; Fledderus, J. O.; Kluin, J.; Hendrikse, S. I. S.; van Dongen, J. L. J.; Sijbesma, E.; Bosman, A. W.; Mes, T.; et al. Early in-Situ Cellularization of a Supramolecular Vascular Graft Is Modified by Synthetic Stromal Cell-Derived Factor-1α Derived Peptides. *Biomaterials* **2016**, *76*, 187–195.

(40) Goor, O. J. G. M.; Brouns, J. E. P.; Dankers, P. Y. W. Introduction of Anti-Fouling Coatings at the Surface of Supramolecular Elastomeric Materials via Post-Modification of Reactive Supramolecular Additives. *Polym. Chem.* **2017**, *8*, 5228–5238.

(41) Pape, A. C. H.; Ippel, B. D.; Dankers, P. Y. W. Cell and Protein Fouling Properties of Polymeric Mixtures Containing Supramolecular Poly(ethylene Glycol) Additives. *Langmuir* **2017**, *33*, 4076–4082.

(42) Yan, W.; Divandari, M.; Rosenboom, J. G.; Ramakrishna, S. N.; Trachsel, L.; Spencer, N. D.; Morgese, G.; Benetti, E. M. Design and Characterization of Ultrastable, Biopassive and Lubricious Cyclic poly(2-Alkyl-2-Oxazoline) Brushes. *Polym. Chem.* **2018**, *9*, 2580–2589.

(43) Tanaka, M.; Mochizuki, A.; Ishii, N.; Motomura, T.; Hatakeyama, T. Study of Blood Compatibility with Poly(2-Methoxyethyl Acrylate). Relationship between Water Structure and Platelet Compatibility in Poly(2-Methoxyethylacrylate- Co -2-Hydroxyethylmethacrylate). *Biomacromolecules* **2002**, *3*, 36–41.

(44) Higaki, Y.; Kobayashi, M.; Murakami, D.; Takahara, A. Anti-Fouling Behavior of Polymer Brush Immobilized Surfaces. *Polym. J.* **2016**, *48*, 325–331.

(45) Fega, K. R.; Wilcox, D. S.; Ben-Amotz, D. Application of Raman Multivariate Curve Resolution to Solvation-Shell Spectroscopy. *Appl. Spectrosc.* **2012**, *66*, 282–288.

(46) Estroff, L. A.; Hamilton, A. D. Water Gelation by Small Organic Molecules. *Chem. Rev.* **2004**, *104*, 1201–1218.

(47) Chebotareva, N.; Bomans, P. H. H.; Frederik, P. M.; Sommerdijk, N. A. J. M.; Sijbesma, R. P. Morphological Control and Molecular Recognition by Bis-Urea Hydrogen Bonding in Micelles of Amphiphilic Tri-Block Copolymers. *Chem. Commun.* **2005**, No. 39, 4967.

(48) Koenigs, M. M. E.; Pal, A.; Mortazavi, H.; Pawar, G. M.; Storm, C.; Sijbesma, R. P. Tuning Cross-Link Density in a Physical Hydrogel by Supramolecular Self-Sorting. *Macromolecules* **2014**, *47*, 2712–2717.

(49) Goor, O. J. G. M.; Hendrikse, S. I. S.; Dankers, P. Y. W.; Meijer, E. W. From Supramolecular Polymers to Multi-Component Biomaterials. *Chem. Soc. Rev.* **2017**, *46*, 6621–6637.

(50) Lavery, K. S.; Rhodes, C.; Mcgraw, A.; Eppihimer, M. J. Anti-Thrombotic Technologies for Medical Devices. *Adv. Drug Deliv. Rev.* **2017**, *112*, 2–11.

(51) Hemker, H. C.; Giesen, P.; AlDieri, R.; Regnault, V.; De Smed, E.; Wagenvoord, R.; Lecompte, T.; Béguin, S. The Calibrated Automated Thrombogram (CAT): A Universal Routine Test for Hyper- and Hypocoagulability. *Pathophysiol. Haemost. Thromb.* **2002**, *32*, 249–253.

(52) Kaplan, A. V.; Baim, D. S.; Smith, J. J.; Feigal, D. A.; Simons, M.; Jefferys, D.; Fogarty, T. J.; Kuntz, R. E.; Leon, M. B. Medical Device Development: From Prototype to Regulatory Approval. *Circulation* **2004**, *109*, 3068–3072.

(53) Mol, A.; Rutten, M. C. M.; Driessen, N. J. B.; Bouten, C. V. C.; Zünd, G.; Baaijens, F. P. T.; Hoerstrup, S. P. Autologous Human Tissue-Engineered Heart Valves: Prospects for Systemic Application. *Circulation* **2006**, *114*, 152–159.

Curriculum Vitae

Bastiaan Dirk Ippel was born on September 21st 1990 in Utrecht, the Netherlands. He grew up in De Bilt and attended grammar school in Utrecht at the Christelijk Gymnasium. He obtained his bachelor degree in Biomedical Engineering at Eindhoven University of Technology in 2012, with a final project relating to the multi-scale analysis of 3D electrospun scaffolds for tissue engineering. In 2015, he completed his master also in Biomedical Engineering at Eindhoven University of Technology. For his thesis he investigated the regulation of cardiac fibroblast phenotype in engineered micro-tissue models with extracellular matrix (an)isotropy under supervision of prof. dr. Carlijn V.C. Bouten. Additionally he completed a research internship on the inflammatory phenotype of differentiating mesenchymal stromal cells at Harvard School of Engineering and Applied Sciences under supervision of prof. David J. Mooney. In 2015, he started his doctoral research at Eindhoven University of Technology under supervision of prof. dr. dr. Patricia Y.W. Dankers and prof. dr. Carlijn V.C. Bouten. The highlights of the research conducted during his PhD are described in this thesis.

Publications related to this thesis

Bastiaan D. Ippel*, Muhabbat I. Komil*, Paul A.A. Bartels, Roy J.E.A. Boonen, Maarten M.J. Smulders, Patricia Y.W. Dankers, *Supramolecular additive initiated controlled atom transfer radical polymerization of zwitterionic brushes on ureido-pyrimidinone-based biomaterial surfaces,* submitted

Bastiaan D. Ippel, Boris Arts, Henk M. Keizer, Patricia Y.W. Dankers, *Combinatorial functionalization with bisurea-peptide and antifouling bisurea additives of a supramolecular elastomeric biomaterial,* submitted

Bastiaan D. Ippel, Eline E. van Haaften, Carlijn V.C. Bouten, Patricia Y.W. Dankers, *Impact of additives on mechanical properties of supramolecular electrospun scaffolds,* in preparation

Bastiaan D. Ippel, Henk M. Keizer, Patricia Y.W. Dankers, *Supramolecular antifouling additives for robust and efficient functionalization of elastomeric materials: molecular design matters*, Advanced Functional Materials **2019**, 29, 1805375

Bastiaan D. Ippel, Patricia Y.W. Dankers, *Introduction of nature's complexity in engineered blood-compatible biomaterials*, Advanced Healthcare Materials **2018**, 7, 1700505

A.C.H. Pape*, Bastiaan D. Ippel*****, Patricia Y.W. Dankers, *Cell and protein fouling properties of polymeric mixtures containing supramolecular poly(ethylene glycol) additives,* Langmuir **2017**, 33, 4076-4082

Geert C. Van Almen, Hanna Talacua**,** Bastiaan D. Ippel, Björne B. Mollet, Mellany Ramaekers, Marc Simonet, Anthal I.P.M. Smits, Carlijn V.C. Bouten, Jolanda Kluin, Patricia Y.W. Dankers, *Development of non-cell adhesive vascular grafts using supramolecular building blocks*, Macromolecular Bioscience **2016**, 16, 350-362

Other publications

Ronald C. van Gaal, A.B.C. Buskermolen, Bastiaan D. Ippel, Peter-Paul K.H. Fransen, Sabrina Zaccaria, Carlijn V.C. Bouten, Patricia Y.W. Dankers, *Functional peptide presentation on different hydrogen bonding biomaterials using supramolecular additives*, submitted

Eline E. van Haaften*, Renée Duijvelshoff*, Bastiaan D. Ippel, Serge H.M. Söntjens, Michel H.C.J. van Houtem, Henk M. Janssen, Anthal I.P.M. Smits, Nicolas A. Kurniawan, Patricia Y.W. Dankers, Carlijn V.C. Bouten, *The degradation and performance of electrospun supramolecular vascular scaffolds examined upon in vitro enzymatic exposure*, Acta Biomaterialia **2019**, 92, 48-59

Mani Diba, Sergio Spaans, Ke Ning, Bastiaan D. Ippel, Fang Yang, Bas Loomans, Patricia Y.W. Dankers, Sander C.G. Leeuwenburgh, *Self-healing biomaterials: from molecular concepts to clinical applications*, Advanced Materials Interfaces **2018**, 5, 1800118

Valentina Bonito, Anthal I.P.M. Smits, Olga J.G.M. Goor, Bastiaan D. Ippel, Anita Driessen-Mol, Tijmen J.A.G. Münker, Anton W. Bosman, Tristan Mes, Patricia Y.W. Dankers, Carlijn V.C. Bouten, *Modulation of macrophage phenotype and protein secretion via heparin-IL-4 funcitonalized supramolecular elastomers*, Acta Biomaterialia **2018**, 71, 247-260

Sergio Spaans, Peter-Paul K.H. Fransen, Bastiaan D. Ippel, Denise F.A. de Bont, Henk M. Keizer, Noortje A.M. Bax, Carlijn V.C. Bouten, Patricia Y.W. Dankers, *Supramolecular surface functionalization via catechols for the improvement of cell-material interactions*, Biomaterials Science **2017**, 5, 1541

Ronald C. van Gaal, Bastiaan D. Ippel, Sergio Spaans, Muhabbat I. Komil, Patricia Y.W. Dankers, *Effectiveness of cell adhesive additives in different supramolecular polymers*, in preparation

Tamar B. Wissing, Eline E. van Haaften, Suzanne E. Koch, Bastiaan D. Ippel, Nicolas A. Kurniawan, Carlijn V.C. Bouten, Anthal I.P.M. Smits, *Shear stress and cyclic stretch distinctively impact the secretory profile of biomaterial-activated macrophages -implications for in situ tissue regeneration,* submitted

*) these authors contributed equally

Patents

Patricia Y.W. Dankers, Björne B. Mollet, Samaneh Kheyrrooz, Bastiaan D. Ippel, Henk M. Keizer, Geert C. van Almen, Frank T.P. Baaijens, *Supramolecular polymer blend*, US Patent App. 15/544,468 **2018**

Dankwoord

En met het schrijven van deze laatste paar pagina´s komt er bijna een eind aan het avontuur dat promoveren heet. Ik wil hierbij even de tijd nemen om iedereen te bedanken die heeft bijgedragen aan dit proefschrift, zowel inhoudelijke als minder inhoudelijke zin.

Patricia, ik wil beginnen met jou te bedanken voor de begeleiding tijdens mijn promotie, en de kans die je mij gegeven hebt om me te ontwikkelen in een voor mij relatief onbekend vakgebied. In het begin wist ik immers een urea niet van een urethaan te onderscheiden en waren moleculen voor mij vreemd. Ik heb me een partij wikipedia-pagina's afgestruind om te begrijpen wat er allemaal in de groepsmeetings besproken werd. Ik heb van jou, en tijdens het werken in de groep, enorm veel geleerd de afgelopen jaren. Ik vond het prettig om op willekeurige momenten even binnen te komen vallen, wat denk ik de basis heeft gelegd aan de prettige samenwerking. Ik hoop van harte dat het wetenschappelijk werk in de groep de komende jaren tot nog meer prachtige hoogstandjes zal leiden!

Carlijn, ik kan me het eerste skype-gesprek om het project waarop ik terecht ben gekomen te introduceren nog goed herinneren, ingesneeuwd en wel op stage. Bedankt voor het vertrouwen, je wist immers al na mijn afstuderen (voordat ik het doorhad) dat ik wel terug zou komen voor een promotie.

Daarnaast wil ik ook Jan, Rint, Bert, Carsten, Anthal en Maarten bedanken voor het deel uitmaken van mijn promotiecommissie en daarbij voor het lezen van mijn proefschrift en het deelnemen aan de verdediging vandaag. Maarten, ook bedankt voor de samenwerking en de discussies over de data in hoofdstuk 6. Jouw scherpe en kritische blik heeft dit stuk enorm verder geholpen.

Mijn onderzoeksproject maakte deel van het befaamde InSiTeVx consortium, waarvoor ik alle deelnemende partners wil bedanken. Uit Utrecht, prof. Marianne Verhaar en Joost Fledderus, bedankt voor de input tijdens de jaarlijkse consortium meetings. Rachelle Toorop wil ik graag bedanken voor het meenemen door het ziekenhuis en het ons laten bijwonen van een operatie waarbij een fistula werd aangelegd. En Xeltis voor het af en toe oplichten van het tipje van de sluier, om een inzicht te krijgen wat er zich bij jullie afspeelt omtrent de ontwikkeling van synthetische bloedvaten.

Iedereen van SyMO-Chem wil ik graag bedanken voor het synthetiseren van de polymeren en additieven die ik heb gebruikt voor mijn onderzoek, en Henk Janssen daarbij ook voor de hulp bij de DSC metingen. Moniek, Marloes, en later Yuana, bedankt voor het in het gareel houden van het zooitje ongeregeld dat rondloopt in het cellab en dat jullie van het lab zo'n prettige werkomgeving hebben kunnen maken. Koen en Merlijn van de ICMS animatiestudio, bedankt voor het maken van de prachtige cartoons. Wijnand, voor het aan de praat houden van de computers uit het jaar kruik die de AFM opstellingen bestuurden, en het beschikbaar stellen van het klimaatlab waar we met meer controle onze samples konden produceren. Tiny, voor het uitvoeren van en helpen bij de XPS metingen, die een belangrijk onderdeel van het onderzoek in dit proefschrift zijn geworden. Marc voor het operationeel houden van de SEM en Joost en Lou voor de hulp op het analytisch lab.

Daarnaast heb ik van een aantal collega's de fijne kneepjes van allerlei technieken

mogen leren, die ik nu even apart wil noemen. Meester Johnick, voor het leren hoe je de prachtigste peptides in elkaar draait. Moniek, voor het goede voorbeeld hoe je omgaat met de fruststraties van de grillige QCM-D (en de support bij het schoonmaken van de sensoren, wat een feestje was dat). Geert voor de eerste kennismaking met het solution-casten, en Olga voor het spin-coaten. Andrea en Wojtek voor het proberen te doorgronden van de electrospin-opstellingen.

Tijdens mijn promotieonderzoek heb ik ook samen kunnen werken met heel veel mensen. Om te beginnen; mijn (en hopelijk onze) promoties waren niet compleet geweest zonder een serieuze samenwerking, Ronald en Sergio. Heel cool om met de Spanish Collab Train te hebben mogen reizen, naar resultaten waar we nog steeds bar weinig van begrijpen – en des te fijner dat Ronald deze heeft mogen opschrijven. Muhabbat, super dat je het afstudeeronderzoek van Paul op hebt gepakt en dat we dit tot een prachtig paper hebben kunnen brengen. Ik ga er vanuit dat je met jouw enthousiasme de komende jaren nog veel meer instagrammable resultaten zal produceren. Eline, met jou samenwerken ging altijd als een speer, als we er dan daadwerkelijk aan toe kwamen. Fijn dat we het nog hebben kunnen afronden tot wat er nu in hoofdstuk 7 staat. En pak die rust. Boris, bedankt voor de synthese van de bisurea-peptides uit hoofdstuk 4, ondanks dat deze wat minder bleken te werken dan we gehoopt hadden. Maaike, ik ben blij dat je TEM afbeeldingen van de OBO het toch gehaald hebben tot in de thesis! Ook wil ik Mylene, Ivo, Paul, en Izy, met wie ik heb samen kunnen werken tijdens hun afstudeerprojecten, bedanken voor hun inzet. Hiervan heeft het werk van Paul de basis gevormd voor hoofdstuk 6 uit dit proefschrift, en de resultaten uit het project van Izy leiden hopelijk tot toekomstig onderzoek, zoals beschreven in het laatste hoofdstuk in dit boekje. Ik wens jullie allemaal veel succes in jullie verdere carrière!

Ook zijn er heel wat projecten begonnen die uiteindelijk, jammer genoeg, niet tot iets tastbaars hebben kunnen leiden. Paul Besseling, jou wil ik in het bijzonder bedanken voor je geduld en flexibilteit bij het wachten op mijn gefunctionalizeerde grafts. Ik had niet voorzien dat het fabriceren hiervan zoveel problemen met zich mee zou brengen en ik hoop van harte dat deze het toch ooit nog tot in een dier zullen schoppen, zonder dat deze snel falen. Simone, samen zijn we naar Utrecht gegaan om te kijken hoe er supramoleculaire scaffoldjes in muizenanusjes werden ingebracht, iets om niet te vergeten (hoe graag je ook zou willen). Nadia en Steven, ondanks dat het voor ons niet ging zoals gehoopt, denk ik dat de high-throughput screening van de supramoleculaire biomaterialen in de toekomst toch van de grond moet kunnen komen. Moniek, de metingen met de QCM waren maar lastig te reproduceren, maar ik had er maar wat graag iets meer uit geleerd. Georgy, ondanks dat ze niet helemaal leken te werken in ons systeem, vond ik het altijd interessant hoe jij naar je moleculen refeerde als je bitches.

Tot zover de inhoudelijke bijdrages; Ronald en Sergio, super dat jullie vandaag op wilden treden als mijn paranimfen, als afsluiter van deze super mooie periode die we nu allemaal achter ons laten als doctor. Ik heb met jullie ontzettend veel plezier gemaakt met bier brouwen (en drinken), gamen, eten, pizza's bouwen, conferenties bezoeken en vanalles anders en hoop dat nog veel langer te blijven doen! Ronald, ik heb met alle waarschijnlijkheid meer tegen jou aangekeken de afgelopen jaren dan dat ik Laura heb gezien, als kantoorbuddy. Bedankt voor al het lachen, samenwerken, random YouTube kennis

en ook zeker niet te vergeten het klagen. Wie weet komt ons adviesbureau ooit nog van de grond. Sergio, ik verwacht nog zeker een tripje naar het warme Aruba voor een flinke chill-sessie en een ritje naar besneeuwde bergtoppen om weer op een snowboard te shinen.

Daarnaast wil ik iedereen uit het DankersLab bedanken, voor alle gezellige kletspraat, koffie-brakes, lunches, borrels, groepsuitjes en tripjes. En in het bijzonder natuurlijk zij die hebben bijgedragen aan het betalen van mijn boete op de winterberg-trip. Dan Jing, voor de horror-nights in combinatie met Chinese lekkernijen, Maaike, voor de volhardendheid mij te blijven vragen om mee te gaan fietsen, Matilde voor de spelletjes-avonden, Moniek voor de guitar-hero sessies, Jiankang (m'n Engels is nog steeds dramatisch), Mani, Giulia, Jingyi, Sabrina, Maxime, Didem en Peter-Paul voor alle post-doc wisdom, Muhabbat voor de game-exchange en ongebreidelde enthousiasme, Johnick voor de overdreven verhalen, Boris voor de collaboration-brew, Annika (als m'n labjas maar niet te strak zit), Joyce, Martin, Paul, en oudgediende DankersLabbers, Geert, Maarten en Olga.

Ook iedereen die ervoor zorgde dat het cellab niet alleen een plek was om fijn te werken, maar ook om gewoon even te komen babbelen over patsaderen, moestuinieren, eten en koken, formule 1 en van alles en nog wat; Tamar, Nicole, Willeke, Noortje, Marc, Rob, Nicole, Eline, Suzanne, Bart, Valentina, Inge, Maike, Gitta, bedankt voor jullie gezelligheid!

Reinier, Jan, Jori, Petra, Eva, Anne-Linde, Sophie en Julia, met z'n allen beter bekend als de entiteit, ik zie jullie misschien maar een paar keer per jaar, met daarin het inmiddels traditiegetrouwe weekendje, maar als we elkaar zien, is het altijd prachtig. Ik vind het daarom ook supermooi dat jullie hier weer bij zijn!

Ineke, Luuk, en Bart, ik vind het super fijn dat ik jullie alweer een hele tijd geleden heb leren kennen. Bedankt voor alle gezellige etentjes, en wie weet word ik vast ooit nog een keertje beter in boeren-bridge.

Opa en oma, dankjewel voor alle support en de interesse in mijn studies al die jaren! Ik vind het superleuk dat je jullie hier bij kunnen zijn. Merel, ik ben ontzettend trots op wat jij nu allemaal doet. En, je kan altijd bellen voor midden-in-de-nacht uit leggen wat het nou ook alweer is wat ik doe.

Papa en mama, wat bof ik me toch een partijtje met zulke toppertjes als ouders. Jullie steunen mij altijd in alles wat ik gedaan heb, doe, en ik weet zeker dat jullie dat ook blijven doen bij wat ik nog ga doen.

Lautje, waar moet ik beginnen. Ik denk dat ik deze hele onderneming niet zo ongeschonden door was gekomen als ik niet iedere dag bij jou thuis had kunnen komen om te ontspannen, samen te koken, te eten, te genieten, voor een peptalk en de niet te ontwijken (en ook stiekem welkome) knuffels. Ik vind het super fijn dat jij al zo lang aan mijn kant staat en kijk enorm uit naar alles wat wij samen nog gaan doen, straks met twee goeie knieën én allebei een PhD.